



University
of Glasgow

Booker, Samuel A. (2011) *Inhibiting inhibition: interactions amongst interneurons of the hippocampus*. PhD thesis.

<http://theses.gla.ac.uk/2995/>

Copyright and moral rights for this thesis are retained by the Author

A copy can be downloaded for personal non-commercial research or study, without prior permission or charge

This thesis cannot be reproduced or quoted extensively from without first obtaining permission in writing from the Author

The content must not be changed in any way or sold commercially in any format or medium without the formal permission of the Author

When referring to this work, full bibliographic details including the author, title, awarding institution and date of the thesis must be given

Inhibiting Inhibition: Interactions amongst Interneurons of the Hippocampus

Samuel Anthony Booker
BSc (Hons)

Submitted in fulfilment of the requirements for the degree of PhD

School of Life Sciences
College of Medical, Veterinary and Life Science
University of Glasgow
Glasgow, G12 8QQ

September 2011

© S Booker 2011

Abstract

Cortical networks comprise excitatory principal cells and interneurons (IN); the latter showing large neurochemical, morphological and physiological heterogeneity. GABA release from IN axon terminals activates fast ionotropic GABA_A or slow metabotropic GABA_B receptors (GABA_BR); ionotropic GABA mechanisms are well described in INs, whereas GABA_BR activity is less well understood.

The primary aim of this thesis is to ascertain GABA_BR mediated inhibition in different IN types containing the neurochemicals parvalbumin (PV), cholecystokinin (CCK) or somatostatin (SSt). Using immunocytochemical techniques, at light and electron microscopic levels, we examined the cellular and subcellular expression of GABA_{B1} receptor subunits in these INs. Application of whole-cell patch clamp techniques in acute slices, allowed analysis of GABA_BR effects pre- and postsynaptically; in response to endogenous GABA release or pharmacological activation.

Light microscopy showed GABA_{B1} expression in INs containing CCK or SSt, equivalent to CA1 pyramidal cells; with low expression in PV INs. Using electron microscopy, we detected GABA_{B1} receptor subunits in dendrites of CCK and PV INs, with densities equivalent or higher than CA1 pyramidal cell dendrites. Unexpectedly, SSt containing dendrites showed a lower density of GABA_{B1} receptor subunits. In axon terminals of CCK and PV containing INs, we found comparable densities of GABA_{B1} receptor subunits.

Electrophysiological recordings confirmed the presence of functional postsynaptic GABA_BR in PV and CCK INs. GABA_BR-mediated slow inhibitory postsynaptic currents (IPSCs) had typically large amplitudes, but with high cell-to-cell variability in both IN types. Morphological separation of PV or CCK INs revealed slow IPSC amplitudes which were large in perisomatic inhibitory (PI)

cells (30.8 ± 8.6 pA and 39.2 ± 5.5 pA, respectively) and small in dendritic inhibitory (DI) cells (4.0 ± 1.7 pA and 11.6 ± 2.4 pA, respectively). Consistently, SSt-immunoreactive DI INs exhibited very small IPSCs (1.5 ± 0.2 pA). Pharmacological activation of GABA_B R by the selective agonist baclofen revealed variable amplitude whole-cell currents, confirming differences between IN subtypes.

Examining presynaptic GABA_BR activity; we minimally stimulated *str. pyramidale* evoking monosynaptic IPSCs in CA1 pyramidal cells. IPSCs mediated by CCK or PV PI axons were pharmacologically isolated by CB1 or M2 receptor activation. Both monosynaptic responses were reduced by baclofen, albeit differentially so. To further investigate this effect we performed paired-recordings from PV or CCK INs coupled synaptically to CA1 pyramidal cells. Baclofen inhibited PV and CCK basket cell mediated IPSCs by 51% and 98%, respectively; with a smaller effect in DI INs.

In summary, we have shown that functional GABA_BRs are expressed pre- and postsynaptically in hippocampal GABAergic INs; with distinct populations of INs under differential GABA_BR control. Postsynaptic inhibition was strong in PI INs, but weak or absent in DI INs, a relationship conserved presynaptically. The observed differential expression of GABA_BRs is likely to play a fundamental role in regulating the excitability and activity of GABAergic INs, regulating synaptic output and potentially contributing to network and oscillatory activity. Consequentially, during periods of high GABA release, GABA_BR activation could act as a switch, allowing DI INs to play a greater role in network inhibition, due to GABA_BR mediated inhibition of perisomatic-targeting INs.

Table of contents

Title page	i
Abstract	ii
List of tables	ix
List of figures	x
Acknowledgments	xiii
Declaration of originality	xv
Abbreviations	xvi
Chapter 1. Introduction	1
1.1: The hippocampus	1
1.2 Location and structure of the hippocampus	3
1.3: Neuronal circuitry of the hippocampus	4
1.3.1: The tri-synaptic loop	4
1.3.2: Other intrinsic and extrinsic pathways innervating the hippocampus	5
1.3.3: Principal cell types	6
1.4 Hippocampal GABAergic inhibitory interneurons	9
1.4.1 Inhibitory microcircuits	9
1.4.2 Functional role of hippocampal INs in hippocampal circuits	11
1.4.3 Neurochemical subtypes of interneuron	14
1.4.4 Morphological subtypes of interneurons	15
1.4.5 Physiological properties of selected interneurons	18
1.5 Molecular mechanisms of inhibition	21
1.5.1 Ionic and molecular basis of synaptic inhibition	21
1.5.2. GABA _A receptors	23
1.5.3 GABA _B receptor	24
1.5.4 GABA _B R in interneurons	26
1.6 Thesis aims	27
Chapter 2. Materials and methods	29
2.1 Animals and procedures	29

2.2 <i>In vitro</i> electrophysiology	29
2.2.1: Acute brain slice preparation	29
2.2.2: Composition of slicing and recording ACSF	30
2.2.3: Whole-cell patch clamp recording of selected cells from acute slices	31
2.2.4: Recording of passive and active membrane properties	32
2.2.5: Whole cell patch clamp recording of slow IPSCs	34
2.2.6: Whole cell patch clamp recording of monosynaptic IPSCs	37
2.2.7: Paired recordings of monosynaptic IPSCs	38
2.3 Morphological analysis of acute slices and perfused tissue	39
2.3.1: Fixation of acute slices following recording	39
2.3.2: Preparation of acute slices for fluorescence microscopy	39
2.3.3: Confocal fluorescence microscopy of brain slices	41
2.3.4: 3D reconstruction of biocytin-filled cells	42
2.3.5 Perfusion fixation for morphological analysis	42
2.3.6 Preparation of perfusion-fixed tissue for light microscopy	43
2.3.7: Preparation of perfusion-fixed tissue for electron microscopy	44
2.3.8 Analysis of immunogold particle density	45
2.4: Statistical analysis	46
2.5: Materials used	46
Chapter 3. Post-synaptic GABA_BR mediated responses in principal cells of the hippocampus	47
3.1 Morphological and physiological characterisation of CA1 pyramidal cells	47
3.2 CA1 pyramidal cells possess postsynaptic GABA _B R conductances	51
3.3 GABA _B R are differentially expressed in basal and apical CA1 pyramidal cell dendrites	54
3.4 GABA _B R responses in CA1 pyramidal cells are mediated by	56

an inward-rectifying K ⁺ -conductance	
3.5 Kinetics of GABA _B R-mediated IPSCs in CA1 pyramidal cells	58
3.6 Morphological and physiological characterisation of CA1 giant radiatum cells (GRCs)	59
3.7 CA1 GRCs possess large postsynaptic GABA _B R conductances	62
3.8 Morphological and physiological characterisation of dentate granule cells (DGCs)	64
3.9 DGCs possess large postsynaptic GABA _B R conductances	67
3.10 Conclusions	69
Chapter 4. Post-synaptic GABA_B receptors in PV-IR interneurons of the hippocampus	71
4.1 CA1 PV-IR INs express GABA _{B1} receptor subunits on dendritic membranes	71
4.2 Presence of Kir3 channel subunit, Kir3.2, on CA1 PV-IR IN dendritic membranes	73
4.3 Identification of PV-IR INs in area CA1 of the hippocampus	74
4.4 PV-IR INs possess GABA _B R conductances, which are different between morphological subtypes	79
4.5 GABA _B R-mediated conductances in PV-IR PI INs are mediated by an inward-rectifying K ⁺ channel	83
4.6 Kinetic properties of GABA _B R-mediated IPSCs in PV-IR PI INs	85
4.7 PV-IR PI INs of the DG also possess functional GABA _B Rs	86
4.8 Conclusions	90
5. Postsynaptic GABA_BRs in CCK-IR interneurons within area CA1 of the hippocampus	91
5.1 CA1 CCK-IR INs express GABA _{B1} subunits at dendritic membranes.	91
5.2 Identification of CCK containing INs in area CA1 of the hippocampus.	93
5.3 CCK-IR INs possess GABA _B R conductances, which were different between morphological subtypes.	99
5.4 GABA _B R-mediated conductances in CCK-IR INs are mediated by an inward-rectifying K ⁺ channel.	104

5.5 Kinetic properties of GABA _B R-mediated IPSCs in CCK-IR INs	106
5.6 Conclusions	107
Chapter 6. Postsynaptic GABA_BR mediated conductances in SSt-IR OLM cells, within area CA1 of the hippocampus	108
6.1 Expression of GABA _{B1} subunits in dendrites of CA1 SSt-IR INs	108
6.2. Identification of SSt-IR INs in area CA1 of the hippocampus	110
6.3 SSt-IR INs possess no observable GABA _B R conductance	114
6.4 Conclusions	116
Chapter 7. GABA_B receptors control presynaptic GABA release from PV and CCK-IR axon terminals.	117
7.1 GABA _{B1} receptor subunits localise to CCK and PV-IR axon terminals in str. pyramidale of CA1	118
7.2 PI interneuron inputs onto CA1 pyramidal cells were pharmacologically separated, revealing two distinct axonal subtypes.	119
7.3 Axons of pharmacologically distinct PI interneurons have different presynaptic GABA _B R profiles	121
7.4 GABA _B Rs mediate presynaptic control of GABA release from identified CCK and PV IR basket cells	125
7.5 CCK and PV IR DI INs coupling to CA1 pyramidal cells is differentially inhibited by GABA _B Rs	128
7.6 Conclusions	131
Chapter 8: Discussion of results	132
8.1 Key findings	132
8.1.1 Intrinsic properties of hippocampal neurons	132
8.1.2 GABA _B R in hippocampal principal cells:	133
8.1.3 Cellular and subcellular localisation of GABA _B Rs in identified hippocampal interneurons	135
8.1.4 PI and DI INs display functional differences in GABA _B R-mediated postsynaptic conductances	136
8.1.5 Presynaptic GABA _B receptors in CCK and PV IR axon terminals	138
8.2 Implications of results	140

8.2.1 GABA _B modulation of synaptic transmission in hippocampal INs.	141
8.2.2 GABA _B Rs in hippocampal network activity and oscillations	143
8.3 Technical considerations and future work	147
8.3.1 Technical considerations	147
8.3.2 Future work	149
8.4 Concluding remarks	150
References	152

List of Tables

Table 2.1 Summary of primary ABs used in immunocytochemistry	40
Table 2.2 Summary of secondary ABs used in immunocytochemistry	41
Table 3.1 Summary of intrinsic properties of CA1 pyramidal cells	51
Table 3.2 Summary of GABA _B R mediated IPSC kinetics in CA1 pyramidal cells	59
Table 3.3 Summary of the intrinsic properties of CA1 GRCs	61
Table 3.4 Summary of the intrinsic properties of DGCs	66
Table 4.1 Summary of intrinsic properties of PI and DI PV-IR INs in CA1	78
Table 4.2 Summary of GABA _B R-mediated IPSC kinetics of PV-IR PI cells, in CA1.	85
Table 4.3 Summary of key intrinsic properties in DG PV-IR PI cells	87
Table 5.1 Summary of intrinsic properties of PI and DI CCK-IR INs in CA1	99
Table 5.2 Summary of GABA _B R-mediated IPSC kinetics in CCK-IR INs, of CA1	106
Table 6.1 Summary of key intrinsic properties of CA1 SST-IR OLM cells.	112
Table 8.1 Summary of GABA _B R mediated currents in principal cells of the hippocampus	134
Table 8.2 Summary of GABA _B R mediated currents in INs of the CA1 subfield	136

List of Figures

Figure 1.1 Schematic diagram of the hippocampal principal cell network, the tri-synaptic loop	3
Figure 1.2 Summary of different types of inhibition within local networks	10
Figure 1.3 Schematic of neurochemical and laminar distributions of INs	15
Figure 2.1: Schematic of whole brain dissection, blocking and slicing.	30
Figure 2.2: Control recordings of GABA _B R-mediated IPSCs in CA1 pyramidal cells	35
Figure 3.1 Morphological identification of a CA1 pyramidal cell	48
Figure 3.2: Comparison of CA1 pyramidal cell intrinsic properties.	50
Figure 3.3 GABA _B R mediated IPSCs in CA1 pyramidal cells elicited by release of endogenous GABA	52
Figure 3.4 Pharmacological characterisation of GABA _B R-mediated currents in CA1 pyramidal cells.	53
Figure 3.5 GABA _B R mediated IPSCs in CA1 pyramidal cells elicited by release of endogenous GABA, in <i>str. oriens</i>	55
Figure 3.6 GABA _B R responses in CA1 pyramidal cells are reversible and inward-rectifying	56
Figure 3.7 Schematic of key GABA _B R IPSC kinetic values	58
Figure 3.8 Morphological and physiological characterisation of CA1 GRCs	60
Figure 3.9 GABA _B R mediated IPSCs in CA1 GRCs elicited by endogenous GABA release	62
Figure 3.10 Pharmacological characterisation of GABA _B R-mediated currents in CA1 GRCs	63
Figure 3.11 Morphological and physiological characterisation of DGCs	65
Figure 3.12 GABA _B R mediated IPSCs in DGCs elicited by release of endogenous GABA.	67
Figure 3.13 Pharmacological characterisation of GABA _B R-mediated currents in DGCs	68

Figure 4.1 Immunocytochemical localisation of GABA _{B1} receptor subunits to CA1 PV-IR INs.	72
Figure 4.2 Immunocytochemical localisation of Kir3.2 channel subunits to CA1 PV-IR INs	73
Figure 4.3 Morphological and neurochemical identification of a PV-IR PI IN, in CA1	75
Figure 4.4 Morphological and neurochemical identification of a PV-IR DI cell, in CA1	76
Figure 4.5 Trains of APs and AP waveforms in PV-IR PI and DI INs.	77
Figure 4.6 GABA _B R mediated IPSCs in CA1 PV-IR INs, elicited by release of endogenous GABA	80
Figure 4.7 Pharmacological characterisation of GABA _B R-mediated currents in PV-IR INs of the CA1.	82
Figure 4.8 GABA _B R responses seen in PV-IR PI cells are reversible and inward-rectifying	84
Figure 4.9 Morphological and physiological characterisation of a PV-IR basket cell in the DG	86
Figure 4.10 GABA _B R mediated IPSCs in DG PV-IR PI cells elicited by release of endogenous GABA.	88
Figure 4.11 Pharmacological characterisation of GABA _B R-mediated currents in PV-IR INs of the DG	89
Figure 5.1: Immunocytochemical localisation of GABA _{B1} subunits to CCK-IR dendrites in CA1	92
Figure 5.2: Morphological and neurochemical identification of a CCK-IR PI IN, in CA1.	94
Figure 5.3: Morphological and neurochemical identification of a putative CCK-IR SCA-type IN.	95
Figure 5.4: Morphological and neurochemical identification of a putative CCK-IR PPA-type IN	96
Figure 5.5 Trains of APs and AP waveforms from representative CCK-IR PI and DI IN subtypes.	97
Figure 5.6 GABA _B R-mediated IPSC in CA1 CCK-IR INs, elicited by release of endogenous GABA	101
Figure 5.7 Pharmacological characterisation of GABA _B R-mediated	103

responses in CCK-IR INs of the CA1	
Figure 5.8 GABA _B R responses seen in all CCK-IR cells are reversible and inward-rectifying	105
Figure 6.1 Immunocytochemical localisation of GABA _{B1} receptor subunits to SSt-IR dendrites, in <i>str. oriens</i> of CA1	109
Figure 6.2 Morphological, neurochemical and physiological identification of a CA1 SSt-IR OLM cell.	110
Figure 6.3 Release of endogenous GABA evoked no or very small slow-IPSCs in CA1 SSt-IR OLM cells.	114
Figure 6.4 Pharmacological characterisation of GABA _B R-mediated responses in CA1 SSt-IR OLM cells	115
Figure 7.1 Immunocytochemical localisation of GABA _{B1} receptor subunits to PV and CCK-IR axon terminals, in <i>str. pyramidale</i> of CA1.	118
Figure 7.2 Monosynaptic IPSCs elicited by minimal stimulation in <i>str. pyramidale</i> were differentially sensitive to CB1 receptor activation	120
Figure 7.3 GABA _B Rs exerts presynaptic control of GABA release in PI axons which is independent of WIN-sensitivity	122
Figure 7.4 Comparison of monosynaptic IPSC amplitudes from M2 and CB1 sensitive afferents	124
Figure 7.5 Monosynaptic IPSCs from CCK-IR PI cells are sensitive to GABA _B R activation	126
Figure 7.6 Monosynaptic IPSCs from PV-IR PI cells are sensitive to GABA _B R activation	127
Figure 7.7 Monosynaptic IPSCs from CCK-IR DI cells are also sensitive to GABA _B R activation.	129
Figure 7.8: Monosynaptic IPSCs from PV-IR DI cells are not sensitive to GABA _B R activation.	130
Figure 8.1 Schematic of presynaptic modulation by GABA _B Rs	139
Figure 8.2 Raster plot of a modelled IN network of fast-spiking PI and DI cells	146

Acknowledgements

As it comes to the end of my time in Glasgow and completion of this thesis, I feel that without the seemingly tireless support and kindness of my supervisor Imre Vida, who although I was drenched to the bone in my initial interview gave me the opportunity of work with him. Without Imre I doubt that I would have ever have reached this stage. Also thanks to his family for allowing him to stay until all hours, helping me get to grips with innumerate conceptual ideas and to nurture my interest in neuroscience. From the bottom of my heart, thank you so very, very much.

As well as Imre, I would like to thank the MRes and undergraduate students who have aided this project immensely, most notably Annabelle Gee, Jacek Baraniecki and also Katarina Pankova.

It would be prudent for me not to acknowledge the immense debt I owe to my colleagues at the Institute of Anatomy, Freiburg (Germany), notably Ákos Kulik for giving me the opportunity to visit his lab in spring 2011 and teaching me the art of electron microscopy. And to Anna Gross, Daniel Althof, Natalie Cailles, Sigrun Nestel and Barbara Jung for data, time, support and kindness.

Without the support of Stuart Cobb; for a friendly ear whenever things have gone a bit-pear shaped or when I have been in need of some chemical, I probably would have come unstuck several times; as well as his lab: Paul Turko, Faye McLeod, Shih Ming Weng (Jonas), Kamal Gadalla and Jian Gian for many, many kindness.

I don't think my 3 years in the West Medical Building would have been as rewarding and fun if it hadn't been for those who have aided and abetted

shenanigans, notably: Graham for countless cigarettes and chats, Rhiannon and everyone else mentioned previously.

Nothing I have done or achieved would be possible without the support and love of my family, who have always been on the end of the phone for a chat or providing some fine wine, cheers Mum, Dad, Jack, Tom and Ned.

And lastly to my girlfriend Cheryl, thank you for putting up with my bad moods, tiredness, and general annoying conversations about neuroscience, over the last 3 or so years. Ta much, luv.

I think it would be good to end these acknowledgements with a quote from the late Richard Feynman:

“... I'm really still a very one-sided person and don't know a great deal. I have a limited intelligence and I've used it in a particular direction.”

Richard P Feynman, talking on the BBC's Horizon, 1981

Declaration of originality

I declare that the work presented in this thesis is entirely my own work, with the exception of figures 4.1, 4.2, 5.1 and 7.1, which was taken from work published as the thesis of Dr Anna Gross (2010), under the supervision of Drs Imre Vida and Ákos Kulik.

Signature.....

Sam A Booker

Where this work has been used, permission has been approved by Drs. Vida and Kulik, supervisors to the below work.

Anna Gross, Differential distribution of GABA_B receptors in CCK and PV-containing hippocampal interneurons; University of Freiburg, Germany, 2010

Abbreviations

7-TM	7-transmembrane domain
AB	Antibody
ABET	Arecaidine but-2-ynyl ester tosylate
ACSF	Artificial cerebrospinal fluid
ADA	Apical dendrite associated
AHP	Afterhyperpolarisation
AIS	Axon-initial-segment
AMPA	2-amino(methyloxo-1,2-oxazolyl)propanoic acid
AP	Action potential
AP-V	D-2-Amino-5-phosphonopentanoic acid
BC	Basket cell
CA	<i>Cornu ammonis</i>
CB	Calbindin
CB1	Endocannabinoid 1 receptor
CCK	Cholecystokinin
CGP-55,845	(3,4- Dichlorophenylethyl amino-2-hydroxypropyl(phenylmethyl) phosphinic acid hydrochloride
CNS	Central nervous system
CR	Calretinin
DAB	Diaminobenzidine
DAP	Depolarising afterpotential
DG	<i>Dentate gyrus</i>
DGC	Dentate granule cell
DI	Dendritic inhibitory
EC	Entorhinal cortex
EPSC	Excitatory post-synaptic current
EPSP	Excitatory post-synaptic potential
E _R	Reversal potential
GABA	γ-aminobutyric acid
GCL	Granule cell layer
GRC	Giant radiatum cell
I _A	A-current
I _h	Hyperpolarisation-activated current

I_M	M-current
IN	Interneuron
IPSC	Inhibitory post-synaptic current
IPSP	Inhibitory post-synaptic potential
IR	Immunoreactive
KCC2	Potassium/Chloride Co-transporter 2
K_{ir3}	G-protein coupled inward-rectifying potassium channel
K_V	Voltage-gated potassium channel
LGIC	Ligand-gated ion-channel
L-M	<i>Lacunosum-moleculare</i>
LTD	Long-term depression
LTP	Long-term potentiation
M2	Muscarinic acetyl choline 2 receptor
mGluR	Metabotropic glutamate receptor
Na_V	Voltage-gated sodium channel
NBQX	2,3-Dioxo-6-nitro-tetrahydrobenzo-quinoxaline-7-sulfonamide
NGS	Normal goat serum
NMDA	n-methyl d-aspartate
OLM	<i>Oriens/lacunosum-moleculare</i>
PB	Phosphate buffer
PBS	Phosphate buffered saline
PI	Perisomatic inhibitory
PPA	Perforant-path associated
PV	Parvalbumin
R_i	Input resistance
R_s	Series resistance
SCA	Schaffer-collateral associated
SEM	Standard error of the mean
SSt	Somatostatin
<i>Str.</i>	<i>stratum</i>
SWR	Sharp wave ripples
TB	Tris buffer
TBS	Tris buffered saline
Tx-100	Triton X-100
VGCC	Voltage-gated calcium-channel

V_M	Membrane potential
WIN-55,212	2,3-Dihydro-5-methyl (4-morpholinylmethyl)pyrrolo[1,2,3- <i>de</i>]-1,4-benzoxazin-6-yl]-1-naphthalenylmethanone mesylate

Chapter 1 Introduction

We set out to determine whether functional metabotropic GABA_B receptors are found on the plasma membranes of inhibitory interneurons (INs) of the mammalian hippocampus and how these receptors effect synaptic transmission in these cells. To understand the role GABA_B receptors in the hippocampal network we first have to recapitulate how this network functions, how INs fit into this network and what is known regarding inhibitory transmission in INs; particularly in regard to metabotropic transmission. This approach takes into account morphological and physiological features of excitatory and inhibitory cells present in the hippocampus, determining how inhibitory synaptic transmission and resulting network activity is potentially modulated by GABA_B.

1.1: The hippocampus

The mammalian CNS is arguably one of the most complicated biological systems with many different regions receiving input from peripheral tissue and other brain regions, integrating and then transmitting electrical and chemical signals for information storage or output. One such brain region is the hippocampus, recognised historically by its characteristic shape, which is conserved amongst mammals. Intrinsic in learning and memory pathways (Squire, 1992), the hippocampus has been identified as being involved in several outcomes of cognition: in humans, through the neurosurgical lesion studies of Scoville and Millner (1957) and in rats, in the generation of new spatial memories (O'Keefe and Nadel, 1979; Eichenbaum et al, 1999); as well as coding for memories which are not necessarily stored in it.

Similar to other cortical regions, the hippocampus is comprised of principal cells, i.e. those which release glutamate as their primary neurotransmitter (Cajal, 1911; Lorente de nó, 1934); which make up approximately 90% of neurons in the hippocampus, the remaining ~10% being comprised of inhibitory INs (IN; Freund

and Buzsáki, 1996) and release the neurotransmitter γ -aminobutyric acid (GABA). As well as neurons the hippocampus contains a large number of glial cells, supporting and modulating neuronal function (Rakic, 1981).

The hippocampus shows robust long-term potentiation (LTP) and depression (LTD), at all main glutamatergic synapses; which are believed to be two mechanisms contributing to memory formation and consolidation (Landfield et al, 1978). Excitatory synapses in the hippocampus have been shown to undergo Hebbian LTP (Bliss and Lømo, 1973), with synapses onto INs undergoing both Hebbian and non-Hebbian LTP and LTD (Lamsa et al, 2007; Nissen et al, 2010). Dysfunction of the hippocampus presumably through alteration of synaptic transmission LTP/LTD mechanisms has been shown to have dramatic effects on learning and memory capabilities (Scoville and Millner, 1957; Zola-Morgan, 1986)

Due to the convergence of strong excitatory transmission onto the hippocampus, within the extensive recurrent network of the CA3 and the synaptic plasticity associated with this transmission, there are several key pathological states strongly associated with hippocampal dysfunction. Probably the most well described is in temporal lobe epilepsy (Sommer, 1880). Input from the cortex into the recurrent CA3 network, to and from dentate gyrus and CA1, combined with a heavy reliance on inhibition to maintain co-ordinated hippocampal activity within these pathways (Klausberger et al, 2003), leaves this region susceptible to seizure generation. In particular the mossy-fibre pathway is highly prone epileptogenic damage and modification, for example axon sprouting and cell-death of dentate granule cells (Mello et al, 1993). Aside from epilepsy, there is evidence that the hippocampus is involved in the development of Alzheimer's disease (Geddes et al, 1986; Braak and Braak, 1991), which in light of hippocampal function in learning and memory, fits well with symptoms of this disease.

Hippocampal coupling to extrahippocampal cortices, i.e. the pre-frontal cortex (Vertes et al, 2006) or the median raphe nuclei (Papp et al, 1999), can suffer

dysfunctional connectivity, which has been suggested as a potential cause of psychiatric disorders. Hippocampal dysfunction has been shown to drive the progression of psychiatric illness, notably schizophrenia, depression and anxiety disorders (Falkai and Bogerts, 1986; Meyer-Lindenberg and Weinberger, 2006; Kehrer et al, 2008).

1.2 Location and structure of the hippocampus.

The hippocampus is found within the temporal lobes of the forebrain, underlying the neocortex, with a cylinder-like shape, turning to form a C-shaped structure present in both hemispheres of the mid brain and are surrounded by the lateral ventricle.

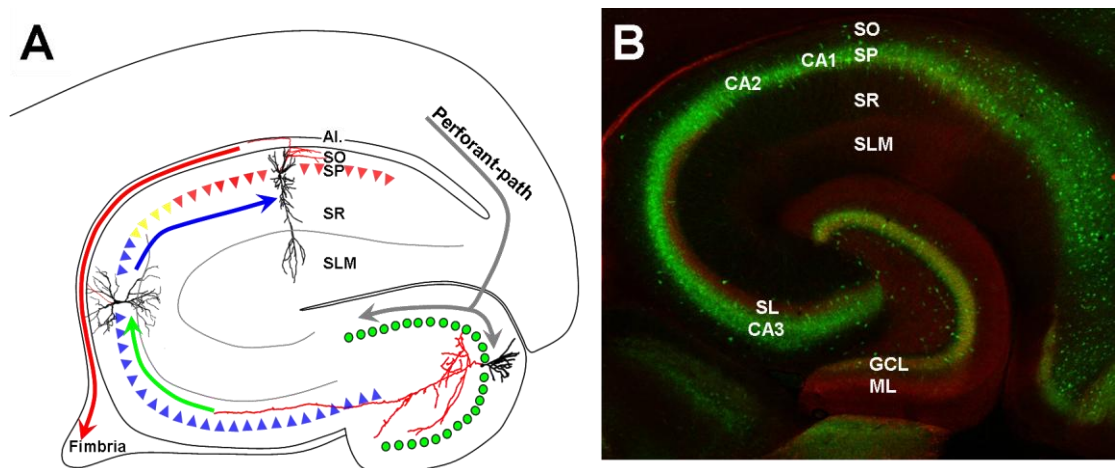


Figure 1.1 Schematic diagram of the hippocampal principal cells network, the tri-synaptic loop. **A**, Dentate granule cells (green circles), CA3 pyramidal cells (blue triangles), CA2 and CA1 pyramidal cells (yellow and red, respectively) are all shown. Arrows dictate orthodromic AP direction along axons. Reconstructions of relevant cells are shown descriptively (not scaled). **B** low power confocal micrograph showing immunoreactivity for PV (green pseudo colour) and CB (red pseudocolour); hippocampal laminations are labelled.

The hippocampus is composed of two distinct regions known as the *dentate gyrus* (DG) and the *cornu ammonis* (CA), with the DG folding around the distal CA, known as the CA3 region. The CA runs parallel to the tangent of the DG, giving rise to regions known as CA2 and CA1 (see figure 1.1) which give

transverse sections of the hippocampus its classical “double C” shape. The hippocampus has an ordered laminar structure, resulting from specific layering of CA1-3 and DG principal cell somatodendritic axes (Cajal, 1911). The neuropil (dendritic region) of the hippocampus is then delineated based upon properties of principal cell dendrites in that field, for example in CA1, principal cell apical dendritic trunks are unilaterally arranged in a region known as *stratum (str.) radiatum*. These thick dendrites bifurcate and produce dendritic tufts in the region *str. lacunosum-moleculare (L-M)*. The basal dendrites of principal cells lie in the neuropil below the somatic layer forming a lamina known as *str. oriens*. Encapsulating the whole CA region is the main projection of the hippocampus, the *alveus* (see figure 1.1.A) consisting of myelinated and unmyelinated, afferent or efferent, axons.

As well as principal cells, INs tightly observe this lamina structure, as seen in figure 1.1.B by the distribution of neurochemical markers, such as parvalbumin (PV; in green) contrasted with that of calbindin (CB; in red); delineating some INs and principal cells, most obviously a dense PV-immunoreactive (IR) axonal plexus in all cell-body layers and CB-IR principal cells in the DG and CA1. The tight lamina structure of area CA1 is similar to the other hippocampal subfields, with some minor differences; for summary of hippocampal architecture see: Cajal (1911); Lorente de nó (1934) and Amaral and Witter, (1989).

1.3: Neuronal circuitry of the hippocampus

1.3.1: The tri-synaptic loop

Synaptic glutamatergic transmission in the hippocampus forms a loop circuit, in three key synaptic zones; referred to as the tri-synaptic loop (see figure 1.1.A). Excitatory input enters the hippocampus from the entorhinal cortex (EC) via DGCs, integrating this input to evoke an action potential (AP) in their axon. CA3 pyramidal cells receive DGC input on apical dendrites; this connection referred

to as the “teacher” synapse, due to low-probability, large-amplitude and highly plastic glutamatergic activity (Henze et al, 2002). APs elicited by CA3 pyramidal cells release glutamate onto dendritic spines of apical and basal dendrites of CA1 pyramidal cells (Collingridge et al, 1983). This excitatory signal then enters the EC from CA1 pyramidal cell axons, closing this loop. Each synaptic group in this loop interconnects with local INs, providing differential inhibition to the local network.

1.3.2: Other intrinsic and extrinsic pathways innervating the hippocampus

This somewhat classical view of the hippocampal glutamatergic network is predominant in transverse hippocampal slices, however *in vivo* the intact hippocampus has a wider variety of intrinsic and extrinsic glutamatergic connections, with many synapse groups converging onto several brain regions. Notably, perforant path afferents do not exclusively ramify in a lamellar fashion onto DGCs, as is suggested in the tri-synaptic loop hypothesis; rather that the perforant-path afferents synapse onto three-dimensional groups of neurons along the axis of the DG (Amaral and Witter, 1989). More interestingly is the strong perforant-path connection to dendrites of principal cell and INs in *str. L-M* of CA1 to CA3, potentially acting to bypass the tri-synaptic loop, with hippocampal input only integrating in area CA1 (Amaral and Witter, 1989).

Perhaps the most pertinent examples of glutamatergic input to hippocampal neurons arising from out with the tri-synaptic loop are the recurrent fibres, principally recurrent mossy-fibres and the recurrent CA3 network. It has been shown that the mossy-fibres of DGCs not only project onto CA3 pyramidal cells, but also back onto hilar mossy cells, DG INs and DGCs (Okazaki et al, 1999; Henze et al, 2000) acting as an excitatory feedback loop, maintaining and synchronising the local excitatory network. The recurrent CA3 network is possibly the most well studied recurrent network, due to the central role it plays in providing feedback excitation to both the CA3 (Amaral and Witter, 1989) and DG (Helen, 2007). The effect of these connections is to provide strong feedback

excitation, which in the CA3 results in synchronised synaptic output, from synaptically coupled groups of CA3 pyramidal cells. Additional to this, CA1 pyramidal cells have been shown to have a strong local axonal arborisation, innervating mainly INs in the local vicinity (Blasco-Ibáñez and Freund, 1995) and are believed to autoregulate glutamatergic transmission, maintaining network synchrony.

Additional to glutamatergic input to the hippocampus many different transmitter systems converge onto the hippocampus, in a three-dimensional manner. For example, the serotonergic connection from the dorsal raphe nucleus (Schmitz et al, 1998), the cholinergic input from the medial septal nucleus and the diagonal band of Broca (Mesulam et al, 1983) and the noradrenergic connection from the locus coeruleus (Jones and Moore, 1977), as well as other extrahippocampal inputs; which generally act to modulate activity within the hippocampal network.

1.3.3: *Principal cell types*

There are 6 main types of principal cell in the hippocampus, dentate granule cells (DGC), hilar mossy cells, CA1, CA2, CA3 pyramidal cells and displaced pyramidal or giant *radiatum* cells (GRC). We will provide full morphological descriptions of the principal cell subtypes we have studied in chapter 3; those not described have been defined, in terms of morphology and physiology, elsewhere (Hilar mossy cells, CA3 and CA2 pyramidal cells: for review see Cutsuridis et al, 2010). There are two common features linking all principal cells: 1) glutamate as the primary neurotransmitter (Dudar, 1974; Storm-Mathieson, 1977; Collingridge et al, 1983) and 2) spine covered dendrites (Cajal, 1911). Principal cells are the primary effectors of the tri-synaptic loop; although extrahippocampal inputs, glutamatergic or otherwise, influence transmission in all cell types.

DGCs and hilar mossy cells

The main principal cell type in the DG is the DGC, these small bipolar cells are localised almost exclusively to the *str. granulosum* or the granule-cell layer (GCL) of the DG. We discuss the physiological and anatomical properties of this cell type in chapter 3. Receiving primary glutamatergic input from entorhinal cortex via the perforant-path (Andersen et al, 1966); DGCs are the primary excitatory input to the recurrent CA network. DGCs give rise to a single unmyelinated axon (mossy-fiber), which forms a narrow lamina in CA3, known as *str. lucidum*; forming mossy-fiber bouton synapses with CA3 pyramidal cell apical dendrites (see Henze et al, 2000; for review). Also within the DG lies another principal cell type, the hilar mossy cell (Ribak et al, 1985) which receive input primarily from DGCs; hilar mossy-cells innervate DGCs and local INs, providing feedback excitation to these local cells.

CA3 pyramidal cells

Within the CA3 subfield, CA3 pyramidal cells are the dominant excitatory cell, receiving excitatory input from the mossy-fibers of DGCs and from the CA3 recurrent pathway. The main axon of CA3 pyramidal cells emerges from the soma and extends several millimetres in the *str. radiatum* (in rat brain), forming the so-called Schaffer-collateral/commissural pathway (Amaral and Witter, 1989). The Schaffer-collaterals are the effectors of the recurrent network, making glutamatergic synaptic contacts with dendrites of principal cells and INs in CA3, CA2 and CA1 subfields (Hjorth-Simonsen, 1973; Collingridge et al, 1983), which in the former region provide recurrent network drive leading to self-amplification of CA3 output (Ishizuki et al, 1990).

CA2 pyramidal cells

The CA2 subfield is the most poorly understood hippocampal region, populated with CA2 pyramidal cells it receives input from the extra-hippocampal, supra-mammillary cortex and CA3 recurrent glutamatergic input, similar to CA1 pyramidal cells (Mercer et al, 2007). CA2 pyramidal cells are believed to drive excitation locally in distinct IN networks and also projecting to extra-hippocampal cortices.

CA1 pyramidal cells

The best studied hippocampal principal cell is the CA1 pyramidal cell, with well described morphological and physiological properties (Schwartzkroin, 1975) which will be further examined in chapter 3.

Robust synaptic connections are formed onto dendritic spines of CA1 pyramidal cells by CA3 Schaffer-collateral in *str. radiatum* and *oriens* (Cajal, 1911; Hjorth-Simonsen, 1973) and perforant-path afferent mainly in *str. L-M* (Cajal, 1911; Colbert and Levy, 1992). CA1 pyramidal cells are the main glutamatergic projection neuron of the hippocampus, with axons extending through *str. oriens* into the *alveus*, projecting into the entorhinal cortex. CA1 pyramidal cells also contribute a small local axon arborisation, which provides feedback excitation to local INs (Blasco-Ibáñez and Freund, 1995; Katona et al, 1999; Gulyás et al, 1999).

Giant radiatum cells of the hippocampus

The last major subset of hippocampal principal cells, present in at least CA3 and CA1 subfields; are known collectively as displaced pyramidal cells or “giant *radiatum* cells” (GRCs). Very little has been published regarding these cells; however two clear subtypes are observed (Gulyás et al, 1998; Bullis et al, 2007): those which are morphologically similar to pyramidal cells or ones with

differential dendritic morphologies (see chapter 3). All GRCs have a high density of dendrites in *str. radiatum* suggesting a large Schaffer-collateral input and show similar physiologies to CA1 and CA3 pyramidal cells (Christie et al, 2000). In CA1 GRCs, axons are believed to project to extra-hippocampal regions, principally the olfactory bulb and septum (Christie et al, 2000).

1.4 Hippocampal GABAergic inhibitory interneurons

As stated previously the hippocampus exhibits a diverse population of INs which act locally or project to other subfields (Khazipov et al, 1995; Sík et al, 1994; Fuentalba et al, 2008) and brain regions (Tóth and Freund, 1992), mediating the synaptic output of both principal and non-principal neurons. Inhibitory INs release GABA from their axon terminals and inhibit synaptic transmission in pre- and post-synaptic compartments, maintaining control of glutamatergic and GABAergic signalling (Freund and Buzsáki, 1996).

There are now over 20 known inhibitory INs in the CA1 of the mammalian hippocampus (Klausberger and Somogyi, 2008) and at this time there is no final consensus on how to classify INs, due to their great morphological and neurochemical diversities. Hence, for this study we will describe both characteristics in 5 key subtypes of IN, containing either PV, cholecystokinin (CCK) or somatostatin (SSt) neurochemicals and with targeting either the perisomatic or dendritic regions or principal cells.

1.4.1 Inhibitory microcircuits

At single synapses, inhibition reduces transmitter release or EPSP amplitude by modulation of release mechanisms or influencing intrinsic properties of membranes (Krnjevic, 1974). Networks of synapses arise from axons of different populations of excitatory and inhibitory neurons converging on many other cells;

in turn leading to synchronisation of AP generation in axons, through inhibition of excitation or inhibition. A wide variety of IN morphological phenotypes confer different subcellular compartments with different inhibitory drive, synchronising and patterning AP generation, controlling network excitability and giving rise to the variety of oscillations seen in the hippocampus. Inhibition therefore plays a central role in ordering excitatory activity in all hippocampal subfields and is defined as: feedforward, feedback or disinhibitive types of inhibition, described below.

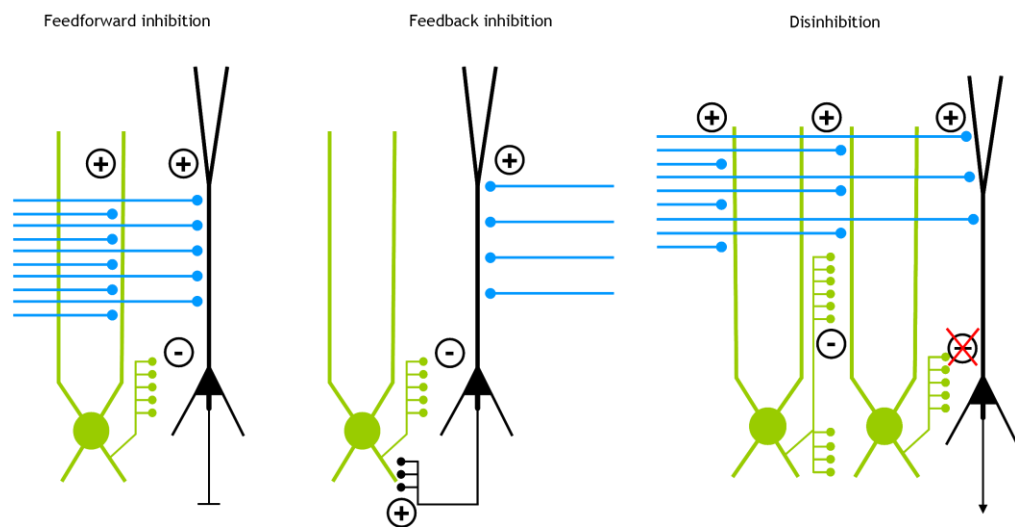


Figure 1.2 Summary of different types of inhibition within small local networks. Excitatory afferents (blue), INs (green) and principal cells (black) are depicted resulting in either excitatory (+) or inhibitory (-) activity.

Feed-forward inhibition arises when excitatory afferents synapse onto excitatory and inhibitory cells simultaneously (figure 1.2, left). Excitation of INs will release GABA onto excited principal cells, to both synaptic and extrasynaptic domains; thereby limiting the amplitude and duration of this excitation in the local region (Alger and Nicoll, 1982; Price et al, 2008; Elfant et al, 2008).

Feedback inhibition requires the excitation of local principal cells, which in turn recruit local INs (figure 1.2, middle) through secondary excitation, which then release GABA onto the same population of local CA1 pyramidal cells which just excited them, preventing recurrent excitation activation within local networks (Bartos et al, 2007).

Disinhibition is broadly similar to feedback inhibition; however 2 IN groups require excitation as well as principal cells (figure 1.2, right). The first IN reduces principal cell excitation in either a feedforward or feedback mechanism, while the second IN group inhibits the first IN, resulting in a decrease in excitation arriving onto the first group of INs; reducing inhibition onto the principal cell, allowing principal cell transmission (Cunha-Reis et al 2004). The overall extent of disinhibition between INs remains unclear, however inhibitory connections between INs have been widely shown (Gulyás et al, 1999; Katona et al, 1999; Bartos et al, 2002; Mátyás et al, 2004; Ali, 2007).

Additional to these direct postsynaptic forms of inhibition, there is a strong component of GABAergic presynaptic inhibition, mediated by GABA_BRs; regulating transmitter release from presynaptic terminals. This presynaptic inhibition can be homosynaptic, with effects observed at direct synaptic connections (i.e paired pulse depression; Davies et al, 1990); heterosynaptic, with effects being observed between different presynaptic terminals (i.e. during activity of the local GABAergic network; Vogt and Nicoll, 1999); or autoreceptors, whereby GABA release from an axon terminal acts upon itself to inhibit further release (Davies et al, 1993).

1.4.2 Functional role of hippocampal INs in hippocampal circuits

The function of most hippocampal INs is to provide GABAergic input onto principal cells and other INs, reducing excitation and resulting synaptic output. The most obvious manifestation of a lack of inhibition is epileptogenesis in hippocampal networks linked to reduction of either GABA_A or GABA_B receptor-mediated inhibition (Ribak et al, 1979; Mangan et al, 1996; Fritschy et al, 1999). Besides counterbalancing excitation, inhibition has roles at the subcellular, cellular and network level; leading to synaptic plasticity, precise timing of hippocampal output and the generation of neuronal oscillations within networks of neurons.

At the subcellular level, inhibition serves to modulate the excitability of local membranes. This is achieved through either hyperpolarisation or shunting of the local membrane to directly inhibit propagation of excitation from synaptic zones.

Temporal summation of excitatory and inhibitory synaptic responses derived from spatially close synaptic zones leads to either the excitation reaching AP threshold or not, dependent on inhibition strength. Strong, repetitive GABA release onto a particular subcellular compartment leads to non-linear increases in inhibition of excitatory transmission (Tamás et al, 2002). Indeed, GABA is positioned to prevent electrical transmission in both directions along dendrites, both ortho- and antidromically, preventing integration of synaptic responses and depolarisation of synaptic terminals; thus reduced voltage-sensitive channel opening in perisynaptic domains (Kanemoto et al, 2011).

In respect to glutamatergic transmission, inhibition results in reduced total depolarisation and hence less temporal summation and reduced NMDA receptor activation, leading to reduced synaptic excitation and Hebbian-LTP through reduced calcium-release (Morrisett et al, 1991). Recently it has been shown that GABA_B directly interacts with NMDA receptors (Chalifoux and Carter, 2010) to additionally reduce postsynaptic transmission; leading to reduced synaptic transmission and plasticity in compartments strongly modulated by GABA_BR activation.

In presynaptic compartments GABAergic inhibition, mediated by the GABA_BR, has been shown to inhibit the release of glutamate and GABA (Bowery et al, 1980; Doze et al, 1995), effectively silencing chemical synapses which receive this GABAergic input. There is evidence that GABA_A receptors are also located in presynaptic terminals, controlling the release of transmitter from neurons (Vautrin, et al 1994). Due to the autoreceptive and heterosynaptic nature of presynaptic inhibition, the action of GABA is not strictly confined to individual synapses, giving rise to inhibition of multiple synapses simultaneously.

The principle role of INs at the cellular level is to provide strong temporal control of AP generation in neurons. Dependent on timing, strength and duration of synaptic inhibition, APs will be inhibited completely and synchronised in respect to the phase of IN firing (Andersen et al, 1963; Cobb et al, 1995; Klausberger et al, 2003; Hajos et al, 2004). Additional to this it has been shown in principal cell and INs that blockade of GABA_A, leads to increase spontaneous AP firing (Suzuki and Smith, 1988) as well as an increase AP discharge frequency in response to depolarising stimuli (Misgeld and Frotscher, 1986).

At the network level, synchronised depolarisation and AP spiking gives rise to the development of electrical up and down states within populations of neurons, developing into oscillatory activity. *In vitro* hippocampal network activity is underpinned by three main subtypes of cortical oscillation, defined by phase-frequency: sharp wave ripples (SWR, 100-300 Hz), gamma (γ , 30-100Hz) and theta oscillations (θ , 2-10Hz) (Stumpf, 1965; Buzáki et al, 1983). Gamma oscillations are driven primarily by Schaffer-collateral/commissural input to CA1 pyramidal cells, acting to provide feedback excitation onto INs (Csicsvari et al, 1999; Hájos et al, 2004) with PV-IR basket cells believed to synchronise the rhythm (Bartos et al, 2002). Theta-oscillations on the other hand, are believed to be produced by SSt-IR OLM cells and CCK-IR INs, due to their slower spiking phenotype and greater neuromodulation (Maccaferri and McBain, 1996; Klausberger et al, 2005; Cea-del Rio et al, 2010). This IN-dependent oscillatory output of hippocampal circuits is intimately linked to plasticity events at excitatory synapses, particularly in spike-time dependent plasticity profiles, due to the harmonising of differential inputs to neurons by oscillatory activity (Hefft et al, 2002; Baroni and Varona, 2010).

The function of hippocampal INs is therefore intrinsically linked to the location of IN axonal arbours with respect to post-synaptic domains of principal cells and INs. This inhibition is dependent on the activation state of the presynaptic IN, leading to modified plasticity and coupling between different cell types.

1.4.3 Neurochemical subtypes of IN

An important criterion for classifying INs is the analysis of neurochemical markers, specific to discrete populations of INs (see figure 1.3). All INs are positive for the glutamate decarboxylase 65 or 67 protein (GAD 65/67), converting glutamate to GABA; as well as axon-terminals containing vesicular GABA transporters (vGAT1-3) and in some cells (CCK/VIP-IR basket cells) vesicular glutamate transporter 3 (vGluT3; Somogyi et al, 2004). There are ever increasing lists of proteins identifying populations of INs, however the most widely accepted markers fall into two categories: calcium-binding proteins and neuropeptides.

Calcium-binding proteins identifying INs in the CA1 comprise: PV, CB and calretinin (CR) and classify two main subclasses of IN: PV or CB immunoreactive (IR), which mainly target CA1 pyramidal cells; or CR-IR which target dendrites of other INs (Gulyás et al, 1996; Freund and Buzsáki, 1996). The other main neurochemical markers are neuropeptides, containing: CCK, SSt, vasoactive intestinal peptide (VIP) and neuropeptide Y (NPY); which mark INs which mainly targeting pyramidal cells (see figure 1.3 for summary). Aside from neuropeptides and calcium-binding proteins, certain receptors delineate some INs. Of particular interest to this study is the presence of endocannabinoid 1 (CB1) and muscarinic acetyl choline 2 (M2) receptors localised to the axon-terminals of CCK-IR (Katona et al, 1999; Ali et al, 2007) and a subset of PV-IR INs (Hajos et al, 1997; Katona et al, 1999; Tsou et al, 1999), respectively.

Although these different neurochemical markers delineate different populations of INs; morphological classification within and across these neurochemical subtypes is still required for a thorough classification of the wide variety of INs present in the hippocampus.

1.4.4 Morphological subtypes of INs

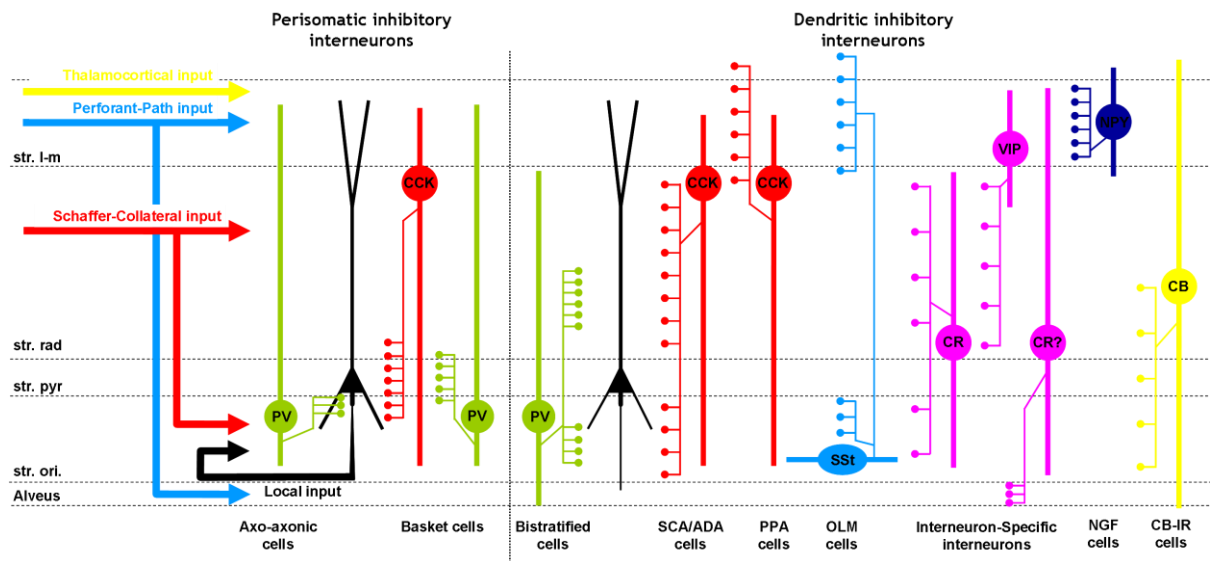


Figure 1.3 Schematic of neurochemical and laminar distributions of INs PV (green), CCK (red), SSt (cyan), CR/VIP (pink), NPY (dark blue) and CB (yellow) IR IN subtypes are portrayed, with respect to CA1 pyramidal cells (black) and afferent input (labelled). Dendritic axes are shown as thick filled lines, whereas axons are shown as thin lines and terminal zones represented as balls. Hippocampal laminations are shown (dashed lines) and labelled. Adapted from: Klausberger and Somogyi (2008).

Morphological identification of hippocampal INs relies heavily on the lamination of the axonal arborisation, conferring postsynaptic targets (see figure 1.3 and Freund and Buzsáki, 1996; Klausberger and Somogyi, 2008). We will describe detailed morphological features of relevant INs in chapters 4 to 6, here we will try to summarise important properties shared between morphologically similar groups of INs. Most INs of the hippocampus share two common characteristics: a) no (or sparse) dendritic spines, receiving synaptic inhibition and excitation on dendritic shafts, b) they release GABA from presynaptic terminals. In figure 1.3 we have shown schematic dendritic and axonal localisations of a selection of neurochemical IN subtypes. Various IN subtypes preferentially targeting principal cells can be divided into those with axon targeting either the perisomatic region or dendrites of neurons, whereas those which exclusively target other interneurons contain CR, VIP or NPY (Gulyás et al, 1996).

Perisomatic inhibitory (PI) INs of the CA1

There are two morphological subtypes of PI INs in CA1: ones targeting both the soma and proximal dendrites of neurons (basket cells) and ones which target pyramidal cell axons (axo-axonic or chandelier cells).

Basket cells have axons which target the somata and proximal dendrites of neurons in and around *str. pyramidale*, inhibiting temporal summation of excitatory input arriving from dendrites; suppressing and timing AP output from the axon-initial segment (AIS). There are two distinct subtypes of basket cell, either containing the calcium binding protein PV (Kawaguchi et al 1987) or the neuropeptide CCK (Pawelzik et al, 2002). Basket cells make up approximately 60% of all PV-IR cells (Baude et al, 2007), whereas CCK-IR basket cells made up ~50% of their respective neurochemical phenotype (Pawelzik et al, 2002). As described later, both CCK and PV-IR basket cells have assumed physiological roles in controlling CA1 pyramidal cell output, leading to modulation of network activity.

Axo-axonic cells form synapses almost exclusively with the AIS of CA1 pyramidal cells; forming candle-like barrels of boutons along individual axons extending into *str. oriens*. Axo-axonic cells make up approximately 15% of all PV-IR cells (Baude et al, 2007) and are to strongly inhibit AP initiation in the AIS, thus controlling hippocampal output to the EC. In contrast it has been suggested that the absence of the K^+/Cl^- co-transporter 2 (KCC2) in the AIS of adult CA1 pyramidal cells results in a local reversal of the Cl^- gradient leading to $GABA_{A}$ -mediated conductances in this subcellular compartment being depolarising, rather than hyperpolarising or shunting; with axo-axonic cells acting to depolarise the AIS, leading to initiation of APs upon $GABA_{A}$ activation (Szabadics et al, 2006).

Dendritic inhibitory (DI) INs of the CA1

Other INs found within the CA1 region of the hippocampus are presumed to be DI subtype and are grouped on the basis of neurochemical content. DI cells serve to provide inhibition to the dendrites of neurons, controlling excitatory responses reaching the soma, thus reducing excitability. For simplicity we will only discuss DI INs containing PV, CCK or SSt, for a thorough review of the remaining subtypes not mentioned here, notably neurogliaform cells, interneuron-specific interneurons and many others; see: Freund and Buzsáki (1996), McBain and Fisahn (2001), Klausberger and Somogyi (2008) and Cutsuridis et al (2010).

PV immunoreactive DI cells make up approximately 25% of all PV-IR cells in CA1 (Baude et al, 2007), with axon localised in *str. radiatum* and *oriens* synapsing with the dendrites of CA1 pyramidal cells and INs, giving them the classification of bistratified cells. As well as containing PV, some bistratified cells also contain the neuropeptide SSt, at low levels (Baude et al, 2007).

DI INs which contain the neuropeptide CCK form a largely heterogeneous population of neurons, providing inhibition to all laminations of the hippocampus. There are three defined CCK-IR DI subtypes, Schaffer-collateral associated (SCA), perforant-path associated (PPA) and apical dendrite associated (ADA) (Vida et al, 1998). There is difficulty in differentiating between both SCA and ADA subtypes, due to a large degree of overlap in axonal distributions in *str. radiatum*, however SCA type also possess axon in *str. oriens*. SCA INs are believed to selectively inhibit excitatory stimulus arising from Schaffer-collateral input onto CA1 pyramidal cells, while ADA type INs inhibit non-specific excitation in CA1 pyramidal cell apical dendrites. PPA INs have an axon which is almost exclusively confined to *str. L-M* of CA1, believed to inhibit excitatory stimuli arriving from the EC, along perforant path afferents.

The last population of INs we discuss here are classified as *str. oriens/L-M* (OLM) type INs, containing the neuropeptide SSt (McBain et al, 1994; Sik et al, 1995), with ~10% of SSt-IR OLM cells also containing PV (Jinno and Kosaka, 2000). OLM cells have a dendritic tree confined entirely to *str. oriens*, receiving strong, excitatory input from local CA1 pyramidal cell axons (Blasco-Ibáñez and Freund, 1995). The axons of OLM cells form a small local arbour in *str. oriens* and also a dense arbour in *str. L-M*, inhibiting excitatory transmission predominantly in CA1 pyramidal cell distal dendrites and somewhat in basal dendrites (Katona et al, 1999).

Another main morphological subtype of IN, which we have not examined in this thesis is the neurogliaform cell. These INs have small somata found generally in *str. L-M*, with very dense, radially orientated axon and dendrites (Vida et al, 1998). Of interest to this report is proximity to the highest density of GABA_BRs on CA1 pyramidal cells (Kulik et al, 2003) and the ability of these cells to evoke unitary GABA_BR mediated responses in paired-recordings with CA1 pyramidal cells (Price et al, 2005). Therefore this IN subtype may constitute a significant source of GABA_BR-mediated signalling in the CA1.

1.4.5 Physiological properties of selected INs

As physiological properties of hippocampal INs in CA1 correlate well with neurochemical identity we shall discuss the physiological properties of those cells described above; details of physiological properties are given in chapters 4-6. Physiological properties are crucial to understanding the role of relevant INs in subcellular and cellular inhibition profiles as well as in network activity. Loosely speaking, INs can be defined as either fast-spiking or regular spiking (Feder and Ranck, 1973; Buszáki and Eidelberg, 1982)

Physiological properties of PV-IR INs

Most PV-IR INs of area CA1 have broadly similar intrinsic membrane properties. It is assumed that these cells have a more leaky membrane and depolarised membrane potential, with associated lower membrane resistance and faster membrane time-constant; due to the presence of a large non-inducible I_h , not observed in response to electrical stimuli (Aponte et al, 2006). The intrinsic properties of PV-IR dendrites lead to fast integration of synaptic responses, with reduced response amplitudes, resulting in rapid conduction along neurites (Nörenberg et al, 2010) and faster recovery from electrical events. In conjunction, the presence of potassium channel K_v3 (Shaw family; 1b and 2 subtypes) in PV-IR somatic and axonal compartments (Weiser et al, 1995; Chow et al, 1999) confers an increased activation and deactivation of potassium conductances associated with the down-stroke of APs (Martina et al 1998). The presence of voltage-gated sodium channels (NaV1.1) in PV-IR INs (Ogiwara et al, 2007) in combination with $K_v3.1b$, gives rise to the characteristic fast-spiking (>50-100Hz) AP discharge pattern of these neurons. Along with conferring a fast-spiking phenotype, the deactivation properties of $K_v3.1b/2$ and absence of I_A (K_v4 ; Martina et al, 2008) are believed to underlie the absence of inter-spike AP accommodation.

PV-IR INs receive a very strong glutamatergic drive from CA3 Schaffer collateral/commissural, perforant path and septal inputs (Gulyás et al, 1999), which in conjunction with their fast-spiking phenotype is thought to result in rapid, high-fidelity release of GABA from PV-IR axon-terminals targeting either the perisomatic or dendritic domains of CA1 pyramidal cells. This rapid response is due to rapid AP discharge and efficient buffering of Ca^{2+} transients by PV, tightly controlling GABA release (Aponte et al, 2008). This GABA binds to $GABA_A$ receptors containing $\alpha 1$, 2 and $\beta 3$ subunits in the postsynaptic domain; the role of which remains contentious (Prenosil et al, 2006; Kasugai et al, 2010). PV-IR DI cells give rise to high-fidelity, rapid responses, with GABA binding to $GABA_A$ $\alpha 5$ containing receptors (Ali and Thomson, 2008).

Physiological properties of CCK-IR INs

CCK-IR INs have been shown to possess broadly similar intrinsic physiological properties across morphological subtypes, with more “pyramidal cell-like” physiologies. They are known to have hyperpolarised membranes ($\sim -65\text{mV}$) and a larger input resistance and membrane time constant than CA1 pyramidal cells of PV-IR INs (Vida et al, 1998); with much lower passive currents across membranes than PV-IR INs, due in part to I_h and I_M comparable to that seen in CA1 pyramidal cells. CCK-IR generally cells show some degree of AP train accommodation, again similar to CA1 pyramidal cells; having been classified as regular-spiking INs to reflect these properties (Lacaille and Schwartzkroin, 1988; Cauli et al, 1997; Vida et al, 1998; Pawelzik et al, 2002; Cea-del Rio et al, 2010 and 2011).

AP and AHP potentials in CCK-IR INs are generally faster than CA1 pyramidal cells, but slower than PV-IR basket cells; due perhaps to the presence of K_v4 channels (I_A) and I_M to a similar level as in CA1 pyramidal cells. Therefore CCK cells are believed to be much slower signalling neurons, receiving reduced excitatory input than PV-IR neurons (Gulyás et al, 1999), responding more slowly (Cauli et al, 1997) with diverse neuromodulatory input (Férezou et al, 2002; Mátyás et al, 2004; Cea-del Rio et al, 2010).

Physiological properties of SSt-IR OLM cells

The presence of PV alongside SSt in OLM cells confers many properties similar to that of PV-IR cells. For example OLM cells are quite often fast-spiking with large, fast AHPs due to the presence of $Kv3.1b/2$, conferring a low accommodation phenotype (Chow et al, 1999). Unlike PV-IR neurons, most OLM cells show a very large I_h mediated “sag” component upon hyperpolarisation (Maccaferri and McBain, 1996) with similar resting membrane potentials to PV-IR neurons, those of which don't exhibit this current show very hyperpolarised membranes (Lupica et al, 2001).

1.5 Molecular mechanisms of inhibition

Inhibition as we have mentioned previously, acts to counterbalance excitation at the subcellular, cellular and network level. The ultimate outcome of this is seen as a reduction in transmitter release from the target cell, achieved either by a reduction in discharge or through direct inhibition of transmitter release from axon terminals.

All synaptically evoked conductances are mediated by ligand-gated ion-channels (LGIC) or through 7-transmembrane receptors (7TM) associated with second messenger cascades. Temporal dynamics of these two receptor subtypes are profoundly different; LGICs act on the order of 5 to ~200 milliseconds (Treyneis et al, 2010) and 7-TM effects are greater than 100-200 milliseconds. GABA binds to a family of LGICs referred to as GABA_A receptors (GABA_AR) and to a 7-TM receptor, GABA_B receptor (GABA_BR); which mediate fast and slow inhibition respectively. GABA receptors are associated with ionic flux of Cl⁻ (GABA_AR) or and increased K⁺ efflux or decreased presynaptic Ca²⁺ influx (GABA_BR, both). Glutamate acts through NMDA, AMPA and kainate LGICs or through metabotropic glutamate receptors (mGluR), a class of 7TM; which we will not discuss (for review see Treyneis et al, 2010). At hippocampal IN synapses NMDA, AMPA and kainate receptors are found in synaptic clusters on dendritic shafts (Baude et al, 1995), with GluR2-containing calcium-permeable AMPA receptors mediating rapid excitation (Koh et al, 1995; Geiger et al, 1995) inducing non-Hebbian plasticity in PV-IR PI and DI cells (Tóth and McBain, 1998; Nissen et al, 2010; Sambandan et al, 2010).

1.5.1 Ionic and molecular basis of synaptic inhibition

Ionic conductances can be either depolarising, hyperpolarising or shunting; determined by the relationship of the reversal potential (E_R ; derived from the Nernst equation) of the relevant ion compared to the membrane potential (V_M).

In adult neurons GABA_A is either hyperpolarising or shunting and post-synaptic GABA_B is predominantly hyperpolarising.

The E_R for chloride (the primary ionic substrate for GABA_AR) is electrically proximal to V_M (-60-70mV vs. -65 mV), therefore at V_M greater than -60-70 mV, Cl⁻ influx hyperpolarises membranes, shifting V_M further from AP threshold. The proximity of $E_{R(Cl^-)}$ can result in no net current flux; known as shunting inhibition. Although there is no Cl⁻ flux, the open channel reduces local membrane resistance, shunting excitatory currents; reducing subsequent EPSP amplitudes, especially slow NMDA receptor mediated currents (Staley and Mody, 1992).

Postsynaptic GABA_BR responses are mediated by K⁺ and always hyperpolarise V_M , as $E_{R(K^+)} \sim -100$ mV, meaning that K⁺ always efflux hyperpolarises V_M toward -100 mV. The slower nature of GABA_BR responses implies that hyperpolarisation is seen as a prolonged shift of V_M from threshold (Bean and Sodickson, 1996). This hyperpolarisation has two key effects, a) to reduce V_M away from AP threshold, making it less likely that an AP is produced (Connors et al, 1988) and b) to increase the driving force of depolarising currents (i.e. those with a net E_R greater than V_M), decrease driving force of other K⁺ conductances and to reverse GABA_A Cl⁻ conductance (Newberry and Nicoll, 1985).

The role of GABA_B in presynaptic transmission has an additive effect to post-synaptic hyperpolarisation, the reduction in transmitter release mediated by GABA_BR inhibition of Ca²⁺ release through either N or P/Q type voltage-gated Ca⁺ channels (VGCC; Doze et al, 1995), leading to reduced synaptic amplitudes (Pitler and Alger, 1993; Davies and Collingridge, 1993), independent of post-synaptic effects.

1.5.2. GABA_A receptors

GABA_A receptors are of the nicotinic acetyl choline receptor-class of LGICs, consisting of a heteropentamer of receptor subunits (α 1-6, β 1-3, γ 1-3 δ , ϵ , π , θ and ρ), creating the pore and the ligand-binding domains. The GABA binding domain is found between α and β subunits and the allosteric modulator benzodiazepine site found at the border between α and γ subunits (Pritchett et al, 1989), while the picrotoxin site is located on the β 1 subunit within the Cl⁻ pore itself (Sigel et al, 1989). GABA_A receptors containing the ρ subunit have been traditionally referred to as GABA_C type, with distinct physiological and pharmacological properties (Shimada et al, 1992; Liu et al, 2004). However, the ρ subunit shows low expression in the hippocampus, suggesting a predominance of typical GABA_A receptors (Rozzo et al, 2002).

GABA_A receptors are selective monovalent anionic channels, allowing influx of Cl⁻ or bicarbonate (CO₃⁻), resulting in an inward negative or no current. In development, due to a neonatal switch of KCC2 pump direction, GABA_A receptor chloride conductances are outward and depolarising (Ben-Ari et al, 1989). The GABA_A receptor has variable activation time, dependent on subunit-composition of the channel, typically inhibitory post-synaptic potentials (IPSP) elicited by GABA_A are on the order of 5-20 ms (Gingrich et al, 1995), all receptors not containing ρ -subunits, are blocked by the antagonist bicuculline (Curtis et al, 1970).

Synaptic clusters of GABA_A receptors are found on dendrites, somata and the AIS of neurons. Interestingly, there seems to be a difference between GABA_A receptor subunit-composition found on somata and axons of CA1 pyramidal cells, compared to that of dendrites (Nusser et al, 1996; Klausberger et al, 2002; Prenosil et al, 2006; Kasugai et al, 2010). As well, there is increasing evidence that GABA_A receptors are found on extrasynaptic membranes, involved in tonic inhibition of neurons and heterosynaptic inhibition (Kasugai et al, 2010)

1.5.3 GABA_B receptor

Metabotropic 7-TM receptors are one of the main neuromodulatory components and are present extrasynaptically in both pre and postsynaptic faces. One of the main inhibitory metabotropic receptors is activated by GABA, known as the GABA_B receptor (GABA_BR; Bowery et al, 1980) which is active for hundreds of milliseconds (Solis and Nicoll, 1992; Otis et al, 1993).

The GABA_BR is formed by the heterodimerisation of two GABA_BR subunits, known as B1, with 2 main splice variants (a/b) and B2, each a 7-TM protein (Kaupmann et al, 1998); at the C-terminus leucine-zipper motif. It was shown (Pagano et al, 2001) that for GABA_BRs to become functional at neuronal membranes, the B1 and B2 subunits must form a heterodimer (Kaupmann et al, 1998). The B2 subunit is required for translocation from the endoplasmic reticulum and correct membrane insertion, whereas the 2 main splice variants of B1 conferring either pre or post-synaptic localisation (B1a - pre, B1b - post; Vigot et al, 2006). In functional receptors, B1 subunits provide ligand binding, whereas B2 facilitates G-protein activation (Pagano et al, 2001).

The majority of GABA_B receptors are located on extrasynaptic membranes, with the suggestion that there is a gradient of GABA_BRs decreasing with distance from glutamatergic synapses (Kulik et al, 2003). GABA_BRs rely on volume-transmission (synaptic spill-over) of synaptic GABA for activation (Isaacson et al, 1993; Olah et al, 2009); indeed heterosynaptic depression, where a small population of GABA releasing terminals provide a cloud of GABA for local GABA_BR (Vogt and Nicoll, 1999) is believed to be the main action of GABA_BR, inhibiting several cellular compartments simultaneously.

GABA_BRs interact directly with the G-protein pathway, G_{i/o}, resulting in cleavage of G_α and G_{βγ} subunits. In neurons the most rapid effects of G_{i/o} 7-TM activity are through G_{βγ} activation of G-protein coupled, inward-rectifying potassium (Kir3)

channels (Lüscher et al, 1997; Kaupmann et al, 1998) or through inhibition of N and P/Q type voltage-gated calcium-channels (VGCCs) (Doze et al, 1995; Wu and Saggau, 1997); G_{α} interacting with phospholipase C to modulate other 7-TMs and intracellular proteins (Sohn et al, 2007).

Kir3-type channels are the primary post-synaptic effectors of the $GABA_B$ R in neurons (Otis et al, 1993; Lüscher et al, 1997), comprising a tetramer of Kir3.1-4 subunits. Kir3 channels are K^+ selective, with inward-rectifying voltage-dependence (Sadja et al, 2003). This rectification however has not been observed in synaptic responses mediated by $GABA_B$ Rs (Otis et al, 1993). $GABA_B$ R and Kir3 channels oligomerise to form receptor/effector complexes (Ciruela et al, 2010), with $GABA_B$ also interacting with Kir2 channels, providing an alternative mechanism of $GABA_B$ activity, again mediated by K^+ efflux (Rossi et al, 2006). $G_{\beta\gamma}$ inhibition of N and P/Q types VGCCs occurs predominantly in presynaptic terminals, reducing exocytosis and thus the release probability of neurotransmitter filled vesicles into the synaptic cleft. $GABA_B$ R inhibits channel opening by facilitating allosteric changes in the pore structure (Forsythe et al, 1998). The resultant reduction in Ca^{2+} influx leads to reduced transmitter release from the presynapse.

Alternatively it has been shown that $GABA_B$ Rs interact directly with the release machinery in presynaptic zones, bypassing the need for Ca^{2+} -channel inhibition, directly inhibiting vesicle release (Scanziani et al, 1992), mostly in principal cells through G_{α} subunit interactions (Sakaba and Neher, 2003). Price et al (2008) showed that $GABA_B$ R mediated inhibition of GABA release from neurogliaform cells was also independent of Ca^{2+} channels, indicating that these INs have similar presynaptic release properties to pyramidal cells. However, it has been shown that other IN subtypes rely on presynaptic Ca^{2+} influx (Harrison et al, 1990), suggesting that different IN subtypes potentially possess divergent $GABA_B$ R transduction mechanisms, one dependent on the G_{α} subunit, the other dependent on $G_{\beta\gamma}$ induced opening of K^+ channels.

1.5.4 GABA_BR in INs

The extent of GABA_BR mediated signalling in hippocampal INs is, at the time of writing, relatively unexplored. Indeed several studies showed in parallel that hippocampal INs do express GABA_BR subunits; firstly Fritschy et al (1999) showed that non-principal cells of the DG express GABA_{B1} subunits at the soma, while simultaneously exhibiting low expression of GABA_A (β2/3) containing receptors, comparative to INs weakly labelled for GABA_{B1}; suggesting preferential fast or slow GABAergic inhibition in some INs. Sloviter et al (1999) characterised the somatic GABA_{B1} labelling of neurochemically defined INs in the hippocampus proper. In regard to the neurochemical subtypes we have discussed earlier, they state that CCK and SSt containing INs both express GABA_{B1} in ~100% of cell immunoreactive for either marker; however PV-IR INs were suggested to contain very low levels of GABA_{B1} at the soma. Kulik et al (2003) backed this up, showing that approximately 50% of neurons expressing GAD67 were immunopositive for GABA_{B1} subunits.

It has been shown (Kulik et al, 2003) that principal and IN somata generally show low-level staining for GABA_{B2} subunits, while accumulating GABA_{B1} in the endoplasmic reticulum, suggestive of a discrepancy in transcription of the two subunits. It is therefore possible that GABA_BRs are present in other IN populations, besides those described with high somatic localisation; in which there is a reduced transcriptional discrepancy between the GABA_{B1} and GABA_{B2} subunits and strong functional GABA_BR activity.

There is some evidence for GABA_BR involvement in post-synaptic inhibition of unidentified fast-spiking basket cells in the dentate gyrus (Mott et al 1999), as a high proportion of these cells contain PV; this observation contradicts the previous observations in CA1, regarding PV and GABA_BR colocalisation. Additional to basket cells, Khazipov et al (1995) show that unidentified INs at the *str. radiatum/L-M* border show a strong post-synaptic current and Lacaille (1991) showed the presence of GABA_BR in unidentified INs in *str. pyramidale* of CA1.

Price et al (2005 and 2008) went further and showed that neurogliaform type INs in *str. L-M* of the CA1 exhibited unitary GABA_BR mediated responses, between pairs of neurogliaform cells; as well GABA_BRs were shown to inhibit post-synaptic effects of GABA release arising from the same neurogliaform cells. It remains unclear to what extent the remaining subtypes of hippocampal IN display GABA_BR-mediated postsynaptic currents.

Presynaptic GABA_BR mediated inhibition of GABA release from identified and unidentified INs has been much better studied (Davies and Collingridge, 1993; Buhl et al, 1995; Lüscher et al, 1997; Ouardouz and Lacaille, 1997; Lei and McBain, 2002; Price et al, 2005; Lee and Soltesz, 2011). The majority of studies haven't identified the IN subtype possessing this inhibition; hence no conclusive classification of GABA_BR influence across all IN subtypes can be made. Indeed Poncer et al 2000 showed that GABA release from several populations of CA3 INs, in PI and DI cells of *str. oriens* and *radiatum* was under the control of GABA_BRs (Hefft et al, 2002; Lee and Soltesz, 2010).

The detection of the GABA_BR in defined populations of INs could lead to a better understanding of the function of slow-inhibition in INs and how this slow inhibition leads to subsequent disinhibition of principal cells, contributing to network function.

1.6 Thesis aims

Localisation and functionality of the GABA_BR, despite being well studied in principal cells at the morphological and molecular level, has not been studied in hippocampal INs types, due in part perhaps, to the inherent difficulty in accurately identifying morphological and neurochemical subtypes of hippocampal INs from physiological recordings.

The aim of the experiments outlined in this thesis is to determine to what extent GABA_B is present on the membranes of hippocampal INs, identified on the basis of neurochemical and morphological characteristics. We set out to determine both the relative density of receptors in both the pre- and postsynaptic compartments and how these values related to functional GABA_BR activity within these compartments, compared to CA1 pyramidal cells.

We performed light and electron microscopic localisation of GABA_BR subunits to the postsynaptic plasma membrane of PV, CCK, CB and SSt INs and the presynaptic membrane of PV and CCK INs, comparing receptor density to local pyramidal cell dendrites. Functional postsynaptic GABA_BR-mediated conductances were determined in PV, CCK and SSt IN subtypes in whole-cell patch-clamp conditions and IPSCs elicited in CA1 pyramidal cells from pharmacologically isolated PV and CCK axons, as well as synaptically-coupled pairs, were tested for pre-synaptic GABA_BR activity.

Developing an understanding of how GABA_BRs influence synaptic transmission in these INs could help resolve questions remaining in regard to the role of INs in hippocampal circuitry and to the network output of the hippocampus as a whole.

Chapter 2: Materials and methods

2.1 Animals and procedures

All procedure performed herein were in full accordance with University of Glasgow and Home Office guidelines under Schedule 1 of the Scientific Procedures Act (Animals) 1986. Wistar rat perfusions performed at the Institute of Anatomy, Albert-Ludwig University, Freiburg; were performed in accordance with EU and institutional guidelines (Licence number: X-11/07S).

Electrophysiological experiments were performed using acute slices produced from juvenile (17-28 day) male or female wistar rats; bred at Central Research Facility, Glasgow University. Anatomical material was prepared from perfusion fixed material of male and female wistar rats aged 30-60 days (100-300 g).

2.2 In vitro electrophysiology

2.2.1: Acute brain slice preparation

Acute brain slices were produced as described previously (Vida et al 1998, Bartos et al 2002). Briefly, we cervically dislocated then decapitated the rat, quickly removing the intact brain (typically <45 seconds) into ice-cold (0°C) artificial cerebrospinal fluid (ACSF) which was bubbled with carbogen (95% O₂/5%CO₂). The whole brain was allowed to chill for 2-3 minutes prior to dissection of the hemispheres. The brain was then sectioned into blocks containing the transverse hippocampus, by removing the cerebellum and approximately 1/3 of the brain (from bregma; figure 2.1.A). The hemispheres were then separated along the midline and the dorsal surface of this block removed according to Bischofberger et al (2006) (Figure 2.1.B/C) and glued (cyanoacrylate, Loctite) to the stage of a

vibratome (Leica VT1200S; figure 2.1.C, right), which was then filled with more ice-cold sucrose ACSF and bubbled throughout slicing with carbogen.

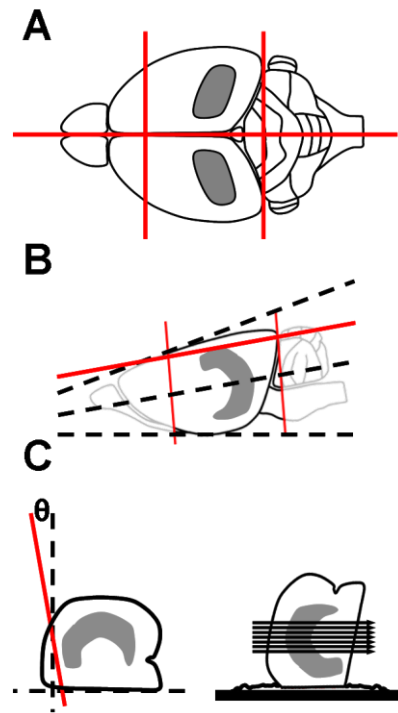


Figure 2.1: Schematic of whole brain dissection, blocking and slicing. **A** Top-down schematic of a rat brain, showing cuts made (red lines) forming a block containing the intact hippocampus (grey). **B** the dorsal surface of the brain is removed (red line), with respect to the dorsal and ventral planes (dashed black lines). **C, left** A front view of the brain block, showing the dorsal cut at $\sim 10^\circ$ to vertical (θ). **C, right** Direction of slicing; relative to the intact hippocampus.

300 μm , transverse hippocampal slices were cut on the vibratome and transferred to a storage chamber containing carbogenated sucrose-ACSF at 35°C . Slices were stored at this temperature for 30 minutes and then slices were cooled to room temperature and stored until recording.

2.2.2: Composition of slicing and recording ACSF

The composition of ACSF we used for handling and slicing the brain was chosen to reduce excitotoxicity and preserve the ultrastructure of neuronal connections adequately. We used a sucrose-based cutting solution, with the composition (in

mM): 87 NaCl, 2.5 KCl, 25 NaHCO₃, 1.25 NaH₂PO₄, 25 glucose, 75 sucrose, 7 MgCl₂, 0.5 CaCl₂, 1 Na-Pyruvate, 1 Ascorbic Acid.

Recording ACSF was similar to that used previously by our group (Vida et al, 1998; Bartos et al, 2009) and was consistent in composition throughout all experiments performed; comprising (in mM): 125 NaCl, 2.5 KCl, 25 NaHCO₃, 1.25 NaH₂PO₄, 25 glucose, 1 MgCl₂, 2 CaCl₂, 1 Na-Pyruvate, 1 Ascorbic Acid.

2.2.3: Whole-cell patch clamp recording of selected cells from acute slices

Once incubated, slices were transferred individually to the recording chamber and perfused with carbogenated recording ACSF. The temperature of the ACSF was 31-35 °C, with a flow rate of 8-10 ml.min⁻¹. Slices were held in place with a platinum ring, strung with several parallel single-strand nylon fibres at intervals of ~1 mm. Slices were visualised with infrared differential interference contrast (IR-DIC) video microscopy on an upright microscope (microscope: Olympus BX50WI; CCD camera: Hamamatsu Orca 285), with Kohler illumination to improve contrast. Cells were selected on the basis of somatic location and dendritic orientation, described in chapters 3-7.

Recording electrodes were pulled from borosilicate glass (\emptyset = 2 mm outer, 1 mm inner (Hilgenberg, Germany)) on a horizontal electrode puller (P-97, Sutter Instrument Co.) and had a tip diameter of ~1 μ m, in some experiment electrodes were fire-polished (Narashige, Japan) to produce a smoother electrode tip. Electrodes were filled with K-Gluconate based intracellular solution for postsynaptic GABA_BR recordings, composition (in mM): 130 K-Gluconate, 10 KCl, 2 MgCl₂, 10 EGTA, 10 HEPES, 2 Na₂-ATP, 0.3 Na₂-GTP, 1 Na₂-Creatinine, 0.1% biotinylated-lysine (*In vitro*gen). In recordings examining monosynaptic IPSCs we utilised a modified intracellular solution (Bartos et al, 2002), which comprised (in mM): 110 K-gluconate, 40 KCl, 10 EGTA, 2 MgCl₂, 10 HEPES, 2 Na₂ATP, 0.3 Na₂ATP, Na₂-creatinine and 0.10% biocytin; which increased the E_R of Cl⁻ to 0

mV. Both intracellular solutions used resulted in a final resistance across the electrode tip of 2-4 M Ω .

Whole-cell patch clamp was achieved through the use of either 1 or 2 AxoPatch 200b amplifiers (Molecular Devices, CA, USA) and cell attached configuration assumed if seal resistance >1G Ω ; monitored with a 5 mV, 1 ms square-wave seal-test. Seals were broken-through into whole-cell mode with several small negative pressure pulses; cells were recorded if $V_M < -50$ mV and $R_S < 30$ M Ω at the time of break-through. In all voltage-clamp recordings R_S was recorded by means of a 1 mV test pulse at the end of each trace record.

All signals were filtered at 10 kHz using an online low-pass Bessel filter built into the Axopatch 200B and were filtered again at 10 kHz through a Brownlee 440 (Brownlee Precision, CA, USA) amplifier and digitized at 20 kHz (CED 1401, Cambridge Instruments; modified for a 10 V input/output range). Traces were collected with WinWCP data acquisition software (John Dempster, Strathclyde University; Glasgow, UK) and stored on a PC (Dell, UK). Online IR-DIC video was viewed using the CCD camera control software (HCImage, Hamamatsu, Japan).

All analysis of electrophysiological data was performed using the Stimfit software package (<http://www.stimfit.org/>; courtesy of C. Schmidt-Hieber, UCL London, UK; and P. Jonas, Physiological Institute, IST, Klosterneuberg, Austria) on a PC running Windows XP operating system.

2.2.4: Recording of passive and active membrane properties

We recorded passive and active intrinsic membrane properties of patch-clamped cells, in current-clamp (I-fast mode); compensating R_S to 100%, with 20 μ s lag, all current-clamp recordings were performed from V_M . A single family of 500 ms hyper-depolarising square-wave current injections was run from -250 to 250 pA

of V_M . If a 250 pA current pulse failed to elicit a train of APs, the pulse amplitude was increased further, to a maximum of 500 pA. Cells were rejected at this stage if depolarizing current pulses failed to elicit APs, confirmed by biasing the V_M of non-firing cells to well above that of AP threshold.

Intrinsic cell properties provided initial identification of recorded neurons, as well as in depth physiological characterisation of recorded cells. Key properties analysed were: membrane potential (V_M); input resistant (R_I); membrane time constant; hyperpolarisation induced voltage “sag” (proportional to I_h); action potential: amplitude, threshold, half-duration, maximal rise and decay rate and their ratio; medium and fast after-hyperpolarisation amplitudes; maximal AP discharge frequency and the accommodation profile of AP discharge trains.

V_M of recorded neurons was taken as the average of the first 50 ms, in response to a 0 pA current injection. R_I and membrane time constant were estimated from voltage response to a 50 pA hyperpolarizing current pulse. To assess R_I we measured the average voltage response over the last 100 ms of the 500 ms pulse, from which we calculated R_I , according to Ohm’s Law ($V=IR$). Membrane time-constant was calculated by fitting a monoexponential curve (Levenberg-Marquardt algorithm) to the decay of the pulses, estimated as time to 63% of the decay. Voltage “sag” proportional to I_h was estimated as the difference between the maximal voltage response and the steady-state of the voltage “sag”; at -250 pA hyperpolarising current. *Post hoc* calculation of this “sag” gave us an estimation of relative I_h contribution in recorded cells (Halliwell and Adams, 1982).

All AP parameters were measured from V_M prior to depolarisation, whereas medium and fast AHP amplitudes were measured from AP threshold (measured as V_M when $dV_M/dt^{-1} = 20 \text{ mV}\cdot\text{ms}^{-1}$). We measured all AP properties from the first AP elicited by sequential 50 pA depolarisations, with all amplitudes measured over 3 data points (150 μs). Maximal AP rise and decay rates were taken as the maxima of the 1st derivative (dV_M/dt) of the rise and decay phase of APs; with

the ratio of rise/decay calculated. AP half-height duration was measured at $\frac{1}{2}$ the maximal AP amplitude from baseline.

Maximal AP discharge frequency was calculated from the number of overshooting spikes over the 250pA, 500 ms depolarizing pulse. AP inter-spike-interval accommodation ratio was determined as the ratio of the instantaneous frequency at the beginning and the end of the AP discharge train.

2.2.5: Whole cell patch clamp recording of slow IPSCs

Following characterisation of intrinsic membrane properties in recorded cells; we elicited GABA_BR- mediated slow-IPSC in INs and principal cells of either the CA1 or DG; in the presence of antagonists to NMDA (AP-5; 50 μ M), AMPA and kainate (NBQX; 10 μ M) and GABA_A (bicuculline or SR95531: both 10 μ M) receptors. Cells were voltage-clamped at a V_M of -65 mV and slow-IPSCs elicited by a 0.2-0.4 M Ω monopolar glass electrode filled with 2M NaCl and inserted into either the *str. radiatum/L-M* border or *str. oriens*. Electrical pulses were delivered to afferent fibres via a constant-voltage stimulator at a rate of 0.05 Hz; due to the very slow kinetics of GABA_BR-mediated IPSCs, R_S was not compensated. We produced slow-IPSCs with a single square wave stimulus (50 μ s duration), interleaved with trains of 3 and 5 stimuli (at 200 Hz), each of the same pulse duration; which we recorded for 10 minutes to determine the amplitude of GABA_BR mediated IPSCs under control conditions, in a subset of experiments we performed this control recording for 20 minutes (figure 2.2); peak measured as the average of 200 points (10 ms), taken from the average trace of 1, 3 or 5 stimulus responses. Activation of receptors other than GABA_B was assessed following application of the selective GABA_BR antagonist CGP-55,845, where any residual current was subtracted from the control recordings, to obtain the true GABA_BR-mediated response.

Neither the peak GABA_BR-mediated IPSC amplitude nor the injected current required to maintain voltage clamp changed more than 10% over the course of a typical 20 minute recording (see figure 2.2), confirming that GABA_BR-mediated effects were not “washed out” into the patch-pipette. We then ran a voltage-ramp command test (-40 to -120 mV, over 100ms) to determine voltage-dependent currents active under control conditions (Bean and Sodickson, 1996).

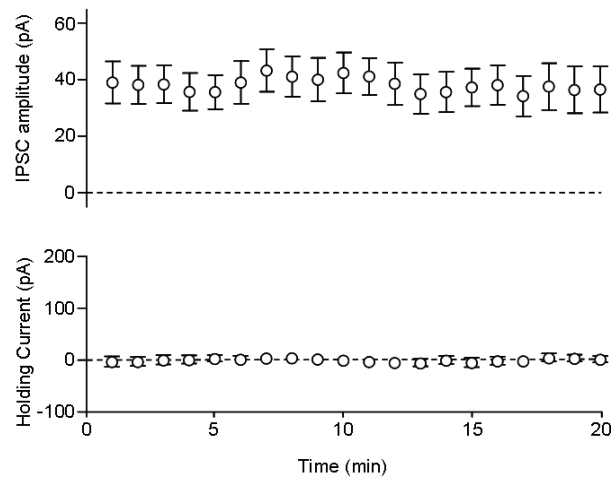


Figure 2.2 Control recordings of GABA_BR-mediated IPSCs in CA1 pyramidal cells. In recordings from 8 CA1 pyramidal cells neither the slow-IPSC amplitude (top) nor the holding current required to maintain -65mV voltage-clamp changed substantially.

If large GABA_BR-mediated IPSCs were observed, we assessed the reversal potential (E_R) of these synaptic responses in current-clamp mode only; as to minimize the effect of “space-clamp” due to passive and active currents in the dendrites modulating the V_M . We elicited IPSPs in response to a 5 stimulus train (as above) and changed the V_M from resting, holding the cell at intervals of ~15 mV, over a range from -50 mV to -110 mV. Plotting of V_M against peak IPSP amplitude allowed determination of the x-axis intercept, giving an approximation of E_R .

Whether GABA_BR-mediated IPSCs or detected or not we applied the selective GABA_BR agonist baclofen (10 μ M) to the bath, following the ramp-command or current-clamp E_R test and allowed 5 minutes for the drug to washin (2 minutes equilibration of drug binding, 3 minutes steady-state drug effect). We measured

the reduction in peak IPSC amplitude, due to pharmacological occlusion of the receptor, along with the change in holding-current required to maintain a -65 mV voltage-clamp, to detect any current flux; a indication of GABA_BR activation. In the presence of baclofen we ran a second voltage ramp-command, subtracting the control test to determine the voltage dependence of currents activated by baclofen. Finally, we removed the baclofen and bath applied 5 μ M CGP-55,845 for 5 minutes, to block all GABA_BR activated currents, which we followed by a final voltage-ramp command, which when subtracted from the baclofen test, gave the voltage-dependence for all functional GABA_BR currents activated by baclofen, including any tonic-currents.

We analysed kinetics of slow IPSCs offline; individual traces were digitally filtered using a Gaussian filter at 0.5 kHz and 10 control responses averaged. Kinetic values calculated from recordings where mean GABA_BR IPSC amplitude, evoked by a single stimulus, had an amplitude >5 pA. Kinetic parameters derived were: onset and peak latencies, half-duration and decay time-constant. Decay time-constants for synaptic responses were fitted with a mono- or biexponential curve (Levenberg-Marquardt algorithm) to the descending phase of the response (Bean and Sodickson, 1996). Latencies were measured from stimulus onset to the peak (peak latency) or beginning of the IPSC (onset latency).

E_R was calculated from voltage-ramp command tests by extracting the average ramp-command data and then subtracting either the baseline or the CGP-55,845 test from the baclofen test. The outward current response plotted against ramp-potential was fitted with a linear regression and the x-intercept was used as an approximation for E_R ; compared between control/baclofen or CGP-55,845/baclofen subtractions.

2.2.6: Whole cell patch clamp recording of monosynaptic IPSCs

To determine the presynaptic effect of GABA_B in CCK and PV axons, we recorded monosynaptic IPSCs evoked in identified CA1 pyramidal cells elicited by putative basket cell afferents. Cells were held a V_M of -65 mV and monosynaptic GABA_AR-mediated IPSCs isolated in the presence of AP-5 (50 μ M) and NBQX (10 μ M). Recording electrodes contained high-chloride intracellular solution to improve signal-to noise of evoked currents and stimulating electrodes were as above; R_S was compensated to 80% with 20 μ s lag. Monosynaptic all-or nothing responses were elicited by single stimuli (50 μ s) in *str. pyramidale*; with stimulation intensity marginally above IPSC generation threshold in a given axon; typically in the range of 0.5-10V, with an average intensity of 3.5 ± 1.2 V. Monosynaptic IPSCs were recorded every 10 seconds and control conditions recorded for 2-5 minutes until stable (i.e. <10% change in response amplitude). In a subset of experiments we applied the highly potent and selective CB1 receptor agonist WIN-55,212 (1 μ M) to the bath for 10 minutes, to allow full drug effect and steady state. Inhibition of unitary response after 10 minutes indicated that CB1 receptors were present on the axon, presumably a CCK-IR basket cell afferent; with WIN-insensitive axons putatively identified as originating from PV-IR basket cells (Katona et al, 1999).

Alternatively, following control recording, WIN-55,212 was applied for 2 minutes then washed out of the bath. If IPSC amplitude was seen to decrease transiently in response WIN-55,212, then that axon was deemed to be WIN-sensitive, putatively identified as a CCK-IR basket cell afferent. If transient WIN-55,212 application had no effect on IPSC amplitude these axons were again putatively identified as WIN-insensitive PV-IR basket cell afferents (Lee and Soltesz 2010). Fast-IPSC amplitudes were measured as a temporal average of 20 data points (1 ms) in every trace with timecourse plots averaging the peak amplitude of 6 traces. Peak pharmacological effect was measured over the 2 minute maximal drug effect window; representative traces shown are the mean trace of this window.

In experiments where WIN-55,212 was washed in for 10 minutes, 10 μ M baclofen was applied for 5 minutes; directly on top of the CB1 receptor agonist. With baclofen effect on IPSC amplitude measured at 3-5 minutes following drug application to the bath. In those experiments where WIN-55,212 was applied transiently, we applied 10 μ M baclofen for 5 minutes, 10 and 15 minutes after WIN-55,212 washout in WIN-insensitive and sensitive fibres, respectively; to allow recovery of the IPSC to control levels. Following baclofen application we then applied 5 μ M CGP-55,845 to remove all presynaptic GABA_BR-mediated inhibition. In a subset of WIN-sensitive and insensitive monosynaptic responses, we applied the selective M2 receptor agonist arecaidine but-2-ynyl ester tosylate (ABET, 10 μ M) on top of CGP-55,845, for 5 minutes; to aid identification of these afferents (Chiang et al, 2010). For comparison of WIN-55,212, baclofen, CGP-55,845 and ABET mediated effects on monosynaptic IPSC amplitudes, elicited by PV and CCK containing afferents; we compared the 2 minute peak effect, relative to control or preceding epoch, of each drug between WIN-sensitive and WIN-insensitive responses.

2.2.7: Paired recordings of monosynaptic IPSCs

To determine the effect of presynaptic GABA_BR on GABA release from identified INs, we performed paired recordings of synaptically coupled cells in the CA1, using 2 Axopatch 200B amplifiers. Using fire-polished recording electrode, filled with high-chloride intracellular solution, we whole cell patch-clamped a CA1 IN and characterised intrinsic properties in current-clamp (as above); in the absence of pharmacological agents. We then approached and patch-clamped a CA1 pyramidal cell in close apposition to this IN, which we identified by intrinsic physiology in current clamp mode.

We evoked monosynaptic IPSCs in the voltage-clamped CA1 pyramidal cell which was held at $V_M = -65$ mV, with $R_S < 15$ M Ω , which was then compensated to 80% with 20 μ s lag. Single APs were evoked in the current-clamped presynaptic IN by a short depolarising current pulse (2 nA, 500 μ s duration) at 0.2 Hz for 5 minutes

(at least 50 traces). Following control recording we applied 10 μ M baclofen to the bath for 5 minutes, followed by 5 μ M CGP-55,845 also for 5 minutes. Recordings were abandoned if $V_M > 50$ mV in either cell and if $R_S > 30$ M Ω in the presynaptic cell. We analysed the peak amplitude of evoked monosynaptic responses as described previously.

2.3 Morphological analysis of acute slices and perfused tissue

Two different aspects of morphological analysis were considered to determine the nature of synaptic transmission between hippocampal neurons. Primarily immunocytochemistry or histological staining was performed following physiological recording to confirm cell identity. Morphological analysis of perfusion fixed material was used for light and electron microscopic analysis of GABA_B receptor subunit localisation within hippocampal neuronal populations.

2.3.1: Fixation of acute slices following recording

Following successful recording an outside-out patch was formed, the electrodes carefully retracted from the slice; which was then transferred to fixative solution (4% paraformaldehyde, 0.1 M phosphate buffer (PB, 0.1 M)) overnight at 4°C. We collected and stored slices for 2-3 weeks in PB at 4°C, to give us a sufficient numbers of slices for the immunolabeling procedure, which were stored in PB. If slices had to be stored for longer than several weeks the PB was exchanged for that containing 0.05% NaN₃. In one case, several slices were stored for 6 months in 15% sucrose, 15% glycerol, 0.05% NaN₃, at -20°C.

2.3.2: Preparation of acute slices for fluorescence microscopy

Slices were rinsed twice in PB, and then in phosphate buffered saline (PBS; 0.025M PB, 0.9% NaCl) three times. Background antigenicity was blocked in PB

containing 10% normal goat serum (NGS), 0.3% Triton X-100 and 0.05% NaN₃ for 1 hour at room temperature (22-25°C). Primary ABs(ABs) (see table 2.1) were diluted in 5% NGS, 0.3% TX and 0.05% NaN₃ and slices incubated in this primary AB containing solution for 72-96 hours, at 4°C.

Antigen	Host	CC.(mg.ml ⁻¹)	Dilution	Supplier
PV	Mouse	1	1:5,000	Swant, Switzerland
PV	Rabbit	1	1:5,000	Swant, Switzerland
CCK	Mouse	1	1:5,000	Gift: CURE,UCLA, USA
CCK	Rabbit	1	1:5,000	AbCam, UK
CB	Rabbit	1	1:5,000	Swant, Switzerland
SSt	Rat	1	1:5,000	Chemicon, USA
SSt	Mouse	0.14	1:100	Genetex, USA
SSt	Rabbit	1	1:5000	Peninsula, USA
GABAB1	Rabbit	Crude serum	1:400	Gift: Ā. Kulik/R Shigemoto
Kir3.2	Guinea-Pig	1	1:200	Genmab, UK

Table 2.1 Summary of primary ABs used in immunocytochemistry. With respect to antigen, host species, stock concentration (CC.), final dilution and source company and country are shown.

Following primary AB incubations slices were rinsed copiously in PBS and secondary ABs applied (table 2.2), diluted in 5% NGS, 0.1% TX and 0.05% NaAZ and incubated at 4°C overnight (>12 hours). To visualize the recorded and biocytin-filled cells, avidin conjugated to AlexaFluor-647 was applied in conjunction with the secondary ABs. To enhance AB penetration and conjugation to antigens, all slices were incubated at room temperature (~22-26 °C) for at least 1 hour before and after refrigeration with all AB solutions. Following secondary AB incubation, slices were rinsed twice in PBS and 3 times in PB before mounting. Slices were mounted on glass slides and cover-slipped, with an aqueous mounting medium comprising 30% glycerol and 10 mM phenylenediamine, in 0.1M PB. Slides were stored at -20 °C and allowed to warm to room temperature before imaging.

Method	Antigen	Host	Dilution	λ /Size (nm)	Supplier
Avidin	Biotin	Bacterial	1:1,000	647	Invitrogen
Antibody	Mouse	Goat	1:500	488/546	Invitrogen
Antibody	Rabbit	Goat	1:500	488/546	Invitrogen
Antibody	Rat	Goat	1:500	488/546	Invitrogen
Antibody	Guinea-pig	Goat	1:500	488/546	Invitrogen
Biotinylated	Mouse	Bacterial	1:50	DAB	Vector Labs
Nanogold	Rabbit	Goat	1:100	1.4 nm gold	Nanoprobes
Nanogold	Guinea-pig	Goat	1:100	1.4 nm gold	Nanoprobes

Table 2.2 Summary of secondary ABs used in immunocytochemistry. Shown in respect to detection method employed are antigens detected, host species, dilution, observable response as wavelength (λ) or otherwise (λ /Size (nm)) and supplier.

2.3.3: Confocal fluorescence microscopy of brain slices

Immunoreactivity of recorded neurons was confirmed on a single-photon confocal microscope (Bio-Rad, UK). Cells were initially identified by imaging crude stacks of 5 μm steps at x20 optical objective magnification, exciting Avidin647, giving us an emission spectra in the far-red range (shown throughout as blue pseudocolour), images at this magnification were collected at a scan speed of 166 line.s⁻¹; giving sufficient resolution of axonal and dendritic distributions.

To confirm IR of IN neurochemical markers in the soma of recovered IN we used x40 objective confocal imaging, with a scan speed of 166 line.s⁻¹; exciting AlexaFluor 488 and 546. If somatic immunofluorescence was sufficiently higher than background levels, the cell was deemed to be IR for the corresponding neurochemical. In some cases where question was raised over immunoreactivity lambda-strobing was applied, stimulating each fluorochrome independently, reducing bleed-through of signal, giving greater confidence in neurochemical IR.

All figures showing immunofluorescence show only a single image from a stack to avoid false positive identification due to overlapping cells. Whereas flattened confocal stacks are shown for x20 images of biotin/avidin fluorescence.

2.3.4: 3D reconstruction of biocytin-filled cells

To clearly convey axonal and dendritic arborisations patterns and morphological characteristics of recorded cells, representative cells for each subtype have been reconstructed in either NeuroLucida (MBF Bioscience, USA) or using Fiji, a modified version of ImageJ; the latter utilising semi-automatic reconstruction techniques in the 'Neurite Tracer Plugin'.

For reconstruction purposes biocytin filled cells were imaged with single channel confocal microscopy, at 1 μm z-axis steps at x40 objective magnification. Image stacks were aligned and segmented offline. Segmentation of dendrites and axons was performed at ~ 1 μm intervals. Complete reconstructions were then compared to x10 objective magnification images to determine relation to hippocampal laminations and boundaries.

2.3.5 Perfusion fixation for morphological analysis

For analysis of protein localisation within the cytoplasm (i.e. neurochemical markers) or on the plasma membrane (GABA_{B1} receptor subunits) in neurons of the hippocampus we used perfusion fixed material as it provided better ultrastructure and antigenicity than tissue produced during *in vitro* experiments, allowing for more accurate determination of protein expression.

We used tissue collected from 5 Wistar rats (100-300 g) for the anatomical characterisation of GABA_BR localisation in this study, which were perfused as described previously (Kulik et al, 2003 and 2006). Briefly, we sedated the rats with isoflurane then they were anaesthetised with Narkodorm-n (180 mg/kg, i.p.; Alvetra, Germany) and allowed 3-5 minutes for the anaesthetic to take effect.

Once anaesthetised, we opened the chest cavity and pericardium, exposing the whole heart and aortic arch. The base of the left ventricle was cut and a gavage needle inserted through the heart into the aorta and the needle clamped in place. 0.9% NaCl was then perfused for 1 minute to removed erythrocytes and plasma, followed by 500mls of fixative comprising: 4% paraformaldehyde, 15% saturated picric acid and 0.05% glutaraldehyde; which was perfused for 13 minutes. In experiments for light microscopy, we excluded glutaraldehyde to reduce background fluorescence and improve antigenicity and AB penetration.

2.3.6 Preparation of perfusion-fixed tissue for light microscopy

To assess the distribution and co-localisation of GABA_{B1} receptor subunits and Kir3.2 channel subunits in populations of hippocampal IN with light microscopy, we processed glutaraldehyde-free perfusion-fixed material for immunofluorescence. 50 µm coronal sections of hippocampus were cut on a vibratome (Leica VT1000) rinsed in PBS several times and antigenicity was blocked in PBS containing: 20% NGS, 0.3% TX-100 and 0.05% NaN₃ for 1 hour at room-temperature. Primary ABs were applied (table 2.1) in PBS containing 2% NGS, 0.3% TX-100 and 0.05% NaN₃ for at least 12 hours incubation or overnight. Slices were rinsed in PBS and secondary ABs applied (table 2.2) in PBS containing 1% NGS, 0.3% TX-100 and 0.05% NaN₃ and incubated for 2 hours at room temperature. Slices were washed once in PBS, then 3 times in PB and mounted on glass slides with hard-setting fluorescence mounting medium (Dako, UK) and then cover-slipped. Light micrographs of perfusion fixed material were imaged as described above.

2.3.7: Preparation of perfusion-fixed tissue for electron microscopy

To determine the relative density of GABA_{B1} receptor subunits and Kir3.2 channel subunits on the plasma-membrane of different neurochemically identified IN sub-populations, compared to CA1 pyramidal cell dendrites; we performed pre-embedding electron microscopy double labelling experiments. Briefly, 50 µm coronal sections of 0.05% glutaraldehyde fixed brains were sliced on a vibratome and washed in 0.1 M PB. Sections were then equilibrated with cryoprotection buffer (10% glycerol, 25% sucrose) and frozen in isopentane (5-6 seconds) floating on Liquid N₂ (-196°C), followed by freezing in Liquid N₂ for 3-4 seconds; then thawed. Sections were washed briefly in PB then 0.05 M Tris-buffered saline (TBS) and blocked in TBS containing 20% NGS for 1 hour.

Primary ABs (table 2.1) were applied overnight, incubated in TBS containing 3% NGS at 4°C. Sections were washed and then secondary ABs applied (Table 2.2), which were incubated with TBS and 2% NGS overnight at 4°C. Primary ABs to IN neurochemical markers were complimented by biotinylated secondary ABs, whereas receptor and channel proteins were revealed by immunogold conjugated secondary ABs (table 2.2). Sections were rinsed in TBS, then PBS and then post fixed with 1% glutaraldehyde. Excess glutaraldehyde was washed away with PBS, then sections rinsed in ultra-pure water. 1.4 nm gold particles were silver-intensified (HQ silver kit, Nanoprobes, USA) to increase particle size to 8-10 nm, allowing observation at lower power magnification. Following silver-intensification, slices were rinsed in TBS and 1:100 avidin conjugated horseradish peroxidase (ABC Elite kit, Vector labs) incubated for 2 hours. Following ABC incubation, sections were rinsed in TB and 0.05% DAB was applied for 20 minutes. DAB end-product was developed with 0.01% H₂O₂, with the reaction monitored to prevent high-background labelling.

Sections were washed in PB and then treated with osmium tetroxide (1% OsO₄ with 6% sucrose) for 40 minutes, dehydrated in 50% ethanol and contrasted with 1% uranyl acetate (in 70% ethanol) for 35 minutes; following which slices were

dehydrated with sequential increasing concentrations of ethanol for 40 minutes. Sections were further dehydrated with 100% propylene oxide for 20 minutes and then embedded in epoxy resin (Durcopan ACM, Sigma-Aldrich). Sections were then flat-embedded and resin polymerised at 56°C overnight. Small blocks (<1 mm²) of hippocampal subfield CA1 were dissected from embedded sections and re-embedded in Durcopan ACM resin capsules. 70 nm serial ultrathin sections were prepared on an ultramicrotome (Leica EM UC6, Leica Microsystems, Germany) and transferred to a transmission electron microscope (LEO 912, Zeiss, Germany). IN dendrites possessing DAB end-product were identified in serial sections and electron micrographs taken at either 6,000x or 10,000x magnification.

2.3.8 Analysis of immunogold particle density

Electron micrographs were analysed offline using the TrackEM plugin of the FIJI software bundle (Cardona et al, 2010; Saalfeld, et al 2010). Chiefly we analysed surface density of silver intensified gold-particles on DAB-end product positive dendrites, axons and somata; which was calculated by counting the number of particles within 20 nm distance on the intracellular face of the plasma membrane. Tracing the perimeter of the neuronal process allowed easy calculation of surface density per 70 nm section. We repeated this process for each serial electron micrograph, giving us a surface density for the whole process. To assess the relative density of receptor and channel protein between experiments, we compared the level of gold-particles in IN dendrites to that of CA1 pyramidal cell dendrites in *str radiatum*; which were identified as having dendritic spines, with excitatory synapses (demarcated by post-synaptic densities) located only on spines. For examination of the GABA_{B1} receptor subunit density in SSt-IR dendrites, serial electron micrographs were also collected in *str. radiatum* where GABA_{B1} labelling in CA1 pyramidal cells is much stronger than in *str. oriens* where SSt-IR dendrites are generally found.

2.4 Statistical analysis

Unless otherwise stated, all data is shown as mean \pm SEM. All statistical analysis was performed in the Graphpad Prism software package (GraphPad, CA, USA). In all experiments statistical significance was compared between groups using the Mann-Whitney non-parametric test, unless stated otherwise. We preferred non-parametric testing due to the inherent non-Gaussian nature of our data due to small experimental numbers. Data was considered significant if $P < 0.05$. Abbreviations used throughout: ns - no significant difference, * - $P < 0.05$, ** - $P < 0.01$, *** - $P < 0.001$.

2.5 Materials used

All reagents used for production of ACSF and buffers were either purchased from Fisher Scientific, UK; or Sigma-Aldrich, UK. Bicuculline, d-APV (5), NBQX, CNQX, ABET, WIN-55,212 and SR95531 were all purchased from Ascent Scientific, UK. Baclofen and CGP-55,845 were both purchased from Tocris, UK.

3 Post-synaptic GABA_BR mediated responses in principal cells of the hippocampus

GABAergic conductances mediated by GABA_BR in hippocampal principal cells have been widely described in the literature (Newberry and Nicoll, 1985; Solis and Nicoll, 1992; Isaacson et al, 1993; Otis et al, 1993; Bean and Sodickson, 1996) and provide us a positive control for later analysis of GABA_BR in identified INs. In particular, CA1 pyramidal cells have been shown to have a large contingent of plasma membrane localised GABA_B receptor subunits as well as abundant levels of Kir3 channel subunits (Fritschy et al, 1999; Kulik et al, 2003 and 2006). Also stimulation of GABAergic afferent boutons proximal of distal apical dendrites has been shown to result in large post-synaptic GABA_BR-mediated currents (Lüscher et al, 1997), resulting from an outward flux of K⁺, hyperpolarising the dendritic membranes.

As all ionic conductances directly relate to the Nernst Equation: ($E_R = (RT/zF) \ln(\text{ion}_{\text{out}}/\text{ion}_{\text{in}})$), differences in slow-IPSC amplitudes could exist between our recordings and those quoted in the literature; due to subtle variations in our experimental design, especially temperature (Mitchell and Silver, 2000). Thus by recording pharmacologically isolated GABA_BR-mediated slow IPSCs in principal cells, especially CA1 pyramidal cells, under identical conditions to that of INs we can compare the relative functional levels of GABA_BR conductance in all cell types we tested. In this chapter we identify GABA_BR-mediated responses in 3 distinct populations of hippocampal principal cell: CA1 pyramidal cells, CA1 GRCs and DGCs; the latter two are compared also to CA1 pyramidal cells.

3.1 Morphological and physiological characterisation of CA1 pyramidal cells

In whole-cell patch clamp experiments we obtained stable recordings from 26 putative CA1 pyramidal cells, based on intrinsic properties observed on-line; we

elucidated identities of these cells *post hoc*, through visualization of the biocytin filled neurons.

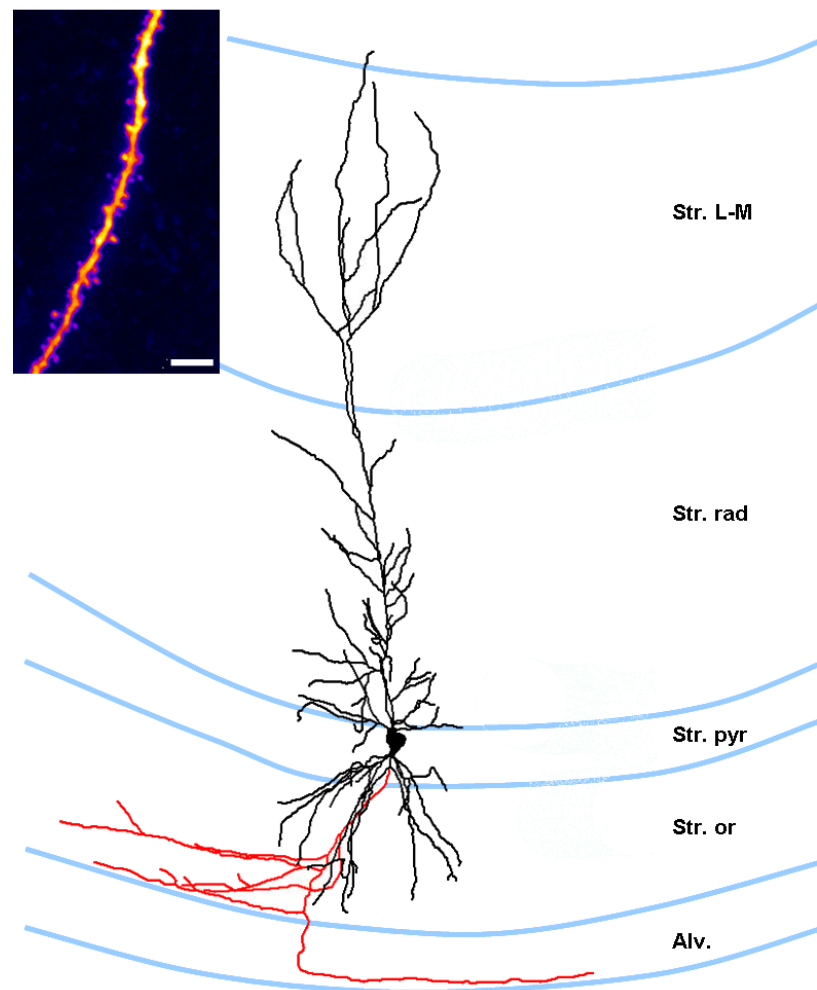


Figure 3.1 Morphological identification of a CA1 pyramidal cell. A flattened NeuroLucida 3D-reconstruction showing the somatodendritic axis (black) and axonal projection and local arbour (red) with respect to CA1 layers (light blue lines); inset, high-power confocal image of a section of dendrite showing dendritic spines. Scale bar - 5 μ m

Cells were defined as CA1 pyramidal cells if they fulfilled these 4 criteria: 1) the soma lay in the *str. pyramidale* or in proximal *str. oriens*; 2) one or occasionally two large calibre, apical dendrites extending into *str. radiatum* which then bifurcated, tufting in *str. L-M*; 3) basal dendrites projecting radially into *str. oriens* and 4) importantly a high density of dendritic spines, as seen in figure 3.1 (inset). Additional to dendritic morphology, the AIS gave rise to a single large axon, which projected vertically into the alveus and projecting along the

transverse axis. Occasionally a small local arborisation of axon was detected in *str. oriens*, but this was not deemed critical for identification. The CA1 pyramidal cell reconstruction seen in figure 3.1 shows this morphology well, in respect to lamina boundaries.

As well as stereotyped morphologies, intrinsic electrophysiological properties of CA1 pyramidal cells are also well defined. Trains of AP's are seen in figure 3.2.A/B (two cells showing different AP discharge patterns) which both show accommodation of inter-spike interval, the firing train on the right comes from a cell where a depolarising after-potential (DAP) was seen, temporally separating both medium and fast AHP components. The train on the left shows no observable DAP and as thus only medium-AHP was detectable. In 63% of cells we observed a DAP component during the AHP.

The CA1 pyramidal cell AP waveform was broad with a very high rise/decay rate ratio and a characteristic long duration AHP predominantly comprising medium-AHP, but fast-AHP was seen in a subset of cells (see above and Azouz et al, 1996); in keeping we saw both subtypes of CA1 pyramidal cell (shown in fig 3.2.E/F). Statistical testing between CA1 pyramidal cells which showed a DAP or did not showed no significant difference in any AP discharge property ($P > 0.05$) except for mAHP amplitude, which one would expect; hence intrinsic properties were pooled (table 3.1). Passive membrane properties were also characterised, typically CA1 pyramidal cells had an input resistance of $\sim 100 \text{ M}\Omega$, determined as the change in V_M from resting; with a membrane time constant of $\sim 20 \text{ ms}$.

A full summary of all intrinsic membrane properties is seen in table 3.1. All of the intrinsic physiological data shown here is consistent with previous reports (Shanes, 1958; Madison and Nicoll, 1984; Spruston and Johnston, 1992) and from other recordings of CA1 pyramidal cells conducted in our lab.

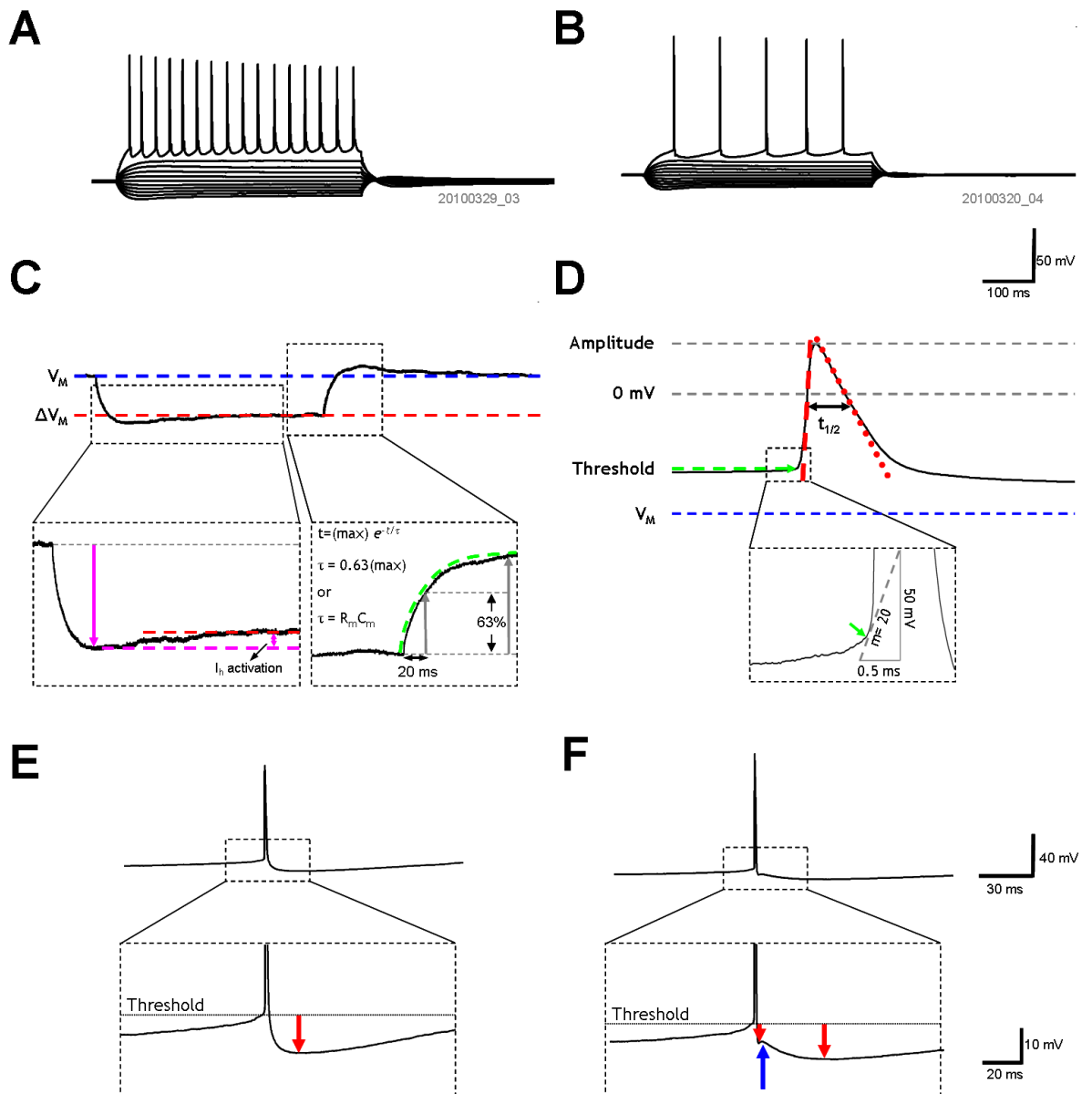


Figure 3.2: Comparison of CA1 pyramidal cell intrinsic properties. A and B AP discharge pattern in response to a family of hyper- to depolarising current commands (50pA steps; -250 to 250 pA range); in a cell showing no DAP (A) or with prominent DAP (B). Determination of passive membrane properties to a -50 pA hyperpolarisation is shown in C, V_M is indicated (blue line) compared to ΔV_M (red line). Inset (left) shows the initial hyperpolarisation followed by putative I_h mediated "sag" component (purple arrow). Inset (right) determination of membrane time constant from a monoexponential decay (Levenberg-Marquardt algorithm) and taken as time to 63% of maximal V_M . Extraction of kinetic data from a single AP waveform is shown in D, V_M and maximal AP amplitude (blue and grey dashed lines, respectively). Maximum rise and decay rates are shown in red (dashed and dotted, respectively). The AP duration at half-height is indicated as $t_{1/2}$. Threshold was determined from the rising phase of the AP (inset). E, F both show single APs expanded to show the AHP. In E, an AHP from a cell where the DAP was not observed (red arrow indicates peak), whereas in F, DAP was seen (blue arrow), with two discrete AHP phases.

Passive membrane properties	CA1 pyramidal cells (n=26)
Membrane potential (mV)	-62.9 ± 1.2
Input resistance (MΩ)	102.2 ± 13.1
Membrane time constant (ms)	22.0 ± 2.6
Putative I _h “sag”(mV)	3.0 ± 0.2
AP Kinetics	
Threshold (mV)	-39.8 ± 1.0
Amplitude (mV)	113.8 ± 2.1
Half-height duration (ms)	0.84 ± 0.04
Maximum rise-rate (mV.ms ⁻¹)	610.6 ± 31.4
Maximum decay-rate (mV.ms ⁻¹)	109.3 ± 4.7
Rise/decay ratio	5.6 ± 0.3
AHP properties	
Amplitude (medium/no DAP) (mV)	10.8 ± 0.6 (9 cells)
Amplitude (medium/with DAP) (mV)	8.6 ± 0.7 (17 cells)
Amplitude (fast/with DAP) (mV)	5.9 ± 0.6 (17 cells)
AP discharge properties	
Maximum frequency (Hz)	23 ± 2
Rheobase (pA)	131.1 ± 13.5
First-last interspike interval ratio	1.55 ± 0.14

Table 3.1 Summary of key intrinsic properties of CA1 pyramidal cells. Which were based on measurements taken, as per figure 3.2. All data shown as mean ± SEM from 26 cells, unless stated otherwise.

3.2 CA1 pyramidal cells possess postsynaptic GABA_B conductances

In 26 CA1 pyramidal cells we electrically stimulated GABAergic afferents at *str. radiatum/L-M border* with single stimulus and trains of 3 and 5 stimuli (200 Hz) in the presence of AMPA, NMDA, Kainate and GABA_A receptor blockers (AP-5 (50 μM), NBQX (10 μM) and bicuculline or SR95531 (both 10 μM)).

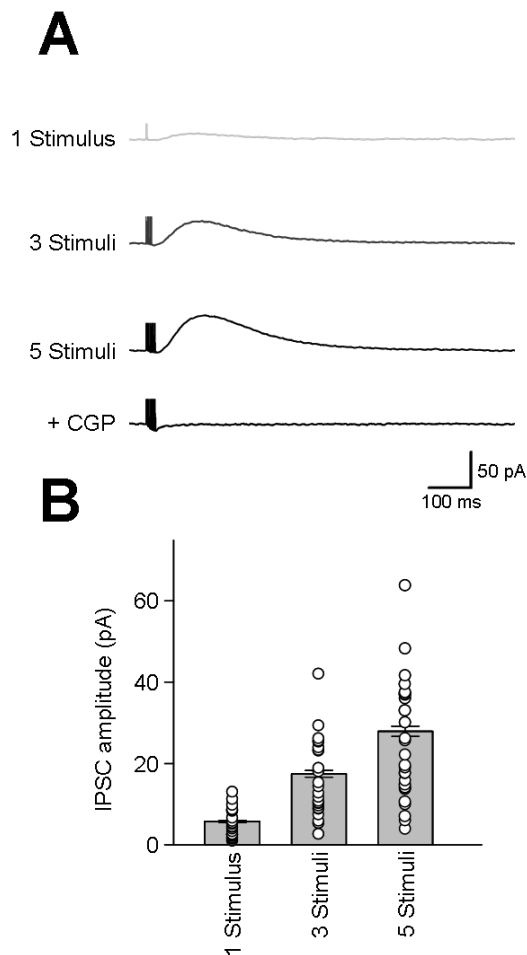


Figure 3.3 GABA_BR mediated IPSCs in CA1 pyramidal cells elicited by release of endogenous GABA. **A** Representative slow IPSCs induced by 1 stimulus (light grey) and 3 or 5 stimulus trains (dark grey and black, respectively) at the *str. radiatum/L-M* border; which were blocked by 5 μ M CGP-55,845 (CGP; black). **B** Mean IPSC amplitudes following the same stimulation as **A**, in 26 CA1 pyramidal cells; individual data is overlain (open circles).

In all 26 cells we observed postsynaptic GABA_BR-mediated slow-IPSCs; representative traces of which can be seen in figure 3.3.A. In CA1 pyramidal cells slow-IPSCs showed a near linear increase in synaptic response, as a function of stimulus number. However, saturation of the finite number of GABA_BRs present within the dendrites of the postsynaptic cell was not reached. The average amplitude of slow-IPSCs following a single stimulation was 5.75 ± 0.77 pA (25 cells), with responses for 3- and 5-stimulus trains averages being 17.48 ± 2.19 pA (25 cells) and 27.96 ± 3.22 pA (26 cells), respectively. We then divided these response amplitudes by the R_i of the recorded cells, to obtain normalised

somatic slow-IPSC amplitudes; the responses (as a ratio of R_i) for CA1 pyramidal cells were: $8.2 \pm 1.6\%$, $25.0 \pm 4.4\%$ and $39.0 \pm 6.3\%$ (respective to above order).

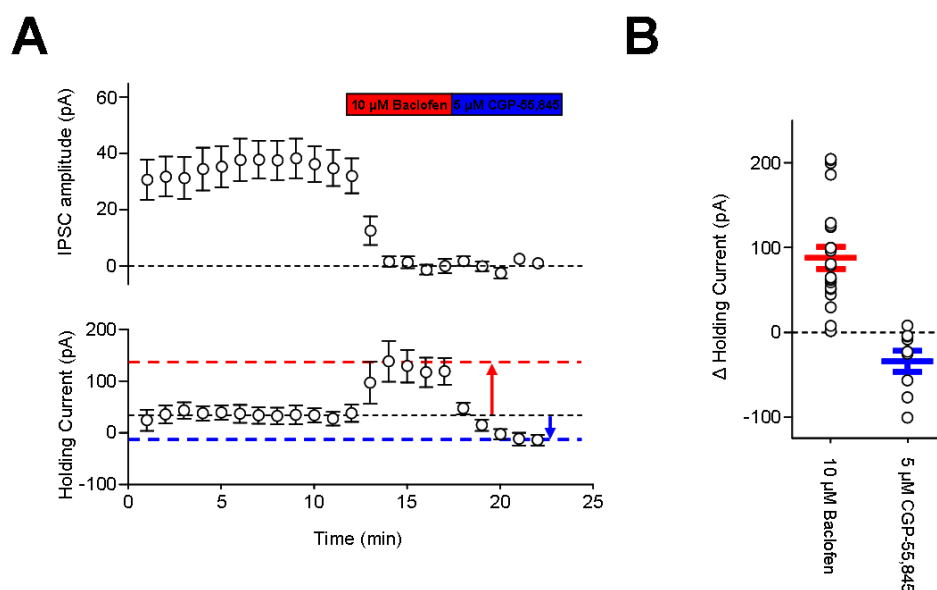


Figure 3.4 Pharmacological characterisation of GABA_BR-mediated currents in CA1 pyramidal cells. **A** Timecourse of mean synaptic amplitude (top, 5 stimulus train IPSCs) and mean holding current (bottom) at 1 minute intervals during control period and following 10 μM baclofen washin (red bar) and 5 μM CGP-55, 845 washin (blue bar). The zero level (dashed line) and maximal holding current change in CA1 pyramidal cells (red-dashed line) are shown; with difference from control indicated (red and blue arrows). **B** Mean maximal holding current change for baclofen (red) and CGP-55,845 (blue) peak levels, in CA1 pyramidal cells. Data is shown overlain by peak responses for individual cells (open circles).

Following at least 10 minutes characterisation of slow-IPSCs we bath applied the selective GABA_BR agonist baclofen (10 μM) to 23 CA1 pyramidal cell recordings; which resulted in a strong outward cationic current, which was compensated by an increase in holding current of the voltage-clamped neuron (figure 3.4.A, bottom, 9 cells); whilst completely occluding IPSCs in all cells (figure 3.4.A (top)). Baclofen failed to result in a change in holding current greater than that of the maximal synaptic response in 3 cells, which were included in the data-set. The average baclofen-induced increase in holding current was 88.25 ± 13.21 pA (Figure 3.4.B) and was larger than the peak amplitude of IPSCs, indicating that we did not activate the whole-cell contingent of GABA_B receptors with extracellular stimulation at the *str. radiatum/L-M* border. As a function of R_i the mean baclofen response in CA1 pyramidal cells was: $124.9 \pm 27.0\%$, again greater than the largest synaptic response.

Following baclofen application we exchanged the perfusing ACSF with that containing the potent and selective GABA_BR antagonist CGP-55,845 (5 μM, 9 cells) to confirm that slow IPSCs and the whole-cell current changes were mediated by GABA_BRs. CGP-55,845 resulted in a rapid and full blockade of GABA_BR currents, evidenced by the reversal of injected current amplitude in figure 3.4.A (bottom), as well as continued suppression of the slow-IPSC (3.4.A, top). In fact CGP-55,845 resulted in a 33.89 ± 13.16 pA reduction in injected current relative to control level (P=0.0195, Wilcoxon matched-pairs), indicated in figure 3.4.A (bottom). The mean CGP-55,845 effect on holding current is shown in figure 3.4.B and suggests the presence of GABA_BR-mediated tonic inhibition in CA1 pyramidal cells under control conditions, in acute slices.

3.3 GABA_BR are differentially expressed in basal and apical CA1 pyramidal cell dendrites

To test whether functional GABA_BRs were equally large across the two main dendritic compartments of CA1 pyramidal cells, we next recorded slow-IPSCs elicited by electrical stimulation in *str. oriens* to activate GABA_BRs on the basal dendrites. In 7 cells we found that slow IPSCs with amplitudes >5pA were only present in 1 cell in response to the same 200Hz 1/3/5 stimulation paradigm as in *str. radiatum*. Slow-IPSCs elicited in *str. oriens* had mean amplitudes of: 1.8 ± 1.6 pA, 3.0 ± 2.0 pA and 4.5 ± 2.1 pA (for 1,3 and 5 stimuli respectively), which was equivalent to 30.5%, 16.9% and 15.7 % of IPSC amplitude elicited in *str. radiatum* (P=0.003, 0.0006, 0.0003 respective to previous order). We confirmed that these *str. oriens* stimulated CA1 pyramidal cells possessed whole-cell GABA_BR responses similar to *str. radiatum* stimulated neurons by bath application of 10 μM baclofen, following recording of IPSCs, in 4 cells. The resulting increase in holding-current required to maintain voltage-clamp was 91.7 ± 46.1 pA, similar to that of *str. radiatum* stimulated cells (+2.3%; P=0.8112). Subsequent application of 5 μM CGP-55,845 resulted in a small inward current of 12.5 ± 38.0 pA in 3 cells, which was not significantly different from that observed in CA1 pyramidal cells stimulated in *str. radiatum* (P=0.3727).

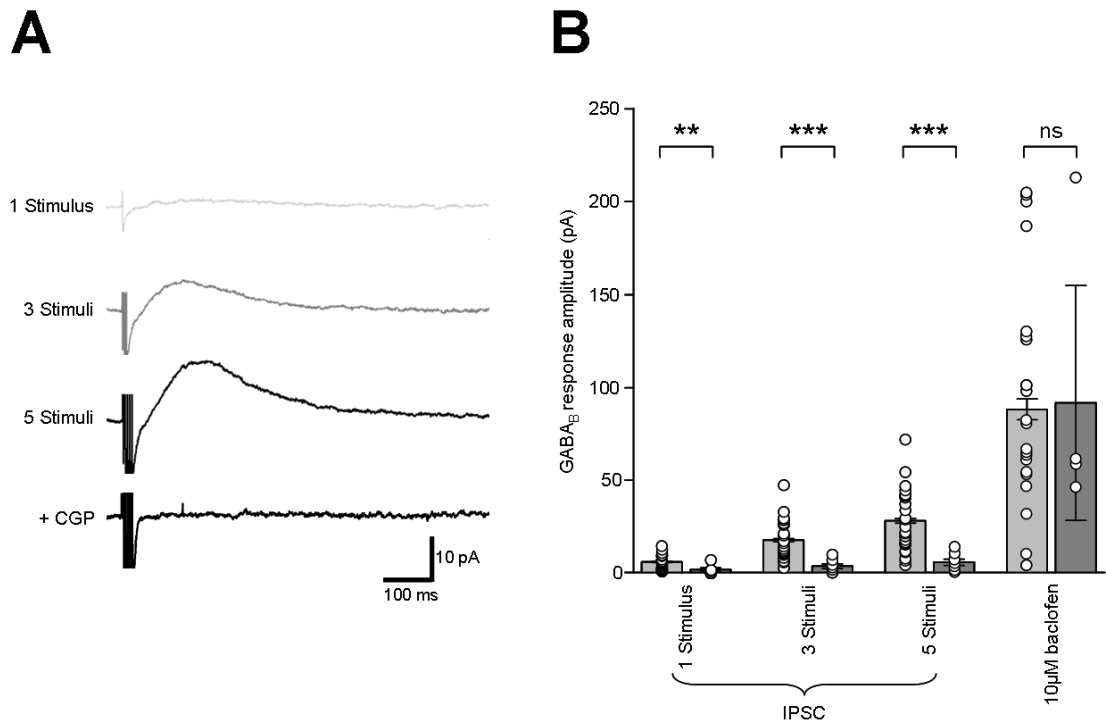


Figure 3.5 GABA_B mediated IPSCs in CA1 pyramidal cells elicited by release of endogenous GABA, in *str. oriens*. **A** Representative slow-IPSCs in a CA1 pyramidal cell in response to 1 stimuli (light grey) or 3 and 5 stimulus trains (dark grey and black, respectively) in *str. oriens*, which were blocked by CGP-55,845 (black, bottom). **B** Slow-IPSCs elicited in *str. oriens* (dark grey) in CA1 pyramidal cells are compared to those from *str. radiatum* (light grey), with stimulation protocol as in A; despite no difference holding-current changes elicited by baclofen (far right). Individual data overlay the mean data (open circles).

This data provides functional confirmation of the previous work by Kulik et al (2003, 2006), which showed that GABA_BR density is not uniform across all sub-cellular compartments. In our data there was a notable difference in GABA_BR-mediated responses seen between *str. oriens* and *radiatum*, in line with the aforementioned literature.

3.4 GABA_BR responses in CA1 pyramidal cells are mediated by an inward-rectifying K⁺-conductance

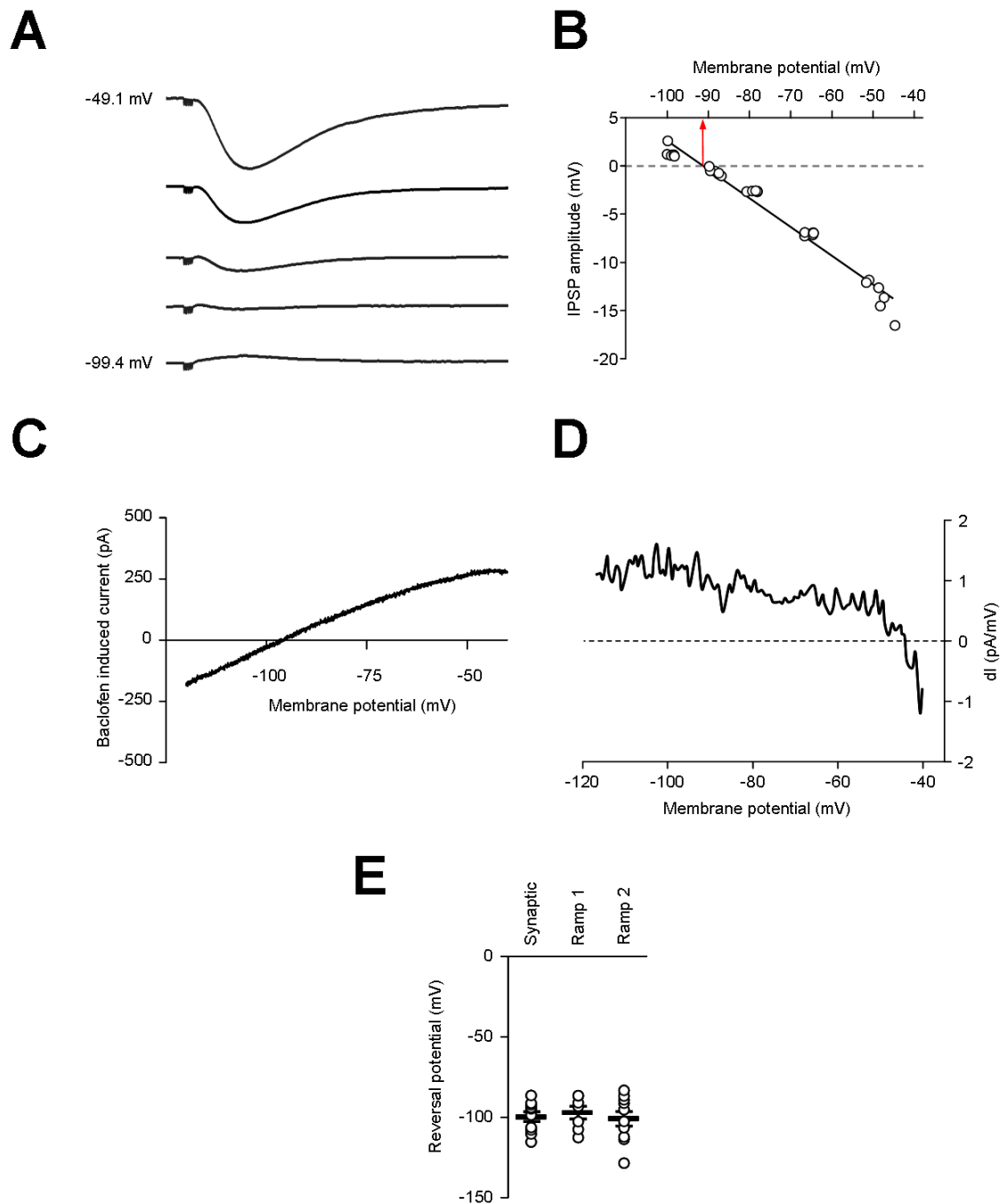


Figure 3.6 GABA_BR responses in CA1 pyramidal cells are reversible and inward-rectifying. **A** A representative synaptic E_R test at 5 membrane potentials (limits indicated), note clear reversal of IPSPs at ~-100 mV. **B** IPSP amplitude plotted against V_M, from the cell in **A**; 0 pA IPSC level (dotted line) and X intercept (red arrow) indicated. **C** Signal average of voltage-ramp protocol (Ramp test 2), with X intercept ~ -100 mV. **D** The same ramp test as in **C**, plotted as the first-differential of current against voltage (dI/dV), highlighting rectification of the current at V_M > 90 mV. **E** comparison of E_R derived from IPSP and voltage-ramp tests, plotted as mean ± SEM, overlain by data from individual experiments (open circles).

To confirm that Kir3 channels mediate the GABA_BR-mediated conductances in CA1 pyramidal cells, we tested the reversal of slow-IPSPs in current clamp mode, changing the membrane potential between -40 and -110 mV; a representative example is shown in figure 3.6.A. The E_R was estimated as the X intercept of the regression line fitted to the IPSPs amplitudes plotted against V_M for each cell (Fig. 3.6 B). The mean value of E_R was -99.6 ± 3.2 mV in 10 pyramidal cells, which was not different from the theoretical E_R of -106 mV, calculated from the Nernst equation for our experimental setup ($P=0.2813$; Wilcoxon signed-rank tests).

Additional to the reversal of slow-IPSPs, we determined the voltage-dependence of baclofen induced GABAB current using voltage-ramp protocol tests, as described by Bean and Sodickson (1996), as seen in figure 3.6.C/D. From voltage-ramp tests we observed inward-rectification of K^+ -currents, showing reduced current transfer at potentials $> \sim -90$ mV, than at more hyperpolarised potentials (representative current trace in figure 3.6.C). This change in current flux was clearest when we plotted the differential of current change against concordant V_M , in the same representative cell; figure 3.6.D. It is apparent that at V_M hyperpolarised relative to E_R there is minimal acceleration/ deceleration of current change, with a rate of $\sim 1-2$ pA.mV⁻¹. At V_M s depolarised to E_R , there was a clear decrease in current change rate approaching 0 pA.mV⁻¹. This data suggests that these is a preferential inward movement of K^+ ions through GABA_BR activated channels, as seen in inward rectifying Kir3 channels.

The interpolated E_R in figure 3.6.C from a representative signal-averaged ramp test, showing baclofen induced currents after subtraction of CGP-55,845 induced current and shows an E_R of approximately ~ 100 mV. From voltage-ramp protocols in 10 cells where currents elicited in the presence of CGP-55,845 were subtracted from baclofen-induced currents, we observed a mean E_R of -98.5 ± 5.9 mV (Ramp 2; fig. 3.6.C/D). In a further 8 cells we determined a mean E_R of -96.4 ± 3.7 mV, by subtracting voltage-ramp currents elicited in control conditions from baclofen-induced currents (Ramp 1, representative trace not shown). Neither E_R determined from voltage-ramp tests were significantly different from the E_R of slow-IPSPs ($P=0.36$ and 0.91 , respectively). The mean E_R

calculated from signal-averaged ramp 1 or ramp 2 tests were not significantly different from the calculated E_R of our experimental setup ($P=0.4375$ and 0.4688 , respectively; Wilcoxon signed-rank tests).

3.5 Kinetics of GABA_BR-mediated IPSCs in CA1 pyramidal cells

To confirm that the slow IPSCs we observed were kinetically similar to other reported values of synaptic GABA_B responses (Williams and Lacaille, 1992; Solis and Nicoll, 1992; Isaacson et al, 1993; Otis et al, 1993) we further investigated the properties of slow-IPSCs in CA1 pyramidal cells. We only analysed GABA_BR mediated responses where the synaptic amplitude >5 pA, elicited by a single stimuli, which resulted in 13 cells for analysis. The schematic in figure 3.7 describes determination of key intrinsic properties: peak amplitude, onset and peak latency, as well as rise and decay time-constants from the Levenberg-Marquardt algorithm.

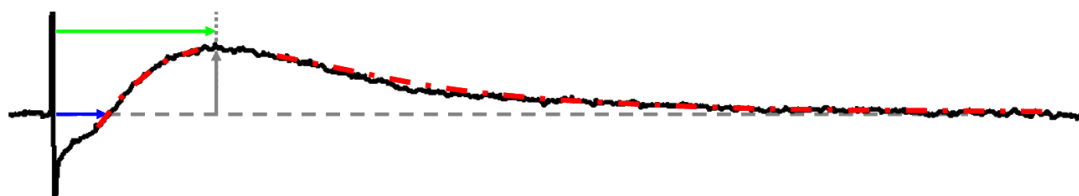


Figure 3.7 Schematic of key GABA_BR IPSC kinetic values. Indicating pre-stimulus baseline (grey line), peak amplitude from baseline (grey arrow), ascending and descending monoexponential curves (red dashed line); as well as onset and peak latency (blue and red arrows, respectively) in reference to the stimulus artefact.

Table 3.2 summarises the key kinetic properties of GABA_B responses. It should be noted that we attempted to fit a biexponential curve to the decay of the IPSC (also the Levenberg-Marquardt form) in line with Otis et al 1993. However the decay time-constants extracted for both mono- and bi-exponential curve fits gave very similar values for the fast decay ($P=0.678$). Whether or not there was a significant slow decay component remains contentious, however when we applied the Fisher test to this data we found that there was no significant

difference between the sum-of-squared error returns from either of the curve fits ($P > 0.30$). Therefore, for the remainder of this thesis we shall consider that the decay time-constant of GABA_BR-mediated IPSCs can be considered as monoexponential and all comparisons to CA1 pyramidal cell kinetics shall refer to the time constant of the monoexponential fit. Kinetic properties we have measured for GABA_BR-mediated slow IPSCs are similar to those observed by Williams and Lacaille (1992) in CA1 pyramidal cells. Principally, we observed shorter peak latencies, due most likely to the overlap of ionotropic glutamate or GABA_A responses with GABA_B IPSPs. Importantly, the decay time of reported GABA_BR IPSCs by Williams and Lacaille (1992) reported, is nearly identical to our reported values for IPSCs originating from the same receptor.

Kinetic properties	CA1 pyramidal cells (13 cells)	SSE
Peak amplitude (pA)	8.8 ± 0.9	n/a
Onset latency (ms)	58.6 ± 4.6	n/a
Peak latency (ms)	114.0 ± 6.7	n/a
Monoexponential curve		
Time constant (rise)	59.3 ± 11.2	635
Time constant (decay)	154 ± 26.8	7017
Biexponential curve:		
Time constant #1 (decay)	145.1 ± 26.26	6377
Time constant #2 (decay)	338.7 ± 94.1	

Table 3.2 Summary of GABA_BR mediated IPSC kinetics in CA1 pyramidal cells. Data from 13 cells where response at 1 stimuli >5 pA. For all kinetic properties we show the mean ± SEM and sum-of-squared-errors, indicating the best fitting exponential curve, where appropriate.

3.6 Morphological and physiological characterisation of CA1 giant radiatum cells (GRCs)

As well as identifying GABA_BR mediated slow-IPSCs in CA1 pyramidal cells, we also tested the GABA_BR content of the other CA1 principal cell type, giant

radiatum cells (GRC), to determine whether their different somatodendritic axis produced differential GABA_BR mediated IPSCs, mediated by the same stimulus.

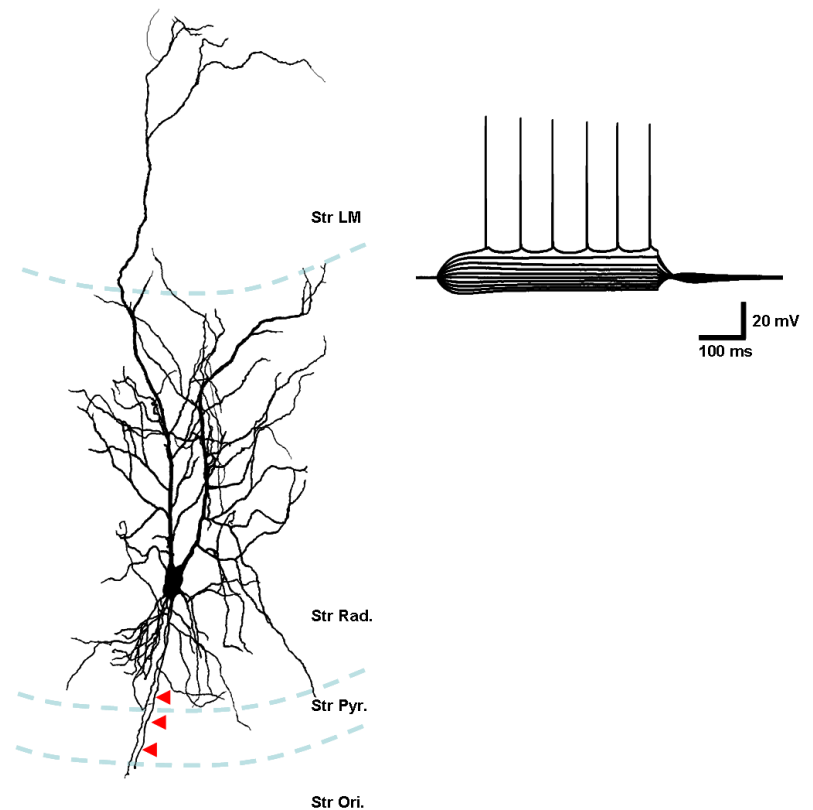


Figure 3.8 Morphological and physiological characterisation of CA1 GRCs. We show a flattened 3D reconstruction of a GRC, displaying the axon (red) and somatodendritic axis (black); in respect to hippocampal lamina (blue lines). Inset, an AP discharge train in response to a family of hyper- to depolarising current steps; note the CA1 pyramidal cell-like pattern of AP discharge.

We recorded slow-IPSCs from 12 GRCs which were identified on the basis of morphology and intrinsic membrane physiology, described previously (Guylas et al, 1998; Christie et al, 2000; Bullis et al, 2007). GRCs were morphologically identified as having large ovoid somata located within *str. radiatum*, with several vertical and radially orientated dendrites which were not restricted to any particular layer; the dendrites of all GRCs possessed dendritic spines (not shown). GRCs showed two main morphological phenotypes, the first dubbed prototypical GRCs; possess a single large-calibre apical dendrite, with oblique dendrites in *str. radiatum*; bifurcating with distal dendritic tufts in *str. L-M*. The basal dendrites of this subtype typically crossed *str. pyramidale* and tufted in *str. oriens* and had an axon resembling that of typical CA1 pyramidal cells.

The dendritic morphology of the other main subtype, dubbed “devil” GRCs (figure 3.8) and consisted of either 1 apical dendrite which bifurcated close (<20 μm) to the soma; or 2 apical dendrites; in both apical dendritic subtypes, distal apical dendritic tufts were similar to CA1 pyramidal cells. Oblique and basal dendrites in both types were typically confined to *str. radiatum*, with an occasional basal dendrite passing into *str. oriens*. Axons of “devil” GRCs generally had a large local arborisation, with local collaterals running parallel to the alveus and ramifying heavily in *str. oriens*; when the axon was preserved a single projection was always observed in the alveus, presumably projecting to either the olfactory bulb or the septum (Gulyas et al, 1998; Bullis et al, 2007).

Passive membrane properties	GRCs (n=11*)
Membrane potential (mV)	60.7 \pm 2.1
Input resistance (M Ω)	126.1 \pm 15.8
Membrane time constant (ms)	21.8 \pm 2.7
Putative I _h “sag”(-250 pA)	3.7 *
AP kinetics	
Threshold (mV)	-41.7 \pm 0.8
Amplitude (mV)	102.3 \pm 4.5
Half-height duration (ms)	0.82 \pm 0.04
Maximum rise-rate (mV.ms ⁻¹)	532.2 \pm 50.4
Maximum decay-rate (mV.ms ⁻¹)	107.3 \pm 5.9
Rise/decay ratio	4.93 \pm 0.4
AHP properties	
Amplitude (fast) (mV)	7.0 \pm 1.4
Amplitude (medium) (mV)	8.7 \pm 0.8
AP discharge properties	
Maximum frequency (Hz)	23.6 \pm 3.4
Rheobase (pA)	89 \pm 1
First-last interspike interval ratio	2.3 \pm 0.5

Table 3.3 Summary of the intrinsic properties of CA1 GRCs. Comparison of the same properties as table 3.1; all data is shown as mean \pm SEM. Note, that voltage-response “sag” data comes from only 1 cell, indicated (*).

The majority of passive and active physiological properties of GRCs were statistically similar to typical CA1 pyramidal cells (table 3.3, $P > 0.05$); the only observed differences came from a ~ 10 mV smaller mean AP amplitude ($P = 0.0132$) and a 40 pA reduction in the mean rheobase required for AP discharge ($P = 0.0371$)

3.7 CA1 GRCs possess large postsynaptic $GABA_B$ R conductances

We observed slow-IPSCs in all 12 identified GRCs; however upon visualisation of biocytin labelling, the apical dendrites had been severed ~ 20 μ m from the soma in 1 cell, which was not analysed further.

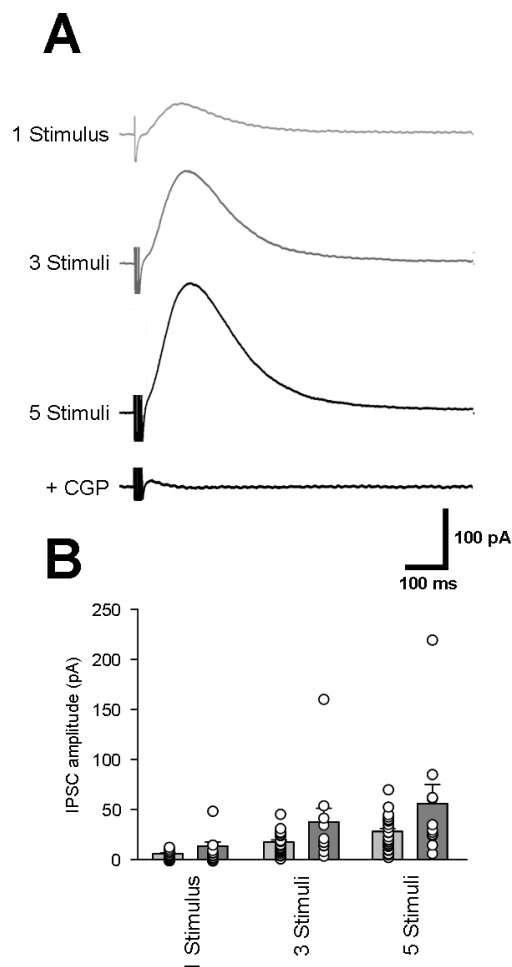


Figure 3.9 $GABA_B$ mediated IPSCs in CA1 GRCs elicited by endogenous GABA release. **A** Representative slow IPSCs a CA1 GRC, induced by 1 stimulus (light grey) and 3 or 5 stimulus trains (dark grey and black, respectively), which were blocked by 5 μ M CGP-55,845 (CGP; black). **B** Mean IPSC amplitudes from the same stimuli as **A**, in 11 CA1 GRCs; individual data is shown overlain (open circles).

Slow-IPSCs could be reliably elicited in GRCs at the border of *str. radiatum/L-M* as for CA1 pyramidal cells, using the 1, 3 and 5 stimuli protocol, which were then blocked by bath application of the selective GABA_BR antagonist CGP-55,845 (5 μ M; figure 3.9.A), confirming that these synaptically evoked slow-IPSCs were mediated by the GABA_BR. We observed mean GABA_BR-mediated responses of 13.2 ± 4.2 pA, 37.4 ± 13.3 pA and 56.0 ± 18.0 pA (respective to the above order) and were equivalent to $11.4 \pm 2.8\%$, $32.2 \pm 8.9\%$ and $48.7 \pm 12.8\%$ of R_i . The amplitudes observed were equivalent to 230%, 214% and 201% of the same responses in CA1 pyramidal cells; albeit only significant following single stimuli ($P=0.0146$) and not so at 3 or 5 stimulus levels ($P= P=0.1145$ and 0.1076 , respectively); at all stimulation levels none of the normalised data were statistically different from regular CA1 pyramidal cells ($P>0.05$, all). However, there is a clear trend for larger GABA_BR mediated responses in GRCs observed at the soma, compared to CA1 pyramidal cells and the lack of significance is most likely due to high variability observed in synaptic GABA_BR-mediated IPSCs within both populations of cells.

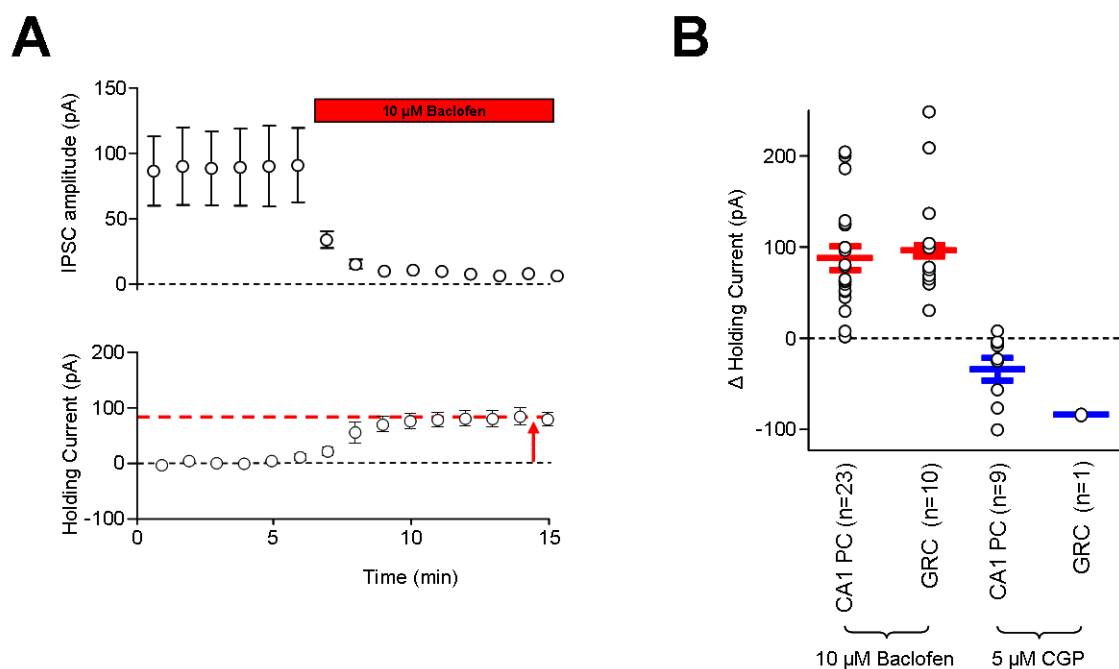


Figure 3.10 Pharmacological characterisation of GABA_BR-mediated currents in CA1 GRCs. A Timecourse of mean synaptic amplitude (top, 5 stimulus train IPSCs) and mean holding current (bottom) at 1 minute intervals during control and 10 μ M baclofen washin (red bar; zero level (dashed line) and maximal change in holding current (red-dashed line and arrow) are indicated.. **B** Peak holding current change in GRCs for baclofen (red; 10 cells) and CGP-55,845 (blue, 1 cell). Data is shown overlain by peak responses for individual cells (open circles).

In addition to determining the level of GABA_B which could be activated by synaptic stimulation, we also quantified the total GABA_BR-mediated conductance in GRCs, as assessed by the application of 10 μM baclofen and then 5 μM CGP-55,845. Baclofen resulted in complete occlusion of GABA_BR-mediated slow-IPSCs in GRCs (figure 3.10.A (top)), consistent with CA1 pyramidal cells, while increasing the holding current required to maintain voltage-clamp in GRCs by an average of 95.7 ± 19.2 pA (figure 3.10.A (bottom)) and $79.0 \pm 13.0\%$ of R_i , neither of which were different to that of CA1 pyramidal cells ($P=0.5701$ and 0.8112 , respectively). This suggests that although GRCs possess larger synaptic GABA_BR responses, this is produced from a pool of receptors no different from that of CA1 pyramidal cells.

The response of GRCs to 5 μM CGP-55,845 was assessed in 1 cell, which compared to pre-baclofen control levels, reduced holding current by 33.9 pA, which was within the same range as CA1 pyramidal cells and suggestive of pre-existing GABA_BR-mediated tonic inhibition in GRCs under control conditions.

3.8 Morphological and physiological characterisation of Dentate Granule Cells (DGCs)

DGCs have been shown previously to have markedly different morphological, physiological and synaptic properties than CA1 pyramidal cells, which we observed in 10 recorded and biocytin-filled DGCs.

The somata of DGCs are small and rounded in shape, with spiny monopolar dendrites (figure 3.11), radiating densely into the molecular layer. A single axon, known as the mossy-fiber, emerges from the hillock at the lower pole of DGC somata, with a small local arborisation in the hilus, and the main axon collateral which projects into *str. lucidum* of area CA3, forming varicose mossy-fibre boutons onto thorny-excrescences on the apical dendrites of CA3 pyramidal cells (indicated in figure 3.11).

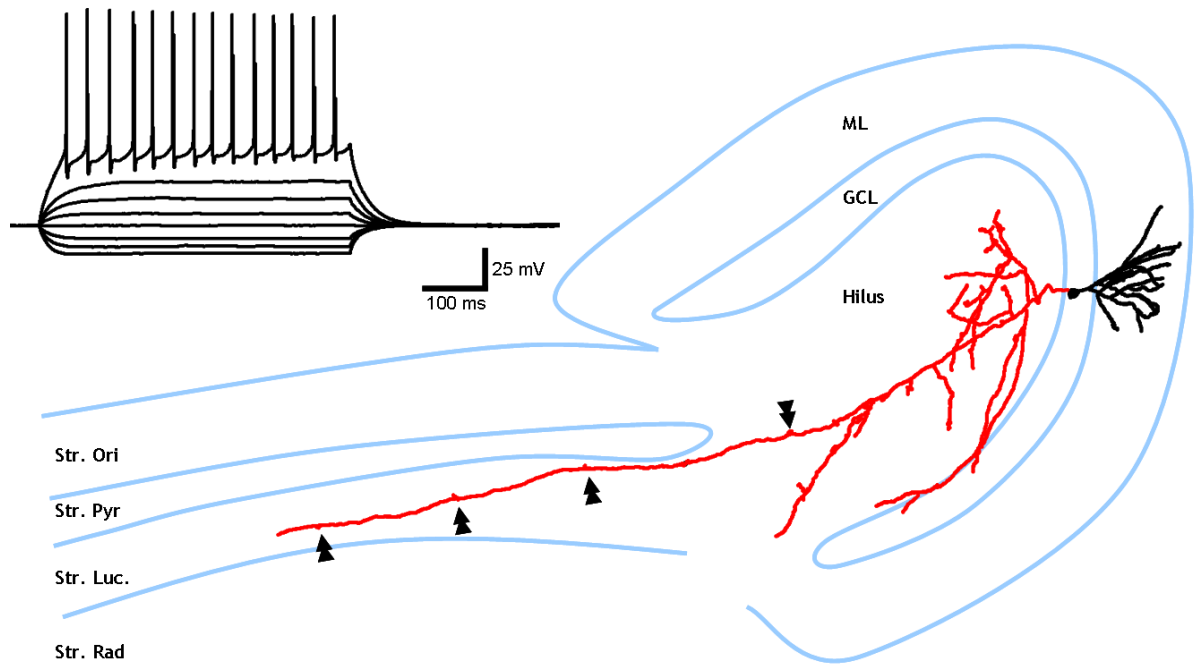


Figure 3.11 Morphological and physiological characterisation of DGCs. A flattened 3D reconstruction of a DGC is shown, with the axon (red) and somatodendritic axis (black) reconstructed in respect to hippocampal and DG lamina (blue lines); mossy-fiber boutons are indicated (double arrowheads). Inset, an AP discharge train in response to a family of hyper- to depolarising current steps; note the large fast-AHP component present following each AP.

Besides being morphologically identifiable, DGCs also have highly unique physiological properties, differing greatly from CA1 pyramidal cells and GRCs (see table 3.4). By comparison to CA1 pyramidal cells, DGCs are more hyperpolarised, with larger R_i than CA1 pyramidal cells ($P=0.0039$ and 0.0002 , respectively) despite having a similar membrane time-constant ($P=0.4216$).

DGC APs waveforms do not differ in amplitude ($P=0.9864$) or maximal rise rate ($P=0.5270$) from CA1 pyramidal cells; however maximal decay rate is significantly faster ($P=0.0051$), resulting in reduced rise/decay ratio, compared to CA1 pyramidal cells ($P=0.0002$); half-height duration is consequentially shorter ($P=0.0274$). These data suggest that DGCs either possess a larger complement or a different population of K_v channels than those present in CA1

pyramidal cell; which was confirmed by fast and medium-AHP components larger than CA1 pyramidal cells with the same properties ($P < 0.0001$ and $P = 0.0053$, respectively). DGCs display AP inter-spike interval accommodation to a similar degree as CA1 pyramidal cells ($P = 0.6366$) and AP discharge in response to 250 pA depolarisation is of similar frequency ($P = 0.3211$).

Passive membrane properties	DGC (n=10*)
Membrane potential (mV)	-72.9 ± 4.3
Input resistance ($M\Omega$)	265.5 ± 44.8
Membrane time constant (ms)	22.5 ± 2.9
Putative I_h “sag” (mV)	0.83 *
AP kinetics	
Threshold (mV)	-31.8 ± 2.0
Amplitude (mV)	111.8 ± 7.6
Half-height duration (ms)	0.68 ± 0.05
Maximum rise-rate ($mV \cdot ms^{-1}$)	537.5 ± 73.8
Maximum decay-rate ($mV \cdot ms^{-1}$)	145.9 ± 13.0
Rise/decay ratio	3.6 ± 0.3
AHP properties	
Amplitude (fast) (mV)	17.8 ± 1.6
Amplitude (medium) (mV)	14.8 ± 1.8
AP discharge properties	
Maximum frequency (Hz)	29.4 ± 6.0
Rheobase (pA)	101 ± 22
First-last interspike interval ratio	1.8 ± 0.4

Table 3.4 Summary of the intrinsic properties of DGCs. Comparison of the same properties as table 3.1; all data is shown as mean \pm SEM. Note, that voltage-response “sag” data comes from only 1 cell, indicated (*).

3.9 DGCs possess large postsynaptic GABA_BR conductances

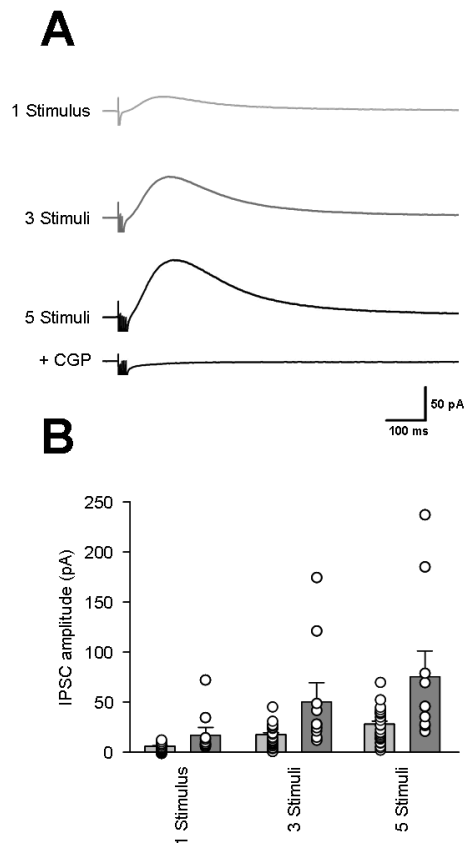


Figure 3.12 GABA_BR mediated IPSCs in DGCs elicited by release of endogenous GABA. A Representative slow IPSCs in a DGC, induced by 1 stimulus (light grey) and 3 or 5 stimulus trains (dark grey and black, respectively), which were blocked by 5 μ M CGP-55,845 (CGP; black). **B** Mean IPSC amplitudes at the same stimulus levels **A**, in 10 DGCs; individual data shown overlaid (open circles).

To confirm the presence of functional GABA_BR in DGCs, under the same circumstances as CA1 pyramidal cells previously, we utilised the same 1, 3 5 stimuli protocol, in the presence of AP-V, NBQX and bicuculline. We observed large (>5pA at 1 stimuli) slow-IPSCs in all 10 cells that were recorded and subsequently morphologically identified (Figure 3.11.A). Slow-IPSCs produced in response to a single stimulus had a mean amplitude of 16.8 ± 6.9 pA, 3 and 5 stimulus trains resulting in mean IPSCs of 50.3 ± 17.8 and 76.1 ± 24.6 pA, respectively, which were abolished in the presence of 5 μ M CGP-55,845 (figure 3.12.A). GABA_BR-mediated slow-IPSCs in DGCs were 262.1%, 250.0% and 247.3% larger than those observed in CA1 pyramidal cells at the same stimulus levels (P=0.0141, 0.0189, 0.0109, respectively). GABA_BR-mediated slow IPSC

amplitudes in DGCs normalised to R_i were: $12.6 \pm 8.1\%$, $35.5 \pm 19.9\%$ and $52.4 \pm 27.2\%$, which were not statistically different from CA1 pyramidal cells ($P > 0.05$, all).

We assessed whether larger IPSCs observed in DGCs were the result of increased $GABA_B$ R content of these cells currents or otherwise; as before we bath applied $10 \mu\text{M}$ baclofen, which resulted in rapid and complete occlusion of the synaptic slow-IPSC, while increasing the holding current required to maintain voltage clamp in 9 cells (figure 3.13). The baclofen mediated response seen in DGCs had a mean amplitude of $111.7 \pm 28.3 \text{ pA}$, which was not different from that of CA1 pyramidal cells ($P = 0.5025$), suggesting a similar level of functional $GABA_B$ Rs in DGCs, as in CA1 pyramidal cells. The baclofen response, normalised to the R_i was equivalent to: $72.4 \pm 29.1\%$, not statistically different from that of CA1 pyramidal cells ($P = 0.3788$)

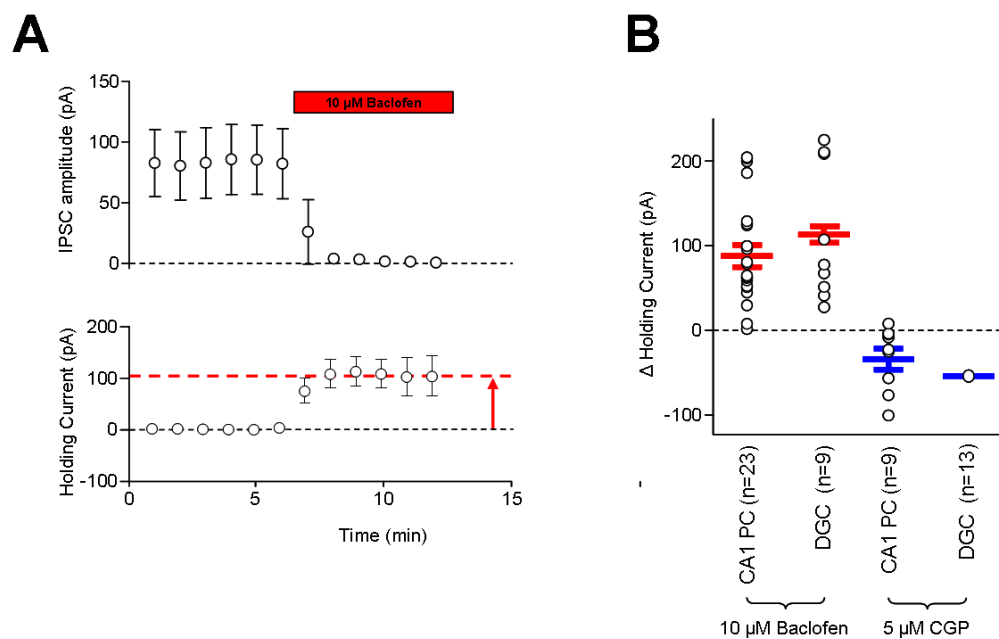


Figure 3.13 Pharmacological characterisation of $GABA_B$ R-mediated currents in DGCs. **A** Timecourse of mean synaptic amplitude (top, 5 stimulus train IPSCs) and holding current (bottom) at 1 minute intervals during control and $10 \mu\text{M}$ baclofen washin (red bar); zero level (dashed line) and maximal holding current change (red-dashed line and arrow) are indicated. **B** Maximal holding current change in DGCs for baclofen (red; 9 cells) and CGP-55,845 (blue, 1 cell). Data is shown overlain by peak responses for individual cells (open circles).

In 1 cell we applied the selective GABA_BR antagonist CGP-55,845 (5 μ M), which resulted in reversal of holding current change observed in the presence of baclofen, resulting in 55.4 pA reduction in holding current, from baseline levels, suggesting the presence of GABA_BR-mediated tonic-inhibition in DGCs.

3.10 Conclusions

From the results presented in this chapter we have confirmed that CA1 pyramidal cells possess a functional GABA_BR-mediated slow-IPSC, which is mediated by inward-rectifying potassium channels, presumably of the Kir 3.n subtype. Additional to this, we have shown for the first time that GABA_BR-mediated currents in CA1 pyramidal cells are different between the two major dendritic arbours of CA1 pyramidal cells, with small GABA_BR currents in basal dendrites, relative to large IPSCs observed in apical dendrites. We have also shown that in GRCs, the other main principal cell type in CA1; show an increased synaptic GABA_BR response resulting from the same stimuli. Finally, we have established that DGCs we observe a GABA_BR-mediated conductance, which is 2-fold larger than that of CA1 pyramidal cells. Suggesting that GABA release acting via GABA_BRs will provide a more robust hyperpolarisation of dendritic membranes in DGCs and GRCs. These overt differences in GABA_BR mediated signalling, arising from either single or repetitive stimulation of inhibitory afferents in CA1 and DG principal cells, are produced from a near identical GABA_B whole cell current, suggesting equivalent populations of functional, membrane localised GABA_B; which fits well with that of Kulik et al (2003), who observed GABA_{B1} and _{B2} receptor subunits in dendritic compartments of CA1, CA3 pyramidal cells and DGCs.

As many INs release GABA onto the dendrites of principal cells, timing them to the prevalent network oscillatory activity (Klausberger et al, 2003), the presence of GABA_BRs on these dendrites suggests a role for this receptor in this synchronisation. Slow theta-oscillations occur on a similar timescale to that of GABA_B activation and inactivation; making it seem likely that these dendritically

located GABA_BRs are involved in feedback inhibition, timed to given oscillation states of the IN network (Scanziani, 2000). The stronger synaptic GABA_BR responses in GRCs and DGCs, suggest that these cells are more inhibited during the down-states of theta-oscillatory activity, than CA1 pyramidal cells, leading to more tight control of glutamate release from these cells, which is synchronised to slow network oscillations.

4. Post-synaptic GABA_B receptors in PV-IR INs of the hippocampus

We aimed to determine the functional GABA_BR content of neurochemically and morphologically identified PV-IR INs in the hippocampus. Previous immunofluorescence work of Sloviter et al (1999) suggested that PV-IR INs in hippocampal subfield CA1 possess very few functional GABA_B receptors at the somatic level. However, electrophysiological work by Mott and Lewis (1999) showed that neurochemically unidentified basket cells in the DG possessed GABA_B receptor-mediated post-synaptic currents. As a major subset of basket cells in the DG express PV, we questioned whether the results from Sloviter et al (1999) were consistent with more sensitive imaging combined with physiological and pharmacological investigation. In the following chapter we show the presence of GABA_B receptors, detected with the use of whole-cell patch-clamp, recorded from morphologically identified PV-IR PI and DI cell types, in both the hippocampus and the DG. Additionally, we also show that the GABA_B receptor-mediated postsynaptic conductance is carried by an inward-rectifying K⁺-channel, further confirmed through the presence of Kir3 effector channels by electron microscopic analysis.

4.1 CA1 PV-IR INs express GABA_{B1} receptor subunits on dendritic membranes.

PV immunoreactivity was easily identified by fluorescence microscopy images, as shown in figure 4.1.A (green pseudocolour) with a high density of dendritic arborisation in *str. radiatum* and with somata located in and around *str. pyramidale*. Consistent with previous immunocytochemical work we observed very low level co-localisation of the GABA_{B1} receptor-subunit (figure 4.1.A; red pseudocolour) with PV, suggestive of a low number of receptors present at the soma. Nevertheless, GABA_{B1} labelling in PV-IR INs was above background, in some cases stronger than that of neighbouring CA1 pyramidal cells.

Furthermore, we assessed the co-localisation of immunogold particles corresponding to the GABA_{B1} receptor subunit in electron-micrographs of HRP/DAB stained PV immunoreactive dendrites; we observed a density of immunogold particles comparable to that of CA1 pyramidal cell dendrites (figure 4.1.C/D). The density of GABA_{B1} receptor labelling in PV-IR dendrites was 12.8 ± 1.3 particles. μm^{-2} (22 dendrites), comparable to that of pyramidal cells (12.1 ± 1.9 particles. μm^{-2} , 9 dendrites; $P=0.8789$). These data show that PV-IR INs express GABA_B receptors in dendritic compartments, based on B1 subunit labelling.

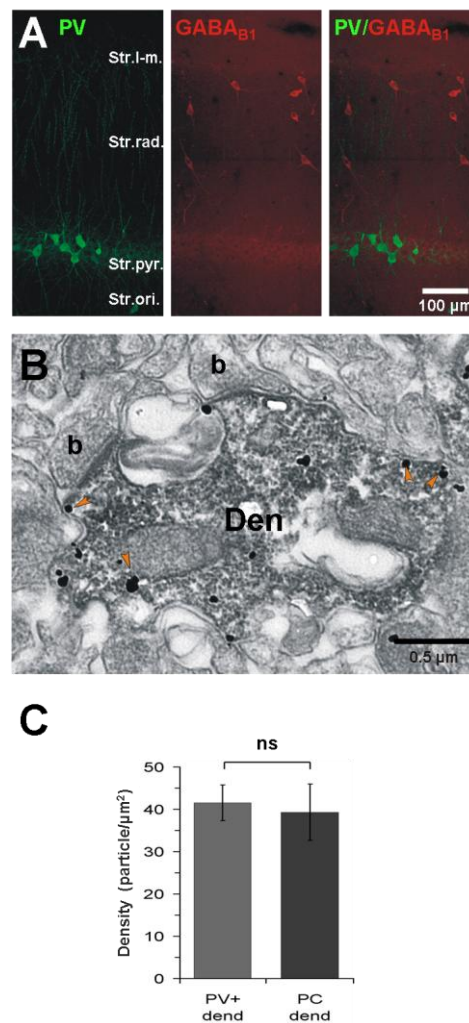


Figure 4.1 Immunocytochemical localisation of GABA_{B1} receptor subunits to CA1 PV-IR INs. **A** Immunocytochemical co-localisation of GABA_{B1} (red pseudocolour) and PV (green pseudocolour) and merged (right); hippocampal laminations indicated. **B** Immunogold particles corresponding to GABA_{B1} receptor subunits (orange arrowheads) at the plasma membrane of PV-IR dendrites (Den); several glutamatergic synapses are present on the dendritic shaft, indicated (b), confirming inhibitory cell-type. **C** Quantification of B1 subunit density in PV-IR dendrites (PV+ dend) and CA1 pyramidal cell dendrites (PC dend). Statistics shown: ns (not significant)- $P>0.05$

4.2 Presence of Kir3 channel subunit, Kir3.2, in CA1 PV-IR IN dendritic membranes

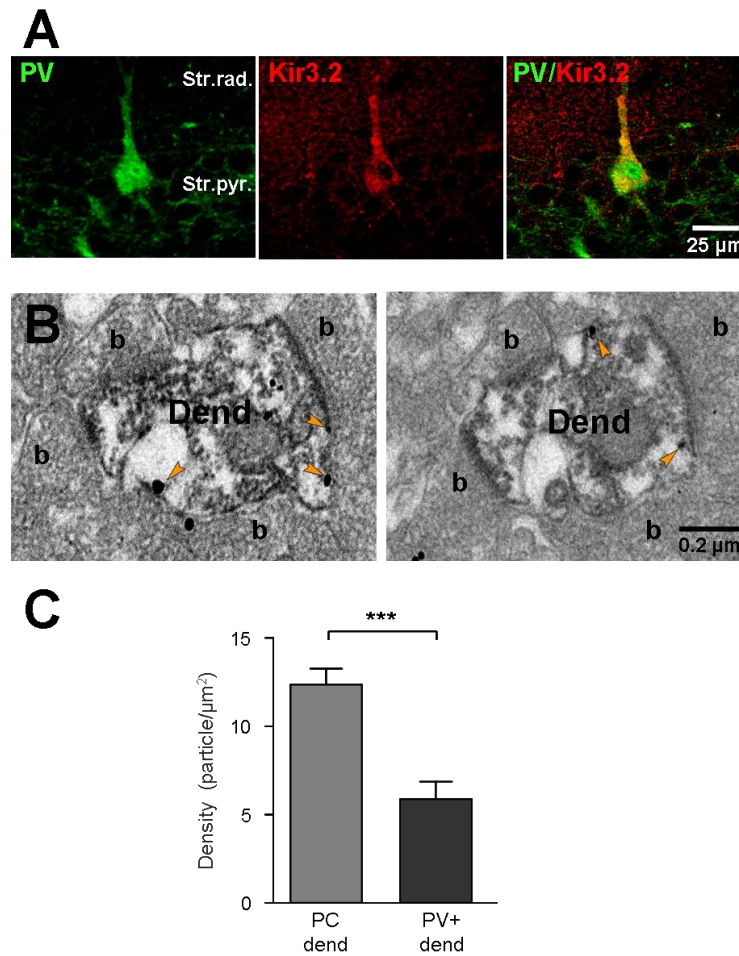


Figure 4.2 Immunocytochemical localisation of Kir3.2 channel subunits to CA1 PV-IR INs. **A** Immunocytochemical co-localisation of Kir3.2 (red pseudocolour) with PV (green pseudocolour) and merged (right); hippocampal laminations indicated. **B** Serial ultrathin sections of a PV-IR dendrite (den) with immunogold labelling for Kir3.2 (orange arrowheads); several glutamatergic synapses are formed with the dendrite, indicated (b). **C** Quantification of Kir3.2 density in PV-IR dendrites (PV+ dend) and CA1 pyramidal cell dendrites (PC dend). Statistics shown: ***- $P < 0.0001$

Additional to the presence of GABA_{B1} subunit, we also saw that effector Kir3.2 channels are also expressed in PV-IR IN somata and apical dendrites, at the light microscopic level (Fig 4.2.A). Immunogold particles corresponding to Kir3.2 channel subunits were detected on the membrane of PV-IR dendrites (figure 4.2.B/C) with a density of 5.9 ± 1.0 particles.µm⁻² (20 dendrites), which was substantially lower than in local CA1 pyramidal cells dendrites (12.4 ± 0.9 particles.µm⁻², 20 dendrites; $P < 0.0001$).

These findings confirm that GABA_BR effector channels are present on the membrane of PV-IR INs, if at a lower level, which may reflect a smaller role for metabotropic receptor/Kir3 signalling overall in PV-IR INs compared to CA1 pyramidal cells. These data confirm the feasibility of observing GABA_B receptor-mediated conductances in neurochemically identified PV INs.

4.3 Identification of PV-IR INs in area CA1 of the hippocampus.

As stated earlier, PV-IR INs display several distinct morphological phenotypes: PI INs, principally basket and axo-axonic cells and DI INs, bistratified cells. At post-synaptic level we have not distinguished between different PI subtypes, but ~90% of cells examined were confirmed as basket-cells, with 1-2 suspected axo-axonic cells which were not confirmed. Basket cells were identified as having a large, pyramidal-like somata located in, or within close proximity to; *str. pyramidale*. Several apical dendrites projected either radially or vertically from the somata, spanning all hippocampal lamina (figure 4.3.A) and occasionally dendritic beading was also observed. A single axon was observed originating from an apical dendrite, with the majority (~80%) of axon ramifying in *str. pyramidale*; occasionally extending into either *str. oriens* or *radiatum*.

DI bistratified cells also have large somata localised to *str. pyramidale* which shows strong labelling for PV (figure 4.4.B), with radially, vertically or horizontally extending dendrites, distinctive from basket-cells. The reconstruction of a bistratified cell in figure 4.4.A shows these dendrites projecting radially, vertically and horizontally in all lamina, bar *str. L-M*. The predominant identifying characteristic of PV-IR DI cells is the dense axonal arborisation in *str. radiatum* and *oriens*, innervating dendritic shafts of CA1 pyramidal cells; axons in both of these lamina account for up to ~90% of the total axonal length, with typically ~10% of axon collaterals found in *str. pyramidale*, mostly passing across from the neuropil.

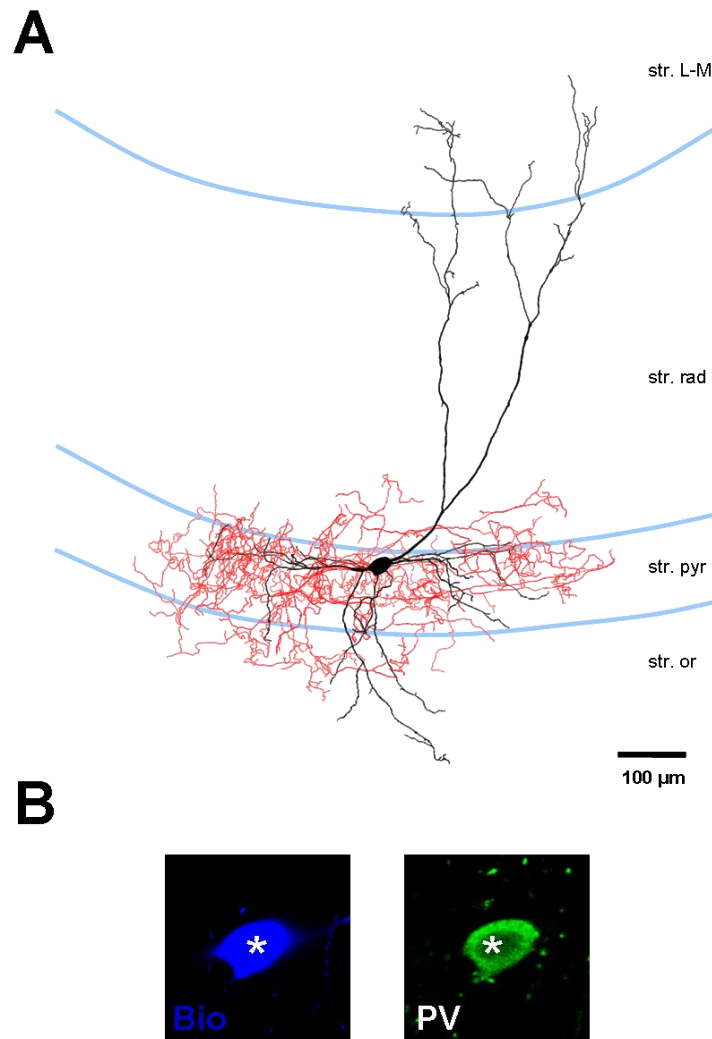


Figure 4.3 Morphological and neurochemical identification of a PV-IR PI IN, in CA1. **A** 3D reconstruction of a CA1 PV-IR basket-cell, with respect to hippocampal lamination (blue lines); somatodendritic axis (black) and axonal arbour (red) are shown. **B** Co-localisation of PV (right, green pseudocolour) with biotin/avidin (left, blue pseudocolour) in the same cell as **A**; immunofluorescence shows near-complete cytoplasmic overlap.

As we saw earlier for CA1 pyramidal cells, morphological analysis confirmed initial physiological identification of neurons, made online. PV-IR INs were reliably identified via physiological characteristics, which in some ways was as reliable as immunocytochemistry to determine subtype due to the unique fast-spiking nature of these cells in the CA1 and DG.

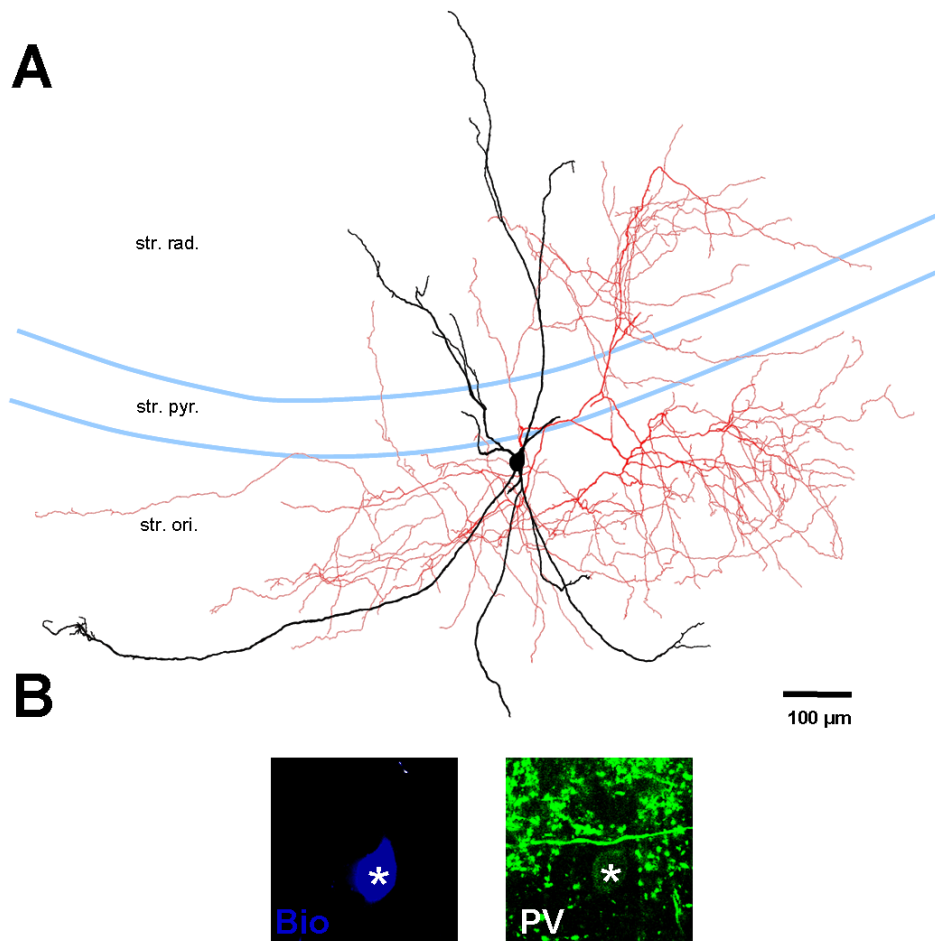


Figure 4.4 Morphological and neurochemical identification of a PV-IR DI cell, in CA1. A 3D reconstruction of a CA1 PV-IR bistratified cell; the somatodendritic axis (black) and axonal arbour (red) are shown, with respect to hippocampal laminations (blue lines). B PV (right, green pseudocolour) and biotin/avidin (left, blue pseudocolour) colocalise in same cell somata.

This fast-spiking phenotype is seen conclusively in figure 4.5.A; where in response to -250 to 250 pA hyper/depolarising current steps, both identified PI and DI cell types display a characteristic high-frequency AP discharge train, which shows no spike-frequency accommodation. Indeed, average maximal AP discharge frequency is ~3-times higher in PI cells than for CA1 pyramidal cells and ~6-times higher in PV-IR DI cells (see table 4.1).

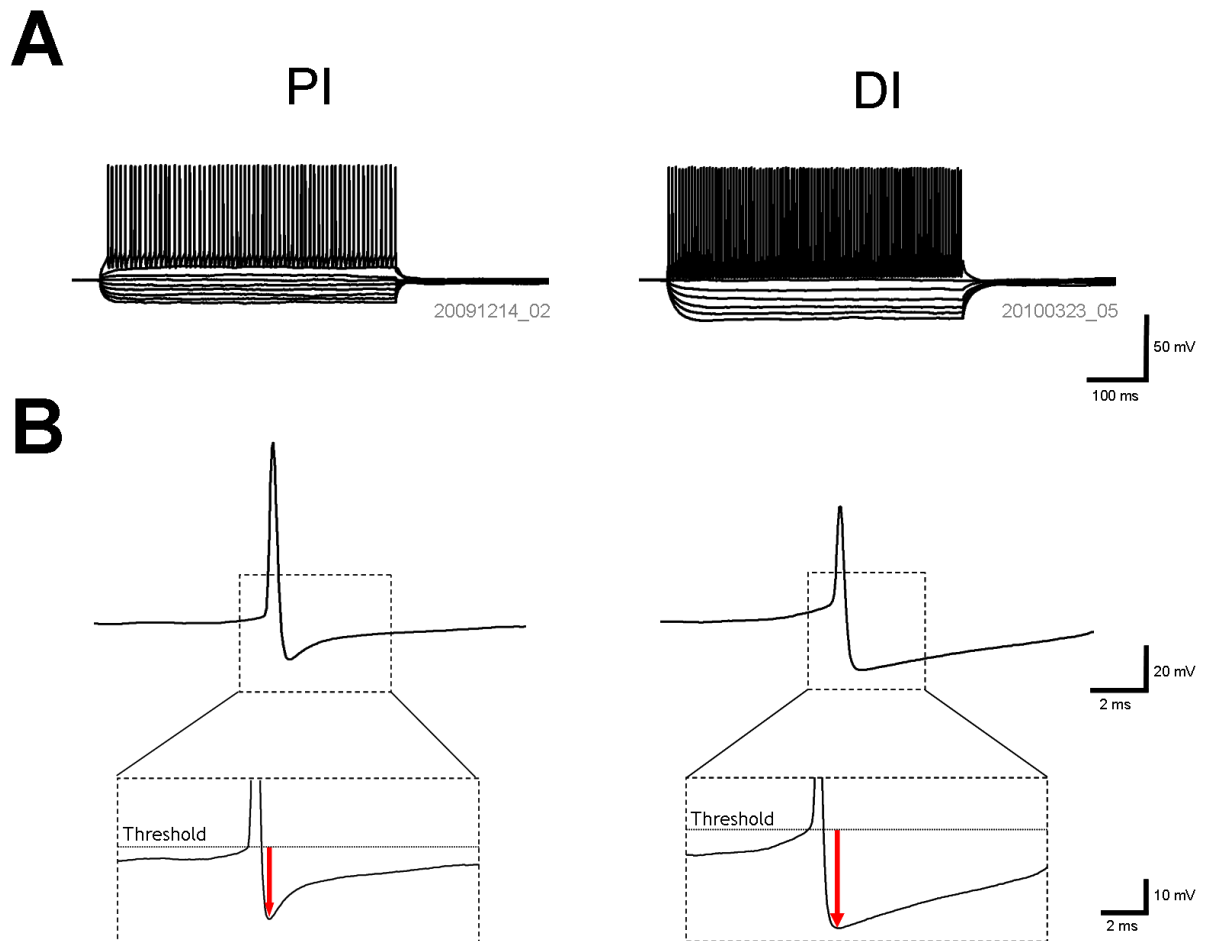


Figure 4.5 Trains of APs and AP waveforms in PV-IR PI and DI INs. **A**, families of hyper-to-depolarising current pulses (50 pA steps, -250 pA to 250 pA range) in representative PV-IR PI (left) and DI (right) cells; only maximal AP discharge has been shown for clarity. **B** The first AP elicited in both cells has been shown; with an expanded view of both threshold and AHP (inset). Red arrows indicate peak AHP amplitude; note the fast-AHP in both traces and the less fast/medium-AHP boundary in the DI trace.

A distinguishing feature of PV-IR IN intrinsic physiology is the absence of I_h mediated voltage-sag following hyperpolarisation, when compared to CA1 pyramidal cells ($P=0.0006$ (PI) and 0.0158 (DI)), suggesting that I_h is not activated by induced hyperpolarisation (Aponte et al 2006). The membrane time-constant is faster in PV-IR PI cells, than for CA1 pyramidal cells albeit not significantly so ($P=0.0832$), while DI cells show no difference ($P=0.9854$), with there being no statistical difference between PI and DI cells ($P=0.2331$).

The R_i of PI and DI cells were similar to that observed in CA1 pyramidal cells ($P=0.9581$ and 0.1250 respectively). These parameters are similar to that quoted for PV-IR INs by Kawaguchi and Kubota (1993) for the frontal cortex and Doischer et al (2008) for basket cells in the DG.

Passive membrane properties	CA1 pyramidal cells (n=27)	PV-IR PI cells (n=15)	PV-IR DI cells (n=9)
Membrane Potential (mV)	-62.9 ± 1.2	-58.2 ± 1.7	-58.6 ± 1.6
Input Resistance ($M\Omega$)	102.2 ± 13.1	91.8 ± 11.9	144.1 ± 29.7
Membrane Time Constant (ms)	22.0 ± 2.6	15.4 ± 2.6	20.6 ± 3.5
Putative I_h "sag" (mV)	3.0 ± 0.2	2.0 ± 0.3	1.9 ± 0.2
AP kinetics			
Threshold (mV)	-39.8 ± 1.0	-34.1 ± 1.3	-31.0 ± 2.4
Amplitude (mV)	113.8 ± 2.1	82.8 ± 3.6	78.5 ± 3.7
Half-height duration (ms)	0.84 ± 0.04	0.38 ± 0.05	0.48 ± 0.07
Maximum rise-rate ($mV.ms^{-1}$)	610.6 ± 31.4	459.7 ± 35.2	304.0 ± 39.0
Maximum decay-rate ($mV.ms^{-1}$)	109.3 ± 4.7	339.0 ± 36.9	238.4 ± 30.6
Rise/Decay Ratio	5.6 ± 0.3	1.57 ± 0.22	1.31 ± 0.08
AHP properties			
Amplitude (fast) (mV)	5.9 ± 0.6	22.6 ± 1.9	23.7 ± 1.9
Amplitude (medium) (mV)	9.4 ± 0.5	12.4 ± 1.8	13.4 ± 1.7
AP discharge properties			
Maximum frequency (Hz)	23 ± 2	81.9 ± 9.6	140.7 ± 24.4
Rheobase (pA)	131.1 ± 13.5	208.0 ± 54.2	1.0 ± 0.1
Interspike interval ratio	1.55 ± 0.14	0.99 ± 0.1	0.94 ± 0.7

Table 4.1 Summary of intrinsic properties of PI and DI PV-IR INs in CA1. Data is shown from identified neurons, with CA1 pyramidal cell data alongside for comparison. All data is shown as mean \pm SEM

Compared to CA1 pyramidal cells, PV-IR PI and DI cells both have much faster APs, characterised by shorter half-height duration (figure 4.5.B and table 4.1). This difference is due, in no small part to a reduced Na_V conductance, evidenced by a smaller maximal rise-rate of both cells ($P=0.0020$ and 0.0006 , respectively)

and a stronger K_v component, seen as an increased decay rate ($P=0.0001$ and 0.0012 , respectively). This overall relationship is reflected well by the rise/decay ratio, which is ~ 4 -times larger in CA1 pyramidal cells, as opposed to both groups of PV-IR neurons ($P<0.0001$, both). PV-IR PI and DI cells had fast-AHPs, much larger than in CA1 pyramidal cells ($P<0.0001$, both) observed in all cells. Medium -AHP was only measurable in 60% of PI cells and 44% of DI cells (see table 4.1), when it was present it was larger than in CA1 pyramidal cells for both cell types, statistically so in DI cells ($P=0.0222$), but not in PI cells ($P=0.1088$). These features of AP discharge are likely due to the presence of $K_v3.1b$ (Du et al, 1996; Chow et al, 1999), endowing PV-IR neurons with rapid K_v activation and a short AP refractory period, leading to the fast-spiking phenotype.

4.4 PV-IR INs possess $GABA_B$ R conductances, which are different between morphological subtypes

We recorded $GABA_B$ R-mediated conductances in PV-IR INs in an identical fashion to that of CA1 pyramidal cells; in that we recorded slow IPSCs in response to stimulation of GABAergic axons at the *str. radiatum/LM* border, in the presence of ionotropic glutamate and GABA receptor blockers ($50 \mu\text{M}$ APV, $10 \mu\text{M}$ NBQX and $10 \mu\text{M}$ bicuculline or SR-95,531). We recorded $GABA_B$ R-mediated currents in 26 INs, physiologically identified as fast-spiking, which were later shown to be PV-IR. The mean $GABA_B$ R-mediated IPSC amplitude in response to 1, 3 and 5 stimuli trains (200 Hz) was $4.0 \pm 1.3 \text{ pA}$, $13.0 \pm 4.1 \text{ pA}$ and $19.5 \pm 5.5 \text{ pA}$ (figure 4.6.A), significantly different from that of CA1 pyramidal cells ($P=0.00339$, 0.0107 , 0.0063 ; respectively). When normalised to the input resistance of the same cells, we saw a rational response amplitude of: $6.6 \pm 2.6\%$, $21.6 \pm 8.3\%$ and $30.3 \pm 11.4 \%$ (relative to the same order as above), still statistically smaller than the same ratios in CA1 pyramidal cells ($P= 0.0151$, 0.0169 , 0.0095 , respectively).

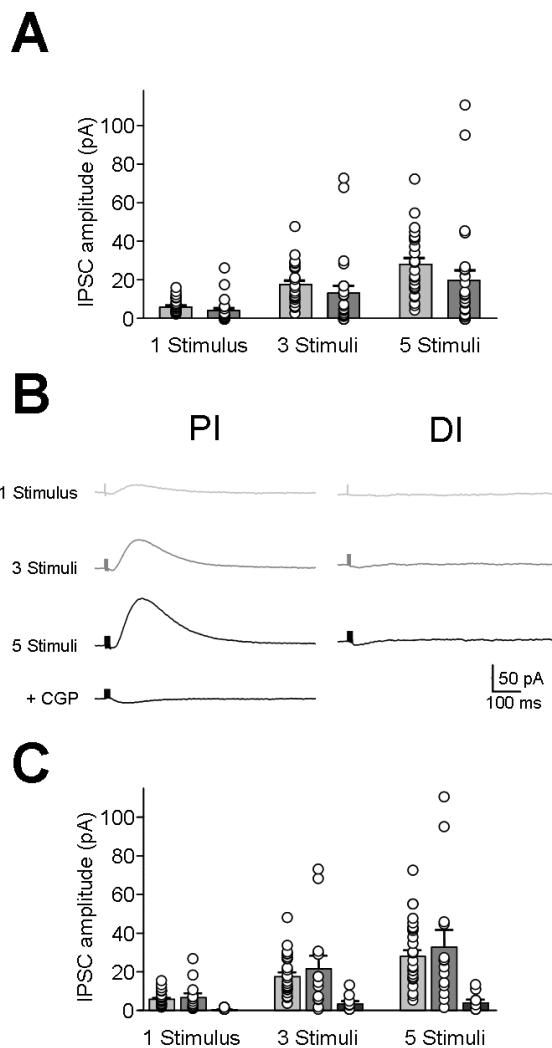


Figure 4.6 GABA_B mediated IPSCs in CA1 PV-IR INs, elicited by release of endogenous GABA. **A** Mean IPSC amplitudes of neurochemically identified PV-IR cells (dark grey bars) compared to CA1 pyramidal cells (light grey bars), at 1, 3 and 5 stimuli levels; data from individual cells is shown overlain (open circles) **B** Representative IPSC traces at 1,3 and 5 stimuli levels (indicated, light, medium and dark grey traces, respectively) in both PV-IR PI cell (left) PV-IR DI cells (right). The GABA_BR antagonist CGP-55,845 (5 μM) fully blocked IPSCs in PI cells (black trace). **C** Bar chart of mean IPSC amplitudes for 1,3 and 5 stimuli levels, with PI (medium grey bar) and DI (dark grey bar) cell types dissected based morphological subtype; compared to CA1 pyramidal cells (lightest grey bar).

These data showed a high degree of heterogeneity; hence we asked whether there is a difference in the functional GABA_BR-mediated conductances between the two morphological classes; PI and DI cells. In figure 4.6.C we show the mean GABA_BR-mediated IPSC amplitudes for both PI and DI, compared to CA1 pyramidal cells. We found that PV-IR PI cells responded to synaptic stimulation with large amplitude, slow- IPSC amplitudes of: 6.4 ± 2.1 pA (14 cells), $20.1 \pm$

6.5 pA (14 cells) and 30.8 ± 8.6 pA (15 cells); at 1, 3 and 5 stimuli levels respectively were not statistically different from the IPSC amplitudes observed for CA1 pyramidal cells, $P= 0.6021, 0.8001$ and 0.8798 (relative to previous ordering). The normalised amplitudes of these responses were: $10.2 \pm 3.9\%$, $32.1 \pm 12.4\%$ and $46.4 \pm 17.2\%$ and were also no different from that of CA1 pyramidal cells ($P=0.6603, 0.4190$ and 0.4009 , respectively).

PV-IR DI cells, by contrast, had substantially lower slow-IPSC amplitudes at all levels: 0.4 ± 0.2 pA, 3.2 ± 1.5 pA and 4.0 ± 1.7 pA at 1, 3 and 5 stimuli respectively. These data are significantly different from both CA1 pyramidal cells ($P=<0.0001, 0.0002, <0.0001$, respectively) and PV-IR PI cells ($P=0.0004, 0.0107, 0.0010$, respectively), suggesting a much lower level of synaptically evoked GABA_BR-mediated currents. We also normalised these mean amplitudes to the R_i of the same cells, which resulted in PV-IR DI cells having relative IPSC amplitudes of: $0.2 \pm 0.1\%$, $3.3 \pm 2.5\%$ and $3.6 \pm 2.3\%$; substantially less than CA1 pyramidal cells ($P= <0.0001, 0.0004$ and 0.0001 , respectively) and PV-IR PI cells ($P=0.0003, 0.0105, 0.0013$, respectively).

As described in chapters 2 and 3, once we characterised 10 minutes of baseline synaptic IPSC recording, we then applied the selective GABA_BR agonist baclofen ($10 \mu\text{M}$) to the bath for 5 minutes, followed by application of the selective GABA_BR antagonist CGP-55,845 ($5 \mu\text{M}$). The time-course of baclofen and CGP-55,845 washin can be seen in figure 4.7. As we would expect the resulting slow synaptic IPSCs were occluded by baclofen in PV-IR PI cells, with no effect on IPSC amplitude in DI cells (fig 4.7.A, top). Slow-IPSCs remained absent following CGP-55,845 washin, due to a switch from occlusion to antagonism of GABA_BRs.

Baclofen induced an increase in holding current in the voltage-clamped PV-IR PI cells of 105.7 ± 18.4 pA (13 cells), which was ~21% larger than principal cells but not significantly so ($P=0.3946$). This response was equivalent to $149.6 \pm 44.5\%$ of R_i , similar to that of CA1 pyramidal cells ($P=0.3232$). Application CGP-55,845 following baclofen application returned holding-current to 3.05 ± 18.02 pA (4

cells) above control levels. This small residual current suggests possible tonic inhibition, mediated by the GABA_BRs, in PV-IR PI INs under control conditions. This result was similar to that observed in CA1 pyramidal cells (P=0.1483), suggestive of a small component of tonic inhibition in the dendrites of both cell types. This is not conclusive due to small numbers of experiments and was merely a *post hoc* observation of the data.

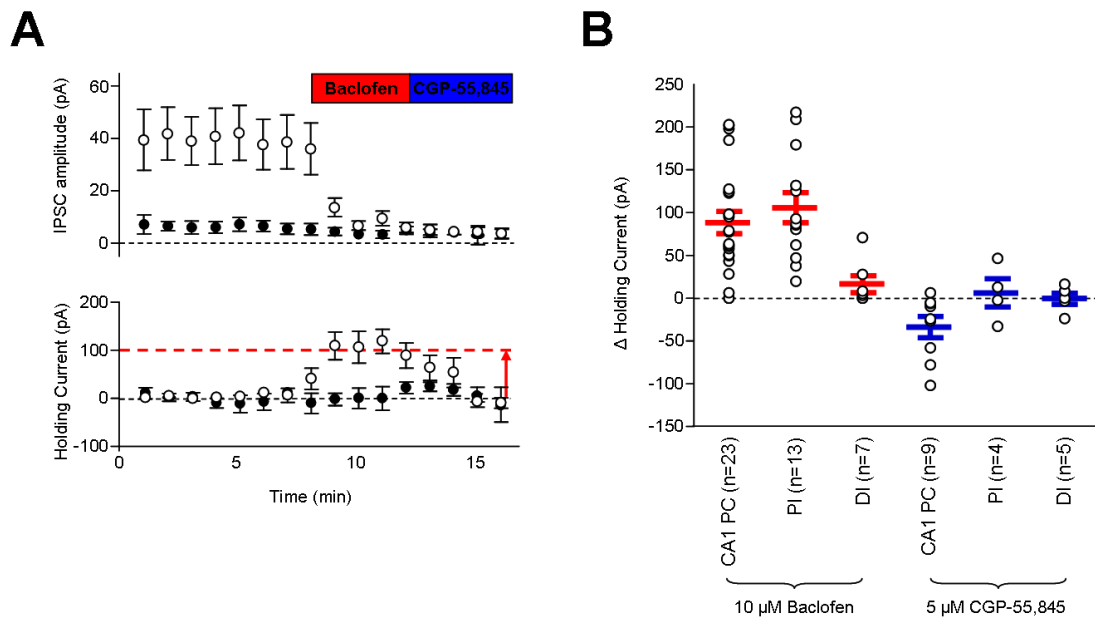


Figure 4.7 Pharmacological characterisation of GABA_BR-mediated currents in PV-IR INs of the CA1. **A** Timecourse of mean synaptic amplitude (top, 5 stimuli train IPSCs) and mean holding current (bottom) at 1 minute intervals during control period (~7 minutes), 10 μ M baclofen washin (red horizontal bar) and 5 μ M CGP-55,845 washin (blue horizontal bar). The zero level (dashed line) and maximal holding current change in PV-IR PI cells (red-dashed line) are shown; with difference indicated (red arrow) for the latter. **B** Maximal responses for both baclofen (red) and CGP-55,845 (blue) for CA1 pyramidal cells (CA1 PC), PV-IR PI cells (PI) and DI cells (DI). Data is shown overlain by peak responses for individual cells (open circles).

PV-IR DI INs, consistent with IPSC data shown above, did not show a large response to the application 10 μ M baclofen to the perfusing ACSF, with a mean increase in holding current of 16.4 ± 10.5 pA (7 cells), equivalent to $16.4 \pm 10.5\%$ of R_i . This response to baclofen was substantially smaller than for PV-IR PI cells and CA1 pyramidal cells both as raw values (P=0.0020 and 0.0052, respectively) or as normalised data (P=0.0015 and 0.0014, respectively). CGP-55,845 resulted in a return of the small baclofen response to 3.6 ± 9.9 pA above control levels,

not significantly different from that observed in PV-IR PI cells ($P=1.000$); suggesting no difference in tonic inhibition in PV-IR DI cells.

This physiological data suggests that IPSC and pharmacological phenomena mediated by the GABA_BR are present in PV-IR INs, showing differential responses between morphological phenotypes. PI INs have GABA_BR-mediated slow-IPSCs and baclofen currents similar to those seen in CA1 pyramidal cells; while DI INs show significantly reduced effects through the same receptor.

4.5 GABA_BR-mediated conductances in PV-IR PI INs are mediated by an inward-rectifying K⁺ channel.

To confirm that the GABA_BR-mediated effects we observed in PV-IR PI cells were produced by a similar mechanism to that seen in CA1 pyramidal cells, we tested the reversal potential and voltage-dependence of both synaptic and pharmacological effects. As seen in figure 4.8.A and B it is clear that slow-IPSPs, recorded in current-clamp; in PV-IR PI cells reverse at -100.9 ± 6.0 mV (4 cells), indicating K⁺ movement across the membrane; similar to that observed in CA1 pyramidal cells ($P=0.6477$). Similar to CA1 pyramidal cells, we saw little evidence of voltage-dependency of the synaptic potential over the V_M range tested.

We also tested the current response of PV-IR PI cells, utilising ramp-test protocols (chapter 3), similar to those suggested by Bean and Sodickson (1996). We tested the current-response before and after baclofen application (Ramp 1, 3 cells) and during baclofen and following CGP-55,845 washin (Ramp 2, 4 cells). Ramp-tests following 10 μ M baclofen washin revealed a mean E_R of -94.6 ± 9.8 mV, which was no different to that observed in CA1 pyramidal cells ($P= 0.8333$). The baclofen to CGP epoch ramp test (ramp 2) gave an average E_R of -95.2 ± 12.0 mV, which was not different from CA1 pyramidal cells, nor from ramp 1 in PI cells ($P=0.7333$ and 0.8571 respectively); this ramp test showed a large inward

rectification at depolarised potentials, as seen in figure 4.8.C. Together the data for PV-IR PI cells agrees with CA1 pyramidal cells, confirming that postsynaptic GABA_BRs act through the inwardly rectifying Kir3 family of K⁺-channels in this cell type.

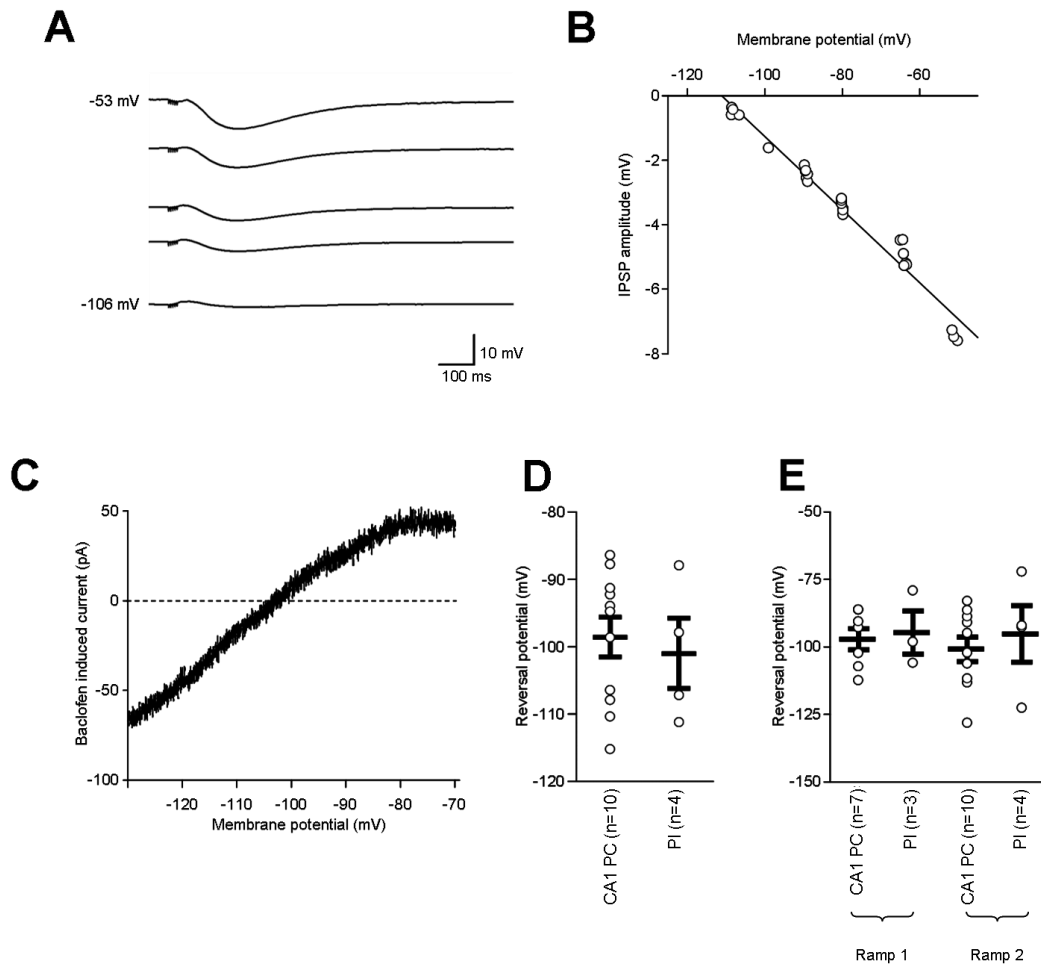


Figure 4.8 GABA_BR responses seen in PV-IR PI cells are reversible and inward-rectifying. **A** Mean representative IPSPs evoked from a PV-IR PI cell, held at a range of V_M levels (indicated). **B** IPSP amplitudes in the same cell are plotted against V_M , fitted with linear regression (black line). **C** Representative ramp-test from the same cell as **A**, showing the CGP-55,845 and baclofen current subtraction (Ramp 2); note, strong rectification at depolarised potentials; zero-level shown (dashed line). **D** Mean IPSP E_R calculated for PV-IR PI cells (PI), compared to CA1 pyramidal cells (CA1 PC); individual data shown as open circles. **E** Mean E_R calculated from voltage-ramp commands in PI cells, compared to CA1 PC.

It should be noted that ramp tests were attempted in PV-IR DI cells, where appropriate pharmacology was applied. However, due to low amplitude responses and poor signal-to-noise ratio, clear results were not produced, preventing further evaluation.

4.6 Kinetic properties of GABA_BR-mediated IPSCs in PV-IR PI INs

We next assessed whether there were any inherent differences in the kinetics of the GABA_BR-mediated IPSCs between those observed in PV-IR PI cells and of CA1 pyramidal cells (table 4.2). These values were obtained as defined in chapter 3, in cells where IPSCs elicited by single stimuli were greater than 5 pA. Interestingly, rise and decay time-constants of the slow-IPSCs calculated in both cell types (CA1 pyramidal cells: 13 cells, PV-IR PI: 6 cells) were not different (Table 4.2, Mann-Whitney tests).

GABA _B IPSC kinetics	PV-IR PI cells (%) (n=6)	P-value
Onset Latency (ms)	87.8 ± 18.4 (149.7%)	0.0484 (*)
Peak Latency (ms)	154.1 ± 5.8 (135.2%)	0.0044 (**)
½ amplitude duration (ms)	78.9 ± 27.9 (147.4%)	0.3132 (ns)
Time Constant (rise)	69.2 ± 13.3 (116.6%)	0.4824 (ns)
Time Constant (decay)	152.9 ± 24.3 (99.2%)	0.8953 (ns)

Table 4.2 Summary of GABA_BR-mediated IPSC kinetics of PV-IR PI cells, in CA1. Shown are the mean values for PV-IR PI cells and comparative level to CA1 pyramidal cells (in parenthesis) and P-values, compared to CA1 pyramidal cells. Statistics shown: ns - non-significant, * - P<0.05, ** - P<0.01

Accordingly, despite IPSC amplitudes being similar (see 4.5) half-height duration of GABA_BR-mediated IPSCs was also statistically similar. From this one can infer that the area-under-the-curve of the IPSC was similar, indicating that synaptic GABA_BR conductances were comparable, between the two cell types. However, IPSCs arrived later, seen as a shift in both mean onset and peak latency of the IPSC (table 4.2), approximately 30-50% later than in CA1 pyramidal cells; equivalent to ~30 ms and ~40 ms shift in onset and peak latencies, respectively. This data suggests that overall conductance of GABA_BR/Kir3 signalling in PV-IR PI cells in area CA1 are broadly similar; however the timing of this response is shifted.

4.7 PV-IR PI INs of the DG also possess functional GABA_BRs

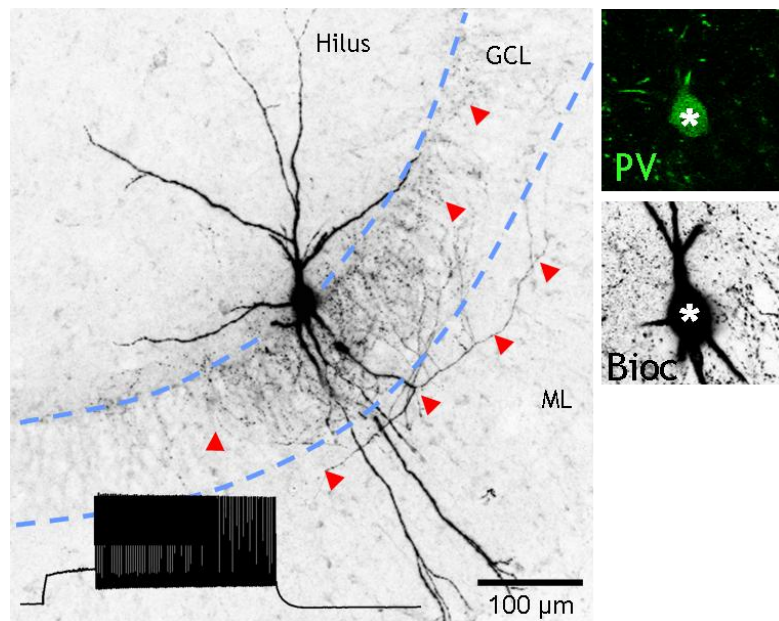


Figure 4.9 Morphological and physiological characterisation of a PV-IR basket cell in the DG. A Flattened confocal stack (x20 objective) of biocytin/avidin signal (blue pseudocolour), axon ramifications (red arrows) and DG laminations are indicated (light blue lines). Somatic localisation of PV (inset, left (top), green pseudocolour) in respect to biocytin/avidin (bottom, black pseudocolour) is shown. A representative AP discharge train is shown (black, inset) in response to a 250 pA current step.

We wanted to investigate the presence of GABA_BR-mediated conductances in PV-IR INs of the DG and whether these currents were of similar amplitude to those seen in CA1 PV-IR INs. As PV-IR INs in the DG have been shown to control feedback inhibition onto DGCs (Bartos et al, 2007), determination of GABA_BR currents in these INs could have an important role in shaping hippocampal inputs. Previously Mott et al (1999) showed that neurochemically unidentified basket cells (BC) in the DG possessed functional currents. As seen in figure 4.9, we could morphologically identify PV-IR BCs in the DG: with axon predominately within the granule-cell-layer (GCL), somata located at the GCL-hilus border and with aspineous dendrites extending into both the hilus and ML; which contained PV (figure 4.9, inset).

Passive membrane properties	CA1 PV-IR PI cells (n=15)	DG PV-IR PI cells (n=9*)
Membrane potential (mV)	-58.2 ± 1.7	-58.0 ± 2.0
Input resistance (MΩ)	91.8 ± 11.9	92.3 ± 9.8
Membrane time constant (ms)	15.4 ± 2.6	9.7 ± 0.4
Putative I _h “sag” (mV)	2.0 ± 0.3	0.7 ± 0.1
AP kinetics		
Threshold (mV)	-34.1 ± 1.3	-29.6 ± 1.7
Amplitude (mV)	82.8 ± 3.6	80.4 ± 4.2
Half-height duration (ms)	0.38 ± 0.05	0.55 ± 0.1
Maximum rise-rate (mV.ms ⁻¹)	459.7 ± 35.2	352.1 ± 48.4
Maximum decay-rate (mV.ms ⁻¹)	339.0 ± 36.9	207.3 ± 28.3
Rise/decay ratio	1.57 ± 0.22	1.7 ± 0.1
AHP properties		
Amplitude (fast) (mV)	22.6 ± 1.9	20.6 ± 1.7
Amplitude (medium) (mV)	12.4 ± 1.8	21.1 ± 2.0*
AP discharge properties		
Maximum frequency (Hz)	81.9 ± 9.6	101.1 ± 22.9
Rheobase (pA)	208.0 ± 54.2	288 ± 59
Interspike-interval ratio	0.99 ± 0.1	0.94 ± 0.06

Table 4.3 Summary of key intrinsic properties in DG PV-IR PI cells. Mean values of DG PV-IR PI cell AP properties, compared to those of CA1 PV-IR PI cells, data are shown as mean ± SEM of 9 cells. Medium-AHP was only observed in 2 DG PV-IR PI cells (*).

DG PV-IR PI cells showed a fast-spiking phenotype (figure 4.9.A, inset) with generally similar intrinsic properties to CA1 PV-IR PI cells (table 4.3). However, DG PV-IR PI cells showed a slightly slower AP, presumably due to a reduced maximal AP decay-rate which was significantly slower in DG PV-IR PI cells (P=0.0134), subsequently resulting in a 44% increase in AP duration (P=0.0254) and an increase in rise/decay ratio (P=0.0179).

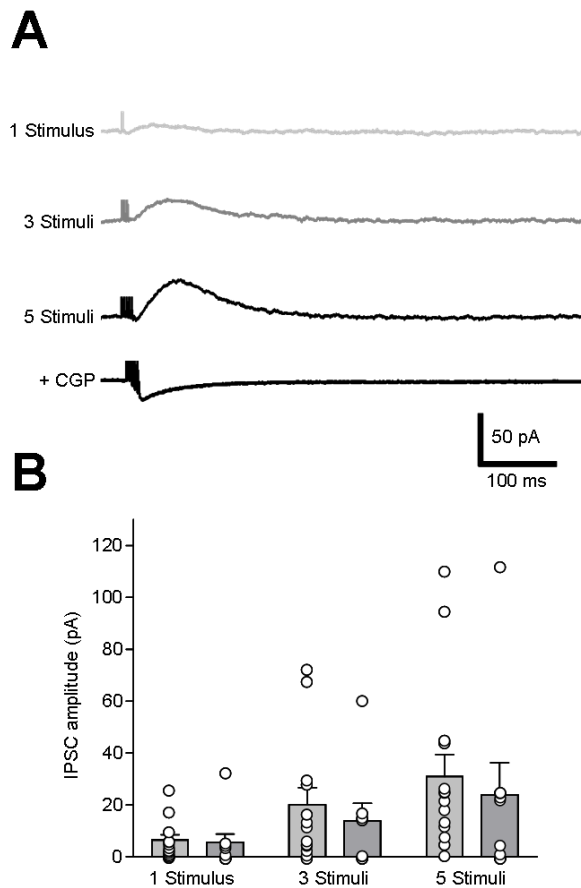


Figure 4.10 GABA_BR mediated IPSCs in DG PV-IR PI cells elicited by release of endogenous GABA. **A** Representative traces of slow-IPSCs elicited in a single cell, stimulated in the DG molecular-layer at 1 (light grey) and 3 or 5 stimulus trains (dark grey and black, respectively); which were blocked with 5 μ M CGP-55,845 washin (bottom, black). **B** Comparison of average slow-IPSC peak amplitude between CA1 PV-IR PI cells (light grey, 14 cells) and 9 DG PV-IR cells (dark grey). Data are overlain by data from individual cells (open circles)

In DG PV-IR BCs we observed slow-IPSCs under the same stimulation protocols (1, 3, 5 stimuli, 200 Hz) as for CA1 neurons. The mean amplitudes of GABA_BR-mediated responses in DG PV-IR BCs were: 1-stimulus: 5.6 ± 3.8 pA; 3 stimuli: 13.9 ± 6.8 pA; 5-stimuli: 24.0 ± 12.4 pA (from 9 cells). The mean GABA_BR-mediated IPSC amplitudes were not dissimilar from CA1 PV-IR PI cells, which was confirmed by statistical analysis between by groups ($P=0.1564$, 0.3950 , 0.2832 , respective to above order); interestingly however, IPSCs in these cells were smaller than those observed in DGCs with the same stimuli ($P=0.0041$, 0.0172 , 0.0057 , respectively). The results were confirmed by the normalisation of slow-IPSCs to R_i which gave percentage amplitudes of: $6.3 \pm 4.4\%$, $15.0 \pm 8.0\%$ and $26.1 \pm 14.7\%$ again not dissimilar from CA1 PV-IR PI cells ($P=0.1388$, 0.2985 and

0.2573, respectively); interestingly these normalised amplitudes were not statistically different from DGCs ($P=0.2110$, 0.3562 and 0.4002 , respectively).

In many recordings from DG PV-IR PI cells a small depolarising inward current was observed (see figure 4.10.A) which we could not identify; which is however likely to be due to the potential presence of nAChR (Jones and Yakel, 1997) or BAR (Cox et al, 2008) in these cells.

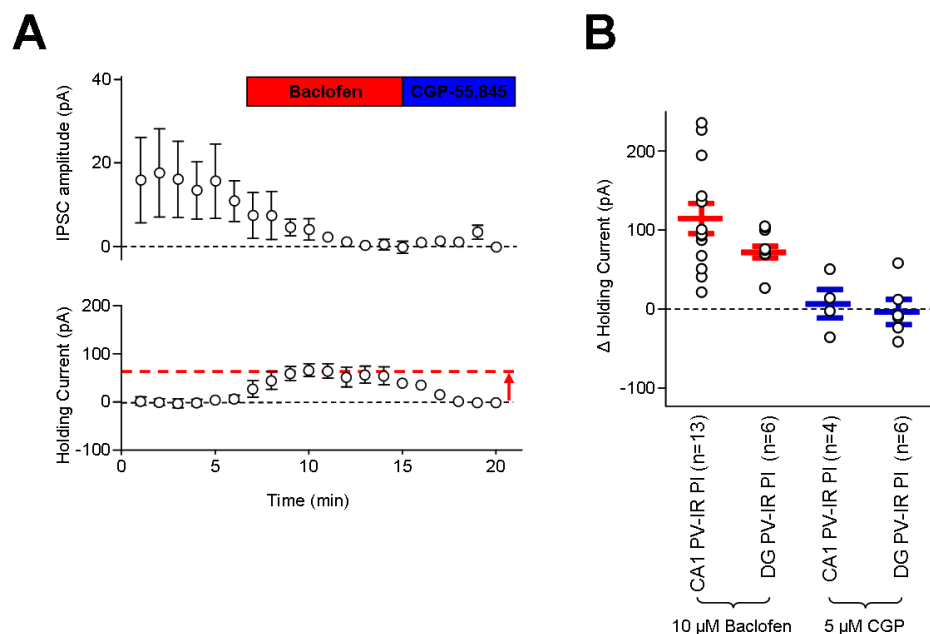


Figure 4.11 Pharmacological characterisation of GABA_BR-mediated currents in PV-IR INs of the DG. **A** Timecourse of mean synaptic amplitude (top, 5 stimulus train IPSCs) and mean holding current (bottom) at 1 minute intervals during control recording, 10 μ M baclofen washin (red horizontal bar) and 5 μ M CGP-55, 845 (blue horizontal bar) washin. Zero levels (dashed lines) and maximal holding current change in PV-IR PI cells are shown (red-dashed line); difference indicated (red arrow). **B** Mean maximal responses for both baclofen (red) and CGP-55,845 (blue) for CA1 PV-IR PI cells (PI) and DG PV-IR PI cells. Data is shown overlain by peak responses for individual cells.

We went on to determine whether pharmacologically evoked GABA_BR-mediated currents were different between DG and CA1 PV-IR PI cells (figure 4.11). As previously, 10 μ M baclofen and 5 μ M CGP-55,845 were both sequentially applied to the bath. Baclofen application resulted in complete occlusion of slow-IPSCs observed in DG PV-IR INs, whilst increasing membrane holding-current by 72.4 ± 12.4 pA, in 6 cells ($76.6 \pm 16.3\%$, normalised to R_i); which were statistically

similar to CA1 pyramidal cells, DGCs and CA1 PV-IR PI cells for the raw data (P=0.9785, 0.6070 and 0.4048, respectively) and for the normalised values (P=0.7672, 0.5287 and 0.2365, respectively).

We applied CGP-55,845 6 cells, resulted in continued suppression of slow-IPSCs, and reversal baclofen effects on voltage-clamp holding current. Following CGP-55,845 washin, holding current returned to -3.98 ± 15.5 pA relative to control (P=0.4375, Wilcoxon signed-rank test), similar to CA1 PV-IR PI cells (P=0.7619); confirming that DG PV-IR cells lack GABA_BR mediated tonic-inhibition, in dendritic compartments.

4.8 Conclusions

From the data shown here it is clear that PV-IR INs in both CA1 and DG subfields possess functional GABA_BRs, confirmed with both immunocytochemistry and electrophysiological techniques.

The GABA_BR-mediated response in CA1 PV-IR INs showed subtype-specific heterogeneity. PV-IR PI cells, our sample included mostly basket cells, expressed GABA_BR mediated currents in response to synaptic stimulation and pharmacological activation comparable to CA1 pyramidal cells. Dendritic inhibitory PV-IR bistratified cells possessed much lower synaptic and pharmacological GABA_BR mediated responses. The presence of GABA_BR mediated responses in PV-IR PI cells was confirmed in DG PV-IR PI cells, where they expressed slow-IPSCs and pharmacological responses to baclofen and CGP, which were similar to their CA1 counterparts; but with synaptic responses smaller than in DGCs, despite similar baclofen effects.

5. Postsynaptic GABA_BRs in CCK-IR INs within area CA1 of the hippocampus

In answering whether INs possess GABA_BR-mediated functional conductances, we tested CCK-IR INs; which were chosen as CCK-IR occurs in discrete populations of both PI and DI cells. As with PV-IR INs, there is some scattered data in the literature on the presence of GABA_BRs on the membranes of CCK-IR INs, most notably Sloviter et al (1999) who showed that in all hippocampal subfields colocalisation of GABA_{B1}R subunits occurs in >80% of CCK-IR cells. Additionally, CCK-IR basket cells receive a greater number of inhibitory synaptic contacts than PV-IR basket cells (Mátyás et al, 2004); implying CCK-IR basket cells receive higher concentrations of GABA at the dendrites. Confounding this Lee and Soltesz 2010 suggest that there is little to no influence of GABA_BR activation on presynaptic release from CB1 receptor containing axons in *str. pyramidale* of CA1, which are predominantly CCK-IR axons (Katona et al, 1999).

In this chapter we aim to determine whether CCK-IR INs possess GABA_BR-mediated currents in postsynaptic compartments and to clarify the extent of GABA_BR-mediated control of dendritic signalling in morphological subtypes of these cells, testing whether GABA_B content is comparable to or greater than that of CA1 pyramidal cells, as suggested by the literature.

5.1 CA1 CCK-IR INs express GABA_{B1} subunits at dendritic membranes.

Immunofluorescent staining for CCK neuropeptide successfully identified a subpopulation of IN somata, dendrites and axon dispersed across all hippocampal laminations, albeit a dense axonal plexus was observed in *str. pyramidale* of CA1 (figure 5.1.A (left)); as previously described (Nunzi et al, 1985; Somogyi et al, 2004). As we have shown previously labelling for the GABA_{B1} receptor subunit (figure 5.1.B (middle panel)) strongly labelled some IN somata (see also figure 5.1.A (middle)); which were found to regularly co-localise with CCK-IR somata (figure 5.1.A (right panel)), confirming results observed by Sloviter et al (1999).

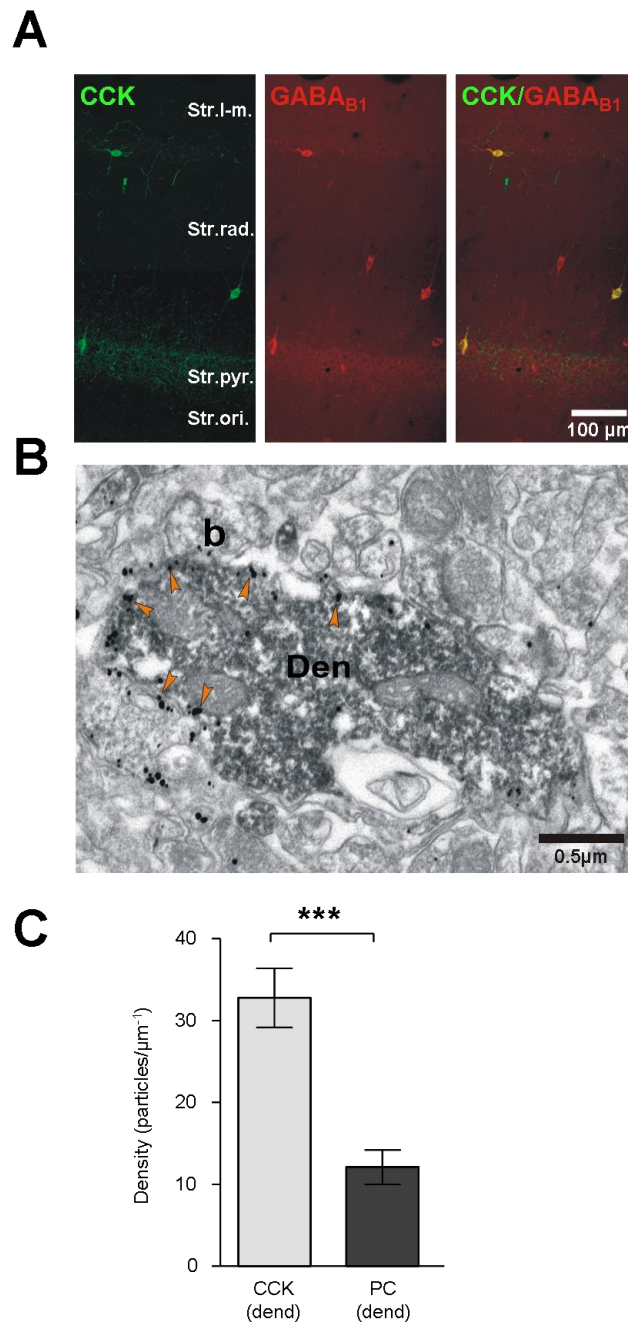


Figure 5.1: Immunocytochemical localisation of GABA_{B1} subunits to CCK-IR dendrites in CA1. **A** Immunofluorescent labelling for CCK neuropeptide (green pseudocolour) and GABA_{B1}R subunit (red pseudocolour) in the CA1 subfield, with merge shown (right). **B** Electron micrograph of a dendrite containing DAB end-product corresponding to CCK localisation (Den) and double-labelled for GABA_{B1} (immunogold particles - orange arrowheads), a presynaptic bouton is visible (b). **C** Quantification of immunogold density in CCK-IR dendrites (light grey bars) compared to putative pyramidal cell dendrites (dark grey bars). Statistics shown: ***- $P < 0.001$.

To determine the density of GABA_{B1} receptor subunits on CCK-IR dendrites, we performed pre-embedding electron microscopy double labelling with the HRP/DAB reaction and 1.4 nm immunogold (figure 5.1.B). In 23 CCK dendrites we

observed surface density of immunogold particle corresponding GABA_{B1}R subunits of 32.8 ± 3.6 particles. μm^{-2} (Figure 5.1.C); ~3-fold higher than that of putative CA1 pyramidal cell dendrites in the same tissue (12.1 ± 2.1 ; $P < 0.0001$, Wilcoxon matched pairs test); confirming a high density of the GABA_BR in CCK-IR dendrites relative to CA1 pyramidal cell dendrites, in line with the immunofluorescence data.

5.2 Identification of CCK containing INs in area CA1 of the hippocampus.

From whole-cell patch-clamp recordings we identified 19 INs in *str. oriens*, *pyramidale* or *radiatum* which exhibited CCK-IR, utilising the filling of cells with biocytin as a positive identification marker; in 14 cells we also applied the primary antibody for calbindin (CB) which is known to colocalise with CCK-IR INs (Sík et al, 1995), of which 9 CCK-IR cells were found to be CB-IR also. Cells were then morphologically subdivided as either being PI or DI cell types as detailed further below, but were not segregated on the basis of CB content; as both morphological subtypes contained CB-IR cells (PI cells: 2 of 6 cells tested; DI cells: 7 out of 8 cells tested).

PI CCK-IR INs consist entirely of basket cells (Nunzi et al, 1985; Pawelzik, et al 2002), which we confirmed; somata were observed in all layers of the hippocampus, but with an increased somatic density at the border of *str. radiatum* and *L-M*. Dendrites of CCK-IR basket cells were aspineous and either vertically or radially orientated, with a general absence of the dendritic beading observed in PV-IR basket cells. Dendrites were usually found in all layers with a single axon of emerging from a proximal dendrite, transversing the lamina to ramify in and around *str. pyramidale* in a usually wide arborisation. Axon collaterals often extended ~50 μm into *str. pyramidale* or *oriens*, with some synaptic contacts observed on presumed apical and basal dendrites of CA1 pyramidal cells.

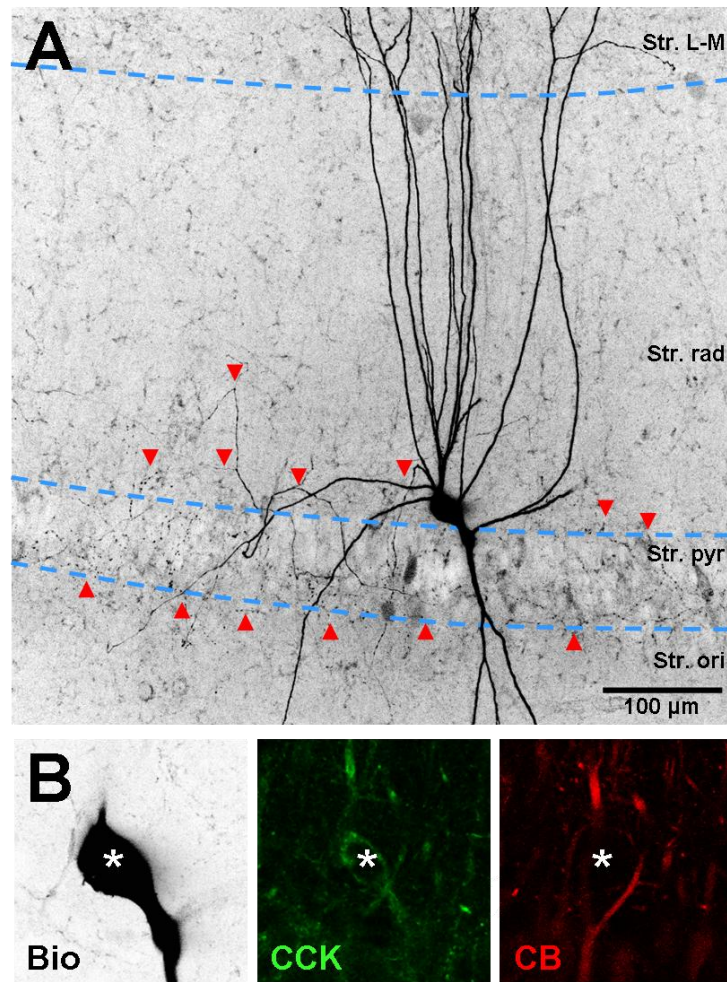


Figure 5.2: Morphological and neurochemical identification of a CCK-IR PI IN, in CA1. A low magnification confocal micrograph of a CCK-IR basket cell visualised by biotin/avidin (black pseudocolour); axon collaterals (red arrowheads) and lamina boundaries (blue dashed lines) are indicated. **B** Co-localisation of biocytin/avidin (right, black pseudocolour) with CCK neuropeptide (middle, green pseudocolour) but not CB (left, red pseudocolour); the somata is indicated (*).

Similarly, CCK-IR DI cells had somata located across all hippocampal lamina, with again a radially or vertically orientated aspineous dendritic tree. Axons of CCK-IR DI cells emerged from proximal dendrites; however ramifying in the neuropil of CA1. Unlike PV-IR DI cells (Vida et al, 1998; Pawelzik et al, 2002), there are three main classes of CCK-IR DI cells in CA1, classified according to the localisation of the primary axonal plexus. The most abundant DI subtype is Schaffer-collateral associated (SCA) type (Vida et al, 1998), with axonal plexi in *str. radiatum* and *oriens* and we observed several clear examples of this subtype (see figure 5.3.A for representative cell). SCA-type CCK-IR DIINs are similar in both somatodendritic and axonal axes to apical dendrite associated (ADA) DI

cells described by Vida et al (1998). The axons ADA cells form synapses with the thick apical dendrites of CA1 pyramidal cells; however we did not observe any clear examples of these cells, potentially due to overlap of axonal distribution with SCA type DI cells.

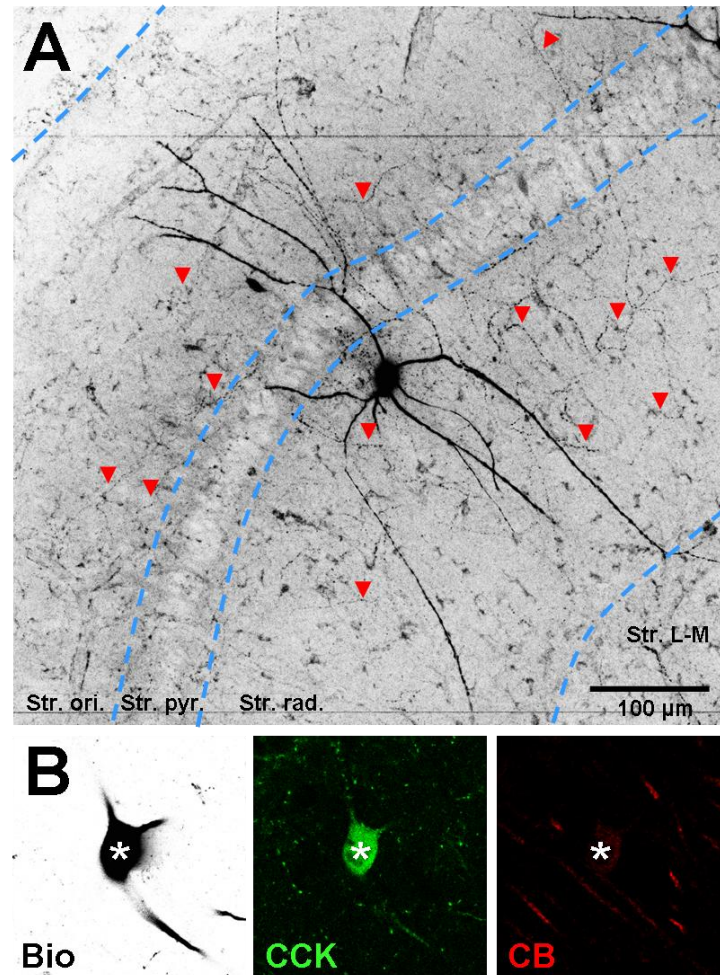


Figure 5.3: Morphological and neurochemical identification of a putative CCK-IR SCA-type IN. A low power magnification flattened confocal stack of a biocytin/avidin reactive cell (black pseudocolour). Axonal plexi in are indicated in *str. oriens* (*str. ori.*) and *radiatum* (*str. rad.*; red arrowheads) in respect to CA1 laminations (blue dashed lines). B Triple co-localisation of avidin/biocytin (left, black pseudocolour), CCK (middle, green pseudocolour) and CB (left, red pseudocolour) to the somata of this cell (*).

The final group of CCK-IR DI cells have a large axonal plexus associated with perforant-path inputs from the EC, in *str. L-M*, known as perforant path associated (PPA) INs. The somatodendritic axis of PPA-type CCK-IR INs is approximately similar to that of other CCK-IR cell types (Vida et al, 1998), which we also observed. CCK-IR PPA cells are believed to inhibit input from the EC on

the distal dendrites of CA1 pyramidal cells (Vida et al, 1998); we observed 3 examples of this cell type (see figure 5.4 for representative example).

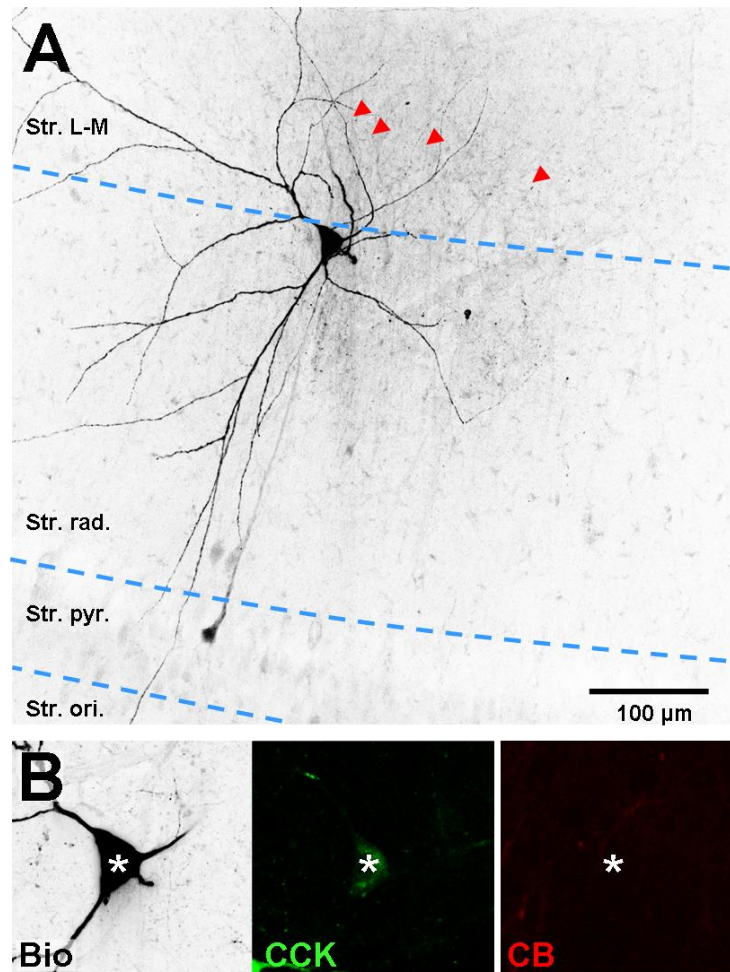


Figure 5.4: Morphological and neurochemical identification of a putative CCK-IR PPA-type IN. A flattened confocal (low power) stack of a biocytin/avidin reactive cell (black pseudocolour). A small axonal plexus in *str.L-M* is indicated (red arrowheads) with respect to CA1 laminations (blue dashed lines). B Co-localisation of avidin/biocytin (left, black pseudocolour) and CCK (middle, green pseudocolour); but not CB (left, red pseudocolour) in the same cell as A, soma indicated (*).

Additional to morphological characterisation of CCK-IR cells, we characterised both passive and active intrinsic physiological properties of these cells as seen in figure 5.5. Table 5.1 highlights the key intrinsic properties extracted from -250 to 250 pA hyper- to depolarising current steps.

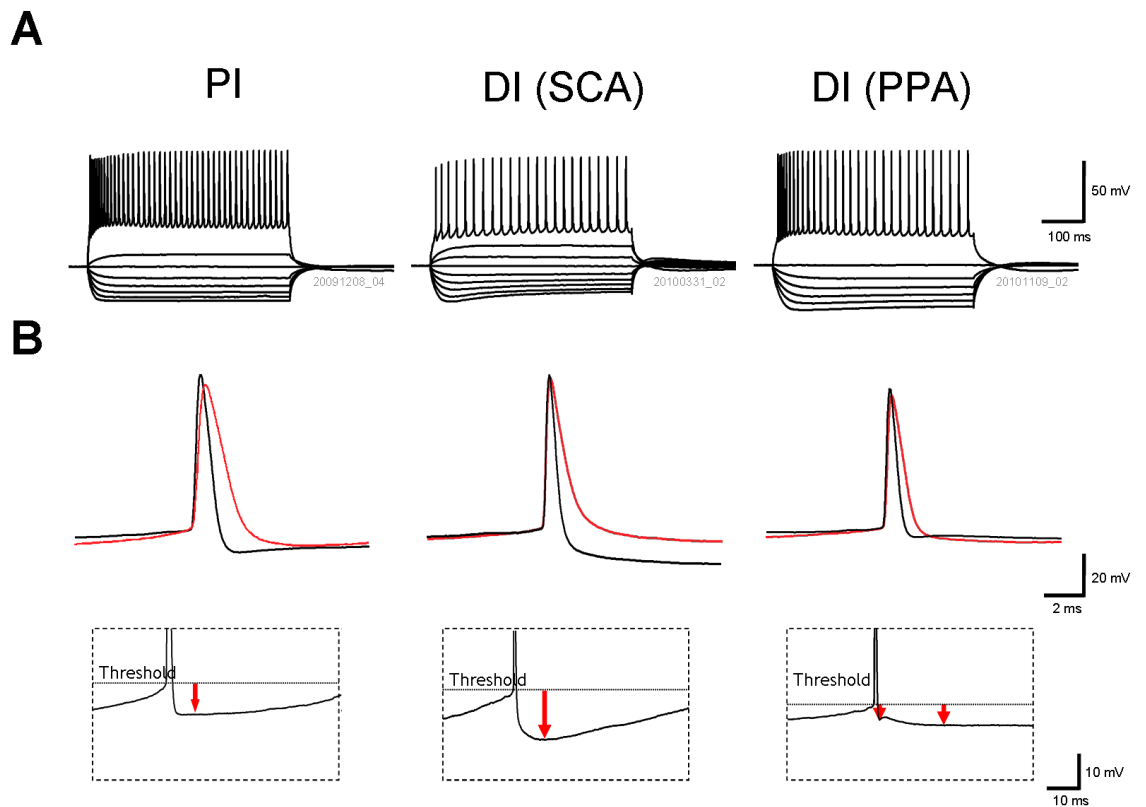


Figure 5.5 Trains of APs and AP waveform from representative CCK-IR PI and DI IN subtypes. **A** families of 50 pA hyper to depolarising responses observed in PI (left) and either SCA or PPA DI cells (middle and right, respectively). **B** an expanded view of the first AP observed in response to depolarisation in the same cells as **A** (black trace), underlain by the last evoked AP (red trace) to highlight accommodation; inset, enlarged view of threshold (dotted line) and AHP (red arrow) of the same AP.

For analysis of intrinsic data we have pooled putative CCK-IR SCA and PPA subtypes, although in PPA cells AP amplitude was significantly smaller ($P=0.0360$) and accommodation was more pronounced ($P=0.0140$); which may have been a result of a small, albeit non-significant depolarisation of PPA cells ($\Delta V_M = 3.9$ mV; $P= 0.3037$).

In CCK-IR PI and pooled DI cells, V_M was similar to CA1 pyramidal cells for both cell types ($P=0.5596$ and $P=0.3026$, respectively); while R_i and membrane time-constant were both longer than in CA1 pyramidal cells, significantly so in CCK-IR DI cells ($P<0.0001$ and $P=0.0102$, respectively), but not in PI cells ($P=0.0653$ and $P=0.0801$, respectively) and R_i was larger in DI than PI cells ($P=0.0355$). As seen in figure 5.5.A there was a larger voltage sag, associated with I_h , in CCK-IR DI

cells than in either CCK-IR PI or CA1 pyramidal cells ($P=0.0002$ and $P=0.0001$, respectively); which was not observed between CCK-IR PI and pyramidal cells ($P=0.7431$). This data suggest that passive membrane properties of CCK-IR cells are inherently different from that of CA1 pyramidal cells, with decreased membrane leakiness at rest. Interestingly, when CCK-IR DI cell membranes are hyperpolarised a larger putative voltage “sag” was produced, indicating a larger I_h than in either CA1 pyramidal cells or CCK-IR PI INs.

CCK-IR cells were generally more reluctant to discharge APs than CA1 pyramidal cells as threshold was higher in both CCK-IR PI and DI cells ($P=0.0143$ and 0.0251 , respectively). APs were smaller in both PI ($P=0.0084$) and DI ($P=0.0002$) cell types, but generally had a similar half-height duration (PI: $P=0.9442$, DI: $P=0.1140$). The reduced AP peak amplitude can be attributed to CCK-IR cells showing a decreased maximal rise rate in both PI and DI cells ($P=0.0014$ and $P<0.0001$, respectively) compared to CA1 pyramidal cells, but with a similar maximal decay rate ($P>0.05$, both). This difference in maximal rise and decay rates was reiterated by the ratio between these two factors, which in both PI and DI cells was much lower than that of CA1 pyramidal cells ($P<0.0001$, both). Recovery after AP discharge was different between CCK-IR cells and CA1 pyramidal cells, as evidenced by an increased medium AHP amplitude ($P<0.05$, both), which manifested itself as a small increase in the level of spike-interval accommodation seen at maximal depolarisation, which was not significant between PI and pyramidal cells ($P=0.1573$), but was when compared to DI cells ($P=0.0317$).

There was no difference between PI and DI fast-AHP components (in 4 cells, $P=0.5714$). Finally, CCK-IR DI cells discharged trains of APs with a frequency 3-fold higher than in CA1 pyramidal cells ($P<0.0001$) and 2-fold faster than PI cells ($P=0.0504$); PI cells discharged to the same frequency as CA1 pyramidal cells ($P=0.3269$).

Passive membrane properties	CA1 pyramidal cells (n=27)	CCK-IR PI cells (n=6)	CCK-IR DI cells (n=13)
Membrane potential (mV)	-62.9 ± 1.2	-62.1 ± 3.6	-61.2 ± 1.4
Input resistance (MΩ)	102.2 ± 13.1	143.5 ± 23.8	199.6 ± 12.9
Membrane time constant (ms)	22.0 ± 2.6	27.9 ± 5.0	25.6 ± 1.8
Putative I _h “sag”	3.0 ± 0.2	2.9 ± 0.6	7.4 ± 0.5
AP kinetics			
Threshold (mV)	-39.8 ± 1.0	-33.6 ± 2.6	-36.3 ± 1.3
Amplitude (mV)	113.8 ± 2.1	96.6 ± 5.4	97.8 ± 2.9
Half-height duration (ms)	0.84 ± 0.04	0.83 ± 0.08	0.78 ± 0.08
Maximum rise-rate (mV.ms ⁻¹)	610.6 ± 31.4	321.5 ± 37.2	350.0 ± 26.7
Maximum decay-rate (mV.ms ⁻¹)	109.3 ± 4.7	110.0 ± 12.4	135.9 ± 13.4
Rise/decay ratio	5.6 ± 0.3	2.9 ± 0.1	2.7 ± 0.1
AHP properties			
Amplitude (fast) (mV)	5.9 ± 0.6	13.0 ± 2.1 ‡	14.4 ± 2.0 ‡
Amplitude (medium) (mV)	9.4 ± 0.5	13.9 ± 1.4	15.1 ± 1.3
AP discharge properties			
Maximum frequency (Hz)	23 ± 2	35.7 ± 12.6	64.4 ± 8.1
Rheobase (pA)	131.1 ± 13.5	158 ± 33	81 ± 15
Interspike interval ratio	1.55 ± 0.14	2.4 ± 0.7	2.1 ± 0.2

Table 5.1 Summary of intrinsic properties of PI and DI CCK-IR INs in CA1. Mean values for morphologically identified CCK-IR cells are shown alongside that of CA1 pyramidal cell, for comparison, in the case of fast AHP this property was only seen in 4 cells (indicated: ‡); all data is shown as mean ± SEM.

5.3 GABA_BR conductances differ between morphological subtypes of CCK-IR INs.

To assess whether CCK cells possessed GABA_BR-mediated conductances, as previously explained (Chapter 2, 3 and 4); blocking ionotropic glutamate and GABA_A receptors pharmacologically, we electrically stimulated the border of *str.*

radiatum and *L-M* with single stimuli or 200 Hz trains of 3 and 5 stimuli. Of the 20 CCK-IR cells recorded we observed slow-IPSCs in 10 cells following trains of 5 stimuli, with the remainder showing small (<5 pA) responses at this level; which have been included in the analysis.

Slow IPSCs were completely abolished by the direct application of CGP-55,845 in 2 cells, confirming that these responses were mediated by the GABA_BR. Figure 5.5.1 shows the slow-IPSC responses at 1, 3 and 5 stimuli levels from all 20 cells, with mean amplitudes of 3.5 ± 0.3 pA, 13.5 ± 1.5 pA and 20.8 ± 2.3 pA, respectively. The observed responses for CCK-IR cells were smaller than those observed in CA1 pyramidal cells at all stimulation levels tested. At 1 stimuli, the mean slow-IPSC in CCK-IR cells was 60.3% of pyramidal cell mean amplitude ($P=0.0257$), and 77.2% and 72.4% at 3 and 5 stimuli ($P=0.0390$ and 0.0254 , respectively). When we normalised for R_i , as before, we saw that the mean CCK-IR slow-IPSC amplitudes were equivalent to: $2.2 \pm 0.2\%$, $9.3 \pm 0.9\%$ and $14.3 \pm 1.3\%$ (same order as above), which were statistically smaller than in CA1 pyramidal cells ($P=0.006$, 0.002 , 0.001 , respectively)

Despite these differences, there were many CCK-IR INs which had large GABA_BR-mediated slow-IPSCs of a similar magnitude to CA1 pyramidal cells, so as for PV-IR cells, we separated the PI and DI subtypes to determine whether there were differential IPSC amplitudes; we further subdivided CCK-IR DI cells into either putative SCA or PPA subtypes, dependent on axonal localisation.

Following dissection of morphological types, CCK-IR PI cells were found to have consistently large GABA_BR-mediated IPSCs (figure 5.5.B (left) and C) which had mean amplitudes of 6.2 ± 0.9 pA, 26.3 ± 4.0 pA and 39.2 ± 5.5 pA (in 6 cells); determined as 107.5%, 150.4% and 140.0% of CA1 pyramidal cell IPSCs, respectively. Although the amplitude of GABA_B IPSCs seen in PI cells was higher overall than CA1 pyramidal cells (figure 5.5.C), there was no statistical difference between the two cell types ($P=0.8280$, 0.2993 and 0.3628 , respectively). These IPSC amplitudes normalised to R_i , gave relative amplitudes

of $4.9 \pm 0.7\%$, $21.6 \pm 3.3\%$ and $32.7 \pm 5.3\%$, which were statistically similar to those observed in CA1 pyramidal cells ($P > 0.05$, all).

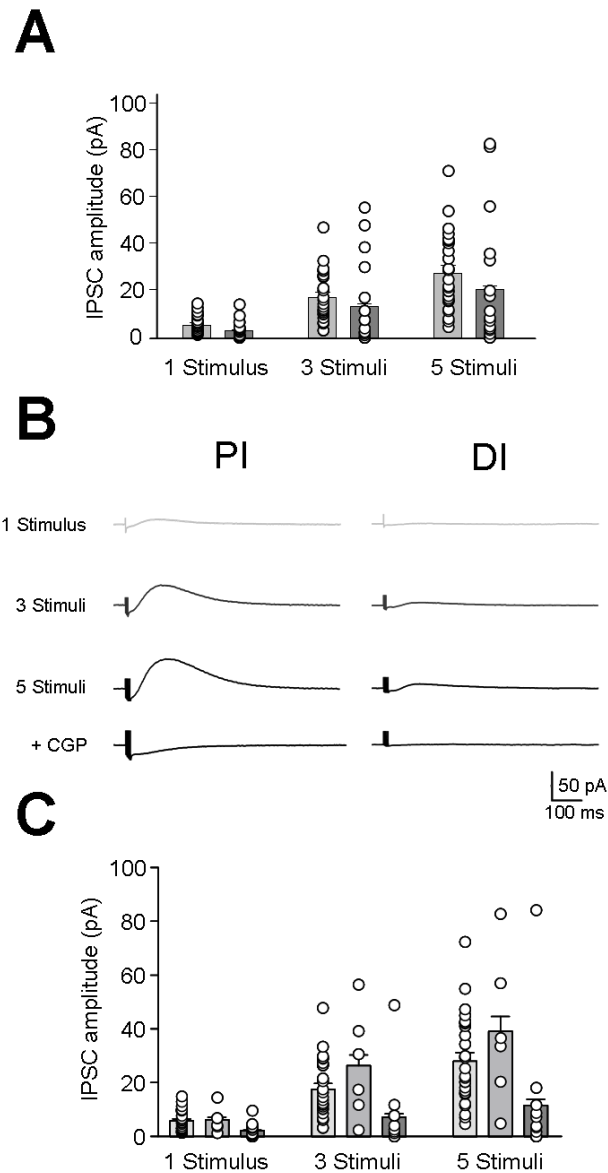


Figure 5.6 GABA_BR-mediated IPSC in CA1 CCK-IR INs, elicited by release of endogenous GABA. **A** Histogram showing mean GABA_BR-mediated IPSCs in CCK-IR INs (dark grey bars) compared to CA1 pyramidal cells (light grey bars), overlain by data from individual cells (open circles). **B** slow-IPSCs from a CCK-IR PI (left) and DI cells (right) at 1 stimuli (light grey) or 3 and 5 stimuli trains (dark grey and black respectively), which was blocked by 5 μ M CGP-55,845 (black, bottom). **C** Mean GABA_BR-mediated responses at the same stimulus levels as **B** in CCK-IR PI (medium grey bars) and DI cells (dark grey bars) and CA1 pyramidal cells (light grey bars).

Mixed CCK-IR DI cells had substantially reduced GABA_BR-mediated IPSC amplitudes at all stimulation levels (see figure 5.6.B (right) and C). The mean

IPSC amplitudes were: 2.1 ± 0.3 pA, 7.1 ± 1.4 pA and 11.6 ± 2.4 pA (14 cells), which were on average 36.7%, 40.7% and 41.3% of CA1 pyramidal cell amplitudes ($P=0.002$, 0.0007 and 0.0004 , respectively) and equivalent to: $0.9 \pm 0.1\%$, $3.1 \pm 0.6\%$ and $5.1 \pm 1.1\%$ of R_i . GABA_BR-mediated IPSCs in CCK-IR DI cells were 34.1%, 27.0% and 29.5% (relative to previous order) smaller than IPSCs resulting from the same stimuli in CCK-IR PI cells, from the raw data ($P=0.0218$, 0.0170 , 0.0170 , respectively), which was confirmed in the normalised data ($P<0.0001$, for all). Interestingly, following $5 \mu\text{M}$ CGP-55,845 application (5.6.B, bottom) a small residual inward current remained, although the absolute identity of this current is unknown, it is potentially due to the presence of 5-HT₃ receptors in CCK INs (Morales and Bloom, 1997).

IPSCs elicited in morphologically distinct SCA and PPA CCK-IR DI cells showed differential amplitudes, in response to the same stimuli. Putative SCA type cells possessing mean GABA_BR-mediated IPSC amplitudes of 1.1 ± 0.15 pA, 2.9 ± 0.4 pA and 4.7 ± 0.7 pA (in 10 cells) at 1, 3 or 5 stimuli, respectively; which were smaller, although not significantly so, than IPSCs observed in PPA-type DI cells, which had mean amplitudes of 3.8 ± 1.4 pA, 14.7 ± 7.7 pA and 24.3 ± 13.3 pA (in 4 cells; $P= 0.2398$, 0.3736 and 0.2398 , respectively).

We next attempted to identify whether CCK-IR PI and DI cells reacted to pharmacological modulation of GABA_BRs to the same extent. As performed previously for both CA1 pyramidal cells and PV-IR INs, we first applied the selective GABA_BR agonist baclofen ($10 \mu\text{M}$) for 5 minutes to assess the whole-cell contingent of GABA_BRs; after which we applied the high affinity antagonist CGP-55,845 ($5 \mu\text{M}$) to block all functional currents, baclofen induced or otherwise. Application of $10 \mu\text{M}$ baclofen to both CCK-IR PI and DI cells induced an increase in the holding current required to maintain a -65 mV voltage clamp (figure 5.6.A, bottom); while simultaneously occluding IPSCs in both cell types (figure 5.6.A, top). The subsequent application of CGP-55,845 resulted in a maintained suppression of the slow-IPSC amplitude whilst reversing the holding current changes induced by baclofen.

Figure 5.6.B shows the mean pharmacological response of both CCK-IR PI and DI cell types, as compared to CA1 pyramidal cells. PI cells had an average peak baclofen-induced response of 70.6 ± 7.6 pA (5 cells) from control levels, smaller than pyramidal cells (80.0%) and PV-IR PI cells (66.8%), but not significantly so ($P=0.5486$ and $P=0.2783$) and had a mean normalised amplitude of $70.6 \pm 7.6\%$, ($P=0.5094$ compared to CA1 pyramidal cells). Pooled CCK-IR DI cells, had a mean baclofen response of 29.9 ± 7.4 pA (in 10 cells), which was 33.8% and 42.3% that of pyramidal and neurochemically similar PI cell responses ($P=0.0050$ and 0.0190 , respectively), as well as amplitudes normalised to R_i ($P=0.0120$ and 0.0019 , respectively). Baclofen responses in mixed CCK-IR DI cells were 162.3% of those observed in PV-IR DI cells ($P=0.6943$); this average being drawn from 8 putative SCA-type DI cells (31.5 ± 19.4 pA) and from 2 putative PPA-type cells (6.8 ± 7.1 pA). Statistically, SCA-type cells were not different from PV-IR DI cells ($P=0.6943$), whereas PPA-type cells could not be tested.

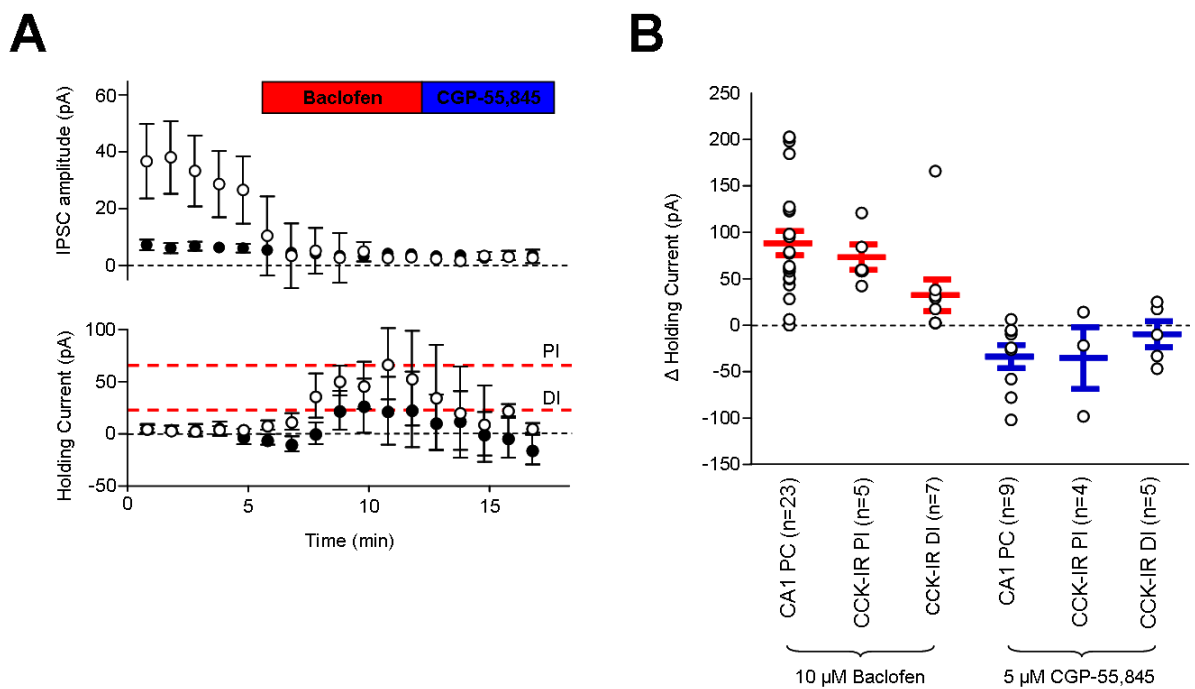


Figure 5.7 Pharmacological characterisation of $GABA_B$ -mediated responses in CCK-IR INs of the CA1. **A** Timecourse of control, 10 μ M baclofen (red bar) and 5 μ M CGP-55,845 (blue bar) effects on IPSC amplitude (top) and voltage-clamp holding-current (bottom), in CCK-IR PI cells (open circles) and DI cells (filled circles); peak baclofen responses are indicated (dashed red lines) for both cell types and zero level shown (dashed black line). **B** Mean holding current changes in CCK-IR PI and DI cells compared to CA1 pyramidal cells (CA1 PC) following baclofen (red) and CGP-55,845 (blue). Mean data is overlaid by individual experiment data (open circles).

Accordingly, CGP-55,845 responses in CCK-IR PI cells showed no apparent difference from those seen in CA1 pyramidal cells (figure 5.6.B). PI cell holding currents overshoot control levels by 37.6 ± 28.6 pA (3 cells), which was 10.8% greater than that observed in CA1 pyramidal cells, not statistically different ($P=0.8636$); however, this responses was larger that that seen in PV-IR PI cells ($+3.05 \pm 15.6$) but not significantly so ($P=0.6286$). By contrast, CGP-55,845 responses in morphologically pooled CCK-IR DI cells CGP-55,845 resulted in a small overshoot holding-current (-7.5 ± 6.4 pA from control; 5 cells), equivalent to 22.2 % of CA1 pyramidal cell and 20.0% of PI cell overshooting responses; albeit these differences were not significant ($P=0.4376$ and $P=0.8376$, respectively). Likewise, CCK-IR DI cell CGP-55,845 mediated responses were similar to those seen in PV-IR DI cells ($P=0.5053$). The mean CGP-55,845 response of CCK-IR DI cells was drawn from 4 putative SCA INs (-2.6 ± 8.9 pA) and 1 putative PPA IN (-30.0 pA), the former was still similar to that of CA1 pyramidal and CCK-IR PI cells ($P>0.05$, both)

Taken together the data suggest that CCK-IR PI cells possessed large synaptic and pharmacologically induced GABA_BR mediated responses which were similar to those seen in CA1 pyramidal cells and PV-IR PI cells. In CCK-IR DI cells we observed synaptic and pharmacological responses smaller than in CA pyramidal and CCK-IR PI cells, which were similar between morphologically distinct CCK-IR PPA and SCA DI subtypes; and not distinct from PV-IR DI cells.

5.4 GABA_BR-mediated conductances in CCK-IR INs are mediated by an inward-rectifying K⁺ channel.

To confirm whether post-synaptic GABA_BR responses in CCK-IR INs are mediated primarily by Kir3.n type K⁺ channels, as in CA1 pyramidal cells, we tested the E_R of synaptic and pharmacological conductances in these cells. Changing the V_M of cells (-50 to -100 mV), whilst recording IPSPs in current-clamp revealed that in both CCK-IR PI and DI cells synaptically evoked GABA_B responses reversed at -87.7 mV (1 PI cell) and -96.4 ± 15.7 mV (2 DI cells), close to the calculated $E_{R(K^+)}$

~ -106 mV , in our setup (figure 5.7.A and B). The voltage-dependence of IPSP amplitude showed a clear reduction in inward K⁺ conductance below ~ -90 mV, indicative of an inwardly-rectification, despite meaningful K⁺ conductances observed at resting V_M. Due to the small number of successful experiments in both CCK-IR PI and DI cells, no statistical evaluation of similarity to CA1 pyramidal cells could be provided.

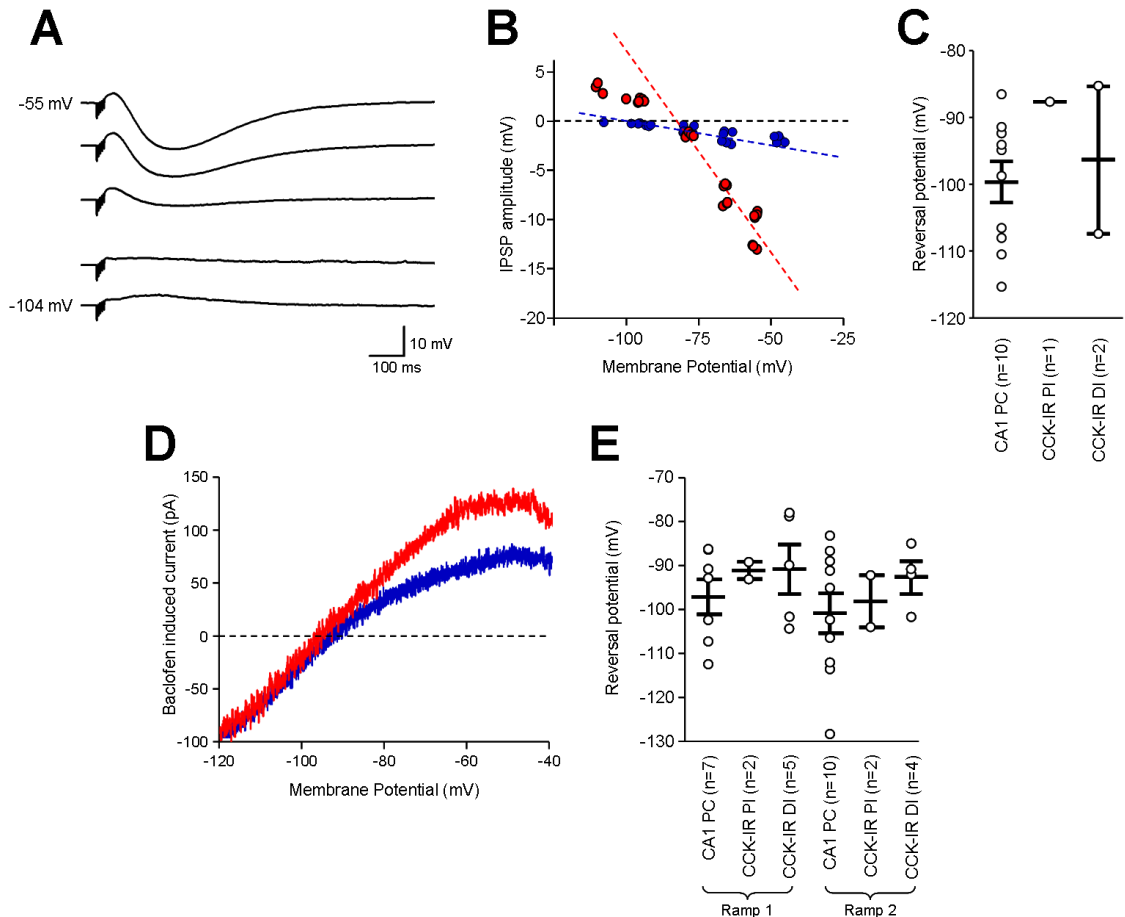


Figure 5.8 GABA_BR responses seen in all CCK-IR cells are reversible and inward-rectifying. **A** Representative IPSPs recorded in current-clamp over a range of V_M (indicated on left) in a CCK-IR PI cell. **B** Voltage-response plot of IPSP amplitude against V_M in the same PI cell as in A (red) and in a CCK-IR DI cell (blue). The linear phase of the voltage-relationship is plotted for each cell in respective colours. **C** Comparison of mean E_R in CCK-IR cells and CA1 pyramidal cells; note that only 1 PI cell and 2 DI cells were recorded. **D** Representative subtracted voltage-ramp commands (ramp test 2) in PI and DI cells (same colours as B); note strong rectification at V_M > -90 mV. **E** Mean E_R calculated from ramp commands tests. In C and E mean data is overlain by data from individual experiments (open circles).

To determine whether current flux resulting from 10 μ M baclofen application was a result of $K_{ir3.n}$ activation, we utilised the voltage-ramp command test as shown by Bean and Sodickson (1996). As described earlier, we tested current differences between control and 10 μ M baclofen (ramp 1) and also between 10 μ M baclofen and 5 μ M CGP-55,845 (ramp 2). In CCK-IR PI cells (n=2) we saw a mean E_R , measured from control levels in ramp 1, of -91.1 ± 2.76 mV; whereas baclofen induced currents in ramp 2 resulted in an E_R of -98.1 ± 8.4 pA. Which were similar to values obtained in CA1 pyramidal cells, but which could not be tested.

In CCK-IR DI cells, ramp 1 gave a E_R of -90.7 ± 3.1 mV (in 5 cells) with ramp 2 giving an E_R of -92.6 ± 2.3 mV (in 4 cells), both values being similar to that recorded from CA1 pyramidal cells (P=0.3434 and 0.3736, respectively) and from PV-IR PI cells (P=0.5714 and 0.6857, respectively). Importantly, E_R in CCK-IR DI cells did not differ from that calculated according to the Nernst Equation for our experimental set-up (Ramp 1: P=0.5000, Wilcoxon signed-rank test).

5.5 Kinetic properties of $GABA_B$ R-mediated IPSCs in CCK-IR INs

GABA _B R IPSC kinetics	CCK-IR PI cells (n=3) (%)	CCK-IR DI cells	PI vs. PC (P-value)
Onset latency (ms)	35.5 \pm 5.4 (79%)	63.8 (105%)	0.0078
Peak latency (ms)	126.0 \pm 9.1(107%)	140.7 (116%)	0.3958
½ height duration (ms)	125.7 \pm 26.2 (235%)	137.5 (257%)	0.0793
Time constant (rise)	41.9 \pm 8.7 (71%)	45.8 (77%)	0.5853
Time constant (decay)	112.8 \pm 16.7 (73%)	148.2 (96%)	0.4618

Table 5.2 Summary of $GABA_B$ R-mediated IPSC kinetics in CCK-IR INs, of CA1. Data is shown as the mean \pm SEM, with % difference of CA1 pyramidal cells (PC) shown in parenthesis and P-values only shown for CCK-IR PI cells.

CCK-IR PI and DI cells generally had similar kinetic properties to those seen in CA1 pyramidal cells (see table 5.2); the similarity of these values suggesting that the molecular mechanisms of GABA_B signal transduction are broadly similar between the two cell types. GABA_BR IPSCs in CCK-IR PI INs showed more rapid onset than CA1 pyramidal cells (see table 5.2). However all other kinetic properties (table 5.2) were statistically similar; ½ amplitude duration was approaching significance, with values in CCK-IR PI cells at least 200% of CA1 pyramidal cell values. Compared to PV-IR PI cells, CCK-IR PI IN IPSCs had similar ½ amplitude duration and rise and decay time constants (P=0.3524, 0.1143 and 0.6095, respectively), Interestingly, CCK-IR PI cells were faster in both onset and peak latency than PV-IR PI cells, by 49.5 % and 81.8% of PV-IR PI values respectively (P=0.0095 and 0.0381, accordingly). Kinetics of IPSC response seen in 1 CCK-IR DI cell were slower than those seen in PI cells, however this could not be tested statistically, due to only 1 DI cell evoking a synaptic response >5 pA.

5.6 Conclusions

We have shown conclusively that CCK-IR INs possess post-synaptic GABA_BR which could be detected at both the immunocytochemical and physiological levels. The conductances mediated by GABA_BR were activated by the selective GABA_B agonist baclofen and blocked by the selective antagonist CGP-55,845. The GABA_B mediated responses detected; both synaptic and pharmacological, were significantly larger in PI type CCK-IR IN, compared to their DI counterparts and these conductances, in both cell types, and were underlain by inwardly rectifying K⁺ conductances.

Finally divergence of GABA_BR-mediated responses in CCK-IR PI or DI INs was almost identical to that seen in PV-IR INs, suggesting that PI INs in general possess large, functional, dendritic GABA_BR responses, while the same responses in DI INs have typically smaller amplitudes.

Chapter 6. Postsynaptic GABA_BR mediated conductances in SSt-IR OLM cells, within area CA1 of the hippocampus

From recordings of CCK and PV IR cells, it was apparent that there were overt differences between INs which showed PI or DI morphologies. We attempted to check whether another prototypical DI cell would show a similar lack of GABA_BR conductances in dendritic compartments. SSt-IR INs in the hippocampus are a morphologically homogenous cell type, across all subfields; in the CA1 the predominant morphological subtype is the OLM cell, which is exclusively DI. In immunocytochemical colocalisation SSt-IR somata have been shown to possess a strong somatic labelling for GABA_{B1} subunits (Sloviter et al, 1999) in >90% of cells of the CA1. Determination of GABA_BR function in the dendrites of these cells ties well to data produced in CA1 PV-IR DI bistratified INs, as there is some overlap of PV and SSt staining in both these and OLM cells. The aim of this chapter was to assess whether under the same conditions as for PV and CCK cells, we could observe functional GABA_BR -mediated postsynaptic effects; utilising anatomical techniques to confirm the previous literature and whole-cell patch-clamp recordings to test whether functional GABA_BR conductances are present in these cells.

6.1 Expression of GABA_{B1} subunits in dendrites of CA1 SSt-IR INs

To detect that GABA_{B1} subunits could be observed in SSt-IR cells in the CA1, we first performed immunofluorescent double-labelling in coronal sections of rat hippocampus, for SSt and GABA_{B1} (see figure 6.1.A). The majority of observed SSt-IR somata localised to *str. oriens* and were immunoreactive for GABA_{B1} with labelling intensity comparable to or higher than that of proximal CA1 pyramidal cell somata.

To confirm that GABA_{B1} subunits were present at the plasma membrane of SSt-IR dendrites we then performed pre-embedding electron microscopy double-

labelling of hippocampal slices, staining for both SSt (DAB end-product) and GABA_{B1} (silver-intensified nanogold; figure 6.1.B). In 9 SSt-IR dendrites recovered from *str. oriens* we observed a very low density of gold-particles (1.9 ± 0.5 particles. μm^{-2}), corresponding to GABA_{B1}. The density of gold-particles on SSt-IR dendrites was significantly lower than the density of gold-particles seen on spiny dendrites of putative CA1 pyramidal cells in *str. oriens* (8.9 ± 1.4 particles. μm^{-2} ; $P=0.0002$) in the same sections.

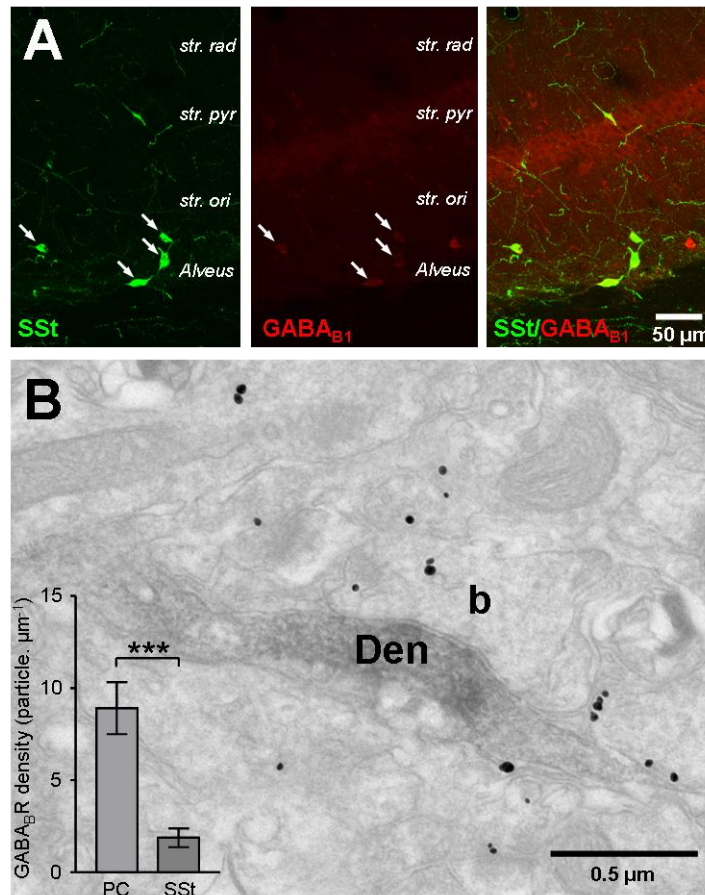


Figure 6.1 Immunocytochemical localisation of GABA_{B1} receptor subunits to SSt-IR dendrites, in *str. oriens* of CA1. **A** Low power confocal micrograph of the CA1 of the hippocampus, double labelled for SSt (green pseudocolour) and GABA_{B1} subunit (red pseudo colour); which was merged (right panel). **B** Electron micrograph of a SSt-IR dendrite (Den, DAB end product) and GABA_{B1} receptor subunit (immunogold); an excitatory bouton is shown (b). Inset, quantification of immunogold density on SSt-IR dendrites, compared to putative CA1 pyramidal cell dendrites in *str. oriens*. Statistics shown: *** - $P<0.001$

6.2. Identification of SSt-IR INs in area CA1 of the hippocampus

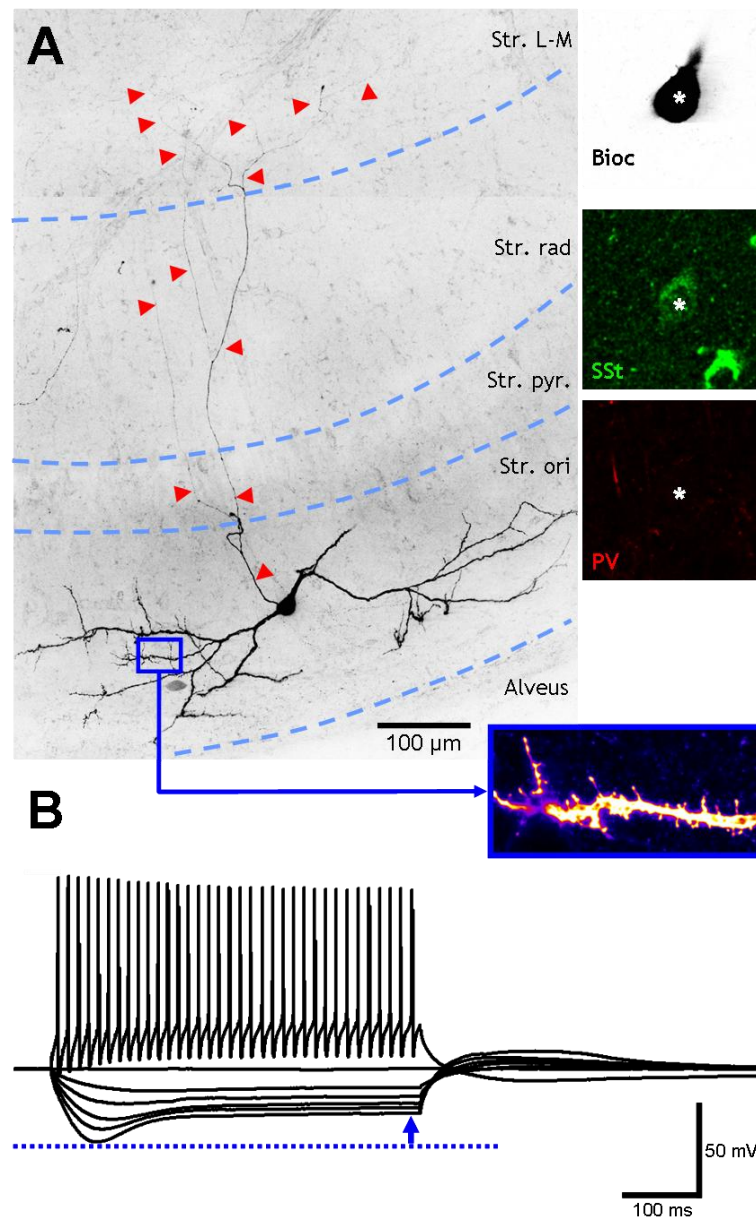


Figure 6.2 Morphological, neurochemical and physiological identification of a CA1 SSt-IR OLM cell. **A** Low-power flattened confocal stack of a biocytin filled SSt-IR OLM cell, with axon indicated (red arrowheads); hippocampal laminations are shown (light blue dashed lines). Inset (right), immunofluorescent triple labelling of the same cell, showing co-localisation of SSt (middle, green pseudocolour) but not PV (bottom, red pseudocolour) with biocytin/avidin (top, black pseudocolour) of the cell somata (*). Inset (bottom) high power confocal micrograph of a dendrite belonging to the same cell (indicated by blue box/arrow), showing sparsely spiny dendrites. **B** A hyper- to depolarising series of current steps (50 pA steps, -250 to 250 pA range) showing intrinsic physiological properties and AP discharge, at 250 pA depolarisation; note the strong sag component produced by hyperpolarising current steps (blue line and arrow).

SSt-IR INs have different morphologies dependent on their location within the hippocampus. In area CA1 the majority of SSt-IR INs are defined as *oriens/L-M* (OLM) cells (McBain et al, 1994; Katona et al, 1999). The somata of OLM cells are found in *the str. oriens* proximal to the *alveus*, with typically 2-3 horizontal dendrites arborising radially within the borders of *str. oriens*. SSt-IR OLM cell dendrites have been shown to possess dendritic spines (figure 6.2.A, inset), quite different from those of CA1 pyramidal cells (McBain et al, 1994; Katona et al, 1999) and have 1 to 3 axon collaterals which traverse *str. pyramidale* and *radiatum* to ramify heavily in *str. L-M*. (figure 6.2.A); occasionally a small local axon arbour is seen in *str. oriens*. OLM cell somata highly express SSt (figure 6.2.A, inset). Approximately 25% of SSt-IR somata in *str. oriens* are also weakly IR for PV (Jinno and Kosaka et al, 2000), an example of which is seen in figure 6.2.A, inset.

Additional to well-defined morphology, SSt-IR OLM cells have a distinctive intrinsic electrophysiological profile. As seen in table 6.1, several key-intrinsic characteristics for OLM cells are quite different from CA1 pyramidal cells; by comparison, membrane potential and AP threshold are not different in OLM cells ($P=0.4009$ and $P=0.1153$, respectively). The defining feature of OLM cell intrinsic characteristics was the large voltage sag component (Maccaferri and McBain, 1996), proportional to I_h (Mayer and Westbrook, 1983), seen in response to hyperpolarising potentials which in our experiments was substantially larger than in CA1 pyramidal cells ($P<0.0001$). As OLM cells also co-express PV, we tested whether the I_h measured for OLM cells was similar to PV-IR neurons. We found that OLM cells dwarf PV-IR INs, with a 10-fold higher “sag” component seen in the OLM subtype ($P<0.0001$). This difference between PV and OLM cells is potentially due to a more active membrane of OLM cells. The longer membrane time-constant and R_i compared to PV-IR INs ($P=0.0003$ and $P=0.0083$, respectively) and CA1 pyramidal cells ($P=0.0004$ and $P=0.0015$, respectively) that we observed would suggest that membranes of OLM cells have less passively open channels than either cell type.

Action-potentials in OLM cells were significantly faster than in CA1 pyramidal cells, as described by the half-height duration ($P=0.0036$); whereas maximal rise rate was slower, but the maximal decay rate faster than for the same cells ($P=0.0008$, both). Interestingly, comparing AP kinetics to PV-IR INs, there was no difference in the maximal rise-rate ($P=0.8512$), but the decay rate was significantly slower in OLM cells ($P=0.0018$); subsequently AP half-height duration was longer ($P<0.0001$).

Passive Membrane Properties	CA1 pyramidal cells (n=27)	SSt-IR OLM cells (n=13)
Membrane Potential (mV)	-62.9 ± 1.2	-61.5 ± 0.4
Input Resistance ($M\Omega$)	102.2 ± 13.1	165.9 ± 5.7
Membrane Time Constant (ms)	22.0 ± 2.6	32.9 ± 0.7
Putative I_h “sag” (-250 pA)	3.0 ± 0.2	17.6 ± 0.6
AP kinetics		
Threshold (mV)	-39.8 ± 1.0	-36.6 ± 0.5
Amplitude (mV)	113.8 ± 2.1	96.8 ± 1.4
Half-height duration (ms)	0.84 ± 0.04	0.64 ± 0.01
Maximum rise-rate ($mV.ms^{-1}$)	610.6 ± 31.4	400.0 ± 13.4
Maximum decay-rate ($mV.ms^{-1}$)	109.3 ± 4.7	175.0 ± 5.7
Rise/Decay Ratio	5.6 ± 0.3	2.32 ± 0.05
AHP properties		
Amplitude (fast) (mV)	$5.9 \pm 0.6\ddagger$	23.9 ± 0.4
Amplitude (medium) (mV)	9.4 ± 0.5	$18.1 \pm 0.9\ddagger$
AP discharge Properties		
Maximum frequency (Hz)	23 ± 2	85 ± 3
Rheobase (pA)	131.1 ± 13.5	60.0 ± 5.6
Interspike interval ratio (ms)	1.55 ± 0.14	1.10 ± 0.10

Table 6.1 Summary of key intrinsic properties of CA1 SSt-IR OLM cells. Data are shown as mean \pm SEM alongside that of CA1 pyramidal cells, for comparison. Fast AHP values were obtained from 17 CA1 pyramidal cells (\ddagger) and medium AHP from 8 OLM cells (\ddagger).

OLM cells have been deemed to be regular spiking (Lacaille and Williams, 1990; McBain et al, 1994) which we tested using depolarisations up to 250 pA. OLM cells fired at 77.6 % of the frequency of PV-IR INs ($P=0.3482$) and at 277.0% of CA1 pyramidal cells ($P<0.0001$) and 162.8% of CCK-IR INs, which was not significant ($P=0.2217$). This quasi fast-spiking phenotype observed is paradoxical to the slower maximal AP decay rate, compared to PV-IR neurons we described earlier. The presence of a large fast-AHP component, similar to that seen in PV-IR INs ($P=0.8512$) in conjunction with a larger medium AHP component than the same PV-IR INs ($P=0.0465$). The K^+ conductances which contribute the fast and medium AHP are also distinct from CA1 pyramidal cells, as both AHP amplitudes were significantly larger ($P<0.0001$ and $P=0.0001$, respectively). Together these data confirm that SSt-IR OLM cells possess a cohort of K_v channels distinct from that of CA1 pyramidal cells or PV-IR INs as described by Zhang and McBain (1995), underpinning differences in AP and AHP kinetics.

This difference in AHP is exemplified by the ratio of interspike-interval leading to accommodation of AP discharge trains in SSt-IR INs, which shows a similar accommodation profile to that of PV-IR INs ($P=0.0549$), while showing less than CA1 pyramidal cells ($P=0.0202$); at 250 pA depolarisation. These distinct AP discharge properties are due to the presence of the Ca^{2+} -dependent, delayed-rectifying K^+ channel (K_v3 or K_v4 ; Lien et al 2002), which has very rapid activation and very slow inactivation, as described by Zhang and McBain (1995) which is temporally different to that observed in CA1 pyramidal cells or PV-IR INs.

In terms of the intrinsic properties of OLM cells, we have shown that there are distinct differences between OLM cells and CA1 pyramidal cells, as well as PV-IR INs. However, there are several clear overlaps in physiology between OLM and PV-IR INs, suggesting that OLM cells are fast-response signalling devices, which due to different voltage sensitive currents are capable of reacting rapidly to excitatory stimuli (Martina et al, 2000).

6.3 SSt-IR INs possess no observable GABA_BR IPSCs

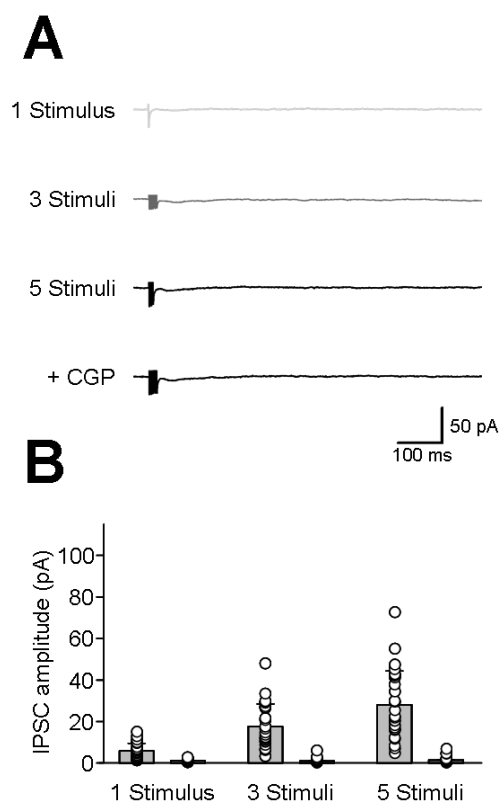


Figure 6.3 Release of endogenous GABA evoked no or very small slow-IPSCs in CA1 SSt-IR OLM cells. **A** Representative traces in responses to 1 stimulus (light grey) and 3 or 5 stimulus trains (dark grey and black, respectively) in SSt-IR OLM cells; 5 μ M CGP-55,845 (bottom, black) had no effect. **B** Mean IPSC amplitudes of SSt-IR OLM cells (dark grey bars), compared to CA1 pyramidal cells (light grey bars); individual experiment data is shown overlain (open circles).

To test whether the low levels of GABA_BR detected by immunocytochemistry corresponded to a reduced functional GABA_BR mediated K⁺ current in SSt-IR OLM cells we stimulated GABA release in *str. oriens*, due to the absence of dendrites in *str. radiatum*; in the presence of APV, NBQX and bicuculline. Using the 1 stimulus or 3 and 5 (200 Hz) stimulus train paradigm outlined earlier we detected no synaptically driven GABA_BR IPSCs in 9 out of 15 cells recorded, in the remaining 6 SSt-IR OLM cells we detected a very small response IPSCs. Slow IPSCs in all identified SSt-IR OLM cells had a mean amplitude of 1.3 ± 0.1 pA in response to single stimuli and of 1.0 ± 0.2 pA and 1.5 ± 0.2 pA, for 3 and 5 stimuli, respectively (figure 6.3.B). Responses seen in SSt-IR OLM cells were

substantially smaller than those of CA1 pyramidal cells (data from 15 cells; $P < 0.0001$, all stimuli levels). The mean normalised IPSC amplitude (to R_i) was: $1.1 \pm 0.4\%$, $0.8 \pm 0.2\%$ and $1.4 \pm 0.4\%$, which were all statistically smaller than in CA1 pyramidal cells ($P < 0.0001$, for all)

As SSt-IR OLM cells show a degree of overlap with PV-IR DI INS in CA1 (Jinno and Kosaka, 2000; Baude et al, 2007) we tested whether both cell types showed similar slow IPSC amplitudes. Mean IPSC amplitudes were larger in OLM cells than PV-IR DI following a single stimuli ($P = 0.0102$, Mann Whitney test), despite no difference in IPSC amplitude at 3 or 5 stimuli ($P = 0.6757$ and $P = 0.8114$, respectively).

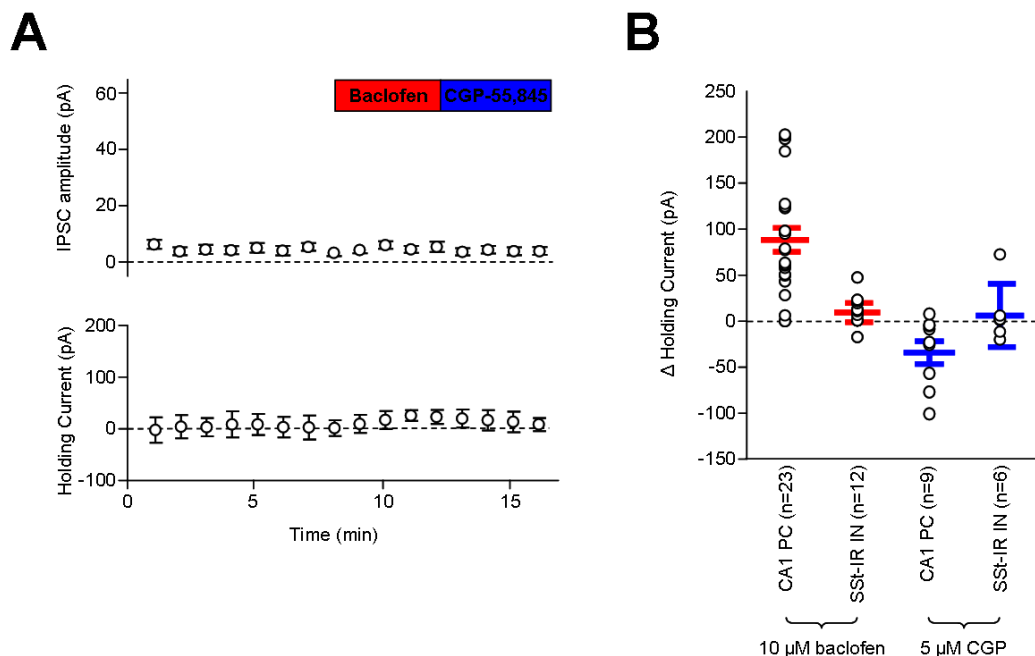


Figure 6.4 Pharmacological characterisation of $GABA_B$ -mediated responses in CA1 SSt-IR OLM cells. A Timecourse of IPSC amplitude (top) and voltage-clamp holding current (bottom), during control and following washin of 10 μ M baclofen (red bar) and 5 μ M CGP-55,845 (blue bar). B Mean baclofen (red) and CGP (blue) effect on holding current in OLM cells, compared to CA1 pyramidal cells. Data are overlain by individual cell responses (open circles).

To confirm that $GABA_B$ Rs present on OLM cells were functionally isolated from Kir3 channels we next tested the effect of 10 μ M baclofen and 5 μ M CGP-55,845 on holding current. It was clear that the small responses evoked by 5 stimuli were not occluded by 10 μ M baclofen nor blocked by 5 μ M CGP-55,845 (6.4.A

(top)). Application of 10 μM baclofen resulted in a minimal increase in mean holding current of 10.9 ± 4.6 pA (in 12 cells), which indicated a very low level of GABA_BR/Kir3 channel interaction, confirming synaptic data, and was equivalent to $8.1 \pm 2.4\%$ of R_i ($P=0.0002$, compared to CA1 pyramidal cells)

Application of 5 μM CGP 55-845 following baclofen application reduced holding current to a mean level of 7.2 ± 6.6 (6 cells; figure 6.4.A); not significantly different from mean baclofen effect on holding current recorded in the same cells ($P=0.6250$; Wilcoxon signed-rank test). Comparison of pharmacological effects in SSt-IR OLM cells to CA1 pyramidal cells (figure 6.4.B) confirmed that the former had a highly reduced baclofen response ($P= 0.0001$) and minimal CGP effect, albeit not significant ($P=0.0663$); confirming that GABA_BR responses produced through interaction with Kir3 channels are all but absent in SSt-IR OLM cells, in area CA1.

6.4 Conclusions

We have shown here that SSt-IR OLM cell dendrites possess very low numbers of GABA_BR, in comparison to CA1 pyramidal cells, in *str. oriens* of the CA1. These results were confirmed by electrophysiological recordings from SSt-IR OLM cells, which showed that there is a substantially lower component of GABA_BR-mediated signalling in the dendrites of these cells, compared to CA1 pyramidal cell basal dendrites; suggesting either complete absence of GABA_BR in SSt-IR dendrites or an absence of functional coupling of GABA_B to Kir3 channels in these dendrites.

Previous data, particularly McBain et al (1994), suggest that INs located within *str. oriens*, with axonal arborisations akin to OLM cells, possess a very high levels of dendritic mGluR1; this fact, combined with our data for absence of typical dendritic GABA_BRs suggest that the predominant slow inhibitory force in these INs may arise from glutamate release from local C1 pyramidal cell axons, rather than GABAergic mechanisms.

Chapter 7 GABA_B receptors control presynaptic GABA release from PV and CCK-IR axon terminals.

Aside from modulating post-synaptic membrane potential, GABA_BRs have a well described role in inhibiting release of transmitter from pre-synaptic terminals of principal cells and INs. Acting through volume transmission, presynaptic GABA_BRs are activated by either heterosynaptic depression, with GABA spillover from other synapses (Vogt and Nicoll, 1999) or via autoreceptor activation, with GABA release binding to GABA_BRs on the same synapse, inhibiting transmission in a retrograde manner (Pittaluga et al, 1987). There is evidence that some INs possess presynaptic GABA_BRs (Davies and Collingridge, 1993; Lei and McBain, 2003; Price et al, 2008; Lee and Soltesz, 2010), therefore we attempted to determine whether presynaptic GABA_BRs were present in either CCK or PV-IR INs. One main issue is that no one group has purposefully determined the relative contribution of GABA_B to inhibiting GABA release from these terminals in a pair-wise fashion, as each subtype of cell is associated with different network functions.

We started by determining, from double immunolabeling electron microscopy, the relative distribution of the GABA_{B1} subunit in PV and CCK immunoreactive boutons, then confirming whether functional differences exist between neurochemical and morphological subtypes. To establish whether GABA_BR receptor activation and antagonism was comparable CCK-IR or PV-IR axons, we first isolated the respective axons pharmacologically. Fortuitously, presynaptic modulators unique to both PV-IR and CCK-IR INs are known in the CA1 region of the hippocampus, particularly CB1 and M2 receptors; in CCK and PV-IR axons, respectively. We utilised the presence of these receptors, by selectively activating them, while recording unitary IPSCs by minimal stimulation of individual axons; activation of either receptor type leading to inhibition of transmitter release from axons containing that receptor subtype. We then pharmacologically probed GABA_BRs effect on pre-synaptic release mechanisms in these cell types, gauged by post-synaptic response amplitude. The most definitive description of unitary coupling between local INs and principal cells is

achieved by recording directly from synaptically coupled pairs of neurons, then testing the presynaptic GABA_BR profile of this coupling. The latter half of this chapter is concerned with applying this technique on representative IN/pyramidal cell pairs.

7.1 GABA_{B1} receptor subunits localise to CCK and PV-IR axon terminals in *str. pyramidale* of CA1.

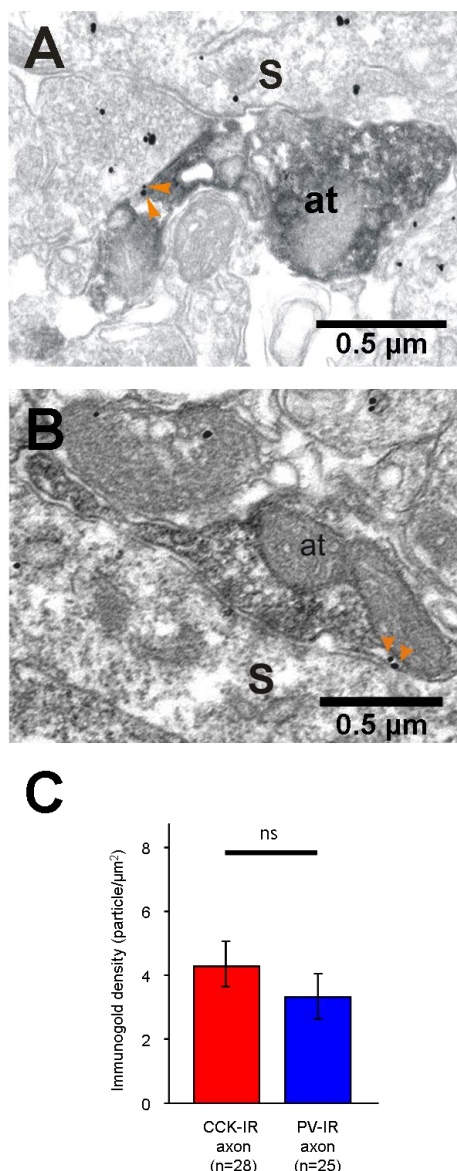


Figure 7.1 Immunocytochemical localisation of GABA_{B1} receptor subunits to PV and CCK-IR axon terminals in *str. pyramidale* of CA1. **A** Electron micrograph of a PV-IR axon terminal (at) containing immunogold particle corresponding to GABA_{B1} receptor subunits (orange arrowheads); contacting a presumed CA1 pyramidal cell somata (S). **B** A CCK-IR axon terminal also exhibiting GABA_{B1} receptor subunit labelling (same scheme as A). **C** Comparison of immunogold labelling in CCK-IR (red) and PV-IR (blue) axon terminals. Statistics shown: ns - not significant, P>0.05.

We attempted to detect GABA_BRs at the level of the plasma membrane in CCK-IR and PV-IR IN axon terminals. In figure 7.1.A and B we see representative electron micrographs displaying low density labelling of GABA_{B1} subunits on axon terminals of PV-IR (A) and CCK-IR (B) INs; which make contact with putative CA1 pyramidal cell soma, in *str. pyramidale*.

Of 28 CCK-IR and 25 PV-IR axon-terminals analysed, we determined that GABA_{B1}R-subunit immunoreactivity in DAB end-product containing boutons was approximately 7-fold lower in CCK-IR boutons, than in CCK-IR dendrites from the same material ($P < 0.05$). Whereas, dendrites of PV-IR cells were lower than those seen in CCK-IR, however axon-terminal labelling was still approximately 3-fold lower in this cell type ($P < 0.05$). At the pre-embedding immunogold electron microscopic level, there was no discernable difference between the labelling seen on PV or CCK immunoreactive axon terminals ($P > 0.05$).

This data shows that firstly GABA_BRs were located on CCK and PV-IR axon terminals found within *str. pyramidale* of the CA1. Secondly there was no difference in GABA_BR content of the two neurochemical cell types, suggesting a lack of difference in presynaptic GABA_B functionality.

7.2 PI IN inputs onto CA1 pyramidal cells were pharmacologically separated, revealing two distinct axonal subtypes.

Isolated unitary IPSCs were obtained from somatic recordings of CA1 pyramidal cells, in the presence of ionotropic glutamate receptor blocker NBQX (10 μ M) and APV (50 μ M); under minimal stimulation paradigms whereby the stimulus intensity resulted in a suprathreshold response, whereas any lower stimulus evoked no response, the mean stimulus intensity was 4.2 V (~20 μ A equivalent). By this method we could reliably obtain recordings from single axons which were present in *str. pyramidale*, presumably of PI subtypes (Katona et al, 1999). Once a stable recording was established for at least 2 minutes we applied the highly

potent and selective CB1 receptor agonist WIN-55,212 (1.0 μM), which in 18 recordings we washed in for 10 minutes (figure 7.2.A). 6 unitary responses responded to CB1 activation, resulting in a significant reduction of IPSCs to 29.2% of control levels ($P=0.0313$, Wilcoxon matched-pairs test) confirming presence of CB1 receptors in the axon terminals; a signature of CCK-IR basket cell axons (Katona et al, 1999; Tsou et al, 1999; Lee and Soltesz, 2010). Monosynaptic IPSCs originating from WIN-sensitive, putative CCK-IR basket cell axons had a mean amplitude of 122.7 ± 8.3 pA, with a onset latency of 1.18 ± 0.08 ms and peak latency of 2.55 ± 0.15 ms.

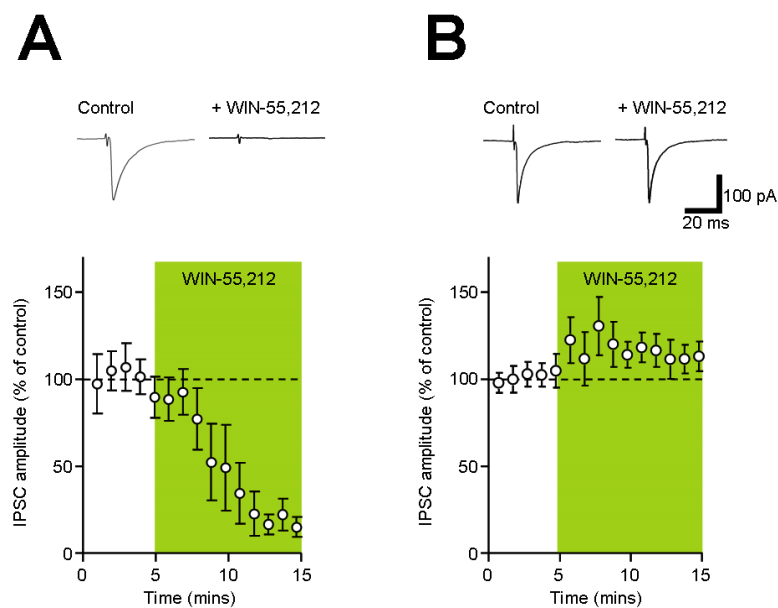


Figure 7.2 Monosynaptic IPSCs elicited by minimal stimulation in *str. pyramidale* were differentially sensitive to CB1 receptor activation. **A** Application of the selective CB1 receptor agonist, WIN-55,212 (1.0 μM , green shading), fully blocked unitary IPSCs after 10 minutes washin in 6 cells. **B** In another set of recordings WIN-55,212 did not reduce IPSC amplitude (12 cells) after 10 minutes washin. Inset (both, top), representative IPSC before (left) and after (right) application of WIN-55,212.

Application of WIN-55,212 in the remaining 12 unitary responses, resulted in no significant change in IPSC amplitude (figure 7.2.B; 107.9% of control, $P=0.3652$, Wilcoxon matched-pairs test). These fibres were deemed to be WIN-insensitive, which due to localisation in *str. pyramidale*, predominately originating from putative PV-IR basket cell axons (Katona et al, 1999). Monosynaptic IPSCs which were not sensitive to WIN-55,212 had a mean peak amplitude of 130.7 ± 15.1 pA

similar to that of WIN-sensitive responses ($P=0.2563$), an onset latency of 0.91 ± 0.04 ms, similar to that of WIN-sensitive responses ($P=0.3499$); and had a peak latency of 2.32 ± 0.08 ms, similar to that of WIN-sensitive responses ($P=0.9734$).

7.3 Axons of pharmacologically distinct PI INs have different presynaptic GABA_BR profiles

In 9 cells, we briefly applied $1.0 \mu\text{M}$ WIN-55,212 (2 minutes), which was then washed out of the bath, to test CB1 receptor sensitivity. This transient application of WIN resulted in a decrease of IPSC amplitudes to 37.9% of control (figure 7.3, bottom, green shading; $P=0.0039$, Wilcoxon matched pairs test) and was a similar reduction to that seen following 10 minute WIN washin (figure 7.2.A; $P=0.2238$); indicating that these 9 unitary responses were sensitive to WIN, therefore the afferent most likely contained the CB1 receptor. Following washout of WIN IPSC amplitudes returned to 90.8% of control levels ($P=0.3008$, Wilcoxon matched-pairs test). WIN-55,212 application had no effect on post-synaptic pyramidal cell holding-current (figure 7.3.A (top); $P=0.2366$, Wilcoxon matched pairs test), indicating that CB1 receptor currents, if present, were minimal in CA1 pyramidal cells.

Once IPSC amplitudes had recovered we applied $10 \mu\text{M}$ baclofen to the circulating ACSF, resulting in a 129.1 ± 15.3 pA increase in holding current in the postsynaptic cell, similar to that seen in chapter 3 for other CA1 pyramidal cells ($P=0.1757$). GABA_BR mediated post-synaptic effect were accompanied by a robust decrease in IPSC amplitude, to 27.3% (in 9 cells) significantly smaller than that seen following IPSC recovery after WIN-55,212 application ($P=0.0039$, Wilcoxon matched-pairs test).

Following baclofen-mediated application, we applied the selective GABA_BR antagonist CGP-55,845 ($5 \mu\text{M}$). Qualitatively, CGP-55,845 resulted in reversal of holding current changes (figure 7.2.B (top, blue bar) to 23.0 ± 10.7 pA below

control levels ($P=0.2188$, Wilcoxon matched pairs test). Simultaneously, IPSC amplitude returned to 115.7% of WIN washout levels (6 cells); overshooting the control level, but not significantly so ($P=0.6875$, Wilcoxon matched pairs test). Following recovery of IPSCs by GABA_BR antagonism, we applied the selective and potent M2 agonist arecaidine but-2-ynyl ester tosylate (ABET, 10 μ M; Chiang et al 2010) to confirm that WIN-sensitive axons did not contain the M2 receptor. In 3 cells ABET had no significant effect on IPSC amplitude compared to CGP-55,845 levels (105.3% of control, $P=0.5000$, Wilcoxon matched-pairs test), confirming the absence of M2 receptors in these axons.

In a further 2 cells we then applied WIN-55,212 for 10 minutes then co-applying 10 μ M baclofen to test whether CB1 and GABA_B receptor responses were mutually exclusive. Baclofen application resulted in no further inhibition of IPSC amplitude from WIN steady-state (113.1% of WIN steady-state, data not shown); in line with previous reports (Lee and Soltesz, 2010), which suggests that these receptors share a common second messenger pathway, in putative CCK-IR presynaptic basket cell axons.

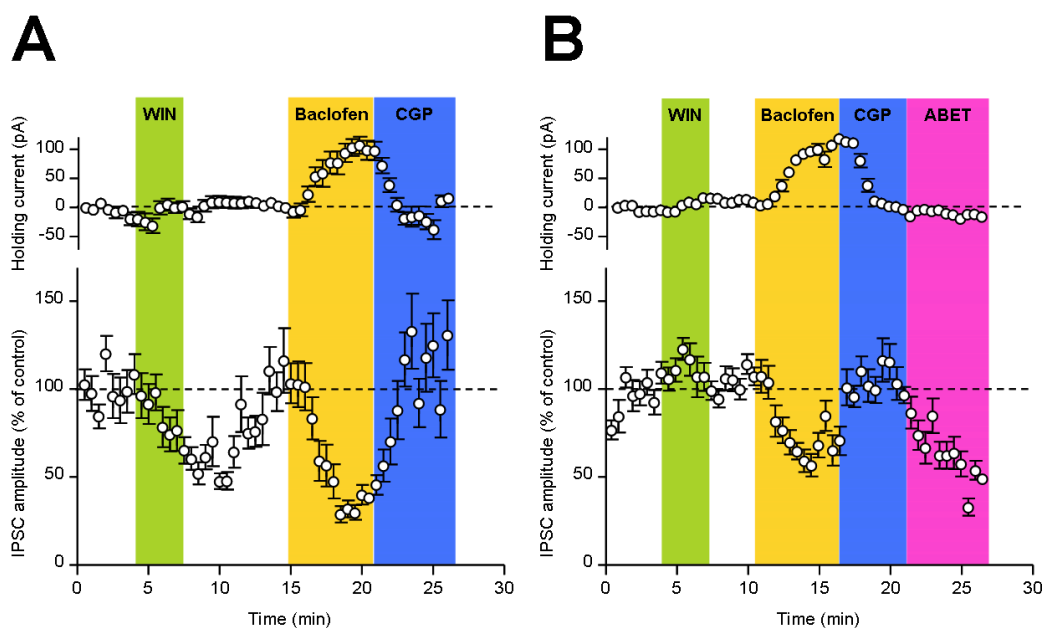


Figure 7.3 GABA_BRs exerts presynaptic control of GABA release in PI axons which is independent of WIN-sensitivity. **A** Timecourse of the washin of 1.0 μ M WIN-55,212 (green shading), 10 μ M baclofen (yellow shading) and 5 μ M CGP-55,845 (blue shading) on monosynaptic IPSC originating from WIN-sensitive fibres (bottom) and pyramidal cell holding current (top); in 7 cells. **B** The same timecourse but in 4 WIN-insensitive afferent recordings (same scheme as **A**), with the subsequent application of 10 μ M ABET (pink shading) following CGP-55845 washin; to determine M2 receptor activity.

As shown above WIN-insensitive unitary responses exist in *str. pyramidale*, putatively arising from PV-IR PI axons which generally lack CB1 receptors (Katona et al, 1999), but contain M2 receptors (Hájos et al, 1997). We therefore surmised that WIN-insensitive unitary responses we detected originated from PV-IR PI cells. We assessed whether WIN-insensitive axonal responses were similarly modulated by GABA_BR activation.

In 11 cells we applied 1.0 μM WIN-55,212, resulting in no decrease in IPSC amplitude (107.9% of control, $P=0.3652$; Wilcoxon matched-pairs test), suggesting that CB1 receptors did not contribute to presynaptic inhibition in these unitary responses. WIN-55,212 resulted in a small increase in holding current (14.7 ± 30 pA), albeit not significant ($P= 0.6250$, Wilcoxon matched-pairs test; figure 7.3.B (top)).

We applied 10 μM baclofen to 15 cells where WIN-55,212 had either been briefly washed in or had reached steady state, resulting in a reduction of monosynaptic IPSC amplitudes to 50.6% of control levels ($P<0.0001$, Wilcoxon matched-pairs test; figure 7.2.B, bottom). Baclofen resulted in a substantial increase in postsynaptic holding current, of 73.1 ± 36.8 pA, not dissimilar from that observed earlier in chapter 3 ($P=0.3865$). In a subset of experiments (5 cells) we applied 5 μM CGP-55,845 for 5 minutes following baclofen effect, partially reversing presynaptic inhibition, returning IPSC amplitudes to 79.5% of pre-baclofen levels ($P=0.1875$, Wilcoxon matched-pairs test); while concordantly returning pyramidal cell holding current to 0.4 ± 18.6 pA of WIN washout levels.

To confirm that WIN-insensitive responses were elicited by PV-IR PI axons we applied the selective M2 agonist ABET (10 μM) on top of CGP-55,845 (4 cells), resulting in large reduction of monosynaptic IPSCs to 49.5% of CGP levels ($P=0.1250$, Wilcoxon matched-pairs test). The effect of ABET, although not significant, due to low experimental numbers, was substantial and comparable to that observed by Chiang et al (2010) in DG PV-IR basket cells.

Comparison of the relative effects of WIN-55,212, 10 μ M baclofen, 5 μ M CGP-55,845 and 10 μ M ABET on IPSCs evoked by either putative CCK-IR or PV-IR axons, can be seen in figure 7.4. Putative CCK-IR axons showed a significant difference in WIN-55,212 response compared to PV-IR axons, as expected ($P=0.0003$). Interestingly, 10 μ M baclofen resulted in a 72.7% decrease of monosynaptic IPSCs produced by putative CCK afferents compared to a 49.4% decrease in putative PV axons ($P=0.0019$). In both axon terminal subtypes, there was no difference in the response to CGP-55,845 following baclofen wash-in ($P=0.5368$), indicating that in our experiments there was no difference in the tonic GABA_B activation between these two cell types. Finally, the selective M2 agonist ABET resulted in no reduction in WIN-sensitive axonal responses, but reduced WIN-insensitive responses by approximately half, although this was not significantly different.

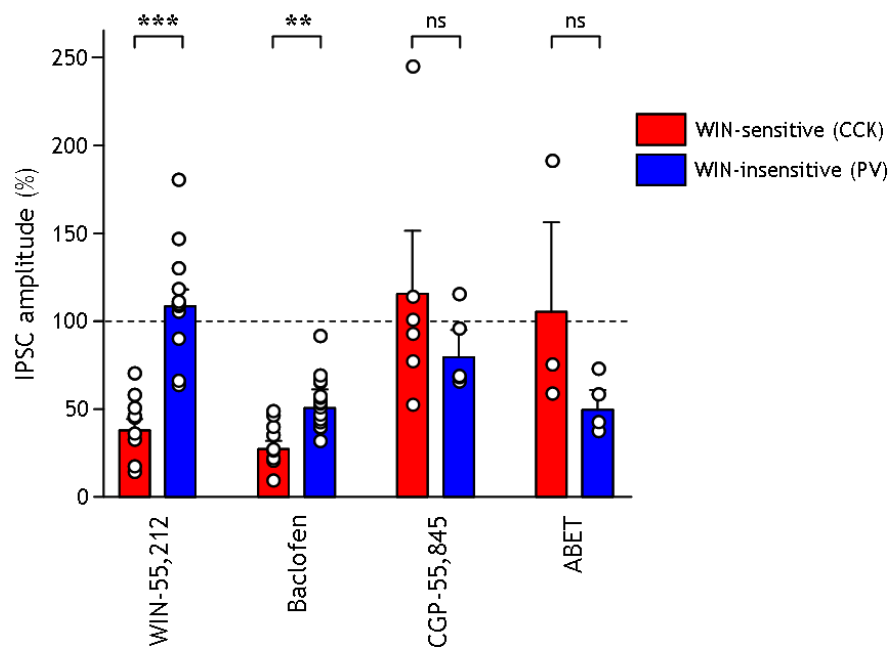


Figure 7.4 Comparison of monosynaptic IPSC amplitudes from M2 and CB1 sensitive afferents. Percentage difference from control (WIN-55212), WIN-55,212 washout (baclofen and CGP-55,845) and CGP-55,845 steady-state (ABET) of monosynaptic IPSCs; produced by WIN-sensitive (CCK-IR, red) and WIN-insensitive (PV-IR, blue) axons in *str. pyramidale* of CA1. Data from individual recordings is shown overlaid (open circles) and statistics shown are: not significant (ns) - $P>0.05$, ** - $P<0.01$ and *** - $P<0.001$. The 100% level of each control level is shown (dashed line).

Thus, pharmacological isolation of putative PV or CCK containing PI axons by either M2 or CB1 activation, respectively, revealed that axons of both

neurochemical subtypes possess GABA_BRs in presynaptic axon terminals. Activation of these receptors reveals that inhibition of GABA release is more strongly controlled by GABA_BRs in axons of putative CCK PI cells, as opposed to PV PI cells.

7.4 GABA_BRs mediate presynaptic control of GABA release from identified CCK and PV IR basket cells

We attempted to record from INs which were synaptically coupled to CA1 pyramidal cells, using paired-recording techniques, to assess GABA_BR control of GABA release from identified cells. This gave us a method to confirm results seen in pharmacological experiments, where the neurochemical subtype could be safely assumed, but not guaranteed. We recorded 6 pairs of synaptically coupled PV-IR or CCK-IR cells, either of the PI or DI morphological subtypes as outlined previously in chapters 3 and 4; identifying them on the basis of immunoreactivity for either PV or CCK content, additionally in CCK-IR INs we checked if CB was co-expressed.

We recorded from 2 CCK-IR basket cell/CA1 pyramidal cell pairs which, briefly, had somata located in *str. radiatum*, had a regular spiking phenotype and showed IR for CCK neuropeptide (Figure 7.5.A). Single APs elicited by depolarising the pre-synaptic CCK-IR basket cell resulted in unitary IPSCs recorded in the post-synaptic pyramidal cell, with amplitudes of 42.4 and 81.7 pA for each cell. Application of 10 µM baclofen to the perfusing ACSF resulted in a complete abolition of synaptic transmission to 1.6% of control amplitude, signifying that all GABAergic transmission from the two cells had ceased in the presence of baclofen. Application of 5 µM CGP-55,845 to these cells fully recovered the IPSC in the post-synaptic cell to 117.2% of pre-baclofen levels (Figure 7.5.B and C). These observations in CCK-IR cell perisomatic synapses, confirm the strong role of GABA_B in inhibiting GABA release from these cells.

By contrast to CCK-IR PI cells, we also obtained paired synaptic responses in 2 presynaptic PV-IR INs, which were identified as basket cells. In figure 7.6.A we see a representative cell from these experiments. Both PV-IR presynaptic INs had a fast-spiking phenotype, somata and axons in and around *str. pyramidale* (inset, red arrows) and were both strongly IR for PV.

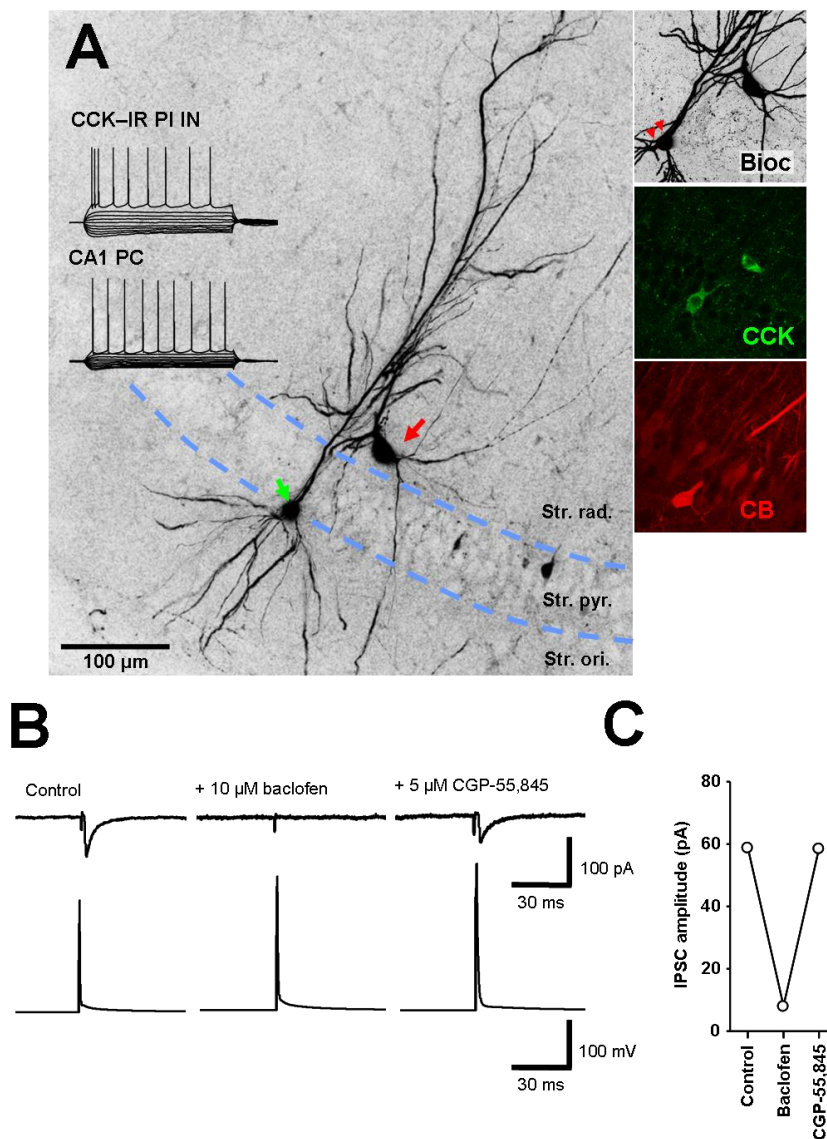


Figure 7.5 Monosynaptic IPSCs from CCK-IR PI cells are sensitive to GABA_B activation. **A** Low power, flattened confocal micrograph of a CCK-IR basket cell (red arrow) synaptically coupled to a CA1 pyramidal cell (green arrow) shown as biocytin/avidin signal (black pseudocolour). Inset (left), representative trains of APs for the paired cells. Inset (right), high power confocal micrograph of cell soma showing colocalisation of biocytin/avidin (black pseudocolour), CCK (green pseudocolour) and CB (red pseudocolour); putative synaptic contacts are shown (red arrowheads). **B** Mean IPSCs during control (top, left) and following baclofen (top, middle) and CGP-55,845 washin (top, right); presynaptic APs shown below respective IPSCs. **C** Average IPSC amplitudes for the cell shown in **B**.

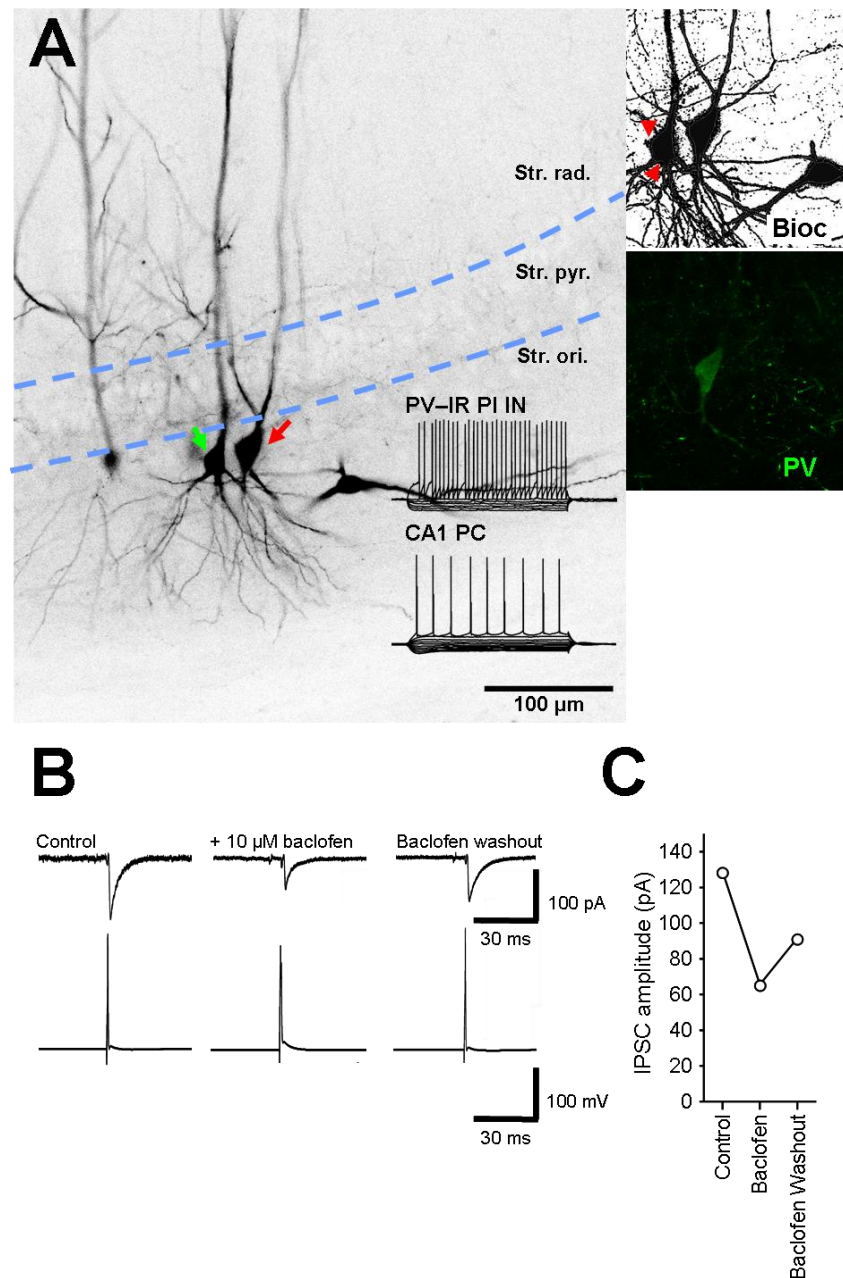


Figure 7.6 Monosynaptic IPSCs from PV-IR PI cells are sensitive to GABA_BR activation. **A** Flattened, low power confocal micrograph showing biocytin/avidin (black pseudocolour) and PV (green pseudocolour) with presynaptic PV-IR basket cell (red arrow) and CA1 pyramidal cell (green arrow) indicated. Inset (near right), representative trains of APs in the paired cells; inset (far right), high-magnification confocal images of the cell soma with colocalisation of biocytin /avidin (black pseudocolour) and PV (green pseudocolour); putative axon contacts are indicated with red arrowheads. **B**, mean IPSCs (top) resulting from presynaptic AP (bottom) before (left) during (middle) and after (right) 10 μ M baclofen application. **C** IPSC amplitudes plotted from the same cell.

PV-IR basket cells also produced a robust IPSC in the post-synaptic pyramidal cell, with amplitudes of 81.4 and 63.6 pA. Once again we applied the selective

GABA_B agonist baclofen (10 μ M), which reduced IPSC amplitude to an average of 51.0% of pre-baclofen levels. Unfortunately, neither of these PV-IR basket cells was tested for their CGP-55,845 response. However the baclofen level observed is almost identical to that seen from extracellular stimulation of presumed CCK axon, suggesting strong concordance of the two data-sets.

7.5 CCK and PV IR DI INs coupling to CA1 pyramidal cells is differentially inhibited by GABA_BRs

From the synaptically coupled paired-recordings in 7.4 we also identified 2 presynaptic DI cells, one of both CCK and PV IR types. Interestingly, the GABA_BR inhibition of GABA release was divergent between these two cell types and from basket cells containing the same neurochemicals. We identified 1 CCK-IR DI cell, which had similar characteristics to a SCA DI cell described in chapter 4 (see figure 7.7.A). In this recording, we observed a mean IPSC in the post-synaptic pyramidal cell of 12.7 pA, substantially smaller than that seen in paired-recordings from CCK-IR basket cells; reflecting the differential distance between synapse location and somatic recording electrode between these two cell types.

Bath application of 10 μ M baclofen reduced the IPSC amplitude to 2.4 pA, reflecting a reduction to 18.4% of control levels (figure 7.7.B and C). Washin of 5 μ M CGP-55,845 was not obtained for this cell. The IPSC amplitude change seen in response to 10 μ M baclofen was somewhat less than that seen in CCK-IR PI cells, however was of a similar order of magnitude to that seen of extracellular activation of WIN-sensitive fibres in figure 7.3.

A single PV-IR DI cell was identified as a putative bistratified cell, with similar physiological and morphological properties as described in chapter 4, notably a fast-spiking phenotype (figure 7.8.A). A small IPSC was detected at the level of the pyramidal cell somata with amplitude of 10.2 pA; close to that seen in the CCK-IR DI cell.

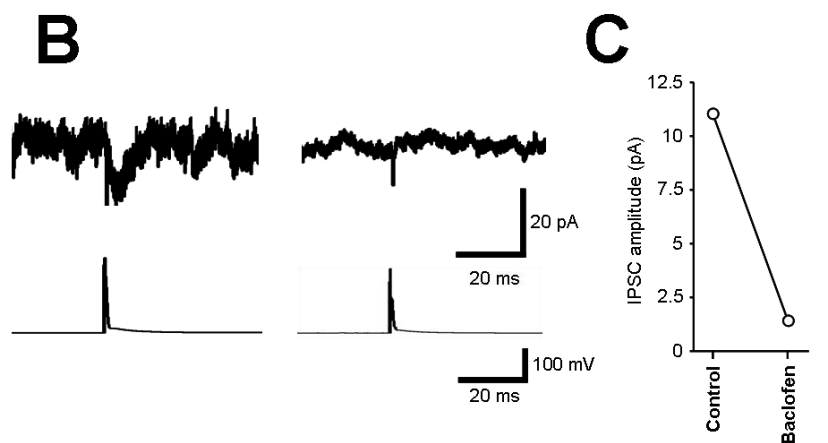
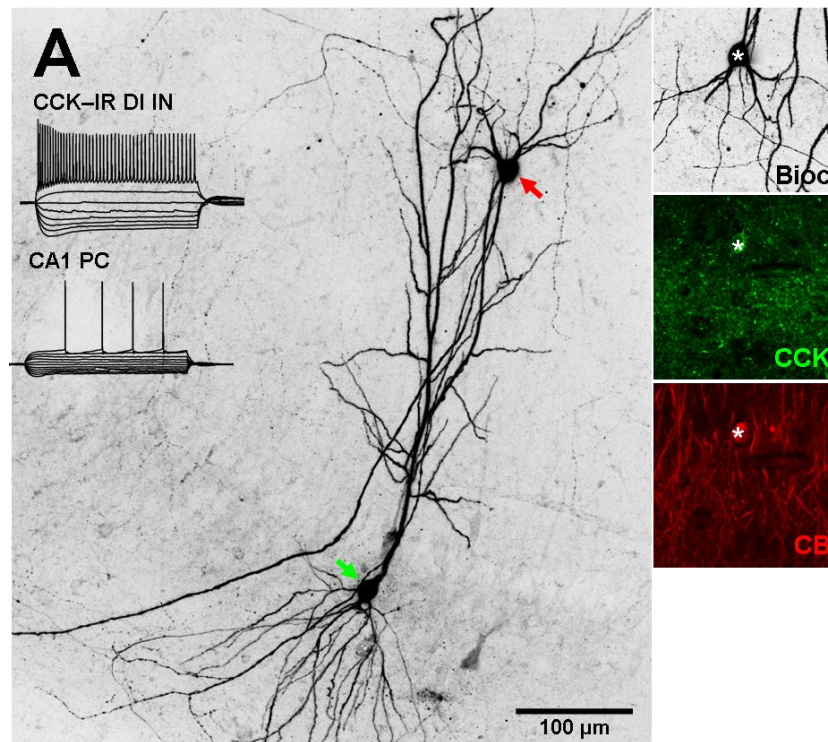


Figure 7.7 Monosynaptic IPSCs from CCK-IR DI cells are also sensitive to GABA_BR activation. **A** Low power, flattened confocal micrograph of biocytin/avidin fluorescent labelling (black pseudocolour); the presynaptic CCK-IR DI cell (red arrow) and CA1 pyramidal cell (green arrow) are both indicated. AP discharge patterns for the two cells are shown inset (left). High-magnification confocal images of the IN somata are shown inset, (far right) for biocytin (black pseudocolour), CCK and CB (green and red pseudocolour, respectively). **B** Small IPSCs (top) were elicited in response to presynaptic APs (bottom) before (left) and during (right) 10 μ M baclofen application. **C** Control and baclofen IPSC amplitudes plotted for the same cell.

Application of 10 μ M baclofen to the perfusing ACSF resulted in no change in IPSC amplitude, with a peak amplitude following baclofen of 10.6 pA, equating to 104.1% of control IPSC amplitude (see figure 7.8.B and C). CGP-55,845 was

not added to the bath as the post-synaptic pyramidal cell patch-clamp was lost following induction of baclofen steady-state.

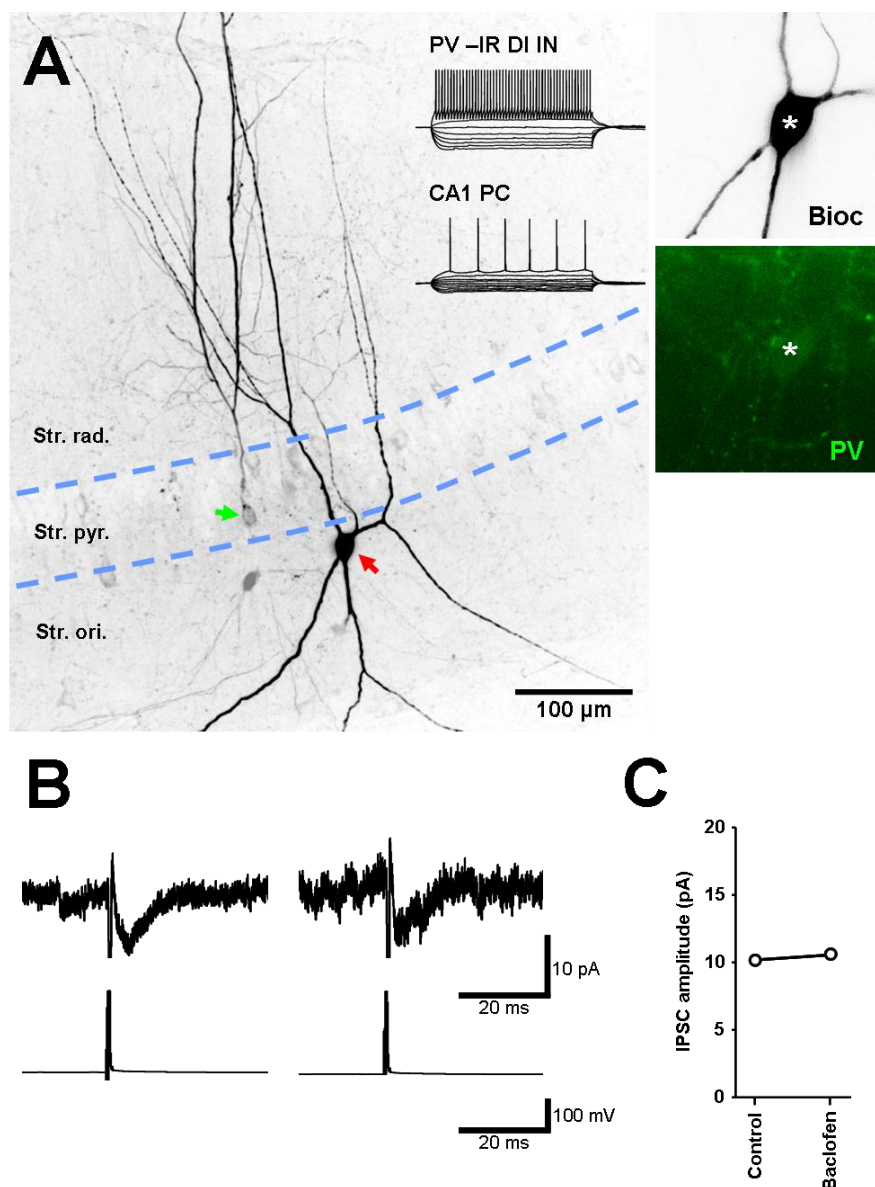


Figure 7.8: Monosynaptic IPSCs from PV-IR DI cells are not sensitive to $GABA_B$ activation. **A** Low power, flattened confocal micrograph with labelling for biocytin/avidin (black pseudocolour) show a presynaptic PV-IR DI subtype cell (red arrow) and CA1 pyramidal cell (green arrow). Representative AP trains for both cells are shown inset (near right). High-magnification images of the DI cell somata (inset, far right) show colocalisation of biocytin/avidin (black pseudocolour) and PV (green pseudocolour). **B** Very small IPSCs (top) were produced in response to presynaptic APs (bottom); before (left) and during (right) 10 μ M baclofen application. **C** Control and baclofen IPSC amplitudes plotted for the same cell.

The data from both PV and CCK-IR DI cells suggests that unlike in basket cells where both neurochemical subtypes of IN possess some degree of presynaptic

GABA_B control, DI CCK or PV-IR cells either have GABA_B in axon terminals (CCK-IR DI cells) or completely lack GABA_BR mediated inhibition of GABA release (PV-IR DI cells).

7.6 Conclusions

Through pharmacological isolation of unitary IPSCs and paired recordings of IPSCs elicited from identified CCK-IR and PV-IR INs we have determined that there are functional GABA_BR localised to the presynaptic terminals of both CCK and PV immunoreactive INs. This finding is confirmed by the presence of immunogold particles for GABA_{B1} on the axon terminals of PV and CCK-IR cells, in *str. pyramidale*. Activation of GABA_BRs differentially modulate the release of GABA from these terminals, with GABA release inhibited more strongly by GABA_BR activation in CCK-IR terminals from both PI and DI IN cell types. On the other hand, we have shown that in PV-IR PI cells, in both sets of experiments performed, GABA_B inhibits GABA release to a lesser degree than in CCK-IR axons. Interestingly, in one identified PV-IR DI cell, selective activation of GABA_B resulted in no change in post-synaptic IPSC amplitude, suggesting an absence of GABA_BR in these terminals.

8. General discussion

8.1 Key findings

We have shown that there are several distinct types of hippocampal neuron with discrete morphological and physiological characteristics possess GABA_BR functional currents of differing levels in postsynaptic domains, as well as in pre-synaptic domains; which was confirmed using immunocytochemical and electrophysiological techniques.

8.1.1 Intrinsic properties of hippocampal neurons

Although evidence exists on the physiological properties of both excitatory and inhibitory hippocampal neurons, there is little quantification of intrinsic membrane properties of either principal cells or interneurons (Han et al, 1993; McBain et al, 1994; Buhl et al, 1995; Gloveli et al 2005). In chapter 3 we provide detailed electrophysiological quantification of key intrinsic properties of principal cells; in particular GRCs (of which no published data exists). In chapters 4-6 we describe the same properties in PV, CCK and SSt IR INs compared to CA1 pyramidal cells, or in the case of DG PV-IR, to CA1 PV-IR Ins.

We confirmed that PV-IR INs have fast-spiking phenotypes, underlying their role in γ and SWR oscillations in both PI and DI cell types (Bartos et al, 2002; and Klausberger et al, 2005), despite PV-IR DI cells firing significantly faster. Interestingly, there is little difference in AP firing between identified SSt-IR OLM cell and PV-IR PI cells; with only passive intrinsic properties differing significantly, due to the large inducible I_h in OLM cells.

We quantified membrane properties of CCK-IR PI and DI cells showing that there are minimal differences between both subtypes of CCK-IR cells with nearly all intrinsic characteristics similar but both cell types generally divergent from CA1 pyramidal cells, consistent with the work of Vida et al, 1999; Pawelzik, et al 2002). Interestingly, there is little difference in AP decay rate between CCK-IR cells and CA1 pyramidal cells, suggesting a similar compliment of K_V channels contributing to the AHP.

Together the intrinsic physiology provided here, provides a thorough description of membrane properties of a selection of hippocampal INs, corroborating and confirming previous data, as well as the first full and thorough description of GRC intrinsic physiology.

8.1.2 $GABA_B$ Rs in hippocampal principal cell

All principal cells possess $GABA_B$ R mediated synaptic and whole cell currents, produced by electrical stimulation or pharmacological manipulation, as summarised in table 8.1.

CA1 pyramidal cells possessed large $GABA_B$ R mediated responses, which we confirmed were mediated by K^+ conductances, shown by Otis et al (1993). In line with anatomical data published by Kulik et al (2003), which indicated that $GABA_B$ R were expressed a lower densities on basal dendrites in *str. oriens* than apical dendrites in *str. radiatum*, we have shown that GABA released selectively in *str. oriens*, results in smaller $GABA_B$ R IPSC amplitudes, compared to those elicited at the *str. radiatum/LM* border, functionally confirming this earlier observation. GABA release from a variety of INs with axon ramifications in this distal neuropil region (i.e. neurogliaform (Price et al, 2008) or SSt cells (Katona et al, 1999) will lead to more efficient control of propagation and summation of excitatory input along apical dendrites via the $GABA_B$ R.

Little is known regarding the synaptic inhibition profile of CA1 GRCs (Savic and Sciancalepore, 2001). We have shown that GRCs possess synaptic GABA_BR responses, larger than in CA1 pyramidal cells, with little difference in baclofen mediated currents; suggesting that the complement of GABA_BRs is similar for both cell types. The larger amplitude IPSCs observed could be due to the higher density of dendritic arborisation in the distal *str. radiatum* (Gulyas et al, 1999), with more dendrites containing functional receptors closer to the stimulation site. This increased local GABA_BR response will enhance the relative weight of GABA_BR-mediated inhibition arising from GABAergic activity in *str. radiatum/L-M*. With dense axon in *str. oriens* these cells could provide substantial feedback excitation onto OLM cells. Strong regulation by GABA_BR transmission could hint that GRCs play a role in the entrainment of hippocampal networks to θ -oscillations (Scanziani, 2000).

Principal cell type (<i>stimulation site</i>)	GABA _B R response	
	IPSC	Baclofen
CA1 pyramidal cell (<i>str. radiatum/LM</i>)	Medium	~100 pA
CA1 pyramidal cell (<i>str. oriens</i>)	Small	~100 pA
GRC (<i>str. radiatum/LM</i>)	Large	=CA1 PC
DGC (<i>outer molecular layer</i>)	Large	=CA1 PC

Table 8.1 Summary of GABA_BR mediated currents in principal cells of the hippocampus. Different stimuli locations of CA1 pyramidal cells are indicated in parenthesis; CA1 PC = CA1 pyramidal cell.

In DGCs, GABA release in the distal molecular layer resulted in the activation of large GABA_BR currents, activated a larger fraction of a total GABA_BR complement; with a similar baclofen response to CA1 pyramidal cells. This suggests that local GABA release in the distal ML has a larger inhibitory effect of DGC dendrites, suppressing EPSP propagation more heavily, due to a denser local dendritic arborisation. This strong synaptic inhibition greater slow inhibition of synaptic inputs to the hippocampus which may contribute to timing of perforant path inputs, through slow feedback inhibition mediated by GABA_BRs.

8.1.3 Cellular and subcellular localisation of GABA_BRs in identified hippocampal INs

Our results show that previous immunocytochemical studies, identifying GABA_BRs in neurochemically identified IN populations; largely underestimated the presence and the functional role of GABA_BRs in PV-IR INs, while potentially overestimating the role of GABA_B in postsynaptic transmission of CCK-IR and SSt-IR INs (Sloviter et al, 1999). From the results we present regarding the nature of GABAergic transmission of IN populations, we are lead to re-examine the relative weight of slow GABA_BR mediated transmission in controlling postsynaptic and presynaptic excitability in these cells.

Morphological assessment of GABA_BRs in CCK, PV and SSt IR INs at the light microscopic level was in general agreement with the results of Fritschy et al (1999) and Sloviter et al (1999). In contrast, electron microscopic investigation showed that on PV and SSt IR INs dendrites GABA_{B1}R subunit labelling was not in accordance with somatic colocalisation. Indeed PV, which showed very low level staining for GABA_{B1}R subunits at the light-microscopic level, had a dendritic surface GABA_{B1}R subunit density similar to that of CA1 pyramidal cells. CCK-IR cells by exception were strongly labelled for GABA_{B1}R subunits in light-microscopy and also showed very strong surface dendritic labelling at the EM level. SSt-IR INs, which showed somatic labelling equivalent or stronger than CA1 pyramidal cells, for GABA_{B1}R subunits, showed dendritic labelling density far lower than local pyramidal cell dendrites, at the EM level.

Interestingly, axons for CCK and PV containing INs in *str. pyramidale* expressed comparable densities of GABA_{B1} subunits. Despite clear differences in dendritic density of GABA_{B1} it appeared as though there should be similar responses to GABA on IPSC output from CCK and PV IR cells.

8.1.4 PI and DI INs display functional differences in GABA_BR-mediated postsynaptic conductances

Physiologically, we have shown that both PV and CCK-IR INs exhibit functional conductances mediated by the GABA_BR, which are different between morphological phenotypes. In contrast, SSt-IR OLM cells possess almost no postsynaptic GABA_B, see table 8.2. The results seen for PV and CCK-IR INs are not altogether unexpected as previous reports have also shown that some IN subtypes do show synaptically driven GABA_BR responses (Khazipov et al, 1995; Mott et al, 1999; Price et al, 2005) although not necessarily in the INs we have identified here.

We found that PV and CCK-IR cell types had GABA_BR conductances substantially larger in PI cells of both IN neurochemical classifications, suggesting a strong dendritic modulation of incoming glutamatergic transmission in these cells. DI cells of the same neurochemical subtypes showed smaller GABA_BR-mediated IPSCs, which were almost completely absent in PV-IR bistratified cells. CCK-IR DI cells, encompassing SCA, ADA and PPA cell types showed more heterogeneity of dendritic GABA_B response; however this was still much smaller than that seen in CCK-IR PI cells. We also confirmed the earlier work of Mott et al (1999) and showed that DG PV-IR basket cells display postsynaptic GABA_BR mediated currents, which were similar in amplitude to those seen in CA1 PV-IR PI cells.

Neurochemical Identity	Perisomatic Inhibitory		Dendritic Inhibitory	
	IPSC	Baclofen	IPSC	Baclofen
PV	Large	=CA1 PC	None/small	<<CA1 PC
CCK	Large	<CA1 PC	Heterogeneous	<CA1 PC
SSt	n/a	n/a	None	<<CA1 PC

Table 8.2 Summary of GABA_BR mediated currents in INs of the CA1 subfield. A comparison of postsynaptic GABA_B R mediated responses, synaptic and pharmacological in INs, relative to CA1 pyramidal cell (CA1 PC).

The ramifications of these data, is that INs which modulate perisomatic inhibition, leading to the precise timing of somatic integration of excitation

(Hájos et al, 2004), in response to GABA will show strong GABA_BR-induced hyperpolarisation of postsynaptic dendritic membranes, resulting in reduced PI IN excitability and GABA release. This will lead to the disinhibition of CA1 pyramidal cell and IN somata, increasing the likelihood of AP discharge in these cells.

The smaller amplitude of postsynaptic GABA_BR currents observed in DI cells, containing either CCK or PV, was somewhat unexpected, as double labelling at the electron microscopic level, suggested no substantial dichotomy in GABA_{B1} subunit density, within populations of neurochemically identified cells. Unfortunately at the EM level we could not determine morphological types of individual dendrites. As PV-IR DI cells make up ~25% of PV-IR cells (Baude et al, 2007) our sample of ~22 dendrites may be too small to pick out a two similar dendritic types expressing differential levels of GABA_{B1} receptor subunit density. An alternative explanation for the discrepancy observed is that GABA_B receptors are present on the dendrites of both PI and DI cells, yet in DI cells are coupled to post-synaptic VGCCs (Bray and Mynlieff, 2011) or phospholipase C (Sohn et al, 2007), resulting in more complex metabotropic actions of the receptor in these dendrites. This is not necessarily true for CCK-IR DI cells as many of these cells possess a small GABA_BR mediated conductance, despite being much smaller than in PI cells containing CCK.

GABA_BR mediated conductances in SSt-IR OLM cells were consistently smaller than those observed in principal cells or PV and CCK-IR PI cells. There were only very small post-synaptic currents sensitive to GABA_BR modulation, consistent with the very low GABA_{B1} density observed by electron micrographic analysis. The low contribution of GABA_B receptor transmission to hyperpolarisation of dendritic membrane in OLM cells is apparent, despite strong somatic labelling for GABA_{B1} at the light microscopic level. The low postsynaptic GABA_{B1} content of OLM cell dendrites raises the possibility of high GABA_BR density in axon terminals.

8.1.5 Presynaptic GABA_B receptors in CCK and PV IR axon terminals

Basket cells, both fast and regular spiking have been shown to possess presynaptic GABA_B receptors (Davies and Collingridge, 1993; Buhl et al, 1995; Poncer et al, 2000; Lee and Soltesz, 2010). Pre-embedding immunogold electron microscopic quantification showed that GABA_{B1} subunits were present on both CCK and PV-IR axon terminals, at low density. Our work showed that these densities were not different, however the relatively low number of terminals quantified and the low particle density observed in them potentially masked differences in GABA_{B1} receptor subunit density.

PV and CCK IR INs were tested to determine whether GABA release from axon terminals of these neurons was inhibited by GABA_BR activation. Utilising the presence of CB1 receptors in presynaptic CCK containing boutons (Katona et al, 1999), we could distinguish unitary IPSCs elicited by either cell type, confirmed with M2 receptor activation which are known to selectively inhibit PV-IR basket cell output (Hájos et al, 1997). Axons containing the CB1 receptor were not inhibited by M2 activation and vice versa; however, IPSCs elicited by both axon types were sensitive to baclofen induced GABA_BR activation. CCK axons were almost 25% more sensitive to baclofen in extracellular stimulation experiments than PV axons, potentially due to the stronger coupling of GABA_BR to N-type VGCCs in CCK-IR terminals, as opposed to P/Q-type VGCCs found in PV-IR cells (Doze et al, 1995; Hefft and Jonas, 2006).

We also tested whether presynaptic effects mediated by GABA_BR were independent of CB1 receptors in CCK-IR/CB1 containing axons. The application of CB1 agonist resulted in ~80% reduction in post-synaptic IPSCs, after which the GABA_BR agonist baclofen had no further appreciable effect on IPSC amplitude. However, following complete washout of CB1 agonist, GABA_B activation resulted in the same reduction as CB1 agonists, in accordance with Lee and Soltesz (2010). This data suggests that both GABA_B and CB1 receptors inhibit the same

pool of N-type VGCCs in CCK-IR axon terminals; following release of GABA and endocannabinoids (Neu et al, 2007; Lee et al, 2010; Lee and Soltesz, 2010).

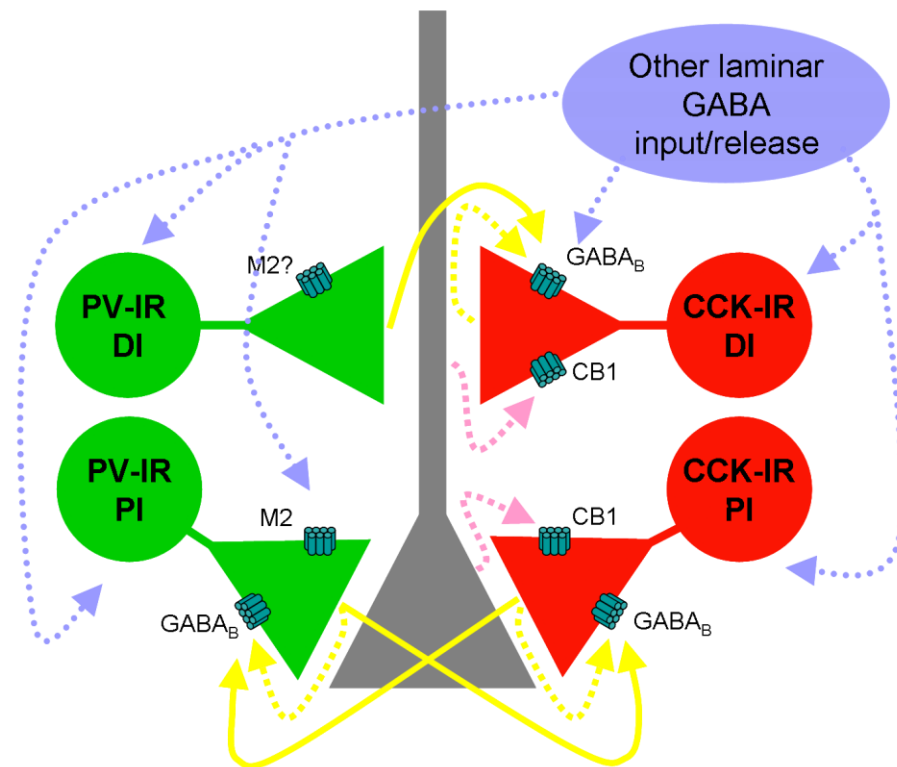


Figure 8.1 Schematic of presynaptic modulation by GABA_BRs. We show the proposed heterosynaptic inhibition pathways mediated by GABA (filled yellow arrows and dashed blue arrows) arising from PV-IR INs (green), CCK-IR INs (red) and other, more general GABA release (blue). Autoreceptive inhibition is shown as dashed yellow arrows and also endocannabinoid signalling (pink dashed arrows); all with respect to CA1 pyramidal cells (grey).

Further distinctions between CCK and PV IR PI cells were made in paired recordings of these INs synaptically coupled to CA1 pyramidal cells. In basket cells containing CCK or PV, GABA_BR activation strongly inhibited GABA release, resulting in reduced postsynaptic IPSCs amplitudes. CCK-IR basket cells were profoundly more sensitive to baclofen application, with the agonist resulting in 100% inhibition of GABA release, which PV-IR basket cells inhibited GABA release by only 50%. These differences were apparent from both extracellular stimulation and paired-recordings: PV-IR basket cell GABA_BR mediated inhibition was identical in both experiments; however, CCK-IR basket cell responses were seemingly more sensitive to baclofen in paired-recordings. These data suggest that similar densities of GABA_BR in both axon subtypes result in stronger

inhibition in CCK-IR terminal containing N-type VGCCs. In DI synapses onto CA1 pyramidal cells, the difference between neurochemical subtypes was exemplified as GABA_BR activation in PV-IR DI axons had no effect on IPSC amplitudes, while in CCK-IR DI cells the same activation resulted in an ~80% reduction IPSCs. In figure 8.1 we show a summary of presynaptic GABA_BR localisation and interactions among GABAergic axon terminals, which we propose on the basis of this data.

Several groups have put forward the hypothesis that CCK containing INs; express GABA_BR-mediated currents in both dendrites and axons; while PV containing INs do not (Sloviter et al, 1999; Freund, 2003; Lee and Soltesz, 2010). We have substantive evidence now, that this is not the case, as both CCK and PV-IR INs both exhibit functional GABA_BR activity, albeit with differential sensitivity in pre- and postsynaptic domains, dependent on morphological phenotype. At the postsynaptic level we observed no difference in GABA_BR activity between these two cell types. However, inhibition observed in response to GABA_BR activation in presynaptic terminals was present in both cell types; however CCK-IR cells were more sensitive to GABA_BR activation. The presence of the GABA_B R in both cell types will have substantial effects on the network role of these interneurons.

8.2 Implications of results

There are several key outcomes of the results presented in this thesis, in regard to GABA_BR-mediated transmission and modulation of GABA release. The presence of functional GABA_BRs in INs will have effects on membrane excitability directly influencing synaptic transmission in these cells. It is the belief of the author, that the most profound role of GABA_B localisation to INs is the role in the timing of GABA release from presynaptic terminals, inhibiting other postsynaptic neurons; the most obvious outcome being the generation and timing of θ -oscillations (Brown et al, 2007; Wang et al, 2010), as well as nested combinations of γ and θ activity (Klausberger et al, 2003).

8.2.1 GABA_BR modulation of synaptic transmission in hippocampal IN

The presence of both CCK and PV IR PI IN dendrites in *str. radiatum* of CA1 and *str. L-M* receiving high GABAergic input (Gulyas et al, 1999) agree with our results that both of these cell types have substantial GABA_BR-mediated effects. GABA_BRs on the dendrites of selected INs will lead to greater modulation of membrane excitability; leading us to rethink the role of inhibition arriving onto INs. GABA_BRs are implicitly involved in hyperpolarising neuronal membranes via K⁺ efflux through Kir3 channels (Otis et al, 1993). This effect will lead to reduction in intrinsic excitability in subcellular compartments containing GABA_BRs, such as the dendrites of INs.

It has been shown that some INs dendrites are electrically active, capable of action potential propagation (Martina et al, 2000) similar to principal cells (Spruston et al 1995); the presence of GABA_BR in these dendrites will therefore result in inhibition of dendritic AP back-propagation, passive spread of depolarisation and associated Ca²⁺ influx (Tsubokawa and Ross, 1996). Dendritic Ca²⁺-spikes display strong temporal attenuation (Spruston et al, 1995) and slow postsynaptic GABA_BR induced hyperpolarisation has been shown to attenuate dendritic Ca²⁺ entry (Pérez-Garci et al, 2006) in CA1 pyramidal cells, augmenting the fast effects of GABA_AR inhibition. The relatively small hyperpolarisation of V_M by GABA_BRs is unlikely to block the large initial dendritic back-propagating APs and the resultant Ca²⁺ influx; however, it is possible that GABA_B blocks the late-phase Ca²⁺ entry, shortening the temporal summation of dendritic Ca²⁺ transients.

Dendritic Ca²⁺ spikes have been examined in PV-IR basket cells (Aponte et al, 2008), where the presence of PV contributes to tight buffering of free-Ca²⁺, particularly fast transients; it is highly likely therefore, that the presence of GABA_B receptors in PV-IR basket cells, but not PV-IR bistratified cells, contributes to attenuation of late-phase Ca²⁺ spikes, which are not buffered well by PV. Recently it has been shown in CCK-IR basket and SCA DI cells, that back-

propagating APs lead to large, summing Ca^{2+} transients (Evstratova et al, 2011); which as for CA1 pyramidal cells, are potentially attenuated by GABA_B Rs, leading to reduced temporal summation; which would not be observed in SCA DI cells. This potential GABA_B R mediated control of Ca^{2+} influx to dendritic compartments, in all INs targeting the perisomatic region of pyramidal cells, will lead to more tightly controlled excitation by GABAergic input, by attenuating VGCCs or repetitive NMDA receptor responses.

In addition to direct modulation of intrinsic excitability of IN membranes GABA_B R cross-talk of GABA_{B2} receptor subunits with M2 and $\text{mGluR1}\alpha$ receptors (Boyer et al, 2009); enhancing muscarinic and metabotropic glutamate signalling. The presence of GABA_{B1} subunits, and presumably GABA_{B2} also, in the dendrites of CCK-IR basket cells; known to possess $\text{mGluR1}\alpha$ receptors (Ferraguti et al, 2004) suggests that neuromodulatory enhancement of glutamatergic inhibition occurs concurrently in these cells. Interestingly, SSt-IR INs show the strongest staining for $\text{mGluR1}\alpha$ in the CA1, which are potentially modulated by the low number of GABA_B Rs observed.

The role of GABA_B R in controlling the excitability of individual cells depends on the location of the initial GABAergic input to those cells, which in the case of CCK and PV-IR INS largely comes from *str. radiatum* and *L-M*. Two key IN populations with axons arborising heavily in these areas are neurogliaform cells and OLM cells, the latter of which has been shown to entrain to θ oscillations (Gloveli et al, 2005). The stimulation of PI INs in this study at the *str. radiatum/LM* border; gives strong credence to the idea that PI and CCK DI INs, to some extent, potentially receive strong feedback inhibition from high levels of GABA released from OLM and neurogliaform cell axons, arborising in these regions.

Cells with small postsynaptic GABA_B R-mediated responses seen (DI cells containing PV, CCK and SSt) may show prolonged depolarisation due to low levels of slow inhibition, allowing these cells to contribute a greater proportion of the

inhibitory tone during periods of high GABA release. This is shown well in PV-IR DI cells, which lack both pre- and postsynaptic GABA_BRs, suggesting that both their input and outputs are void of metabotropic GABAergic modulation.

In contrast, the presence of GABA_BRs in the tightly interspersed presynaptic terminals of PI and CCK-IR DI INs suggests that the output of these cells is not only modulated by autoreceptors, but can be inhibited heterosynaptically by each other (Davies et al, 1991; Lee and Soltesz, 2010). The localisation of PI cell axons, to the *str. pyramidale*, primarily results in a high concentration of extrasynaptic GABA locally, the presence of GABA_BRs on pyramidal cell somata (Kulik et al, 2003), suggesting that local PI IN axons are an important target of this GABA spill-over. The heterosynaptic and autoreceptor properties of GABA_BR-mediated inhibition of GABA release will most likely lead to attenuation of late GABA release, as observed in CCK-IR INs but not in PV-IR (Hefft and Jonas, 2005), but not rapid release (Lu and Trussell, 2000); leading to slower inhibition of GABA release, decreasing release probability of GABA at PI-pyramidal cell synapses during θ -epochs. Further evidence was shown by Scanziani (2000), as application of a GABA_BR antagonist during methacholine-induced θ -oscillations almost doubled the frequency of the θ -phase, suggesting more rapid GABAergic signalling.

8.2.2 GABA_BRs in hippocampal network activity and oscillations

There is much evidence that hippocampal INs are one of the primary factors leading to hippocampal oscillations. Indeed, evidence suggests that θ -oscillations can be produced intrinsically by the hippocampus through activation of cholinergic receptors (Konopacki et al, 1988; Gloveli et al, 2005; Goutagny et al, 2009). Others have shown that a single CA3 pyramidal cell can give rise to γ -oscillations in CA1 (Mikkonen et al, 2006), through interactions with the intrinsic IN network. For this reason, it is likely that all requirements for both θ and γ patterned activity are present within the excised hippocampus, realistically within the inhibitory network.

We have shown evidence for strong post-synaptic GABA_BR modulation in all PI cells in CA1, originating near to *str. L-M*. This suggests that both fast and regular spiking PI cells receive strong inhibition from GABA sources in this area, such as OLM or neurogliaform cells, similar to CA1 pyramidal cells (Katona et al, 1999; Price et al, 2008). Unlike GABA_AR-mediated synaptic inhibition, GABA_BR-mediated inhibition is produced by extrasynaptic receptors, which show a less tight association to synapses (Kulik et al, 2003). So although post-synaptic targets of OLM, neurogliaform cells, as well as other INs with axon localised to the *str. radiatum/L-M* are quite well defined (Lacaille and Schwartzkroin, 1988; Khazipov et al, 1995; Vida et al, 1998; Katona et al, 1999; Maccaferri et al, 2000, Price et al, 2006), any number of intrinsic hippocampal afferents could contribute to inhibition onto dendrites or neurons containing the GABA_BR protein in this region. Additionally, the presynaptic data we provide for PI INs argues that most of these cells receive strong presynaptic inhibition through autoreceptors located on axon terminals (Lee et al, 2010), likely to have a role in silencing GABA release in these cells (Pittaluga et al, 1987) and self-timing GABA release.

It has been proposed that γ frequency oscillations can be generated by networks of fast-spiking cells (Whittington et al, 1995; Wang and Buzsaki, 1996; Bartos et al, 2002) and that these γ -oscillation nest within θ -oscillation to produce an integrated oscillatory output (Klausberger et al, 2005; Wulff et al, 2009), driving learning and memory processes (Murray et al, 2011).

Two cell types tested in this study, seemed to lack post-synaptic GABA_BR mediated post synaptic currents, the PV-IR bistratified cells and SSt-IR OLM cells; while CCK-IR DI cells possessed low but variable levels of GABA_BR conductance. Both PV-IR bistratified and SSt-IR OLM cells have been implicated in the intrinsic timing of oscillation, SWR, γ and θ oscillations.

The near-complete absence of observable GABA_BR mediated effects in both pre and post synaptic domains of PV-IR bistratified cells confirms a lack of GABAergic

neuromodulation of these cells, which may directly affect synaptic output, leading to the tight temporal precision of very-fast (100-200 Hz) SWR oscillations; as suggested for enkephalin-containing INs in the CA1 (Fuentelba et al, 2008). The apparent lack of GABA_B functionality in these cells would imply a reduction in θ -oscillatory control, leaving bistratified cells with oscillatory functions predominantly in the γ and ripple spectra (Gloveli et al, 2005; Klausberger et al, 2005). Absence of post-synaptic GABA_BR-mediated K⁺ conductances in PV-IR or CCK-IR DI cells does not necessarily dictate absence of GABA_BR proteins from these membranes, as immunocytochemical analysis did not show any clear populations of these cells lacking GABA_{B1} receptor subunits; unlike SSt-IR cells, where we observed very low protein content in the membrane, associated with a very small functional current. If GABA_B is present but not coupled to Kir3 channels, rather protein kinase A and C are activated by GABA_B, modulating VGCC transmission (Lambert and Wilson, 1996; Chalifoux and Carter, 2010; Bray and Mynlieff, 2011) through interactions with phospholipase A and C by G_{i/o} α , could lead to profound alterations of transmission through mGluR1 receptors (Sohn et al, 2007), on dendrites of PV-IR DI cells (Ferraguti et al, 2004). It is pertinent to note that 30% of PV-IR cells possess mGluR1 α in dendritic compartments (Ferraguti et al, 2004), a similar proportion of the population as PV-IR DI cells (Baude et al, 2007); however, an overlap of these cell populations has not yet been shown.

OLM cells provide inhibition to other interneurons (Katona et al, 1999), and release GABA timed to θ -oscillations onto distal dendrites of both INs and pyramidal cells. Several groups (Maccaferri and McBain, 1996; Rotstein et al, 2005) suggest that OLM cells provide θ tone, due in part to the large inducible I_h in these cells. Like Gloveli et al (2005), we saw that OLM cells responded with a near fast-spiking phenotype (>50 Hz, *in vitro*) which has been shown to be less *in vivo* (Sík et al, 1995), suggesting that during θ -upstate activation of CA1 pyramidal cells provides feedback excitation to OLM cells, resulting in release of GABA in *str. L-M*. This frequency of synaptic activity according to Scanziani (2000) could be large enough to evoke large GABA_BR-mediated hyperpolarising responses in dendrites CA1 pyramidal cells, as well as local INs, via volume transmission of GABA. This dendritic inhibition would serve to inhibit incoming

EPSPs in PV and CCK-IR PI cells, as well as pyramidal cells (Yanovsky et al, 1997); entraining them to the θ -phase, that are silenced by the feedback inhibition of OLM cells; which themselves are in phase with CA1 pyramidal cells.

There is some evidence from computational modelling data that in thalamocortical pathways GABA_BR are crucial to the generation of waves of inhibition leading to θ -frequency oscillations (Destexhe, 1998), mediated by K⁺ currents. Recent computational modelling data from our lab, suggests that small networks comprising fast-spiking PI cells and regular-spiking DI cells can entrain γ -oscillation phase output of fast-spiking INs into a θ nested pattern, requiring only post-synaptic GABA_B receptors on the dendrites of the fast-spiking PI cells, see figure 8.2.

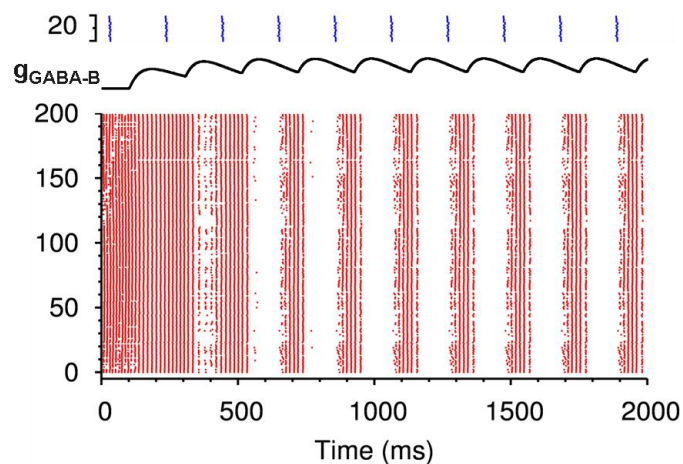


Figure 8.2 Raster plot of a modelled IN network of fast-spiking PI and DI cells. AP output of the network of fast-spiking INs is shown (red) with post-synaptic GABA_B conductance in the same cells (g_{GABA_B} ; black) arising from regular spiking DI stimulation (blue).

Although modulation of many receptor and cell types have been shown to promote oscillatory activity, it seems likely at the time of writing, that the presence or absence of GABA_BR to specific compartments of distinct IN populations plays an integral role in the timing of θ -oscillation in the hippocampus, with possible effects of γ and SWR oscillations.

8.3 Technical considerations and future work

8.3.1 Technical considerations

There were several key technical considerations to overcome throughout the course of this work. Below are highlighted several key factors which were either addressed or not, which may have impinged upon the results presented.

The largest consideration by far, is that all responses recorded here are from acute, *ex vivo* tissue. Although every step was taken to ensure that the highest standards of quality were maintained across all experiments, there is still an element that the evoked responses were due to the artificial nature in which they were managed. Indeed there is evidence that recording temperatures below 37°C result in increased GABA release, leading to a greater GABA_B activation at “rest” (Mitchell and Silver, 2000). Our recording temperature of 32-34°C may have therefore resulted in a reduced synaptic GABA_BR-mediated response, due to increased tonic activation of the receptor. At the same time activity in the slices is lower than *in vivo*; which may counterbalance this. We countered this by application of both selective agonists and antagonists of the GABA_BR, which would have elucidated any tonic conductances in recorded cells. Temperature dependence of GABA_B would account for some of the variability we observed in both synaptic and pharmacological GABA_BR-mediated responses in principal cells, PI and CCK-IR DI cells.

A further significant technical consideration is the possibility that key components of the GABA_BR transduction machinery could potentially be washed out of the cell over the course of the recordings. In figure 2.2 we address this issue, as in a subgroup of control cells we did not apply pharmacology for 20 minutes. Over this period, which was in fact longer than the standard recording period, we saw no substantial change in either the IPSC amplitude or the holding

current, which confirmed that the GABA_BR signal was not being washed out of the recorded cells.

Location of extracellular stimulation sites was generally kept uniform, with the exception of OLM cells; however, dendritic branching patterns of recorded INs and the GABAergic innervation received by these dendrites would affect the amplitude of GABA_BR-mediated IPSCs achievable. Although we stimulated at the border of *str. radiatum/L-M* many of the recorded IN subtypes possess only small dendritic domains within close proximity to this region, for example PV-IR INs generally only have ~20% of dendrites in the distal *str. radiatum/LM regions* (Gulyas et al, 1999). Pharmacological manipulation of recorded cells provided us an independent measure to assess the full complement of GABA_BR, furthermore as the baclofen effect on recorded cells closely followed synaptic amplitudes it validated the results obtained by extracellular stimulation. As with CA1 pyramidal cells, it is possible that hippocampal INs possess a gradient of GABA_BRs (Kulik et al, 2003), which may have been observed if other stimulation sites had been employed routinely, as we performed for CA1 pyramidal cells.

Finally, we have shown through immunocytochemical analysis and comparison that GABA_{B1} receptor-subunit localisation patterns, on principal cells and interneurons. The GABA_{B1} receptor subunit requires the GABA_{B2} subunit for receptor functionality and some could argue that quantification B2 subunit expression levels would be advantageous. However, functional GABA_BRs are comprised of a heterodimer of GABA_{B1} and B₂ with the assumption that this is generally a 1:1 relationship. As we have detected functional currents in all cells where we detected GABA_{B1} receptor subunits, with similar kinetic and pharmacological properties to CA1 pyramidal cell possessing both subunits; GABA_{B2} receptor-subunit must be present. We attempted to localise GABA_{B2} receptor subunits to the plasma membrane of principal cells and neurochemically identified INs with limited success. Immunolabeling achieved with both custom antibodies raised against GABA_{B2} fusion proteins (gifted by A Kulik/R Shigemoto) and a similar commercially available antibody (Chemicon),

gave non-specific and low intensity staining patterns in hippocampal tissue (data not shown).

8.3.2 Future work

Despite determining the profile of GABA_BR-mediated signalling in several key types of hippocampal interneuron and principal cell, several questions remain open-ended in regard to the functionality of this receptor system in hippocampal networks.

We confirmed the GABA_BR-mediated content of PV, CCK and SSt-IR INs, it would be advantageous to determine whether other neurochemical and morphological subtypes of IN show this conductance also. As well it would be fundamental to determine the presynaptic inhibition mediated by GABA_B in SSt-IR OLM cells, as well as other IN types, as yet unexplored. The most interesting class to explore would be calretinin-IR IN-specific INs; which only form synapses onto other INs. The confirmation of GABA_BR in the dendrites and boutons of these two subtypes of INs would have large ramifications for inhibitory transmission, particularly between networks of INs, leading to patterning of excitatory oscillations. We obtained some data from CCK/CB double IR cells, but it would be useful to determine the relative GABA_BR conductance in all IN subtypes, to begin to develop an overarching view of the role of GABA_B in shaping inhibitory networks and to aid the production of more accurate computational network models, taking into account both slow and fast GABAergic transmission. If GABA_B plays as much of a role in inhibitory network formation as we suggest, then correct implementation of this conductance to large scale network models should begin to become standard.

A second consideration which should be tested is the presence or absence of proteins which modulated the function of GABA_BRs IN populations in which we observed GABA_BR subunits, may also contain is the as yet unknown, KCTD 8, 12

or 16 proteins. Recent work suggests that these proteins are abundant in CA1 pyramidal cells and in an as yet unidentified population of non-principal cells (Schwenk et al, 2010). In cultured cells KCTD proteins modulate conductance and desensitization rate of GABA_BRs; when expressed in conjunction with the receptor itself. It is feasible that the presence of KCTD in INs where GABA_BR conductances are absent, but the receptor subunits are possibly expressed (i.e. PV and CCK-IR DI cells), is evidence of functional silencing by KCTD proteins, through increased mobility of the GABA_BR; which could easily be tested.

Finally, it would be meaningful to determine the amplitude of GABA_B responses produced in different IN subtypes during physiological-like network activity. The most straightforward experiment would be to record from PV or CCK-IR INs, whilst inducing θ and γ oscillations via cholinergic modulation and determine whether during theta up or down phases, recorded in field recordings the extent of GABA_BR mediated transmission post-synaptically in these cells. Ultimately, this would aim to corroborate with data from computational network models and expand into the *in vivo* setting, utilising GABA_{B1} subunit knock-out animals, which by comparing the spike and spontaneous synaptic events, would help to establish a role for GABA_BR in different IN populations in a natural setting.

8.4 Concluding remarks

This thesis aimed to assess whether GABA_B receptor mediated transmission exists in INs, modulating either pre- or postsynaptic profiles of these cells.

At the light microscopic level, PV, CCK and SSt cells show different levels of GABA_B receptor subunit colocalisation to the somata, which at EM level was observed in PV and CCK-containing IN dendrites and axons, equivalent to CA1 pyramidal cells. We also show that SSt-containing dendrites express very low GABA_{B1} receptor subunit density in the plasma membrane, far below that of CA1 pyramidal cells.

We confirmed in electrophysiological recordings that both CCK and PV-containing INs possess postsynaptic GABA_BR mediated conductances, mediated by inward-rectifying potassium channels. This GABA_B receptor response was mostly observed in PI IN subtypes; DI IN subtypes of the same neurochemical classifications exhibited far smaller conductances, under the same experimental circumstances. Concordantly, in recordings from SSt-IR OLM cells we observed no or very small postsynaptic GABA_BR mediated responses. Extracellular stimulation and paired-recordings of identified interneuron axons confirmed that GABA_B was present in both PV and CCK-IR PI axon, with a greater effect in CCK-IR axons, which resulted in increased control of GABA release in these axon terminals

Together this data shows that interneurons of different morphological and neurochemical subtypes are under the control of GABA_B receptors in both the pre- and postsynaptic domains, which govern their role in the hippocampal network.

References

Alger BE, Nicoll RA (1982) Feed-forward dendritic inhibition in rat hippocampal pyramidal cells studied *in vitro*. *The Journal of Physiology* 328:105-123.

Ali AB (2007) Presynaptic Inhibition of GABA_A Receptor-Mediated Unitary IPSPs by Cannabinoid Receptors at Synapses Between CCK-Positive Interneurons in Rat Hippocampus. *Journal of Neurophysiology* 98:861-869.

Ali AB, Thomson AM (1998) Facilitating pyramid to horizontal oriens-alveus interneurone inputs: dual intracellular recordings in slices of rat hippocampus. *The Journal of Physiology* 507:185-199.

Ali AB, Thomson AM (2008) Synaptic $\alpha 5$ Subunit-Containing GABAA Receptors Mediate IPSPs Elicited by Dendrite-Preferring Cells in Rat Neocortex Cerebral Cortex 18:1260-1271.

Amaral DG, Witter MP (1989) The three-dimensional organization of the hippocampal formation: A review of anatomical data. *Neuroscience* 31:571-591.

Andersen P, Eccles JC, Løyning Y (1963) Hippocampus of the Brain: Recurrent Inhibition in the Hippocampus with Identification of the Inhibitory Cell and its Synapses. *Nature* 198:540-542.

Andersen P, Holmqvist B, Voorhoeve PE (1966) Entorhinal Activation of Dentate Granule Cells. *Acta Physiologica Scandinavica* 66:448-460.

Aponte Y, Bischofberger J, Jonas P (2008) Efficient Ca²⁺ buffering in fast-spiking basket cells of rat hippocampus. *The Journal of Physiology* 586:2061-2075.

Aponte Y, Lien C-C, Reisinger E, Jonas P (2006) Hyperpolarization-activated cation channels in fast-spiking interneurons of rat hippocampus. *The Journal of Physiology* 574:229-243.

Azouz R, Jensen MS, Yaari Y (1996) Ionic basis of spike after-depolarization and burst generation in adult rat hippocampal CA1 pyramidal cells. *The Journal of Physiology* 492:211-223.

Baroni F, Varona P (2010) Spike timing-dependent plasticity is affected by the interplay of intrinsic and network oscillations. *Journal of Physiology-Paris* 104:91-98.

Bartos M, Vida I, Jonas P (2007) Synaptic mechanisms of synchronized gamma oscillations in inhibitory interneuron networks. *Nat Rev Neurosci* 8:45-56.

Bartos M, Vida I, Frotscher M, Meyer A, Monyer H, Geiger JRP, Jonas P (2002) Fast synaptic inhibition promotes synchronized gamma oscillations in hippocampal interneuron networks. *Proceedings of the National Academy of Sciences* 99:13222-13227.

Baude A, Nusser Z, Molnar E, McIlhinney RAJ, Somogyi P (1995) High-resolution immunogold localization of AMPA type glutamate receptor subunits at synaptic and non-synaptic sites in rat hippocampus. *Neuroscience* 69:1031-1055.

Baude A, Bleasdale C, Dalezios Y, Somogyi P, Klausberger T (2007) Immunoreactivity for the GABA_A Receptor alpha1 Subunit, Somatostatin and Connexin36 Distinguishes Axoaxonic, Basket, and Bistratified Interneurons of the Rat Hippocampus. *Cerebral Cortex* 17:2094-2107.

Ben-Ari Y, Cherubini E, Corradetti R, Gaiarsa JL (1989) Giant synaptic potentials in immature rat CA3 hippocampal neurones. *The Journal of Physiology* 416:303-325.

Bischofberger J, Engel D, Li L, Geiger JRP, Jonas P (2006) Patch-clamp recording from mossy fiber terminals in hippocampal slices. *Nat Protocols* 1:2075-2081.

Blasco-Ibáñez JM, Freund TF (1995) Synaptic Input of Horizontal Interneurons in Stratum Oriens of the Hippocampal CA1 Subfield: Structural Basis of Feed-back Activation. *European Journal of Neuroscience* 7:2170-2180.

Bliss TVP, Lomo T (1973) Long-lasting potentiation of synaptic transmission in the dentate area of the anaesthetized rabbit following stimulation of the perforant path. *The Journal of Physiology* 232:331-356.

Bowery NG, Hill DR, Hudson AL, Doble A, Middlemiss DN, Shaw J, Turnbull M (1980) (-)-Baclofen decreases neurotransmitter release in the mammalian CNS by an action at a novel GABA receptor. *Nature* 283:92-94.

Boyer SB, Clancy SM, Terunuma M, Revilla-Sanchez R, Thomas SM, Moss SJ, Slesinger PA (2009) Direct Interaction of GABAB Receptors with M2 Muscarinic Receptors Enhances Muscarinic Signaling. *The Journal of Neuroscience* 29:15796-15809.

Braak H, Braak E (1991) Neuropathological staging of Alzheimer-related changes. *Acta Neuropathologica* 82:239-259.

Bray JG, Mynlieff M (2011) Involvement of protein kinase C and protein kinase A in the enhancement of L-type calcium current by GABAB receptor activation in neonatal hippocampus. *Neuroscience* 179:62-72.

Brown JT, Davies CH, Randall AD (2007) Synaptic activation of GABAB receptors regulates neuronal network activity and entrainment. *European Journal of Neuroscience* 25:2982-2990.

Buhl EH, Cobb SR, Halasy K, Somogyi P (1995) Properties of unitary IPSPs evoked by anatomically identified basket cells in the rat hippocampus. *European Journal of Neuroscience* 7:1989-2004.

Bullis JB, Jones TD, Poolos NP (2007) Reversed somatodendritic I_h gradient in a class of rat hippocampal neurons with pyramidal morphology. *The Journal of Physiology* 579:431-443.

Buzsaki G, Eidelberg E (1982) Direct afferent excitation and long-term potentiation of hippocampal interneurons. *Journal of Neurophysiology* 48:597-607.

Buzsáki G, Lai-Wo S L, Vanderwolf CH (1983) Cellular bases of hippocampal EEG in the behaving rat. *Brain Research Reviews* 6:139-171.

Cajal SR (1911) *Histologie du système nerveux de l'homme et des vertébrés*. Paris: Maloine.

Cardona A, Saalfeld S, Preibisch S, Schmid B, Cheng A, Pulokas J, Tomancak P, Hartenstein V (2010) An Integrated Micro- and Macroarchitectural Analysis of the *Drosophila* Brain by Computer-Assisted Serial Section Electron Microscopy. *PLoS Biol* 8:e1000502.

Cauli B, Audinat E, Lambolez B, Angulo MC, Ropert N, Tsuzuki K, Hestrin S, Rossier J (1997) Molecular and Physiological Diversity of Cortical Nonpyramidal Cells. *The Journal of Neuroscience* 17:3894-3906.

Cea-del Rio CA, Lawrence JJ, Erdelyi F, Szabo G, McBain CJ (2010) Cholinergic modulation amplifies the intrinsic oscillatory properties of CA1 hippocampal cholecystokinin-positive interneurons. *The Journal of Physiology* 589:609-627.

Cea-del Rio CA, Lawrence JJ, Tricoire L, Erdelyi F, Szabo G, McBain CJ (2011) M3 Muscarinic Acetylcholine Receptor Expression Confers Differential Cholinergic Modulation to Neurochemically Distinct Hippocampal Basket Cell Subtypes. *The Journal of Neuroscience* 30:6011-6024.

Chalifoux JR, Carter AG (2010) GABAB Receptors Modulate NMDA Receptor Calcium Signals in Dendritic Spines. *Neuron* 66:101-113.

Chiang PH, Yeh WC, Lee CT, Weng JY, Huang YY, Lien CC (2010) M1-like muscarinic acetylcholine receptors regulate fast-spiking interneuron excitability in rat dentate gyrus. *Neuroscience* 169:39-51.

Chow A, Erisir A, Farb C, Nadal MS, Ozaita A, Lau D, Welker E, Rudy B (1999) K⁺ Channel Expression Distinguishes Subpopulations of Parvalbumin- and Somatostatin-Containing Neocortical Interneurons. *The Journal of Neuroscience* 19:9332-9345.

Christie BR, Franks KM, Seamans JK, Saga K, Sejnowski TJ (2000) Synaptic plasticity in morphologically identified CA1 stratum radiatum interneurons and giant projection cells. *Hippocampus* 10:673-683.

Ciruela F, Fernández-Dueñas V, Sahlholm K, Fernández-Alacid L, Nicolau JC, Watanabe M, Luján R (2010) Evidence for oligomerization between GABAB receptors and GIRK channels containing the GIRK1 and GIRK3 subunits. *European Journal of Neuroscience* 32:1265-1277.

Cobb SR, Buhl EH, Halasy K, Paulsen O, Somogyi P (1995) Synchronization of neuronal activity in hippocampus by individual GABAergic interneurons. *Nature* 378:75-78.

Colbert CM, Levy WB (1992) Electrophysiological and pharmacological characterization of perforant path synapses in CA1: mediation by glutamate receptors. *Journal of Neurophysiology* 68:1-8.

Collingridge GL, Kehl SJ, McLennan H (1983) Excitatory amino acids in synaptic transmission in the Schaffer collateral-commissural pathway of the rat hippocampus. *The Journal of Physiology* 334:33-46.

Connors BW, Malenka RC, Silva LR (1988) Two inhibitory postsynaptic potentials, and GABAA and GABAB receptor-mediated responses in neocortex of rat and cat. *The Journal of Physiology* 406:443-468.

Cox DJ, Racca C, Lebeau FEN (2008) β -adrenergic receptors are differentially expressed in distinct interneuron subtypes in the rat hippocampus. *The Journal of Comparative Neurology* 509:551-565.

Csicsvari J, Hirase H, Czurka A, Mamiya A, Buzsaki G (1999) Oscillatory Coupling of Hippocampal Pyramidal Cells and Interneurons in the Behaving Rat. *The Journal of Neuroscience* 19:274-287.

Cunha-Reis D, Sebastião AM, Wirkner K, Illes P, Ribeiro JA (2004) VIP enhances both pre- and postsynaptic GABAergic transmission to hippocampal interneurons

leading to increased excitatory synaptic transmission to CA1 pyramidal cells. *British Journal of Pharmacology* 143:733-744.

Curtis DR, Duggan AW, Felix D, Johnston GAR (1970) GABA, Bicuculline and Central Inhibition. *Nature* 226:1222-1224.

Cutsuridis V, Graham B, Cobb S, Vida I, Witter MP (2010) Hippocampal Microcircuits: A computational modellers guide. In: *Hippocampal Microcircuits*, pp 5-26: Springer New York.

Davies CH, Collingridge GL (1993) The physiological regulation of synaptic inhibition by GABAB autoreceptors in rat hippocampus. *The Journal of Physiology* 472:245-265.

Davies CH, Davies SN, Collingridge GL (1990) Paired-pulse depression of monosynaptic GABA-mediated inhibitory postsynaptic responses in rat hippocampus. *The Journal of Physiology* 424:513-531.

Davies CH, Starkey SJ, Pozza MF, Collingridge GL (1991) GABAB autoreceptors regulate the induction of LTP. *Nature* 349:609-611.

Destexhe A (1998) Spike-and-Wave Oscillations Based on the Properties of GABAB Receptors. *The Journal of Neuroscience* 18:9099-9111.

Doischer D, Aurel Hosp J, Yanagawa Y, Obata K, Jonas P, Vida I, Bartos M (2008) Postnatal Differentiation of Basket Cells from Slow to Fast Signaling Devices. *The Journal of Neuroscience* 28:12956-12968.

Doze VA, Cohen GA, Madison DV (1995) Calcium channel involvement in GABAB receptor-mediated inhibition of GABA release in area CA1 of the rat hippocampus. *Journal of Neurophysiology* 74:43-53.

Du J, Zhang L, Weiser M, Rudy B, McBain C (1996) Developmental expression and functional characterization of the potassium-channel subunit Kv3.1b in

parvalbumin-containing interneurons of the rat hippocampus. *The Journal of Neuroscience* 16:506-518.

Dudar JD (1974) *In vitro* excitation of hippocampal pyramidal cell dendrites by glutamic acid. *Neuropharmacology* 13:1083-1089.

Eichenbaum H, Dudchenko P, Wood E, Shapiro M, Tanila H (1999) The Hippocampus, Memory, and Place Cells: Is It Spatial Memory or a Memory Space? *Neuron* 23:209-226.

Elfant D, Pál BZ, Emptage N, Capogna M (2008) Specific inhibitory synapses shift the balance from feedforward to feedback inhibition of hippocampal CA1 pyramidal cells. *European Journal of Neuroscience* 27:104-113.

Evstratova A, Chamberland S, Topolnik L (2011) Cell type-specific and activity-dependent dynamics of action potential-evoked Ca²⁺ signals in dendrites of hippocampal inhibitory interneurons. *The Journal of Physiology* 589:1957-1977.

Falkai P, Bogerts B (1986) Cell loss in the hippocampus of schizophrenics. *European Archives of Psychiatry and Clinical Neuroscience* 236:154-161.

Feder R, Ranck Jr JB (1973) Studies on single neurons in dorsal hippocampal formation and septum in unrestrained rats: Part II. Hippocampal slow waves and theta cell firing during bar pressing and other behaviors. *Experimental Neurology* 41:532-555.

Férézou I, Cauli B, Hill EL, Rossier J, Hamel E, Lambolez B (2002) 5-HT₃ Receptors Mediate Serotonergic Fast Synaptic Excitation of Neocortical Vasoactive Intestinal Peptide/Cholecystokinin Interneurons. *The Journal of Neuroscience* 22:7389-7397.

Ferraguti F, Cobden P, Pollard M, Cope D, Shigemoto R, Watanabe M, Somogyi P (2004) Immunolocalization of metabotropic glutamate receptor 1 α (mGluR1 α) in distinct classes of interneuron in the CA1 region of the rat hippocampus. *Hippocampus* 14:193-215.

Forsythe ID, Tsujimoto T, Barnes-Davies M, Cuttle MF, Takahashi T (1998) Inactivation of Presynaptic Calcium Current Contributes to Synaptic Depression at a Fast Central Synapse. *Neuron* 20:797-807.

Fraser D, MacVicar B (1991) Low-threshold transient calcium current in rat hippocampal lacunosum- moleculare interneurons: kinetics and modulation by neurotransmitters. *The Journal of Neuroscience* 11:2812-2820.

Freund TF (2003) Interneuron Diversity series: Rhythm and mood in perisomatic inhibition. *Trends in Neurosciences* 26:489-495.

Freund TF, Buzsáki G (1996) Interneurons of the hippocampus. *Hippocampus* 6:347-470.

Fritschy J-M, Kiener T, Boullieret V, Loup F (1999a) GABAergic neurons and GABAA-receptors in temporal lobe epilepsy. *Neurochemistry International* 34:435-445.

Fritschy J-M, Meskenaite V, Weinmann O, Honer M, Benke D, Mohler H (1999b) GABAB-receptor splice variants GB1a and GB1b in rat brain: developmental regulation, cellular distribution and extrasynaptic localization. *European Journal of Neuroscience* 11:761-768.

Fuentealba P, Tomioka R, Dalezios Y, Márton L, Studer M, Rockland K, Klausberger T, Somogyi P (2008) Rhythmically Active Enkephalin-Expressing GABAergic Cells in the CA1 Area of the Hippocampus Project to the Subiculum and Preferentially Innervate Interneurons. *The Journal of Neuroscience* 28:10017-10022.

Furtinger S, Bettler B, Sperk G (2003) Altered expression of GABAB receptors in the hippocampus after kainic-acid-induced seizures in rats. *Molecular Brain Research* 113:107-115.

Geddes JW, Chang-Chui H, Cooper SM, Lott IT, Cotman CW (1986) Density and distribution of NMDA receptors in the human hippocampus in Alzheimer's disease. *Brain Research* 399:156-161.

Geiger JRP, Melcher T, Koh DS, Sakmann B, Seeburg PH, Jonas P, Monyer H (1995) Relative abundance of subunit mRNAs determines gating and Ca²⁺ permeability of AMPA receptors in principal neurons and interneurons in rat CNS. *Neuron* 15:193-204.

Gingrich KJ, Roberts WA, Kass RS (1995) Dependence of the GABA_A receptor gating kinetics on the alpha-subunit isoform: implications for structure-function relations and synaptic transmission. *The Journal of Physiology* 489:529-543.

Gloveli T, Dugladze T, Saha S, Monyer H, Heinemann U, Traub RD, Whittington MA, Buhl EH (2005) Differential involvement of oriens/pyramidal interneurons in hippocampal network oscillations *in vitro*. *The Journal of Physiology* 562:131-147.

Goutagny R, Jackson J, Williams S (2009) Self-generated theta oscillations in the hippocampus. *Nat Neurosci* 12:1491-1493.

Gulyás AI, Tóth K, McBain CJ, Freund TF (1998) Stratum radiatum giant cells: a type of principal cell in the rat hippocampus. *European Journal of Neuroscience* 10:3813-3822.

Gulyás AI, Megias M, Emri Z, Freund TF (1999) Total Number and Ratio of Excitatory and Inhibitory Synapses Converging onto Single Interneurons of Different Types in the CA1 Area of the Rat Hippocampus. *The Journal of Neuroscience* 19:10082-10097.

Hájos N, Papp EC, Acsády L, Levey AI, Freund TF (1997) Distinct interneuron types express m2 muscarinic receptor immunoreactivity on their dendrites or axon terminals in the hippocampus. *Neuroscience* 82:355-376.

Hájos N, Pálhalmi J, Mann EO, Németh B, Paulsen O, Freund TF (2004) Spike Timing of Distinct Types of GABAergic Interneuron during Hippocampal Gamma Oscillations *In vitro*. *The Journal of Neuroscience* 24:9127-9137.

Halliwel JV, Adams PR (1982) Voltage-clamp analysis of muscarinic excitation in hippocampal neurons. *Brain Research* 250:71-92.

Han Z-S, Buhl EH, Lörinczi Z, Somogyi P (1993) A High Degree of Spatial Selectivity in the Axonal and Dendritic Domains of Physiologically Identified Local-circuit Neurons in the Dentate Gyms of the Rat Hippocampus. *European Journal of Neuroscience* 5:395-410.

Harrison NL (1990) On the presynaptic action of baclofen at inhibitory synapses between cultured rat hippocampal neurones. *The Journal of Physiology* 422:433-446.

Hefft S, Kraushaar U, Geiger JRP, Jonas P (2002) Presynaptic short-term depression is maintained during regulation of transmitter release at a GABAergic synapse in rat hippocampus. *The Journal of Physiology* 539:201-208.

Hefft S, Jonas P (2005) Asynchronous GABA release generates long-lasting inhibition at a hippocampal interneuron-principal neuron synapse. *Nat Neurosci* 8:1319-1328

Helen E S (2007) The CA3 "backprojection" to the dentate gyrus. In: *Progress in Brain Research*, pp 627-637: Elsevier.

Henze DA, Urban NN, Barrionuevo G (2000) The multifarious hippocampal mossy fiber pathway: a review. *Neuroscience* 98:407-427.

Henze DA, Wittner L, Buzsaki G (2002) Single granule cells reliably discharge targets in the hippocampal CA3 network *in vivo*. *Nat Neurosci* 5:790-795.

Hjorth-Simonsen A (1973) Some intrinsic connections of the hippocampus in the rat: An experimental analysis. *The Journal of Comparative Neurology* 147:145-161.

Isaacson JS, Solis JM, Nicoll RA (1993) Local and diffuse synaptic actions of GABA in the hippocampus. *Neuron* 10:165-175.

Ishizuka N, Weber J, Amaral DG (1990) Organization of intrahippocampal projections originating from CA3 pyramidal cells in the rat. *The Journal of Comparative Neurology* 295:580-623.

Jinno S, Kosaka T (2000) Colocalization of parvalbumin and somatostatin-like immunoreactivity in the mouse hippocampus: Quantitative analysis with optical disector. *The Journal of Comparative Neurology* 428:377-388.

Jones BE, Moore RY (1977) Ascending projections of the locus coeruleus in the rat. II. Autoradiographic study. *Brain Research* 127:23-53.

Jones S, Yakel JL (1997) Functional nicotinic ACh receptors on interneurons in the rat hippocampus. *The Journal of Physiology* 504:603-610.

Kanemoto Y, Matsuzaki M, Morita S, Hayama T, Noguchi J, Senda N, Momotake A, Arai T, Kasai H (2011) Spatial Distributions of GABA Receptors and Local Inhibition of Ca²⁺ Transients Studied with GABA Uncaging in the Dendrites of CA1 Pyramidal Neurons. *PLoS ONE* 6:e22652.

Kasugai Y, Swinny JD, Roberts JDB, Dalezios Y, Fukazawa Y, Sieghart W, Shigemoto R, Somogyi P (2010) Quantitative localisation of synaptic and extrasynaptic GABA_A receptor subunits on hippocampal pyramidal cells by freeze-fracture replica immunolabelling. *European Journal of Neuroscience* 32:1868-1888.

Katona I, Acsády L, Freund TF (1999) Postsynaptic targets of somatostatin-immunoreactive interneurons in the rat hippocampus. *Neuroscience* 88:37-55.

Katona I, Sperl agh B, S ik A, K afalvi A, Vizi ES, Mackie K, Freund TF (1999) Presynaptically Located CB1 Cannabinoid Receptors Regulate GABA Release from Axon Terminals of Specific Hippocampal Interneurons. *The Journal of Neuroscience* 19:4544-4558.

Kaupmann K, Schuler V, Mosbacher J, Bischoff S, Bittiger H, Heid J, Froestl W, Leonhard S, Pfaff T, Karschin A, Bettler B (1998) Human gamma-aminobutyric acid type B receptors are differentially expressed and regulate inwardly rectifying K⁺ channels. *Proceedings of the National Academy of Sciences* 95:14991-14996.

Kawaguchi Y, Kubota Y (1993) Correlation of physiological subgroupings of nonpyramidal cells with parvalbumin- and calbindinD28k-immunoreactive neurons in layer V of rat frontal cortex. *Journal of Neurophysiology* 70:387-396.

Kawaguchi Y, Katsumaru H, Kosaka T, Heizmann CW, Hama K (1987) Fast spiking cells in rat hippocampus (CA1 region) contain the calcium-binding protein parvalbumin. *Brain Research* 416:369-374.

Kehrer C, Maziashvili N, Dugladze T, Gloveli T (2008) Altered excitatory-inhibitory balance in the NMDA-hypofunction model of schizophrenia.

Khazipov R, Congar P, Ben-Ari Y (1995) Hippocampal CA1 lacunosum-moleculare interneurons: modulation of monosynaptic GABAergic IPSCs by presynaptic GABAB receptors. *Journal of Neurophysiology* 74:2126-2137.

Klausberger T, Magill PJ, Marton LF, Roberts JDB, Cobden PM, Buzsaki G, Somogyi P (2003) Brain-state- and cell-type-specific firing of hippocampal interneurons *in vivo*. *Nature* 421:844-848.

Klausberger T, Marton LF, O'Neill J, Huck JHJ, Dalezios Y, Fuentealba P, Suen WY, Papp E, Kaneko T, Watanabe M, Csicsvari J, Somogyi P (2005) Complementary Roles of Cholecystinin- and Parvalbumin-Expressing GABAergic Neurons in Hippocampal Network Oscillations. *The Journal of Neuroscience* 25:9782-9793.

Klausberger T, Somogyi P (2008) Neuronal Diversity and Temporal Dynamics: The Unity of Hippocampal Circuit Operations. *Science* 321:53-57.

Koh DS, Geiger JR, Jonas P, Sakmann B (1995) Ca²⁺-permeable AMPA and NMDA receptor channels in basket cells of rat hippocampal dentate gyrus. *The Journal of Physiology* 485:383-402

Konopacki J, Bland BH, Roth SH (1988) Evidence that activation of *in vitro* hippocampal [theta] rhythm only involves muscarinic receptors. *Brain Research* 455:110-114.

Krnjević K (1974) Chemical Nature of Synaptic Transmission in Vertebrates. *Physiological Reviews* 54:418-540.

Kulik Á, Vida I, Lujan R, Haas CA, López-Bendito G, Shigemoto R, Frotscher M (2003) Subcellular Localization of Metabotropic GABAB Receptor Subunits GABAB1a/b and GABAB2 in the Rat Hippocampus. *The Journal of Neuroscience* 23:11026-11035.

Kulik Á, Vida I, Fukazawa Y, Guetg N, Kasugai Y, Marker CL, Rigato F, Bettler B, Wickman K, Frotscher M, Shigemoto R (2006) Compartment-Dependent Colocalization of Kir3.2-Containing K⁺ Channels and GABAB Receptors in Hippocampal Pyramidal Cells. *The Journal of Neuroscience* 26:4289-4297.

Lacaille JC, Schwartzkroin P (1988) Stratum lacunosum-moleculare interneurons of hippocampal CA1 region. I. Intracellular response characteristics, synaptic responses, and morphology. *The Journal of Neuroscience* 8:1400-1410.

Lacaille JC (1991) Postsynaptic potentials mediated by excitatory and inhibitory amino acids in interneurons of stratum pyramidale of the CA1 region of rat hippocampal slices *in vitro*. *Journal of Neurophysiology* 66:1441-1454.

Lacaille JC, Williams S (1990) Membrane properties of interneurons in stratum oriens-alveus of the CA1 region of rat hippocampus *in vitro*. *Neuroscience* 36:349-359.

Lambert NA, Wilson WA (1996) High-threshold Ca²⁺ currents in rat hippocampal interneurons and their selective inhibition by activation of GABA(B) receptors. *The Journal of Physiology* 492:115-127.

Lamsa KP, Heeroma JH, Somogyi P, Rusakov DA, Kullmann DM (2007) Anti-Hebbian Long-Term Potentiation in the Hippocampal Feedback Inhibitory Circuit. *Science* 315:1262-1266.

Landfield PW, McGaugh JL, Lynch G (1978) Impaired synaptic potentiation processes in the hippocampus of aged, memory-deficient rats. *Brain Research* 150:85-101.

Lee S-H, Soltesz I (2010) Requirement for CB1 but not GABAB receptors in the cholecystokinin mediated inhibition of GABA release from cholecystokinin expressing basket cells. *The Journal of Physiology* 589:891-902.

Lee S-H, Földy C, Soltesz I (2010) Distinct Endocannabinoid Control of GABA Release at Perisomatic and Dendritic Synapses in the Hippocampus. *The Journal of Neuroscience* 30:7993-8000.

Lei S, McBain CJ (2003) GABAB receptor modulation of excitatory and inhibitory synaptic transmission onto rat CA3 hippocampal interneurons. *The Journal of Physiology* 546:439-453.

Lien C-C, Martina M, Schultz JH, Ehmke H, Jonas P (2002) Gating, modulation and subunit composition of voltage-gated K⁺ channels in dendritic inhibitory interneurons of rat hippocampus. *The Journal of Physiology* 538:405-419.

Liu B, Hattori N, Jiang B, Nakayama Y, Zhang N-Y, Wu B, Kitagawa K, Taketo M, Matsuda H, Inagaki C (2004) Single cell RT-PCR demonstrates differential expression of GABAC receptor [ρ] subunits in rat hippocampal pyramidal and granule cells. *Molecular Brain Research* 123:1-6.

López-Bendito G, Shigemoto R, Kulik A, Vida I, Fairén A, Luján R (2004) Distribution of metabotropic GABA receptor subunits GABAB1a/b and GABAB2 in

the rat hippocampus during prenatal and postnatal development. *Hippocampus* 14:836-848.

Lorente de Nò R (1934) Studies on the structure of the cerebral cortex. II. Continuation of the study of the ammonic system. *J Psychol Neurol* 46:113-177.

Lu T, Trussell LO (2000) Inhibitory Transmission Mediated by Asynchronous Transmitter Release. *Neuron* 26:683-694.

Lupica CR, Bell JA, Hoffman AF, Watson PL (2001) Contribution of the Hyperpolarization-Activated Current (I_h) to Membrane Potential and GABA Release in Hippocampal Interneurons. *Journal of Neurophysiology* 86:261-268.

Lüscher C, Jan LY, Stoffel M, Malenka RC, Nicoll RA (1997) G Protein-Coupled Inwardly Rectifying K⁺ Channels (GIRKs) Mediate Postsynaptic but Not Presynaptic Transmitter Actions in Hippocampal Neurons. *Neuron* 19:687-695.

Maccaferri G, McBain CJ (1996) The hyperpolarization-activated current (I_h) and its contribution to pacemaker activity in rat CA1 hippocampal stratum oriens-alveus interneurons. *The Journal of Physiology* 497:119-130.

Maccaferri G, David J, Roberts B, Szucs P, Cottingham CA, Somogyi P (2000) Cell surface domain specific postsynaptic currents evoked by identified GABAergic neurones in rat hippocampus *in vitro*. *The Journal of Physiology* 524:91-116.

Madison DV, Nicoll RA (1984) Control of the repetitive discharge of rat CA 1 pyramidal neurones *in vitro*. *The Journal of Physiology* 354:319-331.

Mangan PS, Lothman EW (1996) Profound disturbances of pre- and postsynaptic GABAB-receptor-mediated processes in region CA1 in a chronic model of temporal lobe epilepsy. *Journal of Neurophysiology* 76:1282-1296.

Manseau F, Marinelli S, Mendez P, Schwaller B, Prince DA, Huguenard JR, Bacci A (2010) Desynchronization of Neocortical Networks by Asynchronous Release of

GABA at Autaptic and Synaptic Contacts from Fast-Spiking Interneurons. PLoS Biol 8:e1000492.

Martina M, Vida I, Jonas P (2000) Distal Initiation and Active Propagation of Action Potentials in Interneuron Dendrites. Science 287:295-300.

Martina M, Schultz JH, Ehmke H, Monyer H, Jonas P (1998) Functional and Molecular Differences between Voltage-Gated K⁺ Channels of Fast-Spiking Interneurons and Pyramidal Neurons of Rat Hippocampus. The Journal of Neuroscience 18:8111-8125.

Mátyás F, Freund TF, Gulyás AI (2004) Convergence of excitatory and inhibitory inputs onto CCK-containing basket cells in the CA1 area of the rat hippocampus. European Journal of Neuroscience 19:1243-1256.

Mayer ML, Westbrook GL (1983) A voltage-clamp analysis of inward (anomalous) rectification in mouse spinal sensory ganglion neurones. The Journal of Physiology 340:19-45.

McBain C, DiChiara T, Kauer J (1994) Activation of metabotropic glutamate receptors differentially affects two classes of hippocampal interneurons and potentiates excitatory synaptic transmission. The Journal of Neuroscience 14:4433-4445.

McBain CJ, Fisahn A (2001) Interneurons unbound. Nat Rev Neuroscience 2:11-23.

Mello LEAM, Cavalheiro EA, Tan AM, Kupfer WR, Pretorius JK, Babb TL, Finch DM (1993) Circuit Mechanisms of Seizures in the Pilocarpine Model of Chronic Epilepsy: Cell Loss and Mossy Fiber Sprouting. Epilepsia 34:985-995.

Mercer A, Trigg HL, Thomson AM (2007) Characterization of Neurons in the CA2 Subfield of the Adult Rat Hippocampus. The Journal of Neuroscience 27:7329-7338.

Mesulam MM, Mufson EJ, Wainer BH, Levey AI (1983) Central cholinergic pathways in the rat: An overview based on an alternative nomenclature (Ch1-Ch6). *Neuroscience* 10:1185-1201

Meyer-Lindenberg A, Weinberger DR (2006) Intermediate phenotypes and genetic mechanisms of psychiatric disorders. *Nat Rev Neurosci* 7:818-827.

Mikkonen JE, Huttunen J, Penttonen M (2006) Contribution of a single CA3 neuron to network synchrony. *NeuroImage* 31:1222-1227.

Misgeld U, Frotscher M (1986) Postsynaptic-gabaergic inhibition of non-pyramidal neurons in the guinea-pig hippocampus. *Neuroscience* 19:193-206.

Mitchell SJ, Silver RA (2000) GABA Spillover from Single Inhibitory Axons Suppresses Low-Frequency Excitatory Transmission at the Cerebellar Glomerulus. *The Journal of Neuroscience* 20:8651-8658.

Morales M, Bloom FE (1997) The 5-HT₃ Receptor Is Present in Different Subpopulations of GABAergic Neurons in the Rat Telencephalon. *The Journal of Neuroscience* 17:3157-3167.

Morrisett R, Mott D, Lewis D, Swartzwelder H, Wilson W (1991) GABAB-receptor-mediated inhibition of the N-methyl-D-aspartate component of synaptic transmission in the rat hippocampus. *The Journal of Neuroscience* 11:203-209.

Mott DD, Li Q, Okazaki MM, Turner DA, Lewis DV (1999) GABAB-Receptor-Mediated Currents in Interneurons of the Dentate-Hilus Border. *Journal of Neurophysiology* 82:1438-1450.

Murray AJ, Sauer J-F, Riedel G, McClure C, Ansel L, Cheyne L, Bartos M, Wisden W, Wulff P (2011) Parvalbumin-positive CA1 interneurons are required for spatial working but not for reference memory. *Nat Neurosci* 14:297-299.

Neu A, Földy C, Soltesz I (2007) Postsynaptic origin of CB1-dependent tonic inhibition of GABA release at cholecystokinin-positive basket cell to pyramidal

cell synapses in the CA1 region of the rat hippocampus. *The Journal of Physiology* 578:233-247.

Newberry NR, Nicoll RA (1985) Comparison of the action of baclofen with gamma-aminobutyric acid on rat hippocampal pyramidal cells *in vitro*. *The Journal of Physiology* 360:161-185.

Nissen W, Szabo A, Somogyi J, Somogyi P, Lamsa KP (2010) Cell Type-Specific Long-Term Plasticity at Glutamatergic Synapses onto Hippocampal Interneurons Expressing either Parvalbumin or CB1 Cannabinoid Receptor. *The Journal of Neuroscience* 30:1337-1347.

Nörenberg A, Hu H, Vida I, Bartos M, Jonas P (2010) Distinct nonuniform cable properties optimize rapid and efficient activation of fast-spiking GABAergic interneurons. *Proceedings of the National Academy of Sciences* 107:894-899.

Nunzi MG, Gorio A, Milan F, Freund TF, Somogyi P, Smith AD (1985) Cholecystinin-immunoreactive cells form symmetrical synaptic contacts with pyramidal and nonpyramidal neurons in the hippocampus. *The Journal of Comparative Neurology* 237:485-505.

Nusser Z, Sieghart W, Benke D, Fritschy JM, Somogyi P (1996) Differential synaptic localization of two major gamma-aminobutyric acid type A receptor alpha subunits on hippocampal pyramidal cells. *Proceedings of the National Academy of Sciences* 93:11939-11944.

O'Keefe J, Nadel L (1979) The hippocampus as a cognitive map. *Behavioral and Brain Sciences* 2:487-494.

Ogiwara I, Miyamoto H, Morita N, Atapour N, Mazaki E, Inoue I, Takeuchi T, Itohara S, Yanagawa Y, Obata K, Furuichi T, Hensch TK, Yamakawa K (2007) Nav1.1 Localizes to Axons of Parvalbumin-Positive Inhibitory Interneurons: A Circuit Basis for Epileptic Seizures in Mice Carrying an Scn1a Gene Mutation. *The Journal of Neuroscience* 27:5903-5914.

- Okazaki MM, Molnár Pt, Nadler JV (1999) Recurrent Mossy Fiber Pathway in Rat Dentate Gyrus: Synaptic Currents Evoked in Presence and Absence of Seizure-Induced Growth. *Journal of Neurophysiology* 81:1645-1660.
- Olah S, Fule M, Komlosi G, Varga C, Baldi R, Barzo P, Tamas G (2009) Regulation of cortical microcircuits by unitary GABA-mediated volume transmission. *Nature* 461:1278-1281.
- Otis TS, De Koninck Y, Mody I (1993) Characterization of synaptically elicited GABAB responses using patch-clamp recordings in rat hippocampal slices. *The Journal of Physiology* 463:391-407.
- Ouardouz M, Lacaille J-C (1997) Properties of Unitary IPSCs in Hippocampal Pyramidal Cells Originating From Different Types of Interneurons in Young Rats. *Journal of Neurophysiology* 77:1939-1949.
- Pagano A, Rovelli G, Mosbacher J, Lohmann T, Duthey B, Stauffer D, Ristig D, Schuler V, Meigel I, Lampert C, Stein T, Pràzeau L, Blahos J, Pin J-P, Froestl W, Kuhn R, Heid J, Kaupmann K, Bettler B (2001) C-Terminal Interaction Is Essential for Surface Trafficking But Not for Heteromeric Assembly of GABAB Receptors. *The Journal of Neuroscience* 21:1189-1202.
- Papp EC, Hájos N, Acsády L, Freund TF (1999) Medial septal and median raphe innervation of vasoactive intestinal polypeptide-containing interneurons in the hippocampus. *Neuroscience* 90:369-382.
- Pawelzik H, Hughes DI, Thomson AM (2002) Physiological and morphological diversity of immunocytochemically defined parvalbumin- and cholecystokinin-positive interneurons in CA1 of the adult rat hippocampus. *The Journal of Comparative Neurology* 443:346-367.
- Pérez-Garci E, Gassmann M, Bettler B, Larkum ME (2006) The GABAB1b Isoform Mediates Long-Lasting Inhibition of Dendritic Ca²⁺ Spikes in Layer 5 Somatosensory Pyramidal Neurons. *Neuron* 50:603-616.

Pittaluga A, Asaro D, Pellegrini G, Raiteri M (1987) Studies on [3H] GABA and endogenous GABA release in rat cerebral cortex suggest the presence of autoreceptors of the GABAB type. *European Journal of Pharmacology* 144:45-52.

Poncer JC, McKinney RA, Gähwiler BH, Thompson SM (2000) Differential control of GABA release at synapses from distinct interneurons in rat hippocampus. *The Journal of Physiology* 528:123-130.

Prenosil GA, Schneider Gasser EM, Rudolph U, Keist R, Fritschy J-M, Vogt KE (2006) Specific Subtypes of GABAA Receptors Mediate Phasic and Tonic Forms of Inhibition in Hippocampal Pyramidal Neurons. *Journal of Neurophysiology* 96:846-857.

Price CJ, Scott R, Rusakov DA, Capogna M (2008) GABAB Receptor Modulation of Feedforward Inhibition through Hippocampal Neurogliaform Cells. *The Journal of Neuroscience* 28:6974-6982.

Price CJ, Cauli B, Kovacs ER, Kulik Á, Lambolez B, Shigemoto R, Capogna M (2005) Neurogliaform Neurons Form a Novel Inhibitory Network in the Hippocampal CA1 Area. *The Journal of Neuroscience* 25:6775-6786.

Pritchett DB, Sontheimer H, Shivers BD, Ymer S, Kettenmann H, Schofield PR, Seeburg PH (1989) Importance of a novel GABAA receptor subunit for benzodiazepine pharmacology. *Nature* 338:582-585.

Rakic P (1981) Neuronal-glia interaction during brain development. *Trends in Neurosciences* 4:184-187.

Reimann W (1983) Inhibition by GABA, baclofen and gabapentin of dopamine release from rabbit caudate nucleus: Are there common or different sites of action? *European Journal of Pharmacology* 94:341-344.

Ribak C, Harris A, Vaughn J, Roberts E (1979) Inhibitory, GABAergic nerve terminals decrease at sites of focal epilepsy. *Science* 205:211-214.

Ribak CE, Seress L, Amaral DG (1985) The development, ultrastructure and synaptic connections of the mossy cells of the dentate gyrus. *Journal of neurocytology* 14:835-857.

Rossi P, Mapelli L, Roggeri L, Gall D, De Kerchove d'Exaerde A, Schiffmann SN, Taglietti V, D'Angelo E (2006) Inhibition of constitutive inward rectifier currents in cerebellar granule cells by pharmacological and synaptic activation of GABAB receptors. *European Journal of Neuroscience* 24:419-432.

Rotstein HG, Pervouchine DD, Acker CD, Gillies MJ, White JA, Buhl EH, Whittington MA, Kopell N (2005) Slow and Fast Inhibition and an H-Current Interact to Create a Theta Rhythm in a Model of CA1 Interneuron Network. *Journal of Neurophysiology* 94:1509-1518.

Rozzo A, Armellin M, Franzot J, Chiaruttini C, Nistri A, Tongiorgi E (2002) Expression and dendritic mRNA localization of GABAC receptor $\rho 1$ and $\rho 2$ subunits in developing rat brain and spinal cord. *European Journal of Neuroscience* 15:1747-1758.

Saalfeld S, Cardona A, Hartenstein V, Tomancak P (2010) As-rigid-as-possible mosaicking and serial section registration of large ssTEM datasets. *Bioinformatics* 26:i57-i63.

Sadja R, Alagem N, Reuveny E (2003) Gating of GIRK Channels: Details of an Intricate, Membrane-Delimited Signaling Complex. *Neuron* 39:9-12.

Sakaba T, Neher E (2003) Direct modulation of synaptic vesicle priming by GABAB receptor activation at a glutamatergic synapse. *Nature* 424:775-778.

Sambandan S, Sauer J-F, Vida I, Bartos M (2010) Associative Plasticity at Excitatory Synapses Facilitates Recruitment of Fast-Spiking Interneurons in the Dentate Gyrus. *The Journal of Neuroscience* 30:11826-11837.

Savić N, Sciancalepore M (2001) Electrophysiological Characterization of "Giant" Cells in *Stratum Radiatum* of the CA3 Hippocampal Region. *Journal of Neurophysiology* 85:1998-2007.

Scanziani M, Capogna M, Gähwiler BH, Thompson SM (1992) Presynaptic inhibition of miniature excitatory synaptic currents by baclofen and adenosine in the hippocampus. *Neuron* 9:919-927.

Scanziani M (2000) GABA Spillover Activates Postsynaptic GABAB Receptors to Control Rhythmic Hippocampal Activity. *Neuron* 25:673-681.

Schmitz D, Gloveli T, Empson R, Heinemann U (1998) Comparison of the effects of serotonin in the hippocampus and the entorhinal cortex. *Molecular Neurobiology* 17:59-72.

Schwartzkroin PA (1975) Characteristics of CA1 neurons recorded intracellularly in the hippocampal *in vitro* slice preparation. *Brain Research* 85:423-436.

Schwenk J, Metz M, Zolles G, Turecek R, Fritzius T, Bildl W, Tarusawa E, Kulik A, Unger A, Ivankova K, Seddik R, Tiao JY, Rajalu M, Trojanova J, Rohde V, Gassmann M, Schulte U, Fakler B, Bettler B (2010) Native GABAB receptors are heteromultimers with a family of auxiliary subunits. *Nature* 465:231-235.

Scoville WB, Milner, B. (1957) Loss of Recent Memory After Bilateral Hippocampal Lesions. *Journal of Neurology Neurosurgery Psychiatry* 20 (1):11-21.

Shanes AM (1958) Electrochemical aspects of physiological and pharmacological action in excitable cells. II. The action potential and excitation. *Pharmacological Reviews* 10:165-273.

Shimada S, Cutting G, Uhl GR (1992) gamma-Aminobutyric acid A or C receptor? gamma-Aminobutyric acid rho 1 receptor RNA induces bicuculline-, barbiturate-, and benzodiazepine-insensitive gamma-aminobutyric acid responses in *Xenopus* oocytes. *Molecular Pharmacology* 41:683-687.

Sigel E, Baur R, Malherbe P, Mähler H (1989) The rat beta1-subunit of the GABAA receptor forms a picrotoxin-sensitive anion channel open in the absence of GABA. *FEBS Letters* 257:377-379.

Sík A, Penttonen M, Ylinen A, Buzsáki G (1995) Hippocampal CA1 interneurons: an *in vivo* intracellular labeling study. *The Journal of Neuroscience* 15:6651-6665.

Sík A, Ylinen A, Penttonen M, Buzsáki G (1994) Inhibitory CA1-CA3-hilar region feedback in the hippocampus. *Science* 265:1722-1724.

Sloviter RS, Ali-Akbarian L, Elliott RC, Bowery BJ, Bowery NG (1999) Localization of GABAB (R1) receptors in the rat hippocampus by immunocytochemistry and high resolution autoradiography, with specific reference to its localization in identified hippocampal interneuron subpopulations. *Neuropharmacology* 38:1707-1721.

Sodickson DL, Bean BP (1996) GABAB Receptor-Activated Inwardly Rectifying Potassium Current in Dissociated Hippocampal CA3 Neurons. *The Journal of Neuroscience* 16:6374-6385.

Sohal VS, Zhang F, Yizhar O, Deisseroth K (2009) Parvalbumin neurons and gamma rhythms enhance cortical circuit performance. *Nature* 459:698-702.

Sohn J-W, Lee D, Cho H, Lim W, Shin H-S, Lee S-H, Ho W-K (2007) Receptor-specific inhibition of GABAB-activated K⁺ currents by muscarinic and metabotropic glutamate receptors in immature rat hippocampus. *The Journal of Physiology* 580:411-422.

Solis J, Nicoll R (1992) Pharmacological characterization of GABAB-mediated responses in the CA1 region of the rat hippocampal slice. *The Journal of Neuroscience* 12:3466-3472.

Sommer W (1880) Erkrankung des Ammonshorns als aetiologisches Moment der Epilepsie. *European Archives of Psychiatry and Clinical Neuroscience* 10:631-675.

Somogyi J, Baude A, Omori Y, Shimizu H, Mestikawy SE, Fukaya M, Shigemoto R, Watanabe M, Somogyi P (2004) GABAergic basket cells expressing cholecystokinin contain vesicular glutamate transporter type 3 (VGLUT3) in their synaptic terminals in hippocampus and isocortex of the rat. *European Journal of Neuroscience* 19:552-569.

Spruston N, Johnston D (1992) Perforated patch-clamp analysis of the passive membrane properties of three classes of hippocampal neurons. *Journal of Neurophysiology* 67:508-529.

Spruston N, Schiller Y, Stuart G, Sakmann B (1995) Activity-dependent action potential invasion and calcium influx into hippocampal CA1 dendrites. *Science* 268:297-300.

Squire LR (1992) Memory and the Hippocampus: A Synthesis From Findings With Rats, Monkeys, and Humans. *Psychological Review* 99:195-231.

Staley KJ, Mody I (1992) Shunting of excitatory input to dentate gyrus granule cells by a depolarizing GABA_A receptor-mediated postsynaptic conductance. *Journal of Neurophysiology* 68:197-212.

Storm-Mathieson J (1977) Localization of transmitter candidates in the brain: the hippocampal formation as a model. *Progress in Neurobiology* 8:119-181.

Stumpf C, Carl CP, John RS (1965) Drug Action on The Electrical Activity of The Hippocampus. In: *International Review of Neurobiology*, pp 77-138: Academic Press.

Suzuki SS, Smith GK (1988) Spontaneous EEG spikes in the normal hippocampus. V. Effects of ether, urethane, pentobarbital, atropine, diazepam and bicuculline. *Electroencephalography and Clinical Neurophysiology* 70:84-95.

- Szabadics J, Varga C, Molnár G, Oláh S, Barzó P, Tamás G (2006) Excitatory Effect of GABAergic Axo-Axonic Cells in Cortical Microcircuits. *Science* 311:233-235.
- Tamás G, Szabadics J, Somogyi P (2002) Cell Type- and Subcellular Position-Dependent Summation of Unitary Postsynaptic Potentials in Neocortical Neurons. *The Journal of Neuroscience* 22:740-747.
- Tóth K, McBain CJ (1998) Afferent-specific innervation of two distinct AMPA receptor subtypes on single hippocampal interneurons. *Nat Neurosci* 1:572-578.
- Tóth K, Freund TF (1992) Calbindin D28k-containing nonpyramidal cells in the rat hippocampus: Their immunoreactivity for GABA and projection to the medial septum. *Neuroscience* 49:793-805.
- Traynelis SF, Wollmuth LP, McBain CJ, Menniti FS, Vance KM, Ogden KK, Hansen KB, Yuan H, Myers SJ, Dingledine R (2010) Glutamate Receptor Ion Channels: Structure, Regulation, and Function. *Pharmacological Reviews* 62:405-496.
- Tsou K, Mackie K, Sañudo-Peña MC, Walker JM (1999) Cannabinoid CB1 receptors are localized primarily on cholecystinin-containing GABAergic interneurons in the rat hippocampal formation. *Neuroscience* 93:969-975.
- Tsubokawa H, Ross WN (1996) IPSPs modulate spike backpropagation and associated $[Ca^{2+}]_i$ changes in the dendrites of hippocampal CA1 pyramidal neurons. *Journal of Neurophysiology* 76:2896-2906.
- Vautrin J, Schaffner AE, Barker JL (1994) Fast presynaptic GABAA receptor-mediated Cl^- conductance in cultured rat hippocampal neurones. *The Journal of Physiology* 479:53-63
- Vertes RP (2006) Interactions among the medial prefrontal cortex, hippocampus and midline thalamus in emotional and cognitive processing in the rat. *Neuroscience* 142:1-20.

Vida I, Halasy K, Szinyei C, Somogyi P, Buhl EH (1998) Unitary IPSPs evoked by interneurons at the stratum radiatum-stratum lacunosum-moleculare border in the CA1 area of the rat hippocampus *in vitro*. *The Journal of Physiology* 506:755-773.

Vigot R, Barbieri S, Bräuner-Osborne H, Turecek R, Shigemoto R, Zhang Y-P, Luján R, Jacobson LH, Biermann B, Fritschy J-M, Vacher C-M, Müller M, Sansig G, Guetg N, Cryan JF, Kaupmann K, Gassmann M, Oertner TG, Bettler B (2006) Differential Compartmentalization and Distinct Functions of GABAB Receptor Variants. *Neuron* 50:589-601.

Vogt KE, Nicoll RA (1999) Glutamate and gamma-aminobutyric acid mediate a heterosynaptic depression at mossy fiber synapses in the hippocampus. *Proceedings of the National Academy of Sciences* 96:1118-1122.

Wang X-J, Buzsáki Gr (1996) Gamma Oscillation by Synaptic Inhibition in a Hippocampal Interneuronal Network Model. *The Journal of Neuroscience* 16:6402-6413.

Wang Y, Neubauer FB, Lüscher H-R, Thurley K (2010) GABAB receptor-dependent modulation of network activity in the rat prefrontal cortex *in vitro*. *European Journal of Neuroscience* 31:1582-1594.

Weiser M, Bueno E, Sekirnjak C, Martone M, Baker H, Hillman D, Chen S, Thornhill W, Ellisman M, Rudy B (1995) The potassium channel subunit KV3.1b is localized to somatic and axonal membranes of specific populations of CNS neurons. *The Journal of Neuroscience* 15:4298-4314.

Whittington MA, Traub RD, Jefferys JGR (1995) Synchronized oscillations in interneuron networks driven by metabotropic glutamate receptor activation. *Nature* 373:612-615.

Williams S, Lacaille J-C (1992) GABA_B receptor-mediated inhibitory postsynaptic potentials evoked by electrical stimulation and by glutamate stimulation of interneurons in *Stratum lacunosum-moleculare* in hippocampal CA1 pyramidal cells *in vitro*. *Synapse* 11:249-258.

Wu L-G, Saggau P (1997) Presynaptic inhibition of elicited neurotransmitter release. *Trends in Neurosciences* 20:204-212.

Wulff P, Ponomarenko AA, Bartos M, Korotkova TM, Fuchs EC, Böhner F, Both M, Tort ABL, Kopell NJ, Wisden W, Monyer H (2009) Hippocampal theta rhythm and its coupling with gamma oscillations require fast inhibition onto parvalbumin-positive interneurons. *Proceedings of the National Academy of Sciences* 106:3561-3566.

Yanovsky Y, Sergeeva OA, Freund TF, Haas HL (1997) Activation of interneurons at the *stratum oriens*/alveus border suppresses excitatory transmission to apical dendrites in the CA1 area of the mouse hippocampus. *Neuroscience* 77:87-96.

Zhang L, McBain CJ (1995) Potassium conductances underlying repolarization and after-hyperpolarization in rat CA1 hippocampal interneurons. *The Journal of Physiology* 488:661-672